



# **Design and Performance of Felodipine-based Solid Dispersions**

by

**Zoe A. Langham**

**Thesis**

Submitted to the University of Nottingham

for the degree of

**Doctor of Philosophy**

**School of Pharmacy**

November 2010



**The University of  
Nottingham**

# Contents

<b>List of Tables</b>	<b>vii</b>
<b>List of Figures</b>	<b>x</b>
<b>Acknowledgments</b>	<b>xxvi</b>
<b>Declarations</b>	<b>xxvii</b>
<b>Abstract</b>	<b>xxviii</b>
<b>Abbreviations</b>	<b>xxix</b>
<b>Summary of Analogues</b>	<b>xxxii</b>
<b>Chapter 1 Introduction</b>	<b>1</b>
1.1 The Problem of Poorly Soluble Drugs . . . . .	1
1.2 Methods of Improving Drug Bioavailability . . . . .	3
1.2.1 Pro-drugs . . . . .	3
1.2.2 Salts . . . . .	4
1.2.3 Co-crystals . . . . .	5
1.2.4 Modification of the Crystal Form . . . . .	5
1.2.5 Lipidic Formulations . . . . .	7
1.2.6 Particle Size Reduction . . . . .	8



1.2.7	Solid Dispersions . . . . .	8
1.3	Review of Solid Dispersion Literature . . . . .	9
1.3.1	Solid Dispersion Classification . . . . .	9
1.3.2	The Advantages of Solid Dispersions . . . . .	17
1.3.3	The Challenges Associated With Using Solid Dispersions . . . . .	18
1.4	Aims of the PhD . . . . .	31
1.4.1	Motivation and Aims of this Research . . . . .	31
1.4.2	Overview of the thesis . . . . .	33
<b>Chapter 2</b>	<b>Materials and Experimental Methods</b>	<b>35</b>
2.1	Materials . . . . .	35
2.1.1	Felodipine . . . . .	35
2.1.2	Copovidone . . . . .	36
2.2	Methods . . . . .	37
2.2.1	Structure Determination . . . . .	37
2.2.2	X-ray Powder Diffraction (XRPD) . . . . .	38
2.2.3	Differential Scanning Calorimetry (DSC) . . . . .	42
2.2.4	Optical Microscopy . . . . .	45
2.2.5	Scanning Electron Microscopy (SEM) . . . . .	46
2.2.6	Atomic Force Microscopy (AFM) . . . . .	46
2.2.7	Dissolution Testing . . . . .	49
<b>Chapter 3</b>	<b>Synthesis of Felodipine Analogues</b>	<b>51</b>
3.1	Introduction . . . . .	51
3.1.1	Rationale for the synthesis of felodipine analogues . . . . .	51
3.1.2	Target Compound Design and Retrosynthetic Analysis . . . . .	53
3.2	Materials . . . . .	58
3.3	Chromatographic Methods . . . . .	58
3.4	Melting Point Determination . . . . .	58

3.5	Spectroscopic Methods . . . . .	58
3.5.1	Nuclear Magnetic Resonance (NMR) . . . . .	59
3.5.2	Mass Spectrometry (MS) . . . . .	59
3.5.3	FTIR . . . . .	59
3.6	Synthetic Methods . . . . .	60
3.6.1	ZAL_001 – O3-ethyl O5-methyl 4-(2,3-dichlorophenyl)-2,6-dimethyl- pyridine-3,5-dicarboxylate . . . . .	60
3.6.2	ZAL_005 – diethyl 2,6-dimethyl-4-phenyl-1,4-dihydropyridine-3,5- dicarboxylate . . . . .	61
3.6.3	ZAL_006 – ethyl 5-cyano-4-(2,3-dichlorophenyl)-2,6-dimethyl-1,4- dihydropyridine-3-carboxylate . . . . .	62
3.6.4	ZAL_007 – diethyl 4-(2,3-dichlorophenyl)-2,6-dimethyl-1,4-dihydropyridine- 3,5-dicarboxylate . . . . .	63
3.6.5	ZAL_008 – 4-(2,3-dichlorophenyl)-2,6-dimethyl-1,4-dihydropyridine- 3,5-dicarbonitrile . . . . .	65
3.6.6	ZAL_009 – ethyl 5-cyano-2,6-dimethyl-4-phenyl-1,4-dihydropyridine- 3-carboxylate . . . . .	66
3.6.7	ZAL_010 – 2,6-dimethyl-4-phenyl-1,4-dihydropyridine-3,5-dicarbonitrile	67
3.6.8	ZAL_011 – diethyl 4-(2,3-dichlorophenyl)-1,2,6-trimethyl-4H-pyridine- 3,5-dicarboxylate . . . . .	68
3.7	Results and Discussion . . . . .	70
3.8	Conclusions . . . . .	75
3.9	Future work . . . . .	75
<b>Chapter 4</b>	<b>Solid State Analysis of Solid Dispersions</b>	<b>78</b>
4.1	Introduction . . . . .	78
4.2	Materials . . . . .	80
4.2.1	Preparation of Solid Dispersion Samples . . . . .	80

4.2.2	Preparation of Amorphous Drug, Copovidone, and Physical Mixture Samples . . . . .	81
4.3	Methods of analysis . . . . .	81
4.3.1	X-ray Powder Diffraction (XRPD) . . . . .	81
4.3.2	Pair Distribution Function Analysis (PDF) . . . . .	82
4.3.3	Differential Scanning Calorimetry (DSC) . . . . .	83
4.3.4	Helium Pycnometry . . . . .	84
4.3.5	Optical Microscopy . . . . .	85
4.3.6	Scanning Electron Microscopy (SEM) . . . . .	85
4.4	Results and Discussion . . . . .	85
4.4.1	Copovidone . . . . .	85
4.4.2	Felodipine . . . . .	86
4.4.3	ZAL_001 . . . . .	99
4.4.4	ZAL_005 . . . . .	99
4.4.5	ZAL_006 . . . . .	102
4.4.6	ZAL_007 . . . . .	105
4.4.7	ZAL_008 . . . . .	109
4.4.8	ZAL_009 . . . . .	109
4.4.9	ZAL_010 . . . . .	112
4.4.10	ZAL_011 . . . . .	115
4.5	Conclusions . . . . .	118
4.6	Future work . . . . .	119

## **Chapter 5 Physical Stability Testing of Felodipine-based Solid Dispersions 120**

5.1	Light Scattering Studies of Felodipine/Copovidone Solid Dispersions . .	121
5.1.1	Introduction . . . . .	121
5.1.2	Materials . . . . .	124
5.1.3	Methods . . . . .	125
5.1.4	Results and Discussion . . . . .	126

5.1.5	Conclusions - Light Scattering Work . . . . .	131
5.2	Polarised Light Microscopy Studies of Felodipine-based Solid Dispersions	135
5.2.1	Introduction . . . . .	135
5.2.2	Materials . . . . .	139
5.2.3	Methods . . . . .	141
5.2.4	Results and Discussion . . . . .	142
5.2.5	Conclusions - Well-plate crystallisation experiments . . . . .	148
5.3	Future Work . . . . .	149
<b>Chapter 6</b>	<b>Dissolution Performance of Felodipine-based Solid Dispersions</b>	<b>151</b>
6.1	Introduction . . . . .	151
6.2	Materials . . . . .	154
6.2.1	Preparation of Solid Dispersion Films . . . . .	154
6.2.2	Pure Drug and Physical Mixture Samples . . . . .	155
6.2.3	Dissolution Media . . . . .	156
6.3	Methods . . . . .	157
6.3.1	Solubility Prediction . . . . .	157
6.3.2	Dissolution Methods . . . . .	157
6.3.3	Complimentary Measurement Techniques . . . . .	162
6.4	Results and Discussion . . . . .	163
6.4.1	Felodipine Dissolution . . . . .	163
6.4.2	Analogue Dissolution and Solubility - Micro-dissolution . . . . .	177
6.5	Conclusions . . . . .	183
6.6	Future work . . . . .	185
<b>Chapter 7</b>	<b>Molecular Descriptors of Felodipine Analogues and Correlation</b>	
	<b>With Measured Properties</b>	<b>186</b>
7.1	Introduction . . . . .	186
7.2	Methods . . . . .	187

7.2.1	<i>In Silico</i> Calculations . . . . .	187
7.2.2	Thermal Properties . . . . .	188
7.2.3	Scoring Analogue Performance . . . . .	188
7.2.4	Determining correlations between modelled and experimental datasets	195
7.3	Results and Discussion . . . . .	196
7.4	Conclusions . . . . .	202
7.5	Future Work . . . . .	203
<b>Chapter 8</b>	<b>Conclusions and Future Work</b>	<b>205</b>
8.1	Conclusions . . . . .	205
8.2	Future Work . . . . .	207
<b>Appendix A</b>	<b>Images from Well-plate Crystallisation Study</b>	<b>209</b>
<b>Appendix B</b>	<b>Analogue Dissolution Results</b>	<b>222</b>
<b>Appendix C</b>	<b>Calculated Molecular Descriptors and Correlations</b>	<b>225</b>
<b>Bibliography</b>		<b>225</b>

# List of Tables

3.1	Summary of the compounds synthesised. . . . .	75
5.1	Table summarising the results of the well-plate crystallisation experiments. Duplicate samples were tested, and both results for each condition are detailed in the table. The numbers indicate the sampling day on which evidence of crystallisation was first seen for that sample; 0 denotes that crystals were seen during the initial analysis carried out prior to storage of the well-plate; '-' denotes that no evidence of crystallisation was observed for this sample for the duration of the experiment (49 days).	143
6.1	Summary of the predicted crystalline and amorphous solubilities for the felodipine analogues tested in this chapter, and the mass of analogue used in micro-dissolution tests. . . . .	158
6.2	Summary of the UV absorption ranges used to determine the solution concentrations of drug in the micro-dissolution experiments. . . . .	159
6.3	The HPLC method, mobile phase gradient used for analysing the drug content of dissolution samples. . . . .	160

6.4	Summary of the data from micro-dissolution experiments carried out on samples containing Felodipine. Data are reported as mean values $\pm$ standard error. All equilibrium solubility values were determined from the micro-dissolution data at 8 hours. <sup>a</sup> Equilibrium solution concentration values could not be determined for the 5% drug-loaded film-cast samples as the solution concentration did not drop to equilibrium levels within the 8 hour experimental time frame. . . . .	164
6.5	Summary of the data from MRI-flowcell dissolution experiments carried out on samples containing Felodipine. <sup>a</sup> Only data for 5% and 15% drug loaded samples is shown as the levels of drug released from the 30% and 50% drug-loaded compacts were below the level of detection for the UV/Vis instrument. . . . .	170
7.1	The scoring system for crystallisation images obtained in chapter 5 applied to the image grid in figure 5.11 for ZAL_011 stored at 25°C/60% Relative Humidity over 7 weeks. . . . .	191
7.2	Summary of the scores determined for each analogue from the crystallisation screening experiment. . . . .	191
7.3	Summary of the Area under the Curve (AUC) values obtained from the dissolution data for solid dispersions of each analogue tested after 60 minutes. Data for 100% drug loaded samples refers to the crystalline form (except for ZAL_001, where this data refers to the oil sample). Data are reported as mean dimensionless scores $\pm$ standard error. . . .	193
7.4	Summary of the scores determined for each analogue from the dissolution data. Scores are determined by calculating the AUC for a graph in which the AUC values for each drug loading have been plotted, and normalised with respect to the 100% crystalline sample. Data are reported as mean values $\pm$ standard error. . . . .	193

B.1	Table summarising the data from dissolution experiments carried out on samples containing analogue ZAL_001. Data are reported as mean values $\pm$ standard error. <sup>a</sup> Analysis of the crystalline form of this compound was not possible as it is an oil. For these samples the oil was dispensed directly into sample vials without any further preparation. <sup>b</sup> The equilibrium solubility determined by HPLC after 18 hours. <sup>c</sup> The equilibrium solubility determined by HPLC after 15 hours. . . . .	222
B.2	Table summarising the data from dissolution experiments carried out on samples containing analogue ZAL_005. Data are reported as mean values $\pm$ standard error. <sup>a</sup> Equilibrium solubility values are obtained by HPLC after 18 hours. <sup>b</sup> Equilibrium solubility values are obtained by HPLC after 48 hours. . . . .	223
B.3	Table summarising the data from dissolution experiments carried out on samples containing analogue ZAL_006. Data are reported as mean values $\pm$ standard error. <sup>a</sup> Initial dissolution rates could not be determined for these samples due to the irregularity of the data. <sup>b</sup> Equilibrium solubility values are obtained by HPLC after 18 hours. <sup>c</sup> Equilibrium solubility values are obtained by HPLC after 48 hours. . . . .	223
B.4	Table summarising the data from dissolution experiments carried out on samples containing analogue ZAL_007. Data are reported as mean values $\pm$ standard error. <sup>a</sup> Only n=1 for this sample. <sup>b</sup> Equilibrium solubility values are obtained by HPLC after 18 hours. <sup>c</sup> Equilibrium solubility values are obtained by HPLC after 48 hours. . . . .	224
B.5	Table summarising the data from dissolution experiments carried out on samples containing analogue ZAL_011. Data are reported as mean values $\pm$ standard error. All equilibrium solubility values are obtained by HPLC after 18 hours. . . . .	224



# List of Figures

1.1	The Biopharmaceutics Classification System. . . . .	2
1.2	Phase diagram for a binary eutectic mixture, with the eutectic composition labelled 'E'. The effect of cooling at the eutectic composition (A to B) results in only the eutectic solidifying, whereas cooling at from a different composition (C to D) results in the solidification of component X, leaving the remaining liquid solution rich in component Y until the eutectic is reached. Reproduced with modifications from [1, 2, 3]. . . .	11
1.3	Schematic showing how a eutectic is an intimately blended physical mixture of the two crystalline components, shown as circles and rectangles.	11
1.4	Phase diagram for a discontinuous crystalline solid solution, whereby region $\alpha$ represents a solid solution of Y in X, and region $\beta$ represents a solid solution of X in Y. Reproduced with modifications from [1, 2, 3]. .	12
1.5	Schematics of a) a substitutional crystalline solid solution and b) an interstitial crystalline solid solution. Solvent molecules are represented with open circles, and filled circles indicate solute molecules. Reproduced from [1, 2]. . . . .	13
1.6	Schematics of a) an amorphous solid solution whereby the both the solvent (open ellipses) and solute (filled ellipses) are small molecules and b) an amorphous solid solution in which the drug molecules (filled circles) are dispersed in an amorphous polymer. . . . .	14

1.7	Schematics showing examples of solid suspensions whereby: a) amorphous material (ellipses) is suspended in a crystalline material (circles); b) drug microcrystals (circles) are suspended in an amorphous polymer (strands); and c) amorphous drug (ellipses) is suspended in an amorphous polymer (strands). . . . .	15
1.8	Schematic of a hot-melt extruder. Numbered labels indicate: 1) Feeding the extruder from a hopper; 2) Movement of the material through the extruder; 3) Flow of material through the die; and 4) Exit of extrudate from the die and down-stream processing. . . . .	20
1.9	Schematic diagram of a typical spray dryer (adapted from [4]). Numbered labels indicate: 1) feed solution; 2) pump; 3) air/N <sub>2</sub> inlet; 4) electric heater; 5) spray nozzle; 6) concentric inlet of the hot air around the spray nozzle; 7) spray cylinder; 8) thermometer for measuring outlet temperature; 9) cyclone to separate particles from gas stream; 10) collecting vessel for dried product; 11) outlet filter; 12) aspirator to pump air through the system. The arrows indicate the flow direction of the hot air (and the sprayed product) . . . . .	23
1.10	a) Schematic to show the miscibility of small molecules A and B, and b) a graph showing how the free energy of mixing ( $F_{mix}$ ) of the system changes with composition ( $\Phi$ ) and dependent on the $\chi$ parameter of the system. Plots represent systems with $\chi$ parameters of -1 (dark blue), 0.5 (purple), 1 (red), 2 (light blue), 3 (green) and 4 (black). . . . .	29
1.11	a) Schematic to show the miscibility of a polymer, A, with a small molecule drug, B, whereby the polymer has a chain length of N monomers. b) a graph showing how the free energy of mixing ( $F_{mix}$ ) of the system changes with composition ( $\Phi$ ) and dependent on the $\chi$ parameter of the system, when $N = \infty$ . Plots represent systems with $\chi$ parameters of -1 (dark blue), 0.5 (purple), 1 (red), 2 (light blue), 3 (green) and 4 (black). . . . .	29

2.1	Molecular structures of copovidone (a) and the chemically similar polymer, pvp (b). . . . .	36
2.2	Diagram showing Bragg reflection from a set of crystal planes with a spacing $d$ (adapted from [5]). . . . .	38
2.3	Schematic showing the nearest neighbour coordination observed using pair distribution functions (adapted from [6]). . . . .	41
2.4	A schematic of a Differential Scanning Calorimeter (DSC). Numbered labels indicate: 1) furnace; 2) sample pan; 3) reference pan; 4) heat flux plate; 5) heating stage thermocouples; 6) purge gas inlet; 7) purge gas vent; 8) temperature and heat flow data is sent to a computer for recording. . . . .	43
2.5	Schematic showing how the glass transition temperature $T_g$ , melting point $T_m$ , and recrystallisation temperature $T_c$ are shown in a thermogram produced by DSC. In this example, exothermic peaks point upwards. . . . .	44
2.6	A schematic of a Scanning Electron Microscope (SEM). . . . .	47
2.7	Schematic of an AFM instrument. Numbered labels indicate: 1) piezoscanner; 2) sample; 3) cantilever; 4) tip; 5) laser; 6) position sensitive detector; and 7) feedback of signal from photodiode to piezoscanner and cantilever. . . . .	48
3.1	Molecular structures of a) felodipine and b) copovidone. . . . .	52
3.2	Molecular structure of felodipine (centre) surrounded with the molecular structures of the target analogues. Clockwise from top: aromatised analogue, 2 oxidation byproducts, diethyl ester, des-chloro diethyl ester, and nitrile ester. . . . .	55
3.3	General reaction scheme for the Hantzsch Dihydropyridine Synthesis. . . . .	56
3.4	Scheme to show the regeneration of the cerium(IV) reagent by reoxidisation by the bromate ion. . . . .	57
3.5	Reaction scheme for ZAL_001 . . . . .	60

3.6	Reaction scheme for ZAL_005 . . . . .	61
3.7	Reaction scheme for ZAL_006 . . . . .	62
3.8	Reaction scheme for ZAL_007 . . . . .	63
3.9	Reaction scheme for ZAL_008 . . . . .	65
3.10	Reaction scheme for ZAL_009 . . . . .	66
3.11	Reaction scheme for ZAL_010 . . . . .	67
3.12	Reaction scheme for ZAL_011 . . . . .	68
3.13	Potential targets in future syntheses of additional felodipine analogues, including a) analogues with modified ester chain length, b) analogues with alkyl chains of varying lengths instead of esters, and c) analogues with amide substituents. . . . .	76
3.14	Potential targets in future syntheses of additional felodipine analogues in which the phenyl ring substituents have been changed or placed at different ring positions. . . . .	77
4.1	X-ray powder diffractograms of the film-cast felodipine/copovidone solid dispersions with drug loadings of 5% (pink), 10% (blue), 20% (green), 30% (grey), 40% (purple) and 50% (light blue). Diffractograms of crys- talline felodipine (red) and copovidone (black) are also shown for com- parison. . . . .	87
4.2	$T_g$ of amorphous felodipine as a function of weight fraction drug. The solid line represents the fit to the Gordon-Taylor equation and the dashed line represents the fit to the Couchman-Karasz equation. . . . .	87
4.3	Comparison of the simulated traces of felodipine/copovidone amorphous physical mixes with the observed traces of the film-cast solid dispersions at drug loadings of a) 15%, b) 30% and c) 50%. . . . .	89

4.4	Images obtained by optical microscopy of spray dried solid dispersions with drug loadings of a) 5%, b) 15%, c) 30% and d) 50%. Scale bars for images a) and d) represent 20 $\mu\text{m}$ and for images b) and c) represent 50 $\mu\text{m}$ . . . . .	91
4.5	SEM images of the spray dried material containing 5% felodipine taken at a) $\times 100$ , b) $\times 1000$ , c) $\times 5000$ and d) $\times 10000$ magnifications. . . . .	92
4.6	SEM images of the spray dried material containing 15% felodipine taken at a) $\times 100$ , b) $\times 1000$ , c) $\times 5000$ and d) $\times 10000$ magnifications. Circled in image b) is a fragmented hollow particle. . . . .	93
4.7	SEM images of the spray dried material containing 30% felodipine taken at a) $\times 100$ , b) $\times 1000$ , c) $\times 5000$ and d) $\times 10000$ magnifications. Circled in image b) is a fragmented hollow particle. . . . .	94
4.8	SEM images of the spray dried material containing 50% felodipine taken at a) $\times 100$ , b) $\times 1000$ , c) $\times 5000$ and d) $\times 10000$ magnifications. Circled in image b) is a fragmented hollow particle. . . . .	95
4.9	X-ray powder diffractograms of the spray dried felodipine/copovidone solid dispersions with drug loadings of 5% (pink), 15% (green), 30% (grey) and 50% (light blue). Diffractograms of crystalline felodipine (red) and copovidone (black) are also shown for comparison. . . . .	97
4.10	X-ray powder diffractograms of the compacted spray dried felodipine/copovidone solid dispersions with drug loadings of 5% (pink), 15% (green), 30% (grey) and 50% (light blue). Diffractograms of crystalline felodipine (red) and copovidone (black) are also shown for comparison. . . . .	97
4.11	Comparison of the simulated traces of felodipine and copovidone amorphous physical mixes with the observed traces of the spray dried solid dispersions at drug loadings of a) 5%, b) 15%, c) 30% and d) 50%. . . . .	98

4.12	X-ray powder diffractograms of samples of crystalline ZAL_005 (red), amorphous ZAL_005 (dark blue), and solid dispersions of ZAL_005 and copovidone with drug loadings of 15% (green), 30% (grey) and 50% (light blue). Copovidone is also shown for reference (black). . . . .	100
4.13	$T_g$ of amorphous ZAL_005 as a function of weight fraction drug. The solid line represents the fit to the Gordon-Taylor equation and the dashed line represents the fit to the Couchman-Karas equation. . . . .	100
4.14	Comparison of the PDF traces generated for each of the amorphous felodipine analogues . . . . .	101
4.15	Comparison of the simulated traces of ZAL_005 and copovidone amorphous physical mixes with the observed traces of the solid dispersion at drug loadings of a) 15%, b) 30% and c) 50%. . . . .	101
4.16	X-ray powder diffractograms of samples of crystalline ZAL_006 (red), amorphous ZAL_006 (dark blue), and solid dispersions of ZAL_006 and copovidone with drug loadings of 15% (green), 30% (grey) and 50% (light blue). Copovidone is also shown for reference (black). . . . .	103
4.17	$T_g$ of amorphous ZAL_006 as a function of weight fraction drug. The solid line represents the fit to the Gordon-Taylor equation and the dashed line represents the fit to the Couchman-Karas equation. . . . .	103
4.18	Comparison of the simulated traces of ZAL_006 and copovidone amorphous physical mixes with the observed traces of the solid dispersion at drug loadings of a) 15%, b) 30% and c) 50%. . . . .	104
4.19	X-ray powder diffractograms of samples of crystalline ZAL_007 (red), amorphous ZAL_007 (dark blue), and solid dispersions of ZAL_007 and copovidone with drug loadings of 15% (green), 30% (grey) and 50% (light blue). Copovidone is also shown for reference (black). . . . .	106

4.20	Comparison of the simulated traces of ZAL_007 and copovidone phase separated solid dispersion with the observed traces of the solid dispersion at drug loadings of a) 15%, b) 30% and c) 50%. . . . .	107
4.21	$T_g$ of amorphous ZAL_007 as a function of weight fraction drug. The solid line represents the fit to the Gordon-Taylor equation and the dashed line represents the fit to the Couchman-Karas equation. . . . .	108
4.22	X-ray powder diffractograms of samples of crystalline ZAL_009 (red), amorphous ZAL_009 (dark blue), and solid dispersions of ZAL_009 and copovidone with drug loadings of 15% (green), 30% (grey) and 50% (light blue). Copovidone is also shown for reference (black). . . . .	111
4.23	$T_g$ of amorphous ZAL_009 as a function of weight fraction drug. The solid line represents the fit to the Gordon-Taylor equation and the dashed line represents the fit to the Couchman-Karas equation. . . . .	111
4.24	$T_g$ of amorphous ZAL_010 as a function of weight fraction drug. The solid line represents the fit to the Gordon-Taylor equation and the dashed line represents the fit to the Couchman-Karas equation. . . . .	114
4.25	X-ray powder diffractograms of samples of crystalline ZAL_010 (red), ZAL_010 subjected to amorphisation (dark blue), and solid dispersions of ZAL_010 and copovidone with drug loadings of 15% (green), 30% (grey) and 50% (light blue). Copovidone is also shown for reference (black). . . . .	114
4.26	X-ray powder diffractograms of samples of crystalline ZAL_011 (red), amorphous ZAL_011 (dark blue), and solid dispersions of ZAL_011 and copovidone with drug loadings of 15% (green), 30% (grey) and 50% (light blue). Copovidone is also shown for reference (black). . . . .	116
4.27	$T_g$ of amorphous ZAL_011 as a function of weight fraction drug. The solid line represents the fit to the Gordon-Taylor equation and the dashed line represents the fit to the Couchman-Karas equation. . . . .	116

4.28	Comparison of the simulated traces of ZAL_011 and copovidone amorphous physical mixes with the observed traces of the solid dispersion at drug loadings of a) 15%, b) 30% and c) 50%. . . . .	117
5.1	Schematic showing a cross-section of the temperature controlled sample cell used in the laser light scattering experiments. . . . .	125
5.2	Photograph showing the experimental setup for the laser light scattering studies. The path of the laser beam is shown in red. . . . .	126
5.3	Graph showing changes in transmission coefficient after water is injected into the sample cell for solid dispersions containing 50% felodipine at four temperatures. . . . .	127
5.4	Semi-log plot of the light scattering data, showing how characteristic nucleation times ( $\tau_N$ ) and growth times ( $\tau_G$ ) can be determined for each sample. . . . .	128
5.5	Arrhenius plots of $\ln(1/\tau_N)$ against $1/T$ for film cast solid dispersions with drug loadings of 50% (blue), 40% (black), 30% (green) and 20% (red). . . . .	129
5.6	Arrhenius plots of $\ln(1/\tau_G)$ against $1/T$ for film cast solid dispersions with drug loadings of 50% (blue), 40% (black), 30% (green) and 20% (red). . . . .	130
5.7	Brightfield optical microscopy images of a 10% felodipine-loaded film prior to water exposure (a), during water exposure (b & c) and after removal of the water droplet (d). All images were taken at $\times 5$ magnification and scale bars represent $500\ \mu\text{m}$ . . . . .	133



5.8	Topographies of Felodipine/Copovidone films as imaged using AFM prior to and after exposure to water. Phase data is shown overlaid on the topographies, with shadings as indicated by the individual scale bars. Images on the left are samples pre-water exposure and images on the right are of samples after exposure to water. Images are of samples with 0% (top images), 10% (middle images) and 50% (bottom images) felodipine-loadings. . . . .	134
5.9	Graphs showing the topography of 10% felodipine loaded films a) pre- and b) post-water exposure along a cross-section of the samples, as determined by AFM. . . . .	134
5.10	A schematic to show the layout of samples in well plates for crystallisation studies. Each well plate was prepared in triplicate to enable storage in three different stability testing rooms. . . . .	140
5.11	Example grid of images obtained from crystallisation experiments. This example shows the images obtained for solid dispersions of ZAL_011 with ranging drug loadings stored at 25°C/60% Relative Humidity over 7 weeks. . . . .	142
5.12	Images showing how entropy of crystallisation is lower for chlorine substituted analogues (a) compared with analogues without chlorine substituents (b) due to the restriction for only $\pi$ face-to-face stacking, compared with the additional possibility of $\pi$ edge-to-face interactions when there are no chlorine substituents. . . . .	146
6.1	Schematic of a single $\mu$ Diss vessel. . . . .	159
6.2	Schematic of the USP IV-style flow cell used in the MRI experiments. . . . .	161
6.3	Schematic of the MRI flow-cell system with in-line UV monitoring. . . . .	162
6.4	Diagram showing the monolithic compact and an example cross-sectional image obtained by MRI. . . . .	162

6.5	Dissolution profiles from micro-dissolution experiments of crystalline felodipine (black plot), amorphous felodipine (grey plot) and physical mixtures of crystalline felodipine with copovidone at drug loadings of 50% (red plot), 30% (pink plot), 15% (green plot) and 5% (blue plot). Mean data is plotted (n=2).	165
6.6	Dissolution profiles from micro-dissolution experiments of spray-dried solid dispersions of felodipine with copovidone at drug loadings of 50% (red plot), 30% (pink plot), 15% (green plot) and 5% (blue plot). In-set shows the first 5 minutes of the experiment in detail. Mean data is plotted (n=2).	166
6.7	Dissolution profiles from micro-dissolution experiments of film-cast solid dispersions of felodipine with copovidone at drug loadings of 50% (blue), 30% (grey), 15% (green) and 5% (pink). Mean data is plotted (n=2).	167
6.8	The initial dissolution rate of the film-cast dried solid dispersion samples as determined from micro-dissolution experiments plotted against drug loading. Mean data is plotted (n=2) and error bars represent the std error.	167
6.9	The maximum solution concentration of the film-cast solid dispersion samples as determined from micro-dissolution experiments plotted against drug loading. Mean data is plotted (n=2) and error bars represent the std error.	168
6.10	The maximum solution concentration of the film-cast solid dispersions plotted against the initial dissolution rate. Mean data measured from micro-dissolution experiments is plotted (n=2) and error bars represent the std error.	168

6.11	Dissolution profiles for spray-dried solid dispersions of felodipine with copovidone at drug loadings of 50% (red plot), 15% (green plot) and 5% (blue plot), as recorded by UV spectrophotometry in MRI experiments. 30% drug loaded sample not shown as the concentration levels were below the detection level of the UV spectrophotometer. . . . .	169
6.12	Example MR images of the 5% (top row) and 50% (bottom row) drug-loaded compacts at a range of time points. . . . .	172
6.13	Graphs to show the changes in the dimensions of the compacts in the MRI experiments with time. . . . .	173
6.14	X-ray powder diffractograms of the compacted spray dried felodipine/copovidone solid dispersions recovered from the MRI flow-cell experiments. The samples with drug loadings of 30% (grey) and 50% (light blue) are shown. Diffractograms of crystalline felodipine (red) and copovidone (black) are also shown for comparison. . . . .	173
6.15	A plot of the aqueous solubility of felodipine in the presence of copovidone ( $S_t$ ) against the concentration of the ligand copovidone ( $L_t$ ). The linear fit from this graph can be used to determine the binding constant ( $K_{11}$ ) for felodipine and copovidone. . . . .	175
6.16	Mean dissolution profiles of samples of ZAL_001 and the corresponding physical mixture and solid dispersion samples (n=2). Profiles for the pure (unprocessed) drug (black), film-cast drug (red) and film-cast drug in media containing 2% w/v copovidone (purple) are shown alongside profiles for physical mixture samples loaded with 15% (light blue) and 50% drug (light green), as well as film-cast solid dispersion samples with drug-loadings of 15% (dark blue), 30% (grey) and 50% (dark green). .	177

6.17	Plots of maximum solution concentration against initial dissolution rate for felodipine analogues ZAL_001 (black), ZAL_005 (red), ZAL_006 (green), ZAL_007 (blue) and ZAL_011 (grey). Mean data (n=2) is plotted and error bars represent the standard error. . . . .	179
6.18	Mean dissolution profiles of samples of ZAL_005 and the corresponding physical mixture and solid dispersion samples (n=2). Profiles for the crystalline drug (black), amorphous drug (red) and amorphous drug in media containing 2% w/v copovidone (purple) are shown alongside profiles for physical mixture samples loaded with 15% (light blue) and 50% drug (light green), as well as film-cast solid dispersion samples with drug-loadings of 15% (dark blue), 30% (grey) and 50% (dark green). The inset shows a zoomed-in area of the graph. . . . .	180
6.19	Mean dissolution profiles of samples of ZAL_006 and the corresponding physical mixture and solid dispersion samples. Profiles for the crystalline drug (black), amorphous drug (red) and amorphous drug in media containing 2% w/v copovidone (purple) are shown alongside profiles for a physical mixture sample loaded with 15% drug (light blue), as well as film-cast solid dispersion samples with drug-loadings of 15% (dark blue), 30% (grey) and 50% (dark green). The inset shows a zoomed-in area of the graph. . . . .	181
6.20	Mean dissolution profiles of samples of ZAL_007 and the corresponding physical mixture and solid dispersion samples. Profiles for the crystalline drug (black), amorphous drug (red) and amorphous drug in media containing 2% w/v copovidone (purple) are shown alongside profiles for physical mixture samples loaded with 15% (light blue) and 50% drug (light green), as well as film-cast solid dispersion samples with drug-loadings of 15% (dark blue), 30% (grey) and 50% (dark green). The inset shows a zoomed-in area of the graph. . . . .	182

6.21	Mean dissolution profiles of samples of ZAL_011 and the corresponding physical mixture and solid dispersion samples. Profiles for the crystalline drug (black), amorphous drug (red) and amorphous drug in media containing 2% w/v copovidone (purple) are shown alongside profiles for physical mixture samples loaded with 15% (light blue) and 50% drug (light green), as well as film-cast solid dispersion samples with drug-loadings of 15% (dark blue), 30% (grey) and 50% (dark green). The inset shows a zoomed-in area of the graph. . . . .	183
7.1	Example grid of images obtained from crystallisation experiments. This example shows the images obtained for solid dispersions of ZAL_011 with ranging drug loadings stored at 25°C/60% RH over 7 weeks. . . . .	189
7.2	A schematic to demonstrate the system used to score the performance of compounds in the crystallisation study carried out in Chapter 5. The 10x8 image grids are scored along diagonals such that the number of images containing crystals along each diagonal is counted, and this number is multiplied by the weighted ranking assigned to that diagonal. . . . .	190
7.3	Plots of AUC <sub>60</sub> against % drug Loading for each felodipine analogue analysed by micro-dissolution. Mean values are plotted (n=2) and error bars represent the standard error. The area under each of these plots ( <i>Z</i> ) is used to score the dissolution preformance of each analogue. . . .	194
7.4	Scores determined from micro dissolution data plotted against scores determined from the crystallisation screening experiments. The linear trendline is shown with its equation and <i>R</i> <sup>2</sup> value, indicating that it is a poor fit. . . . .	196
7.5	Graphs in which the scores obtained from the crystallisation screen are plotted against a) molecular weight (MW), b) amorphous solubility, c) Entropy of Sublimation, d) Polarizability and e) log P. For each plot, the trendline is shown with its equation and <i>R</i> <sup>2</sup> value. . . . .	198

7.6	Copy of the plot of crystallisation screen score vs. molecular weight, with overlays to show regions where different molecular structures dominate. Red circles highlight phenyl substituents, blue circles highlight DHP substituents. . . . .	200
7.7	Graph in which the scores obtained from the crystallisation screen are plotted against $T_m$ . . . . .	202
A.1	Grid of images obtained from crystallisation experiments. This grid contains images obtained for solid dispersions of felodipine with ranging drug loadings stored at 25°C/60% Relative Humidity over 7 weeks. . . . .	209
A.2	Grid of images obtained from crystallisation experiments. This grid contains images obtained for solid dispersions of felodipine with ranging drug loadings stored at 40°C/75% Relative Humidity over 7 weeks. . . . .	210
A.3	Grid of images obtained from crystallisation experiments. This grid contains images obtained for solid dispersions of felodipine with ranging drug loadings stored at 40°C/0% Relative Humidity over 7 weeks. . . . .	210
A.4	Grid of images obtained from crystallisation experiments. This grid contains images obtained for solid dispersions of ZAL_001 with ranging drug loadings stored at 25°C/60% Relative Humidity over 7 weeks. . . . .	211
A.5	Grid of images obtained from crystallisation experiments. This grid contains images obtained for solid dispersions of ZAL_001 with ranging drug loadings stored at 40°C/75% Relative Humidity over 7 weeks. . . . .	211
A.6	Grid of images obtained from crystallisation experiments. This grid contains images obtained for solid dispersions of ZAL_001 with ranging drug loadings stored at 40°C/0% Relative Humidity over 7 weeks. . . . .	212
A.7	Grid of images obtained from crystallisation experiments. This grid contains images obtained for solid dispersions of ZAL_005 with ranging drug loadings stored at 25°C/60% Relative Humidity over 7 weeks. . . . .	212

A.8	Grid of images obtained from crystallisation experiments. This grid contains images obtained for solid dispersions of ZAL_005 with ranging drug loadings stored at 40°C/75% Relative Humidity over 7 weeks. . . . .	213
A.9	Grid of images obtained from crystallisation experiments. This grid contains images obtained for solid dispersions of ZAL_005 with ranging drug loadings stored at 40°C/0% Relative Humidity over 7 weeks. . . . .	213
A.10	Grid of images obtained from crystallisation experiments. This grid contains images obtained for solid dispersions of ZAL_006 with ranging drug loadings stored at 25°C/60% Relative Humidity over 7 weeks. . . . .	214
A.11	Grid of images obtained from crystallisation experiments. This grid contains images obtained for solid dispersions of ZAL_006 with ranging drug loadings stored at 40°C/75% Relative Humidity over 7 weeks. . . . .	214
A.12	Grid of images obtained from crystallisation experiments. This grid contains images obtained for solid dispersions of ZAL_006 with ranging drug loadings stored at 40°C/0% Relative Humidity over 7 weeks. . . . .	215
A.13	Grid of images obtained from crystallisation experiments. This grid contains images obtained for solid dispersions of ZAL_007 with ranging drug loadings stored at 25°C/60% Relative Humidity over 7 weeks. . . . .	216
A.14	Grid of images obtained from crystallisation experiments. This grid contains images obtained for solid dispersions of ZAL_007 with ranging drug loadings stored at 40°C/75% Relative Humidity over 7 weeks. . . . .	216
A.15	Grid of images obtained from crystallisation experiments. This grid contains images obtained for solid dispersions of ZAL_007 with ranging drug loadings stored at 40°C/0% Relative Humidity over 7 weeks. . . . .	217
A.16	Grid of images obtained from crystallisation experiments. This grid contains images obtained for solid dispersions of ZAL_009 with ranging drug loadings stored at 25°C/60% Relative Humidity over 7 weeks. . . . .	217

A.17	Grid of images obtained from crystallisation experiments. This grid contains images obtained for solid dispersions of ZAL_009 with ranging drug loadings stored at 40°C/75% Relative Humidity over 7 weeks. . . . .	218
A.18	Grid of images obtained from crystallisation experiments. This grid contains images obtained for solid dispersions of ZAL_009 with ranging drug loadings stored at 40°C/0% Relative Humidity over 7 weeks. . . . .	218
A.19	Grid of images obtained from crystallisation experiments. This grid contains images obtained for solid dispersions of ZAL_010 with ranging drug loadings stored at 25°C/60% Relative Humidity over 7 weeks. . . . .	219
A.20	Grid of images obtained from crystallisation experiments. This grid contains images obtained for solid dispersions of ZAL_010 with ranging drug loadings stored at 40°C/75% Relative Humidity over 7 weeks. . . . .	219
A.21	Grid of images obtained from crystallisation experiments. This grid contains images obtained for solid dispersions of ZAL_010 with ranging drug loadings stored at 40°C/0% Relative Humidity over 7 weeks. . . . .	220
A.22	Grid of images obtained from crystallisation experiments. This grid contains images obtained for solid dispersions of ZAL_011 with ranging drug loadings stored at 25°C/60% Relative Humidity over 7 weeks. . . . .	220
A.23	Grid of images obtained from crystallisation experiments. This grid contains images obtained for solid dispersions of ZAL_011 with ranging drug loadings stored at 40°C/75% Relative Humidity over 7 weeks. . . . .	221
A.24	Grid of images obtained from crystallisation experiments. This grid contains images obtained for solid dispersions of ZAL_011 with ranging drug loadings stored at 40°C/0% Relative Humidity over 7 weeks. . . . .	221



# Acknowledgments

First and foremost, I would like to thank my academic supervisors Prof. Peter Fischer and Dr. James Sharp for their invaluable help and support over the last four years. I would also like to express my gratitude to my industrial supervisor Dr. Jonathan Booth, whose enthusiasm always provided encouragement, even when things weren't quite going to plan. For funding, I would like to thank AstraZeneca and the EPSRC.

I wish to also express my thanks the following people for their help with specific aspects of my work: Gopal Jadhav for reacquainting me with the practicalities of organic synthesis; Lee Hibbet for NMR and MS access and training; Helen Blade for her assistance in generating PDF data; Les Hughes, Stephen Wren and Gavin Reynolds for their guidance and input with the MRI-dissolution experiments; Ghorkhn Sharma-Singh and Trevor Harris for micro-dissolution access and training; and Caroline Rodger for FTIR access and training.

Over the last four years I have shared labs and office space with too many people to mention here individually. However, I would like to thank all those colleagues who have provided entertaining tea-break conversations, engaged in lively office debates, and aided in lab-based problem-solving sessions. This includes all those with whom I had the pleasure of working with at AstraZeneca (particularly the residents of LG11)- your kindness has meant that my time at Macclesfield felt like a home away from home.

To special friends Cat and Matt for some bringing the good times from Macclesfield to Nottingham, Natasha for our shared writing experience (we finally did it!) and Nicola for your valued, lifelong friendship, I thank you all.

I would like to express my gratitude to my brother Simon, whose globetrotting ways have been inspirational, and are a constant reminder that anything can be achieved. My deepest and most heartfelt thanks go to my Mum and Dad, to whom I am indebted for providing their continual support and encouragement throughout my life, and especially during the last four years. Finally, I would like to say a huge thank-you my boyfriend Simon, whose understanding, kindness and above all friendship have meant so much to me since I have been lucky enough to know you.

# Declarations

I hereby declare that the work contained herein is, unless expressly acknowledged, my own work, with guidance from my supervisors Prof. Peter Fischer, Dr. James Sharp and Dr. Jonathan Booth. Whilst the PDF experimental work in Chapter 4 was carried out by myself, the data analysis was kindly carried out by Helen Blade. The dissolution experiments carried out on spray dried felodipine samples detailed in Chapter 6 were carried out in collaboration with Gavin Reynolds, Stephen Wren and Les Hughes, who also carried out the MRI-flowcell dissolution experiments. Generation of all graphs and figures was carried out solely by the author.

# Abstract

In recent years the pharmaceutical industry has seen a rise in the number of drug compounds with low aqueous solubility, and consequently poor oral bioavailability. One potential solution to this problem is to formulate such compounds as solid dispersions, whereby the drug is dispersed in a carrier matrix in the solid state.

In this thesis, the hypothesis that a number of drug-drug and drug-polymer intermolecular interactions influence the physical stability and dissolution performance of solid dispersions is considered. The aim is to use correlations between drug molecular structure and solid dispersion performance to develop a platform to rapidly assess whether drug compounds will have favourable properties when formulated as a solid dispersion.

Amorphous felodipine/copovidone solid dispersions are used as a model system to develop a suitable testing regime with regards to physical stability and dissolution performance. A laser light scattering technique developed in this work shows that morphological changes in felodipine/copovidone films exposed to water are due to polymer swelling. A combination of dissolution testing methodologies is also used to suggest a mechanism for the dissolution of bulk solid dispersion samples.

Contributions of individual functional groups in the felodipine analogues to the physical stability and dissolution performance of their amorphous solid dispersions are assessed. Blocking of the felodipine amine hydrogen-bond-donor with an N-methyl, and the removal of chlorine substituents are both shown to reduce the physical stability of the solid dispersions.

Correlations between molecular descriptors and data from the above experiments show that drug compounds are more likely to crystallise from solid dispersions with copovidone if they have a low log P, low relative molecular mass and low polarizability. Such correlations can form the basis of a screening method for the molecular design of analogous drug compounds likely to form high-performance solid dispersions with copovidone.

# Abbreviations

IUPAC notation is used for chemical compounds.

The standard symbols for SI units and their scaling prefixes are used throughout this thesis, except where stated otherwise, in which case the abbreviations are defined below.

AFM Atomic Force Microscopy

API Active Pharmaceutical Ingredient

AUC Area Under the Curve

BCS Biopharmaceutics Classification System

CAN Ceric Ammonium Nitrate

d doublet

DHP Dihydropyridine

DSC Differential Scanning Calorimetry

DVS Dynamic Vapour Sorption

FasSIF Fasted-State Simulated Intestinal Fluid

FDA United States Food and Drug Administration

Fel Felodipine

FT-IR Fourier Transform Infrared Spectroscopy

HLB Hydrophile Lipophile Balance

HPLC High Performance Liquid Chromatography

HPMC Hydroxypropylmethylcellulose

HPMCAS Hydroxypropylmethylcellulose Acetate Succinate

log P Octanol/Water Partition Coefficient

m multiplet

MRI Magnetic Resonance Imaging

MS Mass Spectrometry

MW Molecular Weight

NMR Nuclear Magnetic Resonance

PDF Pairwise Distribution Function

PEG Polyethylene Glycol

PLM Polarised Light Microscopy

PVP Poly(vinylpyrrolidone)

PVP-CL Cross-Linked Poly(vinylpyrrolidone), Crospovidone

PVP/VA Poly(vinylpyrrolidone vinyl acetate) copolymer, Copovidone

q quartet

$R_f$  Retention Factor

RH Relative Humidity

s singlet

SEDDS Self-Emulsifying Drug Delivery System

SEM Scanning Electron Microscopy

SMEDDS Self-Microemulsifying Drug Delivery System

t triplet

$T_g$  Glass Transition Temperature

$T_m$  Melting Point

TFA Tetrafluoroacetic Acid

TLC Thin Layer Chromatography

USP United States Pharmacopoeia

UV/Vis Ultraviolet/Visible Spectroscopy

WHO World Health Organisation

XRPD X-ray Powder Diffraction

# Summary of Analogues

Below is a summary of the chemical structures of the molecular analogues synthesised in chapter 3 and used in experiments detailed in the following chapters.

Compound Name	Compound Structure	IUPAC Compound Name
Felodipine		3-ethyl 5-methyl 4-(2,3-dichlorophenyl)-1,4-dihydro-2,6-dimethylpyridine-3,5-dicarboxylate
ZAL_001		O3-ethyl O5-methyl 4-(2,3-dichlorophenyl)-2,6-dimethyl-pyridine-3,5-dicarboxylate
ZAL_005		diethyl 2,6-dimethyl-4-phenyl-1,4-dihydropyridine-3,5-dicarboxylate
ZAL_006		ethyl 5-cyano-4-(2,3-dichlorophenyl)-2,6-dimethyl-1,4-dihydropyridine-3-carboxylate
ZAL_007		diethyl 4-(2,3-dichlorophenyl)-2,6-dimethyl-1,4-dihydropyridine-3,5-dicarboxylate
ZAL_008		4-(2,3-dichlorophenyl)-2,6-dimethyl-1,4-dihydropyridine-3,5-dicarbonitrile
ZAL_009		ethyl 5-cyano-2,6-dimethyl-4-phenyl-1,4-dihydropyridine-3-carboxylate
ZAL_010		2,6-dimethyl-4-phenyl-1,4-dihydropyridine-3,5-dicarbonitrile
ZAL_011		diethyl 4-(2,3-dichlorophenyl)-1,2,6-trimethyl-4H-pyridine-3,5-dicarboxylate

# Chapter 1

## Introduction

### 1.1 The Problem of Poorly Soluble Drugs

The majority of drugs on the market are designed for administration via the oral route, as this is the most convenient method of drug delivery. Typically, compounds delivered via this route will be absorbed into the systemic circulation by transport across the epithelial cells of the small intestine [7]. However, in order for permeation of the drug across the epithelial membrane to occur, the compound must first be presented to the absorbing surface in solution. As the fluids in the body, and more specifically the gastrointestinal tract are aqueous, this goes some way to explaining why the solubility of drug compounds in water is such an important issue in drug development.

In order to better predict the intestinal absorption of drug compounds, the Biopharmaceutics Classification System (BCS) was implemented by the U.S. Food and Drug Administration (FDA) [8]. In this framework, drugs are categorised according to their intestinal permeability, aqueous solubility, and aqueous dissolution [9]. The class boundaries for this classification system are defined as follows:

1. A drug is classed as poorly soluble if the highest dose strength of the immediate release product is not soluble in 250 mL or less aqueous media over the pH range of 1 to 7.5.



2. A drug is classed as having low intestinal permeability when the extent of absorption in humans is less than 90% of the administered dose based on a mass-balance determination or in comparison to an intravenous dose.
3. A drug is classed as rapidly dissolving if  $\geq 85\%$  of the immediate release dose dissolves within 30 minutes using either USP dissolution apparatus I at 100 rpm or USP dissolution apparatus II at 50 rpm in  $\leq 900$  mL of:  
0.1 N HCl or simulated gastric fluid or pH 4.5 buffer  
**and** pH 6.8 buffer or simulated intestinal fluid.

Drugs which have good solubility and permeability within this framework fall into Class I: those with poor solubility, but good permeability are Class II: Class III compounds are those that have good solubility but poor permeability: and drugs that are both poorly soluble and have low permeability are classified as BCS IV (see Figure 1.1). The GI absorption *in-vivo* of a drug depends on its solubility, as the compound cannot pass through the intestinal membrane if it is not first presented to that membrane as individual molecules [10]. Therefore, if a drug has poor oral bioavailability, methods to improve its solubility are often considered first in an attempt to move compounds from BCS classes II and IV into BCS classes I and III, respectively .

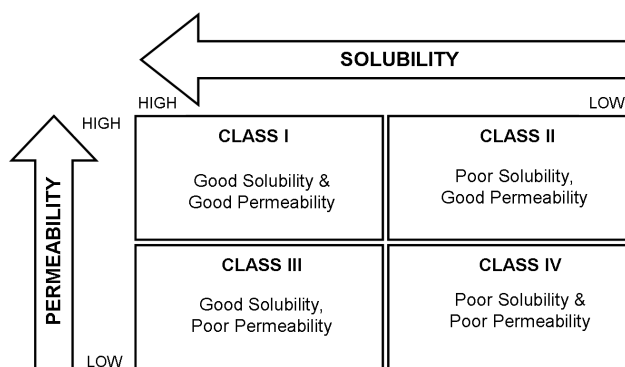


Figure 1.1: The Biopharmaceutics Classification System.

In a 2006 study of the top 200 oral drug products in the United States, Great Britain, Spain and Japan, 30-40% were found to be practically insoluble, and 45% were

shown to be BCS class II or IV, or unclassified [11]. The same study also suggested that 27% more practically insoluble compounds appearing on lists from the above countries, compared to a list from the World Health Organisation (WHO) indicates a trend towards the discovery and development of potent highly lipophilic compounds in developed countries. It has also been shown that whilst most drug compounds under scrutiny in the 1970s and 80s due to bioavailability concerns had aqueous solubility ranging from 20 mg/mL to 100 mg/mL, it is far more common these days to encounter compounds exhibiting intrinsic solubilities lower than 1 mg/mL [12].

## **1.2 Methods of Improving Drug Bioavailability**

As a result of the rise in the number of poorly soluble compounds being identified for pharmaceutical development, the industry has a strong desire to develop strategies to address this problem. A company that is successful in developing such strategies could potentially reduce the rate of attrition of drug candidates, better target research efforts and spending leading to a net reduction in costs, and ultimately produce more effective products [13].

There are a number of strategies to improve drug bioavailability that are currently in use or under consideration, as summarised below.

### **1.2.1 Pro-drugs**

The pro-drug approach is one in which an inactive substance on administration to the patient is metabolised *in-vivo* to produce the active drug compound. By functionalising the API with hydrophilic moieties, this strategy can be used to boost the solubility and absorption of drug compounds. For example, coupling phosphate ester groups to a drug compound has been shown to improve solubility of poorly water-soluble parent drug molecules [14]. This approach to improving drug bioavailability has been in use over many years, and this is evident from the number of commercially available products [15]. Whilst the pro-drug approach is clearly a tried-and-tested method, there are two

main requirements that must be fulfilled in order for this approach to work. Firstly, the compound in question should have suitable functional group(s) to make a pro-drug. Secondly, it is necessary for the body to have the required enzyme or other mechanistic pathway present to enable the compound to be rendered to its active form after administration [16]. If one or both of these requirements can not be met, then formulation of a pro-drug is not a viable option. Two additional drawbacks of this approach are a more complex biopharmaceutical profile, and in some cases, poor stability as a result of the chemistry of the pro-drug [14].

### **1.2.2 Salts**

It was demonstrated by Nelson et al in the 1950s that salt formation can lead to improvements in the dissolution of solid oral dosage forms compared to the free acid or base under the pH conditions of the gastrointestinal tract [17, 18]. This improvement was due to the higher solubility of the free drug in the pH microclimate generated in the aqueous diffusion layer surrounding the solid by the counterion. Since the time of this study, salt formation has been of significant interest to the pharmaceutical industry as a method for improving drug dissolution and solubility, and has become the most commonly used technique to achieve this because it is often the most cost-effective approach [19].

Despite the apparent simplicity of this approach to improve the dissolution rate and solubility of a drug compound, there are limitations. The main consideration is that in order to form a salt, the drug compound must have a group that is ionizable. Furthermore, in order for a stable salt to be formed, it is important that a single ionisation state is formed, and therefore, it is generally recommended that the ionizable group on the drug compound and the salt counter-ion have a difference in pKa values of at least three units in order to prevent dissociation [20]. Because there are a number of cases in which these two requirements cannot be fulfilled (eg. for neutral or very weakly acidic or basic compounds), it can be seen that the technique of salt formation cannot be used

as a panacea for formulating poorly soluble compounds. Also, even if formation of a salt is possible for a drug, it may not deliver the required performance enhancement. For example, during aqueous dissolution there may be rapid conversion to the free form, which can manifest as gelling.

### **1.2.3 Co-crystals**

When the active pharmaceutical ingredient (API) does not have any suitable ionizable groups for salt selection to be a viable option for improving drug solubility, it may be possible to form co-crystals. The definition of a co-crystal is still a subject of debate in the literature [21, 22, 23, 24], but in general they are crystals which contain more than one molecular moiety in the crystal lattice. According to some definitions, the term co-crystal encompasses salts, however, the molecular components of a co-crystal are not necessarily ionically bonded together (there is no proton transfer), but instead may interact in the crystal lattice largely through hydrogen bonds and other non-covalent interactions such as  $\pi$ - $\pi$  stacking [21, 23].

Whilst co-crystallisation appears to present the opportunity for a salt-like formulation of neutral and weakly acidic or basic compounds, it is clear from the lack of any co-crystallised drugs on the market [24] that this approach has some drawbacks. One difficulty in producing co-crystals of an API lies in the unpredictability of whether the drug compound and a co-crystal former will successfully crystallise together, even when the compounds have compatible functional groups for the intermolecular interactions required [21]. A further key issue, is that in many cases co-crystals do not offer the required solubility or dissolution advantage [24].

### **1.2.4 Modification of the Crystal Form**

It is widely known that many drug compounds can exist in several different solid forms ranging from disordered amorphous material to highly ordered crystalline material. Additionally, a drug may exist in two or more crystalline forms, in which the drug molecule

is differently packed in each - a phenomenon termed 'polymorphism'. The subject of polymorphism is of significant interest in the pharmaceutical industry, as different polymorphs have significantly different physical properties of the drug compound, including (but not limited to) solubility, physical stability, and compactability [25]. Because of the effect that the solid-state of a compound has on its properties, much time and money is invested by pharmaceutical companies into determining the polymorph stability hierarchy.

Most commercially available drugs are marketed in the (likely<sup>1</sup>) lowest energy crystalline form, as this is the most thermodynamically stable form. This is of particular importance when considering the large-scale manufacture, and potential long-term storage of both the bulk drug compound and the final product, because it is important to be able to guarantee that the performance of the drug is unaffected after such treatment. Crystalline material is also desirable from a quality control standpoint, as it is easier to quantify and monitor the crystallinity of a material, than to determine if one batch of amorphous material is the same as another batch, as highlighted by recent concerns over the issue of polyamorphism [27].

Despite the convention for using the likely stable crystalline drug form, there are occasions where the formulation of other polymorphs or amorphous material is an attractive option; not least of all, to improve solubility (as will be discussed later). However, there are clearly a number of challenges associated with the formulation of amorphous drugs. For example, the amorphous form of a drug may be more hygroscopic than the thermodynamically stable crystalline form [28, 29], and the main concern with amorphous material, as has already been alluded to, is physical instability with respect to a lower energy crystalline state may lead to the solubility advantage of amorphous material being compromised after long-term storage. This is a topic that will be returned

---

<sup>1</sup>It seems appropriate here to quote Walter McCrone, who famously said that "every compound has different polymorphic forms, and that, in general, the number of forms known for a given compound is proportional to the time and money spent in research on that compound" [26]. In particular, this quote aptly describes how polymorphs have been known to unexpectedly appear or disappear [25], even after lengthy polymorph screening regimes, therefore indicating that it is never possible to say with all certainty that the lowest energy crystalline form of a compound has been identified

to in Chapter 5. As a result of these concerns, very few amorphous drug products reach the market.

### 1.2.5 Lipidic Formulations

Self-Emulsifying Drug Delivery Systems (SEDDS) and Self-Microemulsifying Drug Delivery Systems (SMEDDS) are examples of formulation strategies in which liquid or semi-solid lipids and/or surfactants are used to enhance the bioavailability of the API. A self-emulsifying drug delivery system is an isotropically clear dispersion of oil and non-ionic surfactant. When SEDDS are added to aqueous media and gently agitated (for example, on *in-vivo* administration) they form a fine, thermodynamically stable oil-in-water microemulsion [30], and hence provide a useful method for the delivery of lipophilic drugs to the gastrointestinal tract in a solubilised state [31]. A well-known example where SEDDS were shown to improve drug bioavailability is cyclosporine A, which had a two-fold improvement in bioavailability and decreased variability due to food effects when formulated in this way, compared to another solubilized formulation from which the drug precipitated out in the GI tract [31, 32].

Despite this success, there are only a limited number of commercially available drug products which are formulated in this way, and this may be due to several challenges to the development of lipid-based drug delivery systems. The main hurdle to the wider use of SEDDS in the delivery of an API is that it needs to be soluble in a suitable oil. As many poorly-soluble compounds are considered to be lipophilic, they are often assumed to be soluble in lipids, but it is often found to be the case that solubility of the drug in the oil is too low to make development of a lipidic oral dosage form practical [31]. Additionally, most lipid-based drug delivery systems are liquid, and therefore require administration either as bulk oral solution (which are often inconvenient and unpalatable to the patient) or as liquid-filled soft-gelatin capsules (which require specialist equipment to produce) [31]. Another drawback with lipid formulations is that there are often concerns about the stability (both physical and chemical) of these systems [31].

### 1.2.6 Particle Size Reduction

The Noyes-Whitney equation:

$$\frac{dW}{dt} = \frac{DA(C_s - C)}{L} \quad (1.1)$$

was derived in 1897, and indicates that the rate of dissolution ( $\frac{dW}{dt}$ ) of a solid is directly proportional to the surface area ( $A$ ) of the solid, where  $D$  is the diffusion coefficient,  $C$  is the concentration of solid in the bulk dissolution medium,  $C_s$  is the concentration of the solid in the diffusion layer surrounding the solid, and  $L$  is the thickness of the diffusion layer [33]. Therefore, it follows that the dissolution rate of a solid dosage form can be improved by increasing its surface area through particle size reduction using methods such as milling and micronisation.

Unfortunately, there are a number of disadvantages associated with particle size reduction that means that it is not always a viable option. Firstly, the energy input into the material during the size reduction process may induce a change in the solid-form of the material [34]. Additionally, the handling of sub-micron sized particles is difficult, and the chances of airborne contamination and toxicity by inhalation are very high [16], unless techniques such as wet milling are used to minimise such risks. One of the biggest limitations of crystalline nanoparticles is that there is no solubility improvement and so the potential for increased bioavailability is limited. Therefore, whilst this strategy is often used in early development to identify if the dissolution of a drug compound is the cause of its poor bioavailability, it is not always a viable option for the commercial manufacture of an oral dosage form.

### 1.2.7 Solid Dispersions

Another method for improving the bioavailability of an oral dosage form is to formulate it as a solid dispersion, which, is formed by the dispersion of the drug compound in a carrier matrix in the solid state. This approach has been shown to improve the dissolution profile of a drug substance in some cases, and has therefore been of increasing interest

to the pharmaceutical industry.

In the remainder of this chapter, the topic of solid dispersions will be explored, and the scientific literature surrounding this strategy will be examined in closer detail. Firstly, the types of solid dispersions in terms of physical structure will be discussed, and then the advantages of using this method of formulation and its use in improving drug bioavailability will be considered. Finally, the challenges associated with solid dispersions will be reviewed, as well as the progress made to date in addressing these issues, as well as the questions that remain to be answered with regards to this formulation method before it can be considered for routine use in drug development. Following a review of the literature, the motivation for the work in this thesis will be discussed, and the aims of the experimental work detailed in subsequent chapters will be outlined.

## **1.3 Review of Solid Dispersion Literature**

### **1.3.1 Solid Dispersion Classification**

In a pharmaceutical context the term 'solid dispersion' is one that is widely used to describe a system in which drug particles are homogeneously dispersed in a carrier matrix [1, 35]. However, closer scrutiny of such materials indicates that not all are structured in the same way, and there are a range of materials that are grouped under the umbrella term 'solid dispersions'.

**Simple Eutectic Mixtures** The idea of dispersing a drug compound within a matrix material is widely credited to Sekiguchi and Obi, who showed that eutectics of sulfathiazole with urea dissolved to produce a microcrystalline suspension of the drug in water, and improved the absorption in human compared with crystalline free drug [36]. A eutectic is a two-component material that displays a single solid-to-liquid phase transition as shown in Figure 1.2 [1, 2, 36]. A eutectic is formed when the two components are rapidly solidified from a fused liquid system with a specific composition, and is considered to be an intimate mixture of microcrystals of two crystalline components (see



Figure 1.3). Dissolution enhancement of a compound formulated as a simple eutectic is thought to occur as a result of the increased surface area of the released drug particles [36, 37]. Despite a number of studies investigating the use of eutectics in dissolution enhancement, it appears that the formation of genuine eutectics is rare [3, 38]. This can partially be attributed to the accuracy required in obtaining the eutectic composition, as a small deviation from this composition will result in the independent solidification of one component until the remaining liquor, which is richer in the other component, reaches the eutectic point and solidifies as a dispersion (see Figure 1.2) [3].

**Solid Solutions** Regardless of the number of components, solid solutions consist of just one homogeneous phase. As such, they can be considered to be comparable to liquid solutions, with the difference being that both the solute and solvent are solid [1, 2]. The drug in a solid solution is dispersed in the carrier at the molecular level, and therefore, during dissolution the drug will be released as individual molecules; hence the particle size of the drug has been reduced to its minimum [39]. Solid solutions can be classified in one of two ways: either in terms of the level of miscibility between the two components (continuous or discontinuous solid solutions), or with reference to the crystalline structure of the solid solution (substitutional crystalline, interstitial crystalline or amorphous solid solutions) [1].

A continuous solid solution is one in which the components are miscible in all proportions, and for this to occur, the free energy of mixing must be favourable at all drug loadings. The Gibbs free energy of mixing,  $G_{mix}$  is determined as shown in Equation (1.2), where  $H_{mix}$  is the enthalpy of mixing,  $T$  is the temperature and  $S_{mix}$  is the entropy of mixing.

$$G_{mix} = H_{mix} - TS_{mix} \quad (1.2)$$

As the entropy of mixing is always favourable, this implies that the intermolecular bonding must be stronger between the two components than between molecules of each individual component [1].

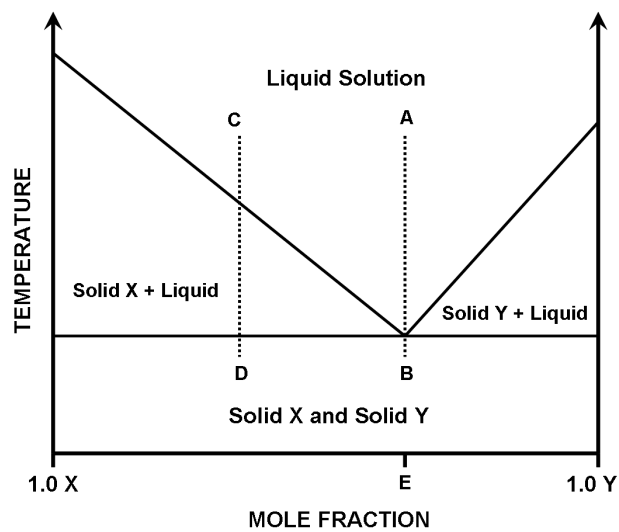


Figure 1.2: Phase diagram for a binary eutectic mixture, with the eutectic composition labelled 'E'. The effect of cooling at the eutectic composition (A to B) results in only the eutectic solidifying, whereas cooling at from a different composition (C to D) results in the solidification of component X, leaving the remaining liquid solution rich in component Y until the eutectic is reached. Reproduced with modifications from [1, 2, 3].

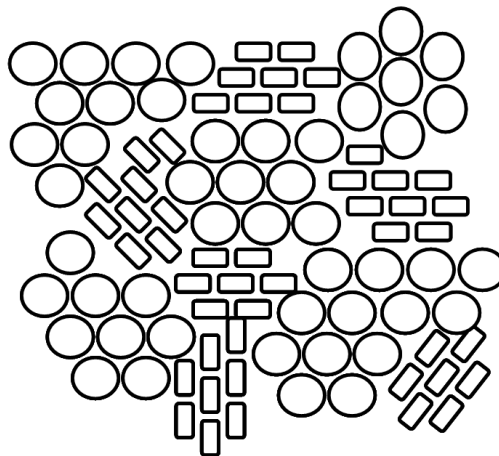


Figure 1.3: Schematic showing how a eutectic is an intimately blended physical mixture of the two crystalline components, shown as circles and rectangles.

Discontinuous solid solutions differ from continuous solid dispersions in that the solubility of one component in the other is limited to particular compositions. A typical phase diagram for this type of system is shown in Figure 1.4, whereby the compositions at which true solid solutions exist are represented by regions  $\alpha$  and  $\beta$  [1].

In practice, it can be expected that all two-component systems demonstrate some degree of solid-state solubility, though this level is often so low that for practical reasons Goldberg et al suggested that the term solid solution should only be applied when solubility of 5% of one component in the other is achieved [39]. However, this measure alone is not always enough to indicate whether a solid solution is suitable for pharmaceutical development. The intended dose of the drug must also be considered. This is because the upper limit for the mass of a tablet or capsule is  $\sim 1$  g, and therefore with only 5% solubility of drug in carrier, doses greater than 50 mg would not be possible [1]. The miscibility of two-component systems will be discussed in more detail below.

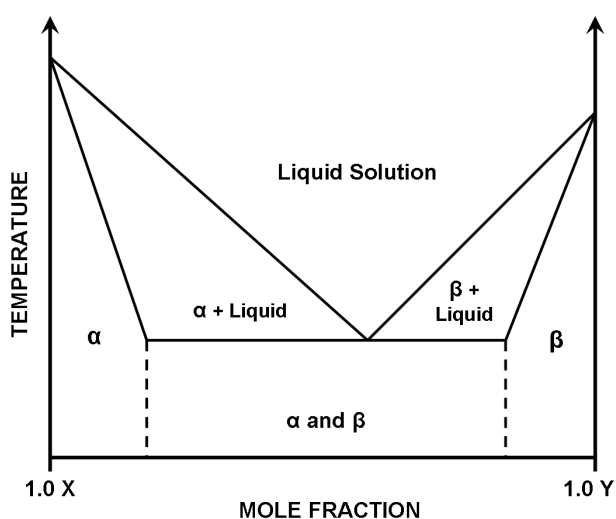


Figure 1.4: Phase diagram for a discontinuous crystalline solid solution, whereby region  $\alpha$  represents a solid solution of Y in X, and region  $\beta$  represents a solid solution of X in Y. Reproduced with modifications from [1, 2, 3].

Substitutional solid solutions are those in which the solute molecules are substituted for solvent molecules in the crystal lattice (see Figure 1.5a). In order for this to

occur, the molecules of the two components must be very similar in size. In general terms, the size of the solute molecules should differ by no more than 15% of the solvent molecule [2].

In interstitial solid solutions the solute molecules lie in the interstitial spaces between the solvent molecules in the crystal lattice (Figure 1.5b). As with substitutional crystalline solid solutions, the molecular size of the solute in relation to that of the solvent is of importance. With respect to this, the volume of the solute molecules should be less than 20% of the solvent, and the molecular diameter should not exceed 0.59 of the solvent molecule's diameter [1]. Large crystalline polymers such as polyethylene glycols tend to favour this type of solid solutions formation [38].

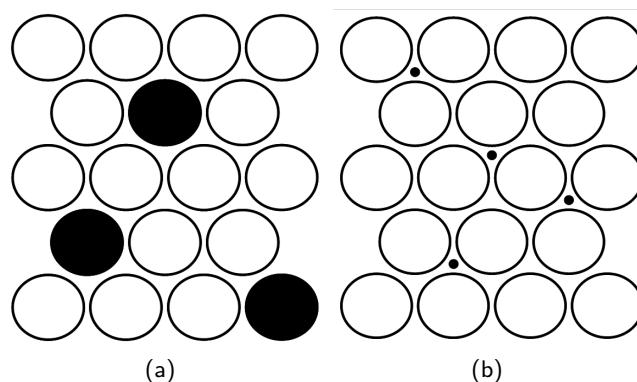


Figure 1.5: Schematics of a) a substitutional crystalline solid solution and b) an interstitial crystalline solid solution. Solvent molecules are represented with open circles, and filled circles indicate solute molecules. Reproduced from [1, 2].

Amorphous Solid Solutions are those in which the solute molecules are molecularly dispersed irregularly within the amorphous solvent (Figure 1.6) [1]. Such solid dispersions are particularly desirable with respect to the formulation of poorly water-soluble drugs, due to the enhanced solubility of amorphous materials compared to their crystalline counterparts (as will be discussed later). Polymer carriers are often used in the formulation of amorphous solid solutions, as they themselves often take an amorphous form. Additionally, the solute molecules often act as a plasticizer, leading to

reduction of the glass transition temperature of the drug.

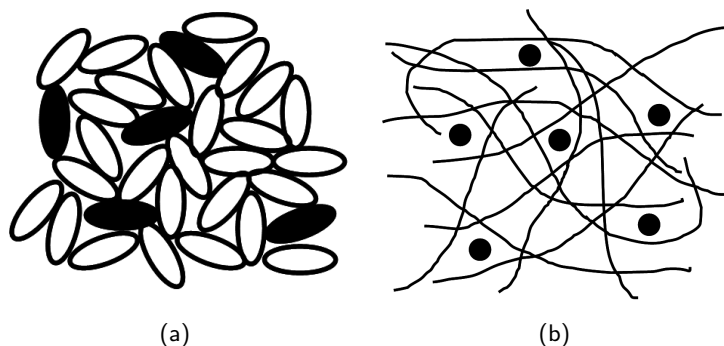


Figure 1.6: Schematics of a) an amorphous solid solution whereby the both the solvent (open ellipses) and solute (filled ellipses) are small molecules and b) an amorphous solid solution in which the drug molecules (filled circles) are dispersed in an amorphous polymer.

**Solid Suspensions** As we have already seen, the term ‘solid solution’ describes systems in which one component (usually the drug) is molecularly dispersed in another component. However, there are examples where dispersion of the drug at a molecular level cannot be achieved. The term ‘suspension’ describes a state in which the particles of a substance are mixed with a fluid but are undissolved. If the word ‘fluid’ in this definition is substituted with ‘solid’, we reach a phrase which better describes the type of system we will discuss here, whereby the drug exists as particles within the carrier material.

It is possible for the drug and carrier components of solid suspensions to exist in different physical forms, and this leads to materials with a diverse physical structures. As discussed previously, a carrier can exist as a crystalline, semi-crystalline or amorphous solid, but as the drug is present as particles, rather than individual molecules, it too can exist in either the amorphous or crystalline state (see Figure 1.7).

**Combinations** Rather than a solid dispersion belonging entirely to any one of the classes detailed above, it is possible that it may contain combinations of the different

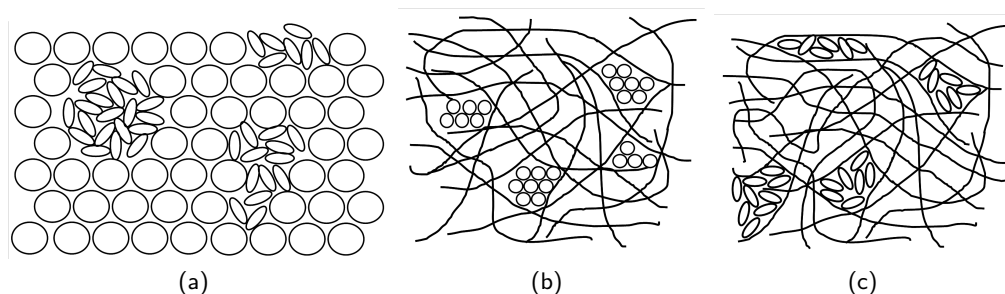


Figure 1.7: Schematics showing examples of solid suspensions whereby: a) amorphous material (ellipses) is suspended in a crystalline material (circles); b) drug microcrystals (circles) are suspended in an amorphous polymer (strands); and c) amorphous drug (ellipses) is suspended in an amorphous polymer (strands).

groups [2]. For example, it may be that a drug is dispersed within a carrier both as microcrystalline particles and individual molecules. Determining how the drug is dispersed throughout the carrier for a particular solid dispersion can prove problematic, and this will be discussed in more detail below and in subsequent chapters.

### Solid Dispersion Matrices

In the time that solid dispersions have been actively researched, a range of materials have been proposed for use as the carrier matrix. Regardless of the type of material chosen for use as the carrier component in a solid dispersion, it is important that it fulfills a several requirements before it can be considered for use [38]. Arguably the most important criteria is that it is non-toxic, as well as pharmacologically inactive. In the USA, the GRAS (generally regarded as safe) status is assigned by the Food and Drug Administration (FDA) to food additives and processing aids that are considered safe for use in products for human consumption (including oral dosage forms), and the use of such substances in formulation is less likely to be challenged by regulatory authorities [40]. The method used to prepare the solid dispersion is an essential consideration when selecting a carrier, as the carrier should be stable to the conditions the components are exposed to during manufacture. For example, if preparation is via melt fusion it is

unacceptable for the carrier to be thermally instable under the required processing conditions. Alternatively, if manufacture is via solvent processes such as spray drying, both the drug and carrier should be able to achieve sufficient solubility in organic solvents for this route to be viable, particularly at large scale. Additionally it is undesirable for the drug to chemically react with the carrier during processing via either a solvent or fusion processes. Finally it is desirable that the carrier is freely water soluble, although there are some examples of solid dispersions formulated with water insoluble matrices.

In Sekiguchi and Obi's initial work producing eutectics containing sulfathiazole, other small molecules, such as nicotinamide, were used as the secondary component [36]. A more recent study by Langer et al in 2003 continues this theme by investigating the use of a sugar alcohol, isomalt, as a carrier material [41]. However, despite several studies using these small molecules as solid dispersion carriers, it is far more widespread in current literature for polymers to be used as carrier matrices in solid dispersions. This is because in general they have less (or no) tendency to crystallise, and can act as better inhibitors of drug crystallisation.

There are a number of polymers that are already widely used in the pharmaceutical industry as excipients in the formulation of oral dosage forms, (for example as a binder, or for coating tablets), and the safety of such materials for use in humans is well-established. A wide range of pharmaceutically relevant polymers are available, which have various properties resulting from their chemical and physical diversity, and this makes them ideal candidates for use as solid dispersion carriers. Previous reviews have provided an excellent summary of the types of polymers that have commonly been used as carrier matrices in studies of solid dispersions, and the advantages and disadvantages of their use [1]. The most commonly used polymers for forming solid dispersions as highlighted by Leuner and Dressman are: polyethylene glycols (PEG); polyvinylpyrrolidone (PVP) and associated polymers such as polyvinylalcohol (PVA), crospovidone (PVP-CL) and polyvinylpyrrolidone/vinylacetate copolymer (PVP/VA). Also cellulose derivatives such as hydroxypropylmethylcellulose (HPMC); and polyacrylates and polymethacry-

lates. It is known that the selection of polymer carrier has a direct influence on the dissolution profile of the dispersed drug, and hence the choice of a water-soluble polymer will result in faster release of the drug than if a poorly soluble polymer is selected [2]. There are also examples in the literature where a combination of polymeric carriers are used in order to tailor the performance of the solid dispersion in terms of dissolution and physical stability properties [42, 43].

As well as using polymers as the carrier matrix in solid dispersions, many studies have included a surfactant in the solid dispersion. The addition of the surfactant is known to enhance the release of the drug from the solid dispersion through improved wetting and solubilisation of the drug [1]. A study by Janssens, Van Humbeeck and Van den Mooter showed that this was indeed the case when Inutec SP1, a poorly water soluble polymeric surfactant derived from Inulin, was added to solid dispersions of itraconazole in PVP/VA [44]. However, Ghebremeskel, Vemavarapu and Lodaya had mixed results with regards to dissolution improvement in their studies in which surfactants were incorporated into solid dispersions using various polymers as the carrier [45], which they suggested was as a result of the sample preparation method. They attempted to relate the dissolution with the hydrophile lipophile balance (HLB) value of the surfactant, but could not establish a link.

### **1.3.2 The Advantages of Solid Dispersions**

There are a number of aspects of solid dispersion formulation that make this approach particularly attractive to the pharmaceutical industry as a strategy for improving oral bioavailability. It could be seen that solid dispersion formulations incorporate a number of the advantages demonstrated by the other solubility-enhancing strategies described above. For example, it is known that the amorphous form of a drug is more soluble than its crystalline counterpart, but that physical instability of the amorphous state with respect to crystallisation is often a barrier to formulating amorphous oral dosage forms. Therefore, in an amorphous solid dispersion the solubility advantage can be realised,



whilst the amorphous form is stabilised by the carrier. If the drug in this amorphous solid dispersion was shown to be molecularly dispersed, this would further enhance the apparent solubility, as this is effectively the highest level of particle size reduction possible [39]. The intermolecular interactions that have been shown to exist between drug molecules and the polymeric carrier are similar to those observed in co-crystals, and finally, the addition of a surfactant to an amorphous solid solution provides similarities with lipidic formulations.

Despite the advantages of producing solid dispersion (particularly with regards to dissolution enhancement), relatively few drugs have been marketed as solid dispersions considering Sekiguchi and Obi's first suggestion of using eutectics was made in 1961. As of February 2010, there were only six solid dispersion products on the market [46], and the reason that there are not more marketed solid dispersions is likely to be due to a number of challenges associated with this method of formulation that still remain to be overcome.

### **1.3.3 The Challenges Associated With Using Solid Dispersions**

#### **Methods of Preparation and Scale-up for Manufacture**

Numerous methods have been reported for the preparation of solid dispersion samples for use in small-scale experiments. However, an initial challenge associated with the formulation of solid dispersions was the large-scale manufacture of solid dispersions. This is particularly so as the scale-up of many of the processes used to produce laboratory-scale batches would prove to be inefficient and costly.

There are two main routes to producing solid dispersions, which are from the melt (fusion method) or from solution with solvent evaporation. Below we explain how these methods are used to produce small batches of material for laboratory experiments, the potential problems that may be encountered in scaling up these methods, and the manufacturing-scale solutions to these challenges.

**Melt Fusion** The first pharmaceutical eutectics produced by Sekiguchi and Obi were prepared using the fusion method. The methodology consisted of the two components being accurately weighed in the eutectic composition into a platinum crucible, mixed thoroughly, and heated to just above the eutectic point in a furnace. The molten mixture was then rapidly cooled in an ice bath with vigorous stirring until the material solidified. The resultant solid was then crushed with a mortar and pestle prior to their use [36]. For lab-scale production of solid dispersions via melting, this method is still widely used [47, 48].

A more appropriate method for producing bulk material on a manufacturing-scale by melt fusion is hot-melt extrusion (HME). The technical details of hot-melt extrusion are beyond the scope of this thesis, but a brief overview of the technique will be outlined here. Further information about this method can be found in several review articles [49, 50, 51, 52, 53].

Melt extrusion consists of four steps as shown in Figure 1.8 [49]:

1. Feeding the extruder
2. Conveying of mass (melting, mixing and reduction of particle size)
3. Flow through the die
4. Exit from the die (and down-stream processing).

Feeding the extruder generally occurs from a hopper which is loaded with the material to be melt extruded. Movement of material through the extruder often occurs via the use of either one or two rotating screws located inside a stationary cylindrical barrel. The extruder can be sub-divided into three sections: The feed zone, where material enters the extruder from the hopper; the compression zone, where the material is melted, homogenised and compressed; and the metering zone, in which the flow of the extrudate is stabilised to ensure uniform thickness of the product (see Figure 1.8). The function of each of the three zones is determined by the geometry of the screw(s) in that section, the temperature, and the screw speed. In a number of extruders the barrel is manufactured

as interchangeable sections that can be assembled in different configurations to allow control of the conditions in each zone. Upon the exit of the molten material from the screw section, it is passed through the die plate, which determines the shape of the product. After the extruded product has cooled following exit from the die, it may be that further processing of the extrudate (e.g. milling) is required [49, 52].

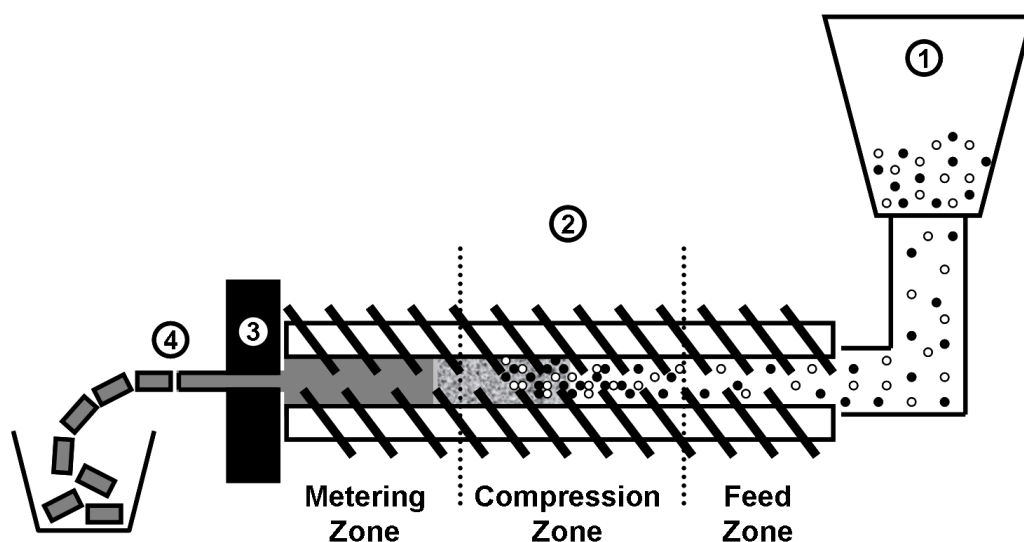


Figure 1.8: Schematic of a hot-melt extruder. Numbered labels indicate: 1) Feeding the extruder from a hopper; 2) Movement of the material through the extruder; 3) Flow of material through the die; and 4) Exit of extrudate from the die and down-stream processing.

The use of hot-melt extrusion in increasing numbers of literature studies indicates that this method is gaining prominence in the field of solid dispersions [42, 54, 55]. An advantage of this method, that may explain its increased use, is that the relatively compact equipment can be used throughout the drug development process, from the lab to the pilot plant and then onwards to manufacture. Processes, such as spray drying, which require the use of solvents are often time-consuming, costly, and there are environmental concerns surrounding their use [35]. On the other hand, extrusion is a solvent-free process, and therefore avoids these issues. Extrusion is also well-suited to

scale up for use on a manufacturing plant, because it is a continuous process. Because the material can be subject to continuous throughput, the product is likely to be more uniform because all the material experiences the same processing conditions.

Despite these advantages, there are also issues with hot-melt extrusion that means that it is not always a suitable method for production of particular solid dispersions. The main is that the use of high temperatures to melt the drug and polymer may lead to the thermal degradation of some compounds and excipients. The potential for thermal degradation may be mitigated by the use of additives as plasticizers which reduce the glass transition temperature of the polymer and the melting point of the drug, enabling lower processing temperatures to be used. However, even with the use of plasticizing additives, this manufacturing approach is not suitable for all formulations as the processing conditions may cause degradation of the components. Additionally, the number of different variables in the melt extrusion process, such as the feed rate, screw speed and extrusion temperature, means that method optimisation may be a lengthy process.

**Solvent Evaporation** An alternative to forming solid dispersions by melting is solvent evaporation. In this method, the drug and carrier compounds are both completely dissolved at the desired ratio in a common organic solvent, which is subsequently evaporated [35]. Several methods exist for the preparation of samples for small-scale feasibility studies on a microgram to tens of grams scale . At the smallest scale, thin film samples for microscopy and spectroscopy studies can be produced by spin-coating, whereby the solution containing drug and carrier is deposited onto a spinning substrate (e.g. a microscope slide). The solution is spread thinly across the substrate by centrifugal force, and the solvent evaporates simultaneously, leaving behind a thin solid dispersion film [56, 57]. Solid dispersions can also be film cast on static substrates [58], but this method results in thicker films. In cases where an amorphous solid dispersion is desired it is important to be aware that crystallisation of the drug may occur as a result of slower solvent evaporation, and this could lead to false negative results.

For lab-scale batches of powder, many studies use rotary evaporation to remove the solvent (e.g. [29, 59, 60]). However, other commonly used methods include spray drying and freeze drying (lyophilisation). Spray drying is an attractive option to the pharmaceutical industry for a number of reasons, including: low thermal stress, particle engineering for specific applications, rapid evaporation of the solvent preventing drug crystallization, and expanded process capability during scale-up [61]. During the spray drying process, the feedstock solution is passed through a spray nozzle, which atomises it, into a hot gas (typically nitrogen due to the use of flammable organic solvents). Because of the small droplet size, the solvent rapidly evaporates from the droplets, to precipitate solid particles, which pass through a cyclone to the collection chamber (see diagram in Figure 1.9).

Spray drying offers the advantage of producing material with a consistent particle size distribution. Also, the temperatures used during spray drying are generally lower than during hot-melt extrusion, so this method can therefore be used to produce solid dispersions of thermally-sensitive drug compounds. Despite the disadvantages of the organic solvent use associated with spray drying, this method is considered to be one of the more proven solvent-based methods for use in large scale manufacturing, as it is less costly and more scalable than freeze drying, and produces free-flowing powder. However, total recovery of the solid dispersion powder from the spray drier may be difficult due to material collecting elsewhere around the spray drier other than in the collecting vessel, and issues arising from the static nature of the product.

The important factors for consideration when using any of the above solvent evaporation methods is that firstly both components must be fully dissolved in the solvent prior to evaporation, and secondly, that the selected solvent is volatile enough to evaporate rapidly. The complete dissolution of both components is important as any undissolved particles may act as seeds for the crystallisation of the drug. It is important that the solvent evaporates rapidly, as slow evaporation might lead to the crystallisation of the drug in the case of an amorphous solid dispersion, or the evolution of a different

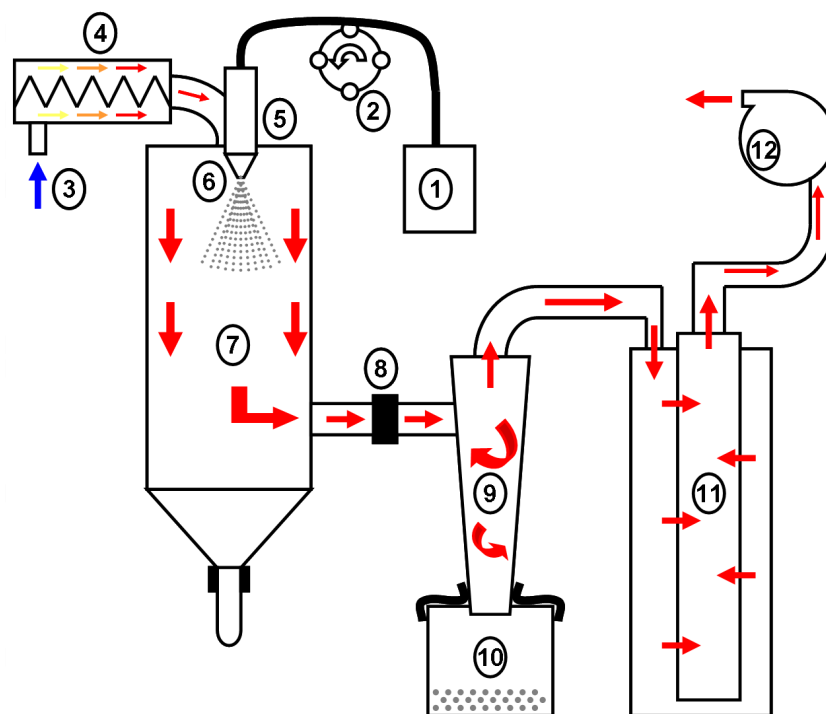


Figure 1.9: Schematic diagram of a typical spray dryer (adapted from [4]). Numbered labels indicate: 1) feed solution; 2) pump; 3) air/N<sub>2</sub> inlet; 4) electric heater; 5) spray nozzle; 6) concentric inlet of the hot air around the spray nozzle; 7) spray cylinder; 8) thermometer for measuring outlet temperature; 9) cyclone to separate particles from gas stream; 10) collecting vessel for dried product; 11) outlet filter; 12) aspirator to pump air through the system. The arrows indicate the flow direction of the hot air (and the sprayed product)

polymorphic form in the case of crystalline solid dispersions. Residual solvent in the resultant solid could also serve to alter the physical properties of the solid dispersion (e.g. by acting as a plasticiser).

**Other Methods** In addition to melt and solvent evaporation methods of solid dispersion formation, there are several other methods that have been reported in the literature, such as compression moulding [62], co-grinding [63], solvent wetting [64] and microwave irradiation [65]. These methods will not be described in any further detail here, and the

reader is directed towards the references for further explanation of the specifics of the techniques.

### **Solid State Analysis of Solid Dispersions**

Earlier in this chapter it was discussed how a solid dispersion may exist in one (or several) of many physical states, and it remains difficult in many cases to determine how the drug is dispersed in the carrier. Both, the physical stability of a solid dispersion and the dissolution properties of a solid dispersion, have been shown to be strongly influenced by the solid state structure, and hence the elucidation of physical structure is of particular importance. Here the general uses and limitations of different analytical techniques will be discussed, with specific reference to the determination of the physical structure of solid dispersions. The particular analytical techniques used in the work reported in the subsequent chapters of this thesis will be described in more detail in Chapter 2.

Traditionally, methods such as X-ray powder diffraction (XRPD), differential scanning calorimetry (DSC) and hot-stage microscopy have provided the principal means of probing the structure of a solid dispersion. In the first instance, XRPD can be used to determine if the solid dispersion is crystalline or amorphous within a specific level of detection. If the material is shown to be crystalline, characteristic peaks in the diffractogram can be attributed to either the drug or carrier components through comparison with diffractograms of the crystalline free form drug and carrier, thus indicating that perhaps a eutectic or solid suspension has been formed. If the particles are very small, this may be manifest in the XRPD diffractogram through peak broadening. This is demonstrated by Kanaze et al, who used the identification of characteristic peaks in XRPD diffractograms to show that the flavonoid drugs were present as microcrystallites when formulated as solid dispersions with either amorphous PVP or crystalline PEG [66]. In the case that the solid dispersion is shown to be completely amorphous by XRPD, it is not possible simply from looking at the diffractogram to determine if the drug is molecularly dispersed in the polymer or if a solid suspension has formed.

DSC analysis will also be able to identify if the material is crystalline, amorphous or a mixture by the identification of melting and glass transition temperatures (denoted  $T_m$  and  $T_g$  respectively) for each of the components. It is also widely accepted that in the case of amorphous solid dispersions, the appearance in the thermogram of a single  $T_g$  that is intermediate to the  $T_g$ s of the individual amorphous components indicates that a molecular dispersion has been formed [67]. However, DSC may not be sensitive enough in most cases to accurately differentiate between a nanosuspension and a solid solution [68] (see Chapter 2). Hot-stage microscopy provides complimentary information to the data from XRPD and DSC, in that the melting or crystallisation temperatures of solid dispersions can be observed with this technique. Nevertheless, molecular resolution cannot be obtained with optical microscopy, and so the existence of a solid solution cannot be absolutely confirmed using this technique.

Spectroscopic methods such as Fourier-transform infrared spectroscopy (FTIR) and Raman mapping can be used to provide more information about drug-drug and drug-polymer intermolecular bonding in solid dispersions, and aid in elucidating whether the material is a solid solution or solid suspension. An example of how FTIR can be used to supplement the information obtained from XRPD and DSC is Lin et al's study of a theophylline-Eudragit L system, in which the collection of FTIR spectra over a range of temperatures shows how intermolecular bonding patterns change with temperature [58]. Karavas et al were able to show with Raman mapping that in higher drug-loaded solid dispersions of felodipine in PVP, the drug was not molecularly dispersed throughout the polymer matrix, but was instead present as microparticles [69].

More recently analysis of XRPD data using the Pairwise Distribution Function (PDF) method has enabled a more detailed understanding of the distribution of components within a solid dispersion material. For example, Bates et al showed that this technique could be used to distinguish different types of structuring within amorphous samples of the same compound [6]. Also, Newman et al showed that the PDFs of dextran/PVP and trehalose/dextran solid dispersions from XRPD data could be predicted



using combinations of the PDFs of the individual components, thus indicating that they were likely to be solid suspensions. Conversely, the PDF of indomethacin/PVP solid dispersions did not match the prediction, suggesting that for this sample it was more likely that the indomethacin was molecularly dispersed in the polymer carrier [68].

What is apparent, is that no single technique can provide all of the answers with regards to the solid-state structure of a solid dispersion. Instead, a combination of analytical methods should be used to probe the physical structure of solid dispersion, and hence enable a better understanding of the associated physical properties. The challenge is to develop a solid-state testing protocol that can be used implemented as early as possible, within the context of a wider pharmaceutical development strategy in which there may be limited amounts of drug compound available.

### **Physical Stability**

The most important challenge to overcome with regards to solid dispersions is the issue of their physical stability, as this directly links to product shelf-life and *in vivo* performance. Solid dispersions can be prone to phase separation, whereby the two components do not remain intimately mixed and migrate into discrete domains. The thermodynamic instability of many amorphous solid dispersions means that there is also a particular risk that the drug or carrier may crystallise out. In some cases it has been shown that it is possible for an amorphous polymer carrier to crystallise [35].

In order to prevent the crystallisation of a drug from the amorphous state, the drug compound should not be able to form in concentrated pockets, as crystals would be more likely to nucleate and grow from such regions. However, the production of a molecularly dispersed system, in which the grouping of drug molecules can be interrupted by polymer chains, may be less likely to lead to the nucleation and growth of drug crystals. This is because the polymer chains would lead to the disruption of any potential crystal lattice, and hence provide both a steric and energetic barrier to crystallisation.

Having stated the importance of producing a molecular dispersion, rather than

a system that is phase separated, it is also important to understand that the production of a molecularly dispersed system depends on the miscibility of the drug and polymer compounds, which itself is dependant on the molecular structure of the drug and polymer compounds. As shown by the Gibbs equation (Equation (1.2)), the miscibility of a system is due to the balance between energy and entropy [70, 71, 72]. The mixing of two similarly-sized components, A and B, is represented in Figure 1.10a, and the free energy of mixing ( $F_{mix}$ ) for such a system is given by Equation (1.3), where  $\Phi$  is the volume fraction of the component,  $k$  is the Boltzmann constant, and  $T$  is the temperature [71].  $\chi$  is a dimensionless parameter that characterises the strength of the energetic interaction between the molecules A and B relative to their self-interactions [70, 71].

$$\frac{F_{mix}}{k_B T} = \Phi_A \ln \Phi_A + \Phi_B \ln \Phi_B + \chi \Phi_A \Phi_B \quad (1.3)$$

As shown in Figure 1.10b, Equation (1.3) can be plotted using different values for  $\chi$ . In Figure 1.10b it can be seen that when  $\chi \leq 2$ , the two components are miscible at all proportions. However, when  $\chi > 2$ , a 'miscibility gap' appears, in which phase separation will occur (for  $\chi = 3$ , this is when  $\Phi_A > 0.1$  and  $< 0.9$ ). Therefore, it can be said that the critical value of  $\chi$ ,  $(\chi_{crit})$ , = 2.

Many solid dispersions consist of a small molecule drug (B) dispersed in a polymeric carrier (A), and in these cases the entropic gain that arises from mixing of the components is less than when both components have a similar volume, due to the reduced number of configurations of the two components [72]. This is illustrated in the schematic shown in Figure 1.11a. In such cases the expression for calculating the free energy of mixing must be modified accordingly, as shown in Equation (1.4), where  $N$  is the number of monomeric units in the polymer [73].

$$\frac{F_{mix}}{k_B T} = \frac{\Phi_A}{N} \ln \Phi_A + \Phi_B \ln \Phi_B + \chi \Phi_A \Phi_B \quad (1.4)$$

The plots of  $\chi$  shown in Figure 1.11b are for a system in which  $N \rightarrow \infty$ . It can be seen that in this case  $\chi_{crit} \sim 0.5$ , and for systems with higher values of  $\chi$  miscibility can only

be achieved at low drug drug loadings. For systems with other values of  $N$ , it can more generally be said that  $\chi_{crit} \approx \frac{1}{2} + \frac{1}{\sqrt{N}}$ .

Some studies have sought to predict the miscibility of solid dispersions, using solubility parameters or experimentally derived thermal properties of the drug compound [72, 74, 75, 76], but these have only had limited success. In other work, rather than seeking to predict miscibility, the focus has been to identify the storage conditions that induce phase separation and crystallisation from a particular miscible system [29, 56, 60]. Or an alternative approach is to look to identify by experimental means an amorphous polymer that inhibits the crystallisation of a particular drug [56]. There are studies that have investigated the interactions that a series of drugs has with a particular polymer [48, 59, 77], but the drug compounds used in these studies are not always analogous. Or, if they are, they may differ by several functional groups from the other compounds in the series, making it difficult to identify the contribution that each functional group has on drug/polymer miscibility. Despite the vast number of studies in the literature investigating physical stability in solid dispersions, it still remains difficult to predict when drugs will crystallise, even after phase separation has been detected.

### **Understanding the Mechanisms of Dissolution Enhancement**

It is well known that the amorphous form of a compound has a higher solubility than its crystalline counterpart [28, 78], and this is largely because the lattice enthalpy does not have to be overcome in the dissolution of amorphous materials. This solubility advantage and the associated dissolution enhancement is often the main reason that solid dispersions are developed. However, the mechanism by which this dissolution enhancement occurs is still not fully understood. This issue was addressed by Craig in his 2002 review article [3], where his survey of the different results reported in the literature highlighted the ongoing debate about whether the dissolution properties of solid dispersions are drug- or carrier-mediated.

It was shown, with the aid of examples of work by Corrigan [79, 80] Dubois and

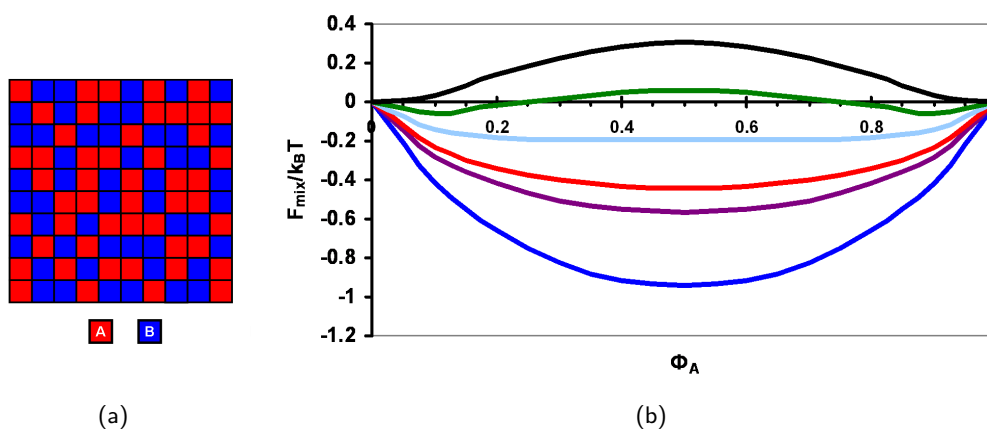


Figure 1.10: a) Schematic to show the miscibility of small molecules A and B, and b) a graph showing how the free energy of mixing ( $F_{mix}$ ) of the system changes with composition ( $\Phi$ ) and dependent on the  $\chi$  parameter of the system. Plots represent systems with  $\chi$  parameters of -1 (dark blue), 0.5 (purple), 1 (red), 2 (light blue), 3 (green) and 4 (black).

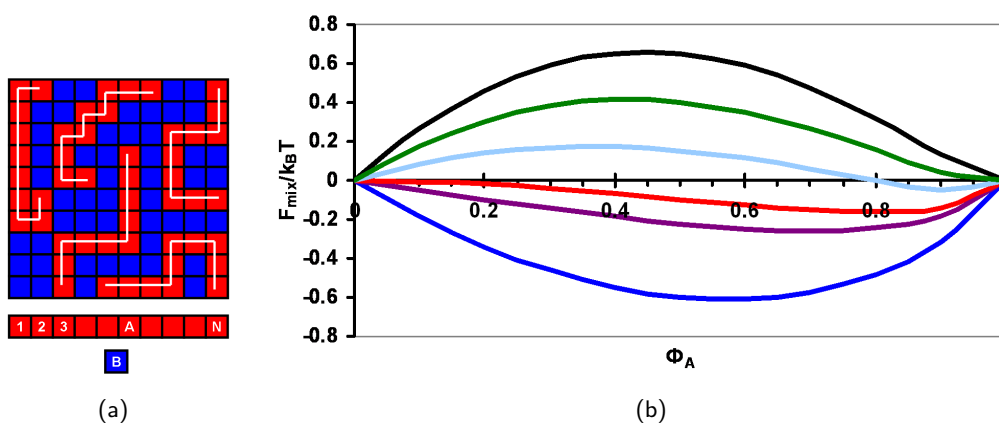


Figure 1.11: a) Schematic to show the miscibility of a polymer, A, with a small molecule drug, B, whereby the polymer has a chain length of N monomers. b) a graph showing how the free energy of mixing ( $F_{mix}$ ) of the system changes with composition ( $\Phi$ ) and dependent on the  $\chi$  parameter of the system, when  $N = \infty$ . Plots represent systems with  $\chi$  parameters of -1 (dark blue), 0.5 (purple), 1 (red), 2 (light blue), 3 (green) and 4 (black).

Ford [47], and Craig and Newton [81], that when the dissolution rate of the drug in the polymer carrier, and the dissolution rate of the polymer alone are equivalent, then the dissolution of the solid dispersion can be deemed to be carrier-controlled. However, this is not the case for all solid dispersions, as illustrated by Craig with an example by Sjökvist-Saers and Craig [82] who observed a linear relationship between the intrinsic dissolution rate and drug solubility of solid dispersions based on a homologous series of drug molecules. This provided evidence that for some systems, dissolution is drug-controlled (rather than carrier-controlled).

There have been a number of studies since the publication of Craig's review which measure the dissolution of solid dispersions with ranges of drug loadings. However, these mostly focus on solid dispersions with drug loadings below 30%, and/or are focussed on producing controlled release dosage forms. Kanaze et al [66] investigated the dissolution enhancement of poorly water-soluble flavonoids when formulated as solid dispersions, and found that there was a clear improvement in the dissolution of them in a concentration dependant manner. However, the flavonoids were found to remain crystalline in the solid dispersion formulations, and hence the dissolution advantage of using amorphous material was not able to be realised in this study. Similarly, Okonogi and Puttipatkhchorn [83] investigated the dissolution of high drug-loaded systems (above 50% w/w drug) of ofloxacin in PEG, both with and without the addition of surfactant, and found that all solid dispersions demonstrated improved dissolution over the crystalline drug, in a concentration dependant manner. However, these solid dispersions were also shown to be crystalline.

### **In Vitro/In Vivo Correlation**

Even if an improvement in the solubility profile of a drug formulated as a solid dispersion can be shown, it is not clear that this always correlates with improved bioavailability of the API *in vivo*. In cases where the *in vivo* performance is not improved, despite enhancement of the dissolution profile, it could be that the intrinsic intestinal permeability

of the drug is low. Several studies have carried out investigations to determine if *in vitro* and *in vivo* performance are correlated for solid dispersion systems [84, 85, 86].

## **1.4 Aims of the PhD**

### **1.4.1 Motivation and Aims of this Research**

A number of studies in the literature have suggested that intermolecular interactions between the drug and polymer components lie at the heart of understanding the performance and stability of solid dispersions. However, most of these studies seem only to have identified the dominant intermolecular bonding motif in a particular system, and investigated this with reference to a particular property. By contrast, it appears that there are few reports in which a broader series of drug molecules has been used as a means to identify and further understand the contributions of all intermolecular interactions on the stability and performance of a solid dispersion system. All of the aforementioned challenges associated with the development solid dispersions could be addressed with a more fundamental understanding of the ways in which the drug and polymer components of a solid dispersion interact. Therefore, the research detailed in this thesis aims to address, in part, this gap in the knowledge, by seeking to identify if any trends exist between the physicochemical properties of solid dispersions and the molecular structure of the drug compound used in the solid dispersion. The identification of correlations between drug descriptors and solid dispersion performance could then be used as a screening tool to assess the suitability of new pharmaceutical drug compounds for formulation as solid dispersions.

The main solid dispersion system under investigation in this work is that of felodipine in copovidone. Studies of the very similar felodipine/PVP system indicate that a hydrogen bonding interaction between the drug and polymer components is dominant in this particular system, which lends physical stability to the drug [87], and enables enhanced dissolution of the drug [88]. It is expected that the same hydrogen-

bonding motif will be present in the felodipine/copovidone system. Other drug-polymer interactions have not been investigated in other studies, and it is the impact of the molecular structure of felodipine and its derivatives on the physicochemical properties of the solid dispersion that are investigated in this work. In order to do this, a series of structural analogues of felodipine were synthesised (Chapter 3), and the properties of solid dispersions containing these analogues were measured, and directly compared with the results of the felodipine system. Thus the contribution of each functional group could be assessed.

If successful, this approach could be used to better enable formulators to recognise the potential risks or benefits of producing a solid dispersion of a particular drug compound. It may also aid in the design of more effective solid dispersion screening protocols. Furthermore, if information about the ability of specific functional groups to impact in either a positive or a negative way on solid dispersion formation could be determined, this could be used as a high-throughput screening tool to direct discovery chemists towards synthesising compounds that can be more successfully formulated (as a copovidone solid dispersion in this case, but the principle could be applied more widely).

The secondary aim of this work is to investigate the potential of emerging analytical methods and techniques for characterising solid dispersion systems. It is hoped that such systems might either be more effective than existing methods, or provide information about the system that cannot be easily determined via other means. In Chapter 5 the use of a laser light scattering technique to provide information about morphological changes in solid dispersion systems will be explored, with the view that this method could potentially be developed as a screening tool. In Chapter 6 magnetic resonance imaging (MRI) with integrated ultraviolet (UV) detection system will be used to further understand the dissolution mechanism of a spray dried felodipine/copovidone solid dispersion system.

### 1.4.2 Overview of the thesis

A number of the experimental techniques that can be used to investigate the physical and chemical properties of solid dispersions have already been alluded to in this introductory chapter. In the next chapter, the techniques used during the course of this work to analyse solid dispersions will be described in more detail. The theory and rationale for the use of these techniques will be outlined.

The synthesis of the felodipine analogues used for the studies reported in Chapters 4, 5, 6 and 7 is described in Chapter 3. In this chapter the rationale for the selection of synthetic target analogues will first be discussed, and then the synthetic methods will be described in more detail. For those compounds that were successfully synthesised, the total amounts of material yielded will be detailed, as this will prove to be a fundamental issue in the planning of experiments in the following chapters.

Chapter 4 summarises the attempts to produce solid dispersions of these materials, and their initial analyses. This chapter will focus on the solid state analysis using x-ray powder diffraction, pair-distribution function analysis and differential scanning calorimetry.

The physical stability of felodipine and its analogues in solid dispersions with copovidone is reported in Chapter 5. Firstly, experiments using a novel laser light scattering method to investigate morphological changes in felodipine/copovidone films will be detailed. In the second part of this chapter polarised light microscopy was used to assess the ability of copovidone to inhibit the crystallisation of felodipine and its analogues in a series of well-plate experiments.

In Chapter 6 the dissolution performance of felodipine and its analogues on felodipine/copovidone solid dispersions produced using spray drying, using an MRI flow-cell technique with an in-line UV/Vis detector is reported. The studies in which the spray dried material was used, attempt to shed light on the mechanisms by which the dissolution of poorly soluble compounds is improved when formulated as solid dispersions. To do this, two very different dissolution methods were employed: One is a



'micro-dissolution' method in which very small samples can be assessed using fibre-optic ultraviolet (UV/Vis) measurement; the other uses magnetic resonance imaging of a bulk sample in a dissolution flowcell in combination with an in-line UV spectrophotometer. Following on from this initial study, a series of experiments were carried out using micro-dissolution to compare the performance of film-cast solid dispersion samples containing the analogue compounds with crystalline and amorphous drug, and physical mixtures, and these experiments are also detailed in Chapter 6.

In Chapter 7, we attempt to correlate the data from the well-plate crystallisation experiments conducted in Chapter 5 and the dissolution experiments on the analogue compounds carried out in Chapter 6 with molecular descriptors and physical properties.

Finally, in Chapter 8 the conclusions from each chapter will be drawn together, and the overall conclusions of the thesis will be laid out. Avenues for future work will also be explored.

## Chapter 2

# Materials and Experimental Methods

This chapter serves to provide an overview of the materials and techniques used throughout this thesis for the analysis of solid dispersion samples. Here, the general theories behind the techniques and how they work will be presented, and the reasoning behind their use will be discussed. The full details of the experimental parameters used will not be addressed in this chapter, as these will be given as the experiments are encountered in subsequent chapters.

### 2.1 Materials

#### 2.1.1 Felodipine

Felodipine (O5-ethyl O3-methyl 4-(2,3-dichlorophenyl)-2,6-dimethyl-1,4-dihydropyridine-3,5-dicarboxylate) is a calcium-channel blocker, which is prescribed predominantly for use as a treatment of hypertension [89]. It is widely documented as a BCS class II compound, and has been the subject of a number of studies which investigate improving the bioavailability of this drug by formulation as a solid dispersion [55, 56, 57, 60, 69, 72, 75, 87, 88, 90, 91, 92, 93, 94]. The glassy state of felodipine has also been

the subject of several studies [95, 96, 97]. The information available about felodipine from these previous studies, made this drug ideal for use as a model compound in the following experiments, and provided a structural basis for design of analogue compounds for synthesis and testing.

## Felodipine Analogues

The experiments in this thesis aimed to investigate the impact of drug molecular structure on the formation of soluble and physically stable solid dispersions with a polymer. Therefore, a series of compounds which are structural analogues of felodipine were synthesised and used directly in the following work. The rationale for which analogues were synthesised, as well as their chemical structures and methods of synthesis are detailed in Chapter 3.

### 2.1.2 Copovidone

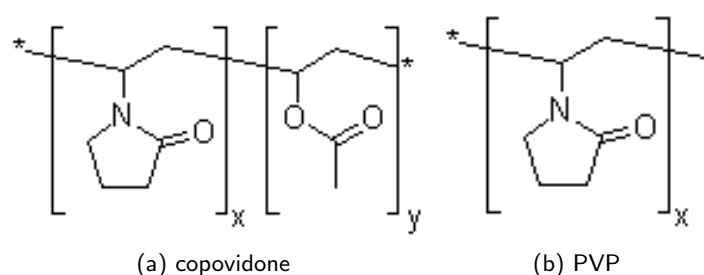


Figure 2.1: Molecular structures of copovidone (a) and the chemically similar polymer, pvp (b).

Copovidone (poly vinylpyrrolidone-vinyl acetate co-polymer - see Figure 2.1a) is a water-soluble polymer, commonly used as a dry binder excipient, granulating agent or retarding and film forming agent in pharmaceutical tablet manufacture processes [98]. Copovidone is chemically similar to polyvinylpyrrolidone (PVP - see Figure 2.1b) which is also a polymer commonly used as an excipient in pharmaceutical tablet manufacture, and has been used in solid dispersion formation in a number of previous studies [66,

99, 100, 101, 102, 103], several of which use felodipine as the API of interest [56, 57, 72, 75, 87, 88, 91, 92, 93, 94]. In these studies, PVP was shown to both inhibit the crystallisation, and enhance the dissolution performance of the drug compounds when used in solid dispersion formation, and it seems logical to suggest that due to their similarities in molecular structure and physical properties, copovidone may provide another suitable option for solid dispersion formulation.

The good aqueous solubility of copovidone may prove to be an advantage over less soluble polymers if dissolution of the drug in solid dispersions is carrier-controlled. Although copovidone is less soluble than PVP, it is also less hygroscopic [98], and hence may prove to be a more attractive option for this reason.

## **2.2 Methods**

### **2.2.1 Structure Determination**

Successful synthesis of the felodipine analogues as detailed in chapter 3 was largely confirmed with the use of three analytical techniques: mass spectrometry (MS), nuclear magnetic resonance (NMR) and Fourier transform infrared spectrophotometry (FTIR). These methods are commonly used for structure determination in synthetic chemistry, and a full description of these methods is both beyond the scope of this work, and more effectively covered in a number of organic and analytical chemistry textbooks. In short:

- MS is used to determine the molecular mass of the compound under testing;
- NMR is used to determine the connectivity of the atoms in the molecule - experiments based on Hydrogen and Carbon atoms are carried out in this work;
- FTIR enables the identification of functional groups present in the molecule.

### 2.2.2 X-ray Powder Diffraction (XRPD)

X-ray powder diffraction (XRPD) is probably the most useful technique for determining the level of crystallinity (or lack thereof) in a sample, and due to the relative ease with which samples can be analysed using this method, it forms the basis of most solid-state testing regimens in the pharmaceutical industry.

In XRPD analysis, a micro-crystalline powder sample if correctly prepared, should present a random selection of crystal orientations at the powder interface. The radiation of this surface with monochromatic x-ray radiation should hence provide information on all the possible atomic spacings in the crystal lattice [104]. The sample is slowly rotated and the scattering angle  $\theta$  is determined by one of two methods: either the scintillation counter measures the angle of diffracted x-rays with respect to the angle of the incident beam; or the detector is moved around the sample, to determine the angle of the diffracted x-rays, whilst the angle between the sample and x-ray source is kept constant.

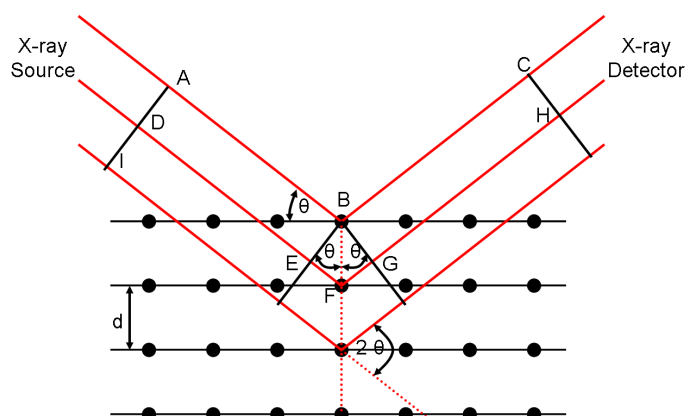


Figure 2.2: Diagram showing Bragg reflection from a set of crystal planes with a spacing  $d$  (adapted from [5]).

Smart and Moore explain that the constructive and destructive interferences of Bragg reflections from the sample gives rise to the powder diffraction pattern produced, as demonstrated in figure 2.2 [5]. In this figure the lines of black dots represent the

parallel planes of a crystal lattice which have spacing  $d$ . During analysis, the crystal is irradiated with a parallel beam of monochromatic x-rays represented by the red lines A, D and I, at an incident angle  $\theta$  with respect to the crystal planes. The atom at position B causes ray A to be scattered, and similarly, ray D is scattered at atom F. The reflected beams must arrive at the detector in phase with each other in order for them to register with a sufficient intensity, and therefore the pathlengths of the beams must differ by an integer number of wavelengths in order for constructive interference to occur. By drawing lines perpendicular to the incident and reflected x-rays at BE and BG, it is possible to determine the difference in path length between the two beams, as:

$$\text{difference in path length} = EF + FG$$

We can also see from figure 2.2 that

$$EF = FG = d \sin \theta$$

and therefore

$$\text{difference in path length} = 2d \sin \theta$$

As the difference in path length must be equal to an integer number,  $n$ , of wavelengths for constructive interference to occur (and hence for a peak to register in the diffractogram), it can be seen that if the wavelength of the x-rays is  $\lambda$ , then

$$n\lambda = 2d \sin \theta \tag{2.1}$$

Following this, it can be seen that for a crystalline powder sample, the x-ray powder diffractogram will contain a series of peaks at characteristic scattering angles, unique to the crystallography of that material. Hence, polymorphs of the same compound will have distinctly different diffractograms. Conversely, if the sample is completely amorphous we can see that there will be no Bragg peaks featured in the diffractogram, and instead an amorphous halo will be seen. For semi-crystalline samples, the Bragg peaks will be broader than for fully crystalline samples, and they will be superimposed on an amorphous halo.

For a more detailed description of XRPD and the practicalities of this technique, the reader is directed to the books by Klug and Alexander [105] and Dinnebier and Billinge [106], which both provide more comprehensive explanations of this technique.

### Pair Distribution Function (PDF)

Looking at a powder diffractogram for an amorphous two-component system cannot directly give information about whether those components are fully miscible or not; it can only tell us that both components are mostly amorphous. Whilst other techniques such as differential scanning calorimetry can be used to determine this information, there are limitations as to the resolution of such techniques (as discussed below). The pair distribution function (PDF) is a method by which XRPD data of an amorphous material is used to produce a plot showing the interatomic distances that define a solid form [107]. Therefore, this technique can be used to better understand the solid state structure of a solid dispersion, and has already been used in several studies for this purpose [55, 57, 68].

Billinge and Kanatzidis [108] define the atomic PDF  $G(r)$ , as

$$G(r) = 4\pi r[\rho(r) - \rho_0] \quad (2.2)$$

where  $\rho_0$  is the average atomic number density,  $\rho(r)$  is the atomic pair density and  $r$  represents radial distance. Hence, the function  $G(r)$  indicates the number of atoms in a spherical shell of a unit thickness at a distance  $r$  from the reference atom as represented in the schematic in figure 2.3. In order to obtain the PDF of an XRPD diffractogram, the measured scattering intensities must first be corrected for background and other experimental effects, and then normalised by the flux and number of atoms in the sample, to give  $I^{coh}(Q)$ . This can then be used to determine the total scattering structure function  $S(Q)$  using equation (2.3)

$$S(Q) = \frac{I^{coh}(Q) - \sum c_i |f_i(Q)|^2}{|\sum c_i f_i(Q)|^2} + 1 \quad (2.3)$$

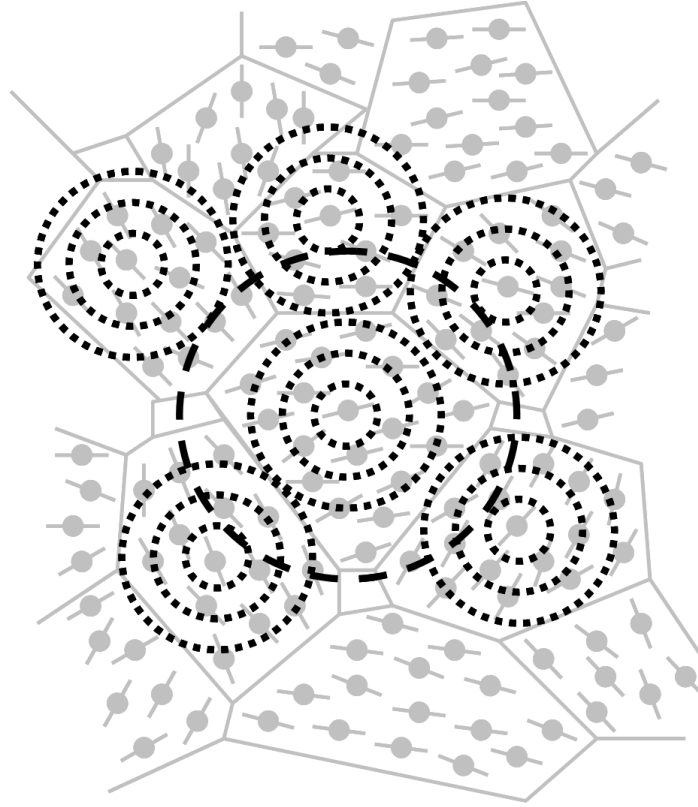


Figure 2.3: Schematic showing the nearest neighbour coordination observed using pair distribution functions (adapted from [6]).

where  $C_i$  and  $f_i$  are the atomic concentration and x-ray atomic form factor respectively for the atomic species of type  $i$ . A sine Fourier transform can then be applied to  $S(Q)$  in order to obtain the PDF of the data as shown in equation 2.4

$$G(r) = (2/\pi) \int_{Q=0}^{Q_{max}} Q[S(Q) - 1] \sin(Qr) dQ \quad (2.4)$$

The plotted PDF essentially indicates the probability of there being two atoms separated by distance  $r$ , whereby the peaks correspond to commonly occurring interatomic distances [6, 109].

It is important to note that calculating the PDF  $G(r)$  does not produce data,



but simply provides another way to represent the diffraction data. Nevertheless, this presentation of the XRPD data in real space has particular advantages in aiding the understanding of structurally disordered materials. This is because whilst the PDF reflects the long-range order of crystalline materials manifest in the diffractogram as Bragg peaks, it can also pick out the diffuse components of the diffraction pattern due to local structural imperfections. This is because, as shown in equations (2.3) and (2.4) the total scattering contributes to the PDF. Additionally, analysis of the data using this method does not presume periodicity, which therefore makes it useful for characterising disordered materials [108].

### **2.2.3 Differential Scanning Calorimetry (DSC)**

Of all thermal analysis techniques performed in pharmaceutical research, differential scanning calorimetry (DSC) is probably the most common, due to its ease of use and wide range of applications. In the field of solid dispersions, DSC is most useful for identifying if a material is crystalline or amorphous (and the temperature ranges over which the associated phase transitions occur) and more importantly, whether the components of the solid dispersion are miscible.

To perform differential scanning calorimetry (DSC) on a sample, 1-7mg of material is prepared in a suitable sample pan. An identical pan, which does not contain any sample is also prepared for use as a reference. The sample and reference pans are placed in a furnace on individual heating stages linked with measurement thermocouples (Figure 2.4). The sample and reference pans are heated (or cooled) at the same rates, and the heat flow required to maintain the sample at the required temperature relative to the reference is measured [104]. Flow of a suitable gas through the furnace cell ensures the atmosphere is inert, and any volatiles produced during the process are purged, as well as assisting in heat transfer. Phase transitions of the material under testing can be identified from the thermogram as endotherms (for melting or solvent loss events), exotherms (for crystallisation events) and glass transitions (Figure 2.5).

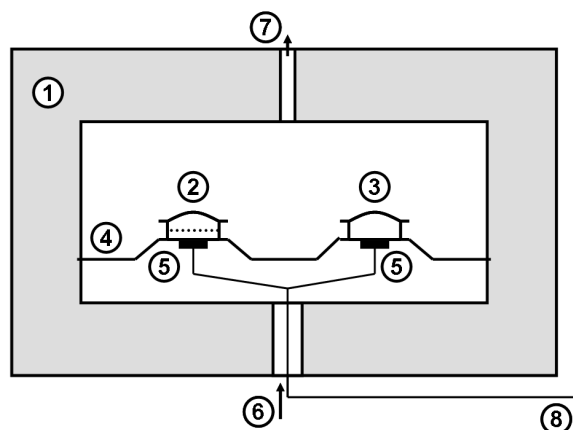


Figure 2.4: A schematic of a Differential Scanning Calorimeter (DSC). Numbered labels indicate: 1) furnace; 2) sample pan; 3) reference pan; 4) heat flux plate; 5) heating stage thermocouples; 6) purge gas inlet; 7) purge gas vent; 8) temperature and heat flow data is sent to a computer for recording.

It is well-known that if a 2-component system is fully miscible it will exhibit a single glass transition temperature  $T_g$ , which is intermediate to the  $T_g$ s of the individual components. However, if the blend is immiscible, then two separate  $T_g$ s will be observed - one for each component. Assuming that the free volumes of the components are additive, the  $T_g$  of a miscible drug/polymer blends can be predicted using the Gordon-Taylor equation (2.5):

$$T_g = \frac{w_1 T_{g1} + K w_2 T_{g2}}{w_1 + K w_2} \quad (2.5)$$

where  $w_i$  are the weight fractions and  $T_{gi}$  are the glass transition temperatures of the individual components. The subscript 2 refers to the component with the higher  $T_g$ . The constant K is calculated as shown in Equation (2.6), where  $\rho_i$  are the densities of the pure amorphous components [87, 110].

$$K = \frac{\rho_1 T_{g1}}{\rho_2 T_{g2}} \quad (2.6)$$

The Couchman-Karasz model can also be used to predict the  $T_g$  of a miscible 2-component system, and this equation takes the same form as Equation (2.5), but instead K is calculated as shown in Equation (2.7), where  $\Delta C_P$  is the change in specific heat

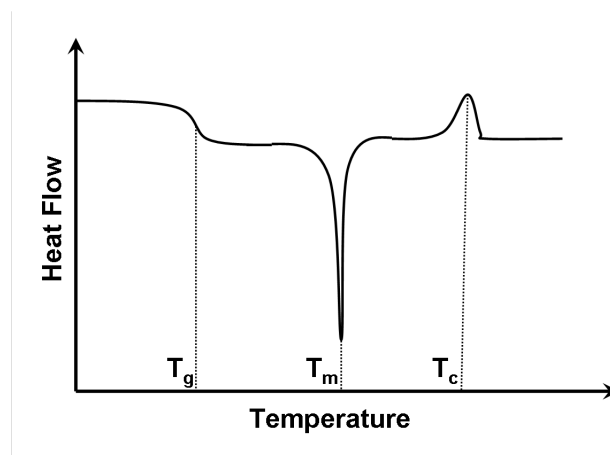


Figure 2.5: Schematic showing how the glass transition temperature  $T_g$ , melting point  $T_m$ , and recrystallisation temperature  $T_c$  are shown in a thermogram produced by DSC. In this example, exothermic peaks point upwards.

capacity at the  $T_g$  of each compound [87, 111].

$$K = \frac{\Delta C_{P1}}{\Delta C_{P2}} \quad (2.7)$$

A key limitation of DSC for determining the miscibility of amorphous solid dispersions is the detection limits associated measuring glass transition temperatures ( $T_g$ ). As discussed above, it is generally accepted that the presence of a single  $T_g$  for a 2-component system indicates that it is fully miscible. However, if the  $T_g$ s of the 2 components are less than 10°C apart, and the phase separated domains are not large enough (typically less than ~30nm) to be detected by the thermal changes measured by DSC, this 2-component system may appear to be fully miscible [68]. An additional drawback of DSC is that due to the numerous types of events that can be detected using this technique, many of which are shown as either endotherms or exotherms, interpretation of the thermograms can often prove challenging, and correct interpretation often depends on the knowledge and experience of the researcher [112]. These issues indicate that despite the potential of DSC to provide the answers to a number of questions about a sample, it is important to use this technique in combination with others before drawing any firm conclusions.

#### **2.2.4 Optical Microscopy**

Optical microscopy is arguably one of the techniques most widely employed by scientists from a range of disciplines due to its versatility. Optical microscopes are available in a range of designs, but in general a microscope consists of a stand which holds a sample stage perpendicular to the optical axis, a tube which contains the objectives and eyepieces, and an system to illuminate the sample that usually involves use of a lamp and condenser [113]. The reader is directed to Bradbury's clear and informative book for further details and a practical guide of optical microscopy [113].

In terms of providing a further understanding solid dispersion systems, optical microscopy can be used to view the morphology of solid dispersion particles and films (Chapter 4). However, it is particularly useful in observing changes that can occur to the materials upon exposure to different environmental conditions, especially with regards to both phase separation and crystallisation, as has been shown extensively in the literature, and will be demonstrated in Chapter 5.

#### **Polarised Light Microscopy**

When detection and observations of crystal growth are required, the use of plane-polarised light can provide a considerable advantage over brightfield microscopy, as most crystals are birefringent. In this form of optical microscopy, polarising filters are positioned above and below the sample stage. The light incident to the sample is constrained by the first polariser to vibrate in one plane only, and the polariser positioned after the sample (termed the analyser) is rotated to a  $90^\circ$  angle with respect to the first polariser; an arrangement in which the polarisers are said to be 'crossed'. In this way, only light that is rotated by the sample is transmitted to the eyepiece [114]. When amorphous solid dispersions are viewed through cross-polarisers, the field of view will be dark. However, if the drug crystallises from the solid dispersion, the anisotropy of the crystals will cause the refraction of light in two slightly different directions to form two rays, and the crystals will be more easily viewed than with standard brightfield

microscopy.

### **2.2.5 Scanning Electron Microscopy (SEM)**

Scanning electron microscopy (SEM) is a technique in which the sample is scanned using a high-energy beam of electrons, to produce images at much higher levels of magnification than is possible with optical microscopy.

Sample preparation for pharmaceutical materials involves fixing the material to a specimen stub, and coating the surface of the material in an ultrathin layer of gold. This is because in order for a sample to be imaged by SEM, the surface of the sample must be electrically conductive, and electrically grounded to prevent the accumulation of electrostatic charge on the sample. A high-energy beam of electrons (typically 0.5 to 40 eV) is emitted from an electron gun at the top of the vacuum column (see Figure 2.6). This beam of electrons is focussed through a series of magnetic condensing lenses to a spot which is in the range of 0.4 to 5 nm in diameter. Lower down the vacuum column, a set of scanning coils moves the focussed beam line by line across the sample, and as this occurs, secondary electrons are emitted from the sample surface through inelastic scattering. These secondary electrons are detected and amplified to produce an image which is essentially a map of the emitted signal intensities from the sample.

The following references provide examples where SEM has been used to investigate the solid state and physical morphology of solid dispersions [54, 115, 116, 117].

### **2.2.6 Atomic Force Microscopy (AFM)**

Atomic Force Microscopy (AFM) is a type of scanning probe microscopy. In AFM, a cantilever with a sharp tip at the end is used to probe the surface of the sample as it is moved back and forth (see Figure 2.7). The radius of the tip is in the order of nanometers, which can lead to the production of images with atomic resolution. When the tip is brought close to the sample surface, forces between the sample and the tip lead to the deflection of the cantilever according to Hooke's law. The deflection of the

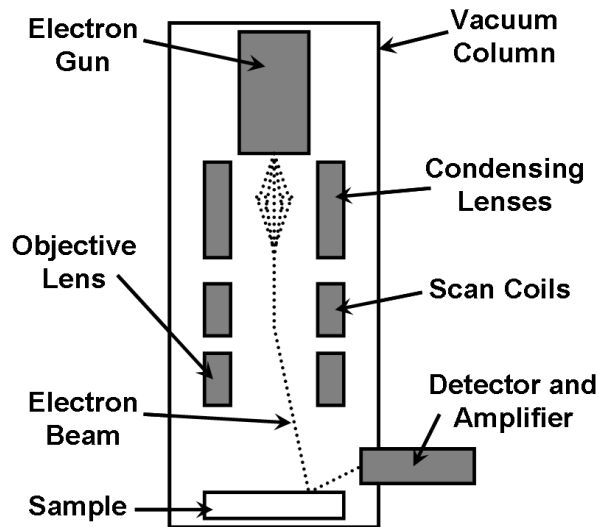


Figure 2.6: A schematic of a Scanning Electron Microscope (SEM).

cantilever is measured through the reflection of a laser spot from the top of the cantilever to a position sensitive photodetector. In order to prevent the tip from crashing into the sample surface, a feedback loop from the photodiode detector to the cantilever and piezoscanner is used to adjust the tip-to-sample distance. The AFM has several modes of operation, which can be divided into static (or contact) modes, and dynamic (or non-contact) modes in which the cantilever is vibrated. In this thesis, samples were analysed using tapping mode, and this will be described below. For information regarding other AFM imaging modes, the reader is directed to the following reference [118].

In tapping mode AFM, the cantilever is oscillated at its resonant frequency with an amplitude of typically 100 to 200 nm. This is done by a piezoelectric element mounted on the AFM tip holder. The amplitude of the cantilever oscillations decreases when the tip approaches the sample surface as a result of forces such as Van der Waals forces, dipole-dipole interactions and electrostatic forces etc. acting on the tip. The height of the cantilever above the sample is adjusted to maintain the amplitude by the piezoelectric actuator controlled by an electronic servo. In tapping mode AFM, the image is formed by imaging the forces experienced by the tip when it makes intermittent

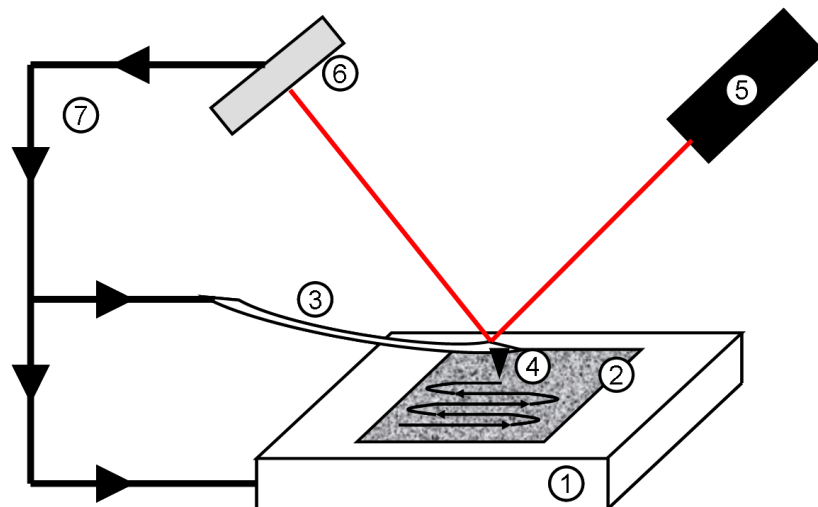


Figure 2.7: Schematic of an AFM instrument. Numbered labels indicate: 1) piezoscanner; 2) sample; 3) cantilever; 4) tip; 5) laser; 6) position sensitive detector; and 7) feedback of signal from photodiode to piezoscanner and cantilever.

contact with the sample [119, 120].

With tapping mode AFM, as well as measuring the topography of a sample surface, it is also possible to observe differences in the material properties of the sample. This is because there is a phase difference between the drive and the response of the cantilever oscillations. In air, the phase difference between the cantilever drive and response oscillations is  $90^\circ$ , but when the tip comes into contact with the sample, this phase difference changes as a result of the different material properties in the samples. Monitoring of the signal phase during tapping mode AFM is called 'phase imaging' [118]. This technique is particularly relevant to analysis of solid dispersions, as it can be used to give an indication of how well mixed two components are.

AFM has several advantages over SEM for imaging samples. Firstly, samples analysed by AFM do not require any special preparations prior to imaging, which could change or damage the sample. Also, AFM provides a three-dimensional surface profile of the surface, whereas electron microscopes only provides a two-dimensional projection

or image of the sample.

### 2.2.7 Dissolution Testing

There are a wide range of dissolution testing methodologies that are used in during the drug development process, and the selection of a suitable dissolution method depends on a number of factors, including the stage the compound has reached in the drug development process, the delivery route of the drug, and the type of dosage form under testing [121]. *In-vitro* dissolution testing methodologies can be used to determine the key factors that influence the performance of a drug (both alone and when formulated as a dosage form) *in-vivo*.

All dissolution tests involve submerging the drug material or dosage form in a suitable medium which is kept moving at a constant speed. From these tests, the rate at which the drug is released and dissolved into the medium from the dosage form is measured using appropriate sampling and analysis techniques (typically the concentration of drug is measured at regular timepoints using UV analysis) [122]. The methods by which the dosage form is presented to the medium, and the medium is kept in motion, differ between dissolution apparatus [121, 123], and these differences, as well as differences in the geometries of the dissolution vessels, can influence the hydrodynamics of the system, and hence impact upon the dissolution rates. Also, the experimental parameters, such as temperature and pH of the dissolution media etc, can effect the dissolution rate. Therefore, as dissolution testing is considered so important in formulation selection, monitoring and quality control, standard methods are published by the United States Pharmacopeia (USP), the European Pharmacopoeia (EP), and the Japanese Pharmacopoeia (JP) [121, 122].

In chapter 6 two methods of dissolution testing are used, neither of which are pharmacopoeial techniques. The techniques used are micro-dissolution, and an MRI flow-cell method, both of which are described in full in chapter 6. The micro-dissolution method is used for the main reason that very little sample is required, and this was a



key consideration for the testing of the felodipine analogue compounds as only limited amounts of material were available. The MRI flow-cell system was used to provide additional mechanistic information about the dissolution process. All of the dissolution tests detailed in this thesis were carried out at a temperature of 37°C, and in media with a pH of 6.5 as these conditions are biologically relevant when considering dissolution and absorption in the small intestine.

## Chapter 3

# Synthesis of Felodipine Analogues

### 3.1 Introduction

#### 3.1.1 Rationale for the synthesis of felodipine analogues

The main hypothesis under test in this thesis is that the properties and performance of a solid dispersion are directly affected by the intermolecular interactions between the drug and polymer molecules. It is also well-documented that increasing numbers of the compounds synthesised showing promising results in terms of their drug properties, are difficult to formulate into oral solid dosage forms. Combining these two points, it is clear that it would be desirable to be able to provide guidance to medicinal chemists about which molecules from an analogue series of drug candidates might be easier to develop as solid dispersions, if it is known that this formulation route might ultimately be used. Additionally, the ability to be able to distinguish molecules that are more likely to produce 'good' solid dispersions, from ones that are harder to effectively formulate in this way, may enable formulation scientists to target their resources more effectively towards drug compounds that are more likely to successfully be formulated as solid dispersions. Consequently, attrition of poorly soluble compounds from the drug development process may be reduced.

In many of the experiments detailed in this thesis, felodipine (see figure 3.1a)

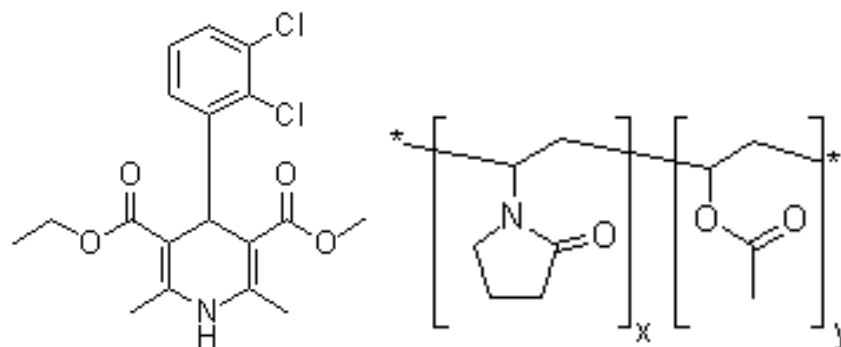


Figure 3.1: Molecular structures of a) felodipine and b) copovidone.

was initially used as a model compound. Felodipine is a calcium channel blocker, used to control hypertension, that is well-known to be poorly water-soluble. As a result of this, felodipine is a BCS Class II drug. Felodipine is a well-documented example of a drug that may benefit from formulation as a solid dispersion, which made this compound a good starting point for use in the experiments detailed later in this work. Therefore, to in order to investigate the effect of drug structure on the properties of solid dispersions, analogues of felodipine were synthesised.

Two main considerations for the structural modification of felodipine were considered. Firstly, potential sites of intermolecular bonding between the drug and copovidone polymer were identified, and modifications that would either enhance or disrupt these interactions were sought. The most obvious candidate group for modification in this way, was the nitrogen of the dihydropyridine ring, which is well known to engage in hydrogen bonding with the carbonyl group in the pyrrolidone ring of PVP, a polymer structurally similar to copovidone (see figure 3.1b) [69, 87, 88]. Secondly, modifications that might typically be carried out by a medicinal chemist to adapt a compound structure in the lead optimisation process were considered.

### 3.1.2 Target Compound Design and Retrosynthetic Analysis

Taking the above factors into account, a list of synthetic targets was identified, which included N-methyl, aromatised, diethyl ester, des-chloro and nitrile analogues (see figure 3.2 for full list of synthetic targets). The first compound to be identified for synthesis was the aromatised analogue, in which the dihydropyridine was oxidised to pyridine, and this choice arose from a desire to investigate the impact of removing the -NH hydrogen bond donor which has been shown in the literature to interact with the carbonyl group of pyrrolidone in PVP [87] - a group which is also present in copovidone. There are a number of methods described in the literature that would enable the oxidation of felodipine, the most common of which involves heating with nitric acid [124, 125]. However, a more effective method that was used in this work was oxidation with ceric ammonium nitrate (CAN), which was shown to be a simple and high-yielding reaction [126]. It was also shown that the CAN oxidation can be carried out catalytically with sodium bromate in acetonitrile to give two oxidation byproducts in low yield. The bromate ion acts to reoxidise the reduced form of the cerium (see figure 3.4) [127, 128]. The addition of an extra -OH group in one of these products may provide additional hydrogen bonding capability with copovidone in a solid dispersion, and was therefore of particular interest. The other oxidation byproduct containing a lactone ring was also of value as it provided further diversity in the chemical structures of the analogues. As a result, these two compounds were added to the list of synthetic targets.

The synthesis of the N-methyl analogue would be another method of blocking the hydrogen-bonding capability of felodipine, and is hence another target compound. The synthesis of this molecule could be undertaken through N-alkylation using methyl iodide and potassium hydroxide in DMSO, as shown in the literature for a closely related compound [129].

Felodipine is an asymmetrical compound as the ester alkyl portions are of different lengths, with one being a methyl group, and the other an ethyl. Therefore, it followed that one of the analogues should be symmetrical, with the two side-chains of

equal length, thus leading to the diethyl ester compound becoming one of the synthetic targets. Hydrolysis to the acid of a diester similar to felodipine, followed by conversion to the salt and re-esterification with DMF/Mel to a diester has been previously described [130], and could be a valid pathway from felodipine. However, a cheaper, faster and more straightforward method was identified in the one-step total synthesis from ethyl acetoacetate, 2,3-dichlorobenzaldehyde and ammonium acetate, following the Hantzsch dihydropyridine synthesis [131, 132]. The Hantzsch dihydropyridine synthesis proceeds via a series of steps (see figure 3.3), the first typically being a Knoevenagel condensation reaction between a suitable aldehyde (in this case 2,3-dichlorobenzaldehyde) and a keto-ester to produce an unsaturated carbonyl compound. The enone formed in the previous step then undergoes a Michael addition with a second enolate molecule, and then addition of ammonia to one of the ketones occurs. Synthesis of the dihydropyridine is completed when cyclization of the imine or enamine on to the other ketone occurs [133]. Use of phenylboronic acid (which is cheap and widely available) as a catalyst, effectively reduces reaction times and increases yields, and can also be recovered from the reaction for re-use if required [134]. It is this methodology which has been used in this work. The des-chloro diethyl ester was also identified as a synthetic target in order to assess the influence of the electronegative chlorine atoms on the intermolecular interaction with copovidone, and synthesis of this compound could also be undertaken using the phenylboronic acid catalysed Hantzsch dihydropyridine method detailed above.

A further potential analogue to be identified was the nitrile ester, as the replacement of ester groups with the strongly electron-withdrawing nitrile group would both increase the polarity of the compound. Additionally, the nitrile has only one lone pair available to accept a hydrogen bond, which is arranged linearly along the axis of the triple bond, compared to the ester which has four hydrogen bond acceptor sites at different orientations. In their paper, Ohsumi et. al. showed the synthesis of a dimethoxy phenyl substituted nitrile ester also using a one-pot, three-component Hantzsch dihydropyridine method [135], which could also be applied to the dichloro phenyl target identified here.

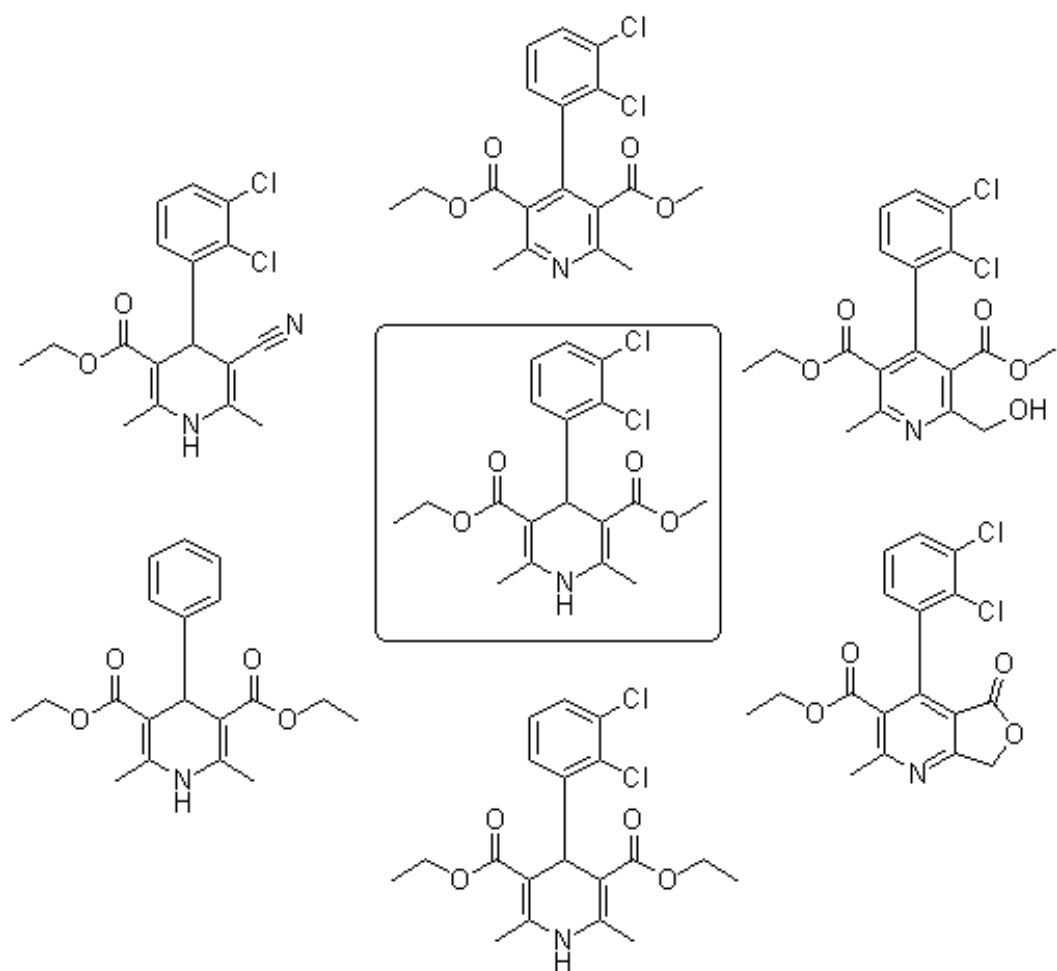


Figure 3.2: Molecular structure of felodipine (centre) surrounded with the molecular structures of the target analogues. Clockwise from top: aromatised analogue, 2 oxidation byproducts, diethyl ester, des-chloro diethyl ester, and nitrile ester.

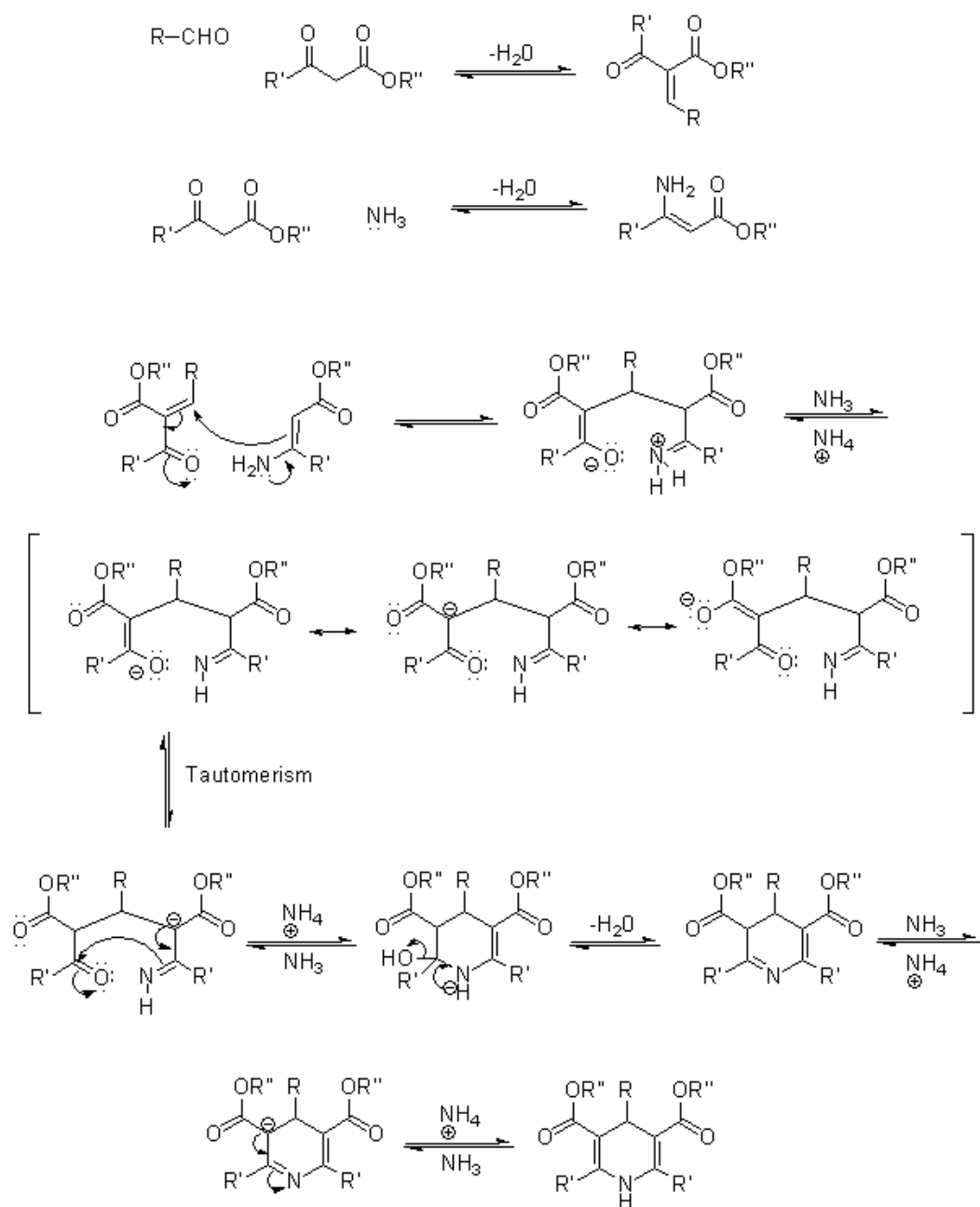


Figure 3.3: General reaction scheme for the Hantzsch Dihydropyridine Synthesis.

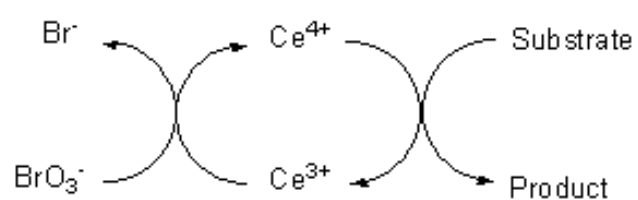


Figure 3.4: Scheme to show the regeneration of the cerium(IV) reagent by reoxidisation by the bromate ion.



## 3.2 Materials

All reagents were used as supplied by Sigma Aldrich and all solvents were used as supplied by Fisher Scientific. The petroleum ether used in this work was the 40-60°C fraction.

## 3.3 Chromatographic Methods

Thin layer chromatography (TLC) was carried out on aluminium sheets coated with TLC Silica 60 F<sub>254</sub>. Spots were visualised with UV light.

Flash column chromatography was carried out for purification of some compounds [136] using silica gel (40-63 $\mu$  60A).

## 3.4 Melting Point Determination

The melting points of the synthesised compounds were determined by DSC. Material for testing (1.5-7 mg) was weighed directly into a 50  $\mu$ L aluminium sample pan and hermetically sealed. The sample was then analysed using a PerkinElmer Jade DSC (PerkinElmer, Massachusetts, USA). An Indium sample was used to calibrate both the temperature and heat flow of the instrument prior to analysis of each set of samples. The sample chamber was purged with nitrogen gas flowing at 50 mL/min. Samples were analysed in standard DSC mode. Each sample was heated from 25°C to 300°C at 10°C/min and then cooled back to 25°C at the same rate. This cycle was repeated three times for each sample. Data analysis was performed using Pyris Thermal Analysis software v8.0 (PerkinElmer, Massachusetts, USA). The onset and peak of the melting endotherm are given.

## 3.5 Spectroscopic Methods

A variety of spectroscopic methods were used to confirm that compounds had been successfully synthesised.

### 3.5.1 Nuclear Magnetic Resonance (NMR)

NMR spectroscopy was performed using a 400 MHz Bruker instrument. Samples were prepared in 5 mm NMR tubes in a suitable deuterated solvent. Analysis of NMR spectra was aided by reference to work by Jung et al on assigning the  $^1\text{H}$  and  $^{13}\text{C}$  NMR spectra of felodipine [137]. Chemical shifts are expressed as ppm with reference to residual undeuterated solvent ( $\text{CHCl}_3$  or DMSO). Peaks are assigned as singlets (s), doublets (d), triplets (t), quartets (q) or multiplets (m), or a combination thereof, and J coupling values for the splitting patterns are given (in Hz).

### 3.5.2 Mass Spectrometry (MS)

An LCT Micromass Mass Spectrometer with electrospray ionisation was used to perform mass spectrometry. Less than 1 mg of the compound to be tested is dissolved in a suitable solvent. For positive ion work, 10  $\mu\text{L}$  of the sample solution is added to a mixture of 200  $\mu\text{L}$  of acetonitrile with 0.1% formic acid and 200  $\mu\text{L}$  of water containing 0.1% formic acid. For negative ion work, sample preparation is the same, except that the acetonitrile and water do not contain formic acid.

### 3.5.3 FTIR

FTIR analysis was performed on all synthesised material using a Nicolet 6700 instrument with golden gate diamond ATR crystal. A background scan was performed prior to each sample analysis with no sample in the instrument, and this was subtracted from the sample data. Powdered samples were placed directly onto the diamond crystal, and the anvil lowered to ensure the sample was in full contact with the diamond. For each sample 32 scans were recorded, with a resolution of  $2\text{ cm}^{-1}$ .

## 3.6 Synthetic Methods

### 3.6.1 ZAL\_001 – O3-ethyl O5-methyl 4-(2,3-dichlorophenyl)-2,6-dimethyl-pyridine-3,5-dicarboxylate

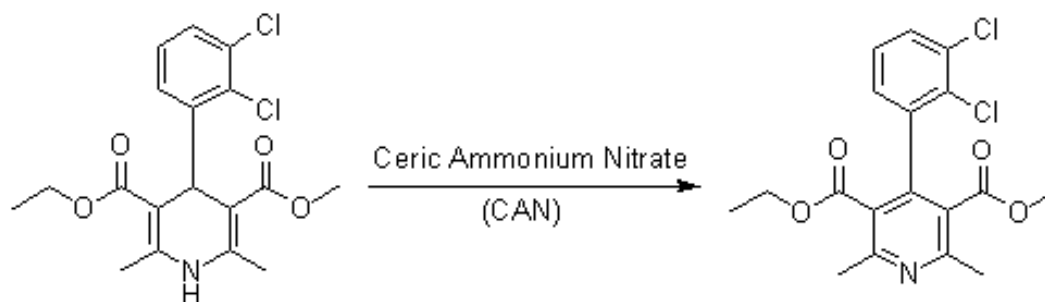


Figure 3.5: Reaction scheme for ZAL\_001

To a solution of felodipine (97 mg, 0.25 mmol) in acetone (15 mL) was added a solution of  $(\text{NH}_4)_2\text{Ce}(\text{NO}_3)_6$  (307 mg, 0.56 mmol) in  $\text{H}_2\text{O}$  (3.5 mL) fairly rapidly, dropwise from a hand-held pipette at room temperature. The mixture was left to stir for 30 min, after which time the orange colour of the reagent had disappeared and the mixture was colourless. Upon further addition of CAN the reaction no longer turned colourless, indicating completion of the reaction. The resulting solution was concentrated to a small volume under reduced pressure.  $\text{H}_2\text{O}$  ( $\sim 20$  mL) is added and the mixture was extracted with DCM ( $2 \times \sim 30$  mL). The organic phase was washed with brine ( $\sim 20$  mL), dried ( $\text{Na}_2\text{SO}_4$ ) and evaporated under reduced pressure. A yellow oil was obtained (93%). TLC  $R_f$  (30% acetone/70% pet. ether) = 0.45.

$^1\text{H}$  NMR (400 MHz,  $\text{CDCl}_3$ ):  $\delta$  0.95 (t, 3H,  $J=7.2$ ,  $\text{COOCH}_2\text{CH}_3$ ), 2.65 (d, 6H,  $J=5.6$ ,  $\text{RC}(\text{CH}_3)\text{NC}(\text{CH}_3)\text{R}$ ), 3.56 (s, 3H,  $\text{COOCH}_3$ ), 4.02 (dq, 2H,  $J_A=7.2$ ,  $J_B=1.6$ ,  $\text{COOCH}_2\text{CH}_3$ ), 7.07 (dd, 1H,  $J_A=7.6$ ,  $J_B=1.6$ ,  $-\text{CC}(\text{Cl})\text{C}(\text{Cl})\text{CHCHCH}-$ ), 7.21 (t, 1H,  $J=7.8$ ,  $-\text{CC}(\text{Cl})\text{C}(\text{Cl})\text{CHCHCH}-$ ), 7.47 (dd, 1H,  $J_A=8.0$ ,  $J_B=1.6$ ,  $-\text{CC}(\text{Cl})\text{C}(\text{Cl})\text{CHCHCH}-$ ).  $^{13}\text{C}$  NMR (100 MHz,  $\text{d}_6\text{-DMSO}$ ):  $\delta$  13.14 ( $-\text{OCH}_2\text{CH}_3$ ), 22.92 and 22.99 ( $\text{RC}(\text{CH}_3)\text{NC}(\text{CH}_3)\text{R}$ ), 52.26 ( $\text{COOCH}_3$ ),

61.05 (COOCH<sub>2</sub>CH<sub>3</sub>), 125.61 and 125.67 (-CCCIC<sub>2</sub>CHCHCH-), 127.82, 128.72 and 130.21 (-CCCIC<sub>2</sub>CHCHCH-), 131.61 and 131.69 (RC(CH<sub>3</sub>)NC(CH<sub>3</sub>)R), 137.07 (-CCCIC<sub>2</sub>CHCHCH-), 143.43 (C<sub>2</sub>H<sub>5</sub>OCOC(R)CH(R')C(R)COOCH<sub>3</sub>), 156.06 and 156.23 (C<sub>2</sub>H<sub>5</sub>OCOC(R)CH(R')C(R)COOCH<sub>3</sub>), 165.90 and 166.51 (C<sub>2</sub>H<sub>5</sub>OCOC(R)CH(R')C(R)COOCH<sub>3</sub>). HRMS (ESI+): m/z [M + H]<sup>+</sup> calcd for C<sub>18</sub>H<sub>18</sub>Cl<sub>2</sub>NO<sub>4</sub> 382.0613, found 381.8327

### 3.6.2 ZAL\_005 – diethyl 2,6-dimethyl-4-phenyl-1,4-dihydropyridine-3,5-dicarboxylate

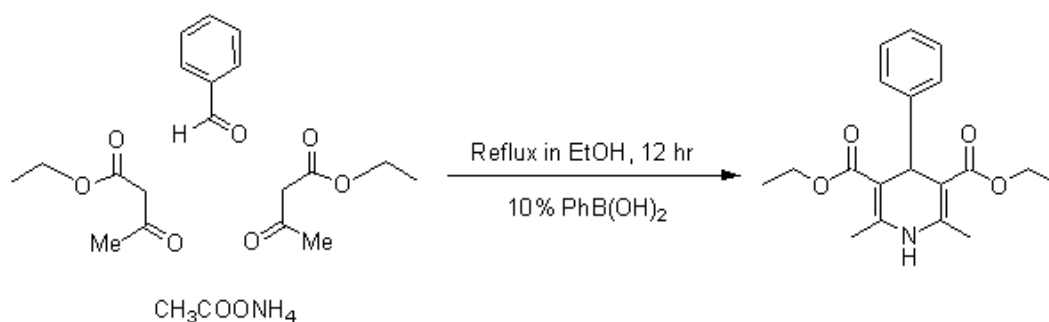


Figure 3.6: Reaction scheme for ZAL\_005

A mixture of benzaldehyde (85 mg, 82  $\mu$ L, 8 mmol), ethyl acetoacetate (208 mg, 202  $\mu$ L, 16 mmol), (NH<sub>4</sub>)<sub>2</sub>OAc (123 mg, 16 mmol) and PhB(OH)<sub>2</sub> (11 mg, 0.8 mmol, 10 mol%) were refluxed in EtOH (10 mL) overnight. The reaction mixture was cooled and the solvent was removed by rotary evaporation. The reaction mixture was then dissolved in EtOAc (~ 10 mL) and poured into cold water (~ 5 mL). The product was extracted with EtOAc (2  $\times$  ~ 15 mL). The organic extract was washed with brine and dried (Na<sub>2</sub>SO<sub>4</sub>), before being filtered and concentrated by rotary evaporation. The product was recrystallised from EtOH and washed with cold EtOH, before being dried *in vacuo*. A yellow solid was yielded (27.4%) with melting point onset at 101.5°C and peak at 107.2°C. TLC R<sub>f</sub> (50% EtOAc/50% pet. ether) = 0.54.

<sup>1</sup>H NMR (400 MHz, d<sub>6</sub>-DMSO):  $\delta$  1.13 (t, 6H, J=7.2, COOCH<sub>2</sub>CH<sub>3</sub>), 2.25

(s, 6H,  $\text{RCC}(\text{H}_3)\text{NHCC}(\text{H}_3)\text{R}$ ), 3.98 (tt, 4H,  $J_A=13.8$ ,  $J_B=3.6$   $2 \times \text{COOCH}_2\text{CH}_3$ ), 4.85 (s, 1H,  $\text{CHCCOOCH}_2\text{CH}_3$ ), 7.09 (tt, 1H,  $J_A=7.2$ ,  $J_B=1.2$ ,  $-\text{CCHCHCHCHCH}-$ ), 7.15 (d, 2H,  $J=6.8$ ,  $-\text{CCHCHCHCHCH}-$ ), 7.18 (d, 2H,  $J=7.2$ ,  $-\text{CCHCHCHCHCH}-$ ), 8.78 (s, 1H, NH).  $^{13}\text{C}$  NMR (100 MHz,  $d_6$ -DMSO):  $\delta$  14.13 ( $2 \times \text{COOCH}_2\text{CH}_3$ ), 18.17 ( $\text{RC}(\text{CH}_3)\text{NHC}(\text{CH}_3)\text{R}$ ), 38.83 ( $\text{ROC}=\text{OC}(\text{R})\text{CH}(\text{Ph})\text{C}(\text{R})\text{C}=\text{OOR}$ ), 58.93 ( $2 \times \text{COOCH}_2\text{CH}_3$ ), 101.82 ( $\text{RC}(\text{CH}_3)\text{NHC}(\text{CH}_3)\text{R}$ ), 125.82, 127.29 and 127.80 (aromatic CH), 145.27 (quaternary C of Ph), 148.12 ( $\text{ROC}=\text{OC}(\text{R})\text{CH}(\text{Ph})\text{C}(\text{R})\text{C}=\text{OOR}$ ), 166.91 ( $\text{ROC}=\text{OC}(\text{R})\text{CH}(\text{Ph})\text{C}(\text{R})\text{C}=\text{OOR}$ ).  $m/z$  (+ve ES-MS) 284.0565 and 285.0565 ( $\text{M}-\text{C}_2\text{H}_5\text{O}$ ).

### 3.6.3 ZAL\_006 – ethyl 5-cyano-4-(2,3-dichlorophenyl)-2,6-dimethyl-1,4-dihydropyridine-3-carboxylate

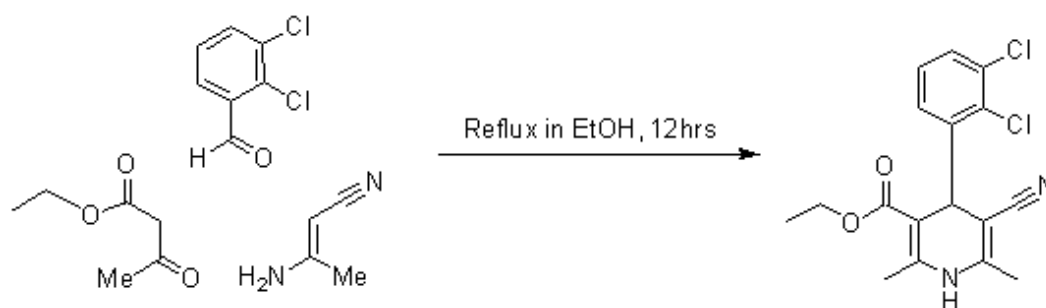


Figure 3.7: Reaction scheme for ZAL\_006

A mixture of 2,3-dichlorobenzaldehyde (525 mg, 3 mmol), ethyl acetoacetate (390 mg, 380  $\mu\text{L}$ , 3 mmol) and 3-aminocrotonitrile (246 mg, 3 mmol) was refluxed in ethanol (30 mL) for 12 hours. The reaction mixture was cooled and the solvent removed by rotary evaporation. The reaction mixture was then dissolved in  $\sim 20$  mL EtOAc, and poured into cold water ( $\sim 25$  mL). The product was extracted with a further 2 portions of EtOAc ( $\sim 20$  mL each). The organic extract was then washed with brine and dried ( $\text{Na}_2\text{SO}_4$ ). The solution was filtered, and concentrated by rotary evaporation. The product was recrystallised from EtOAc and the crystals were washed with cold EtOAc,

and dried in vacuo. A very pale yellow coloured solid was yielded (41%) with melting point onset at 165.3°C and peak at 168.3°C. TLC  $R_f$  (50% EtOAc/50% pet. ether) = 0.26.

$^1\text{H}$  NMR (400 MHz,  $d_6$ -DMSO):  $\delta$  0.94 (t, 3H,  $J=7.2$ ,  $\text{COOCH}_2\text{CH}_3$ ), 1.99 (s, 3H,  $\text{NHC}(\text{CH}_3)\text{CCN}$ ), 2.29 (s, 3H,  $\text{NHC}(\text{CH}_3)\text{CCOOCH}_2\text{CH}_3$ ), 3.85 (m, 2H,  $\text{COOCH}_2\text{CH}_3$ ), 5.15 (s, 1H,  $\text{C}(\text{COOCH}_2\text{CH}_3)\text{CH}(\text{R})\text{C}(\text{CN})$ ), 7.28 (dd, 1H,  $J_A=6.4$ ,  $J_B=1.6$ ,  $-\text{CC}(\text{Cl})\text{C}(\text{Cl})\text{CHCHCH}-$ ), 7.35 (t, 1H,  $J=7.6$ ,  $-\text{CC}(\text{Cl})\text{C}(\text{Cl})\text{CHCHCH}-$ ), 7.50 (dd, 1H,  $J_A=8.0$ ,  $J_B=1.6$ ,  $-\text{CC}(\text{Cl})\text{C}(\text{Cl})\text{CHCHCH}-$ ), 9.25 (s, 1H, NH).  $^{13}\text{C}$  NMR (100 MHz,  $d_6$ -DMSO):  $\delta$  13.70 ( $\text{COOCH}_2\text{CH}_3$ ), 17.37 and 18.20 ( $\text{RC}(\text{CH}_3)\text{NHC}(\text{CH}_3)\text{R}$ ), 59.08 ( $\text{COOCH}_2\text{CH}_3$ ), 99.23 and 99.50 ( $\text{RC}(\text{CH}_3)\text{NHC}(\text{CH}_3)\text{R}$ ), 128.68, 128.75 and 128.90 ( $-\text{CC}(\text{Cl})\text{C}(\text{Cl})\text{CHCHCH}-$ ), 129.08 and 131.47 ( $-\text{CCCICICICHCHCH}-$ ), 146.74 ( $\text{RCN}$ ), 146.83 ( $\text{RC}(\text{CN})\text{R}'$ ), 146.88 ( $-\text{CCCICICICHCHCH}-$ ), 147.23 ( $\text{CC}=\text{OOC}_2\text{H}_5$ ), 165.97 ( $\text{CC}=\text{OOC}_2\text{H}_5$ ). HRMS (ESI+):  $m/z$   $[\text{M}+\text{H}]^+$  calcd for  $\text{C}_{17}\text{H}_{16}\text{Cl}_2\text{N}_2\text{O}_2$  351.0667, found 350.8992.

### 3.6.4 ZAL\_007 – diethyl 4-(2,3-dichlorophenyl)-2,6-dimethyl-1,4-dihydropyridine-3,5-dicarboxylate

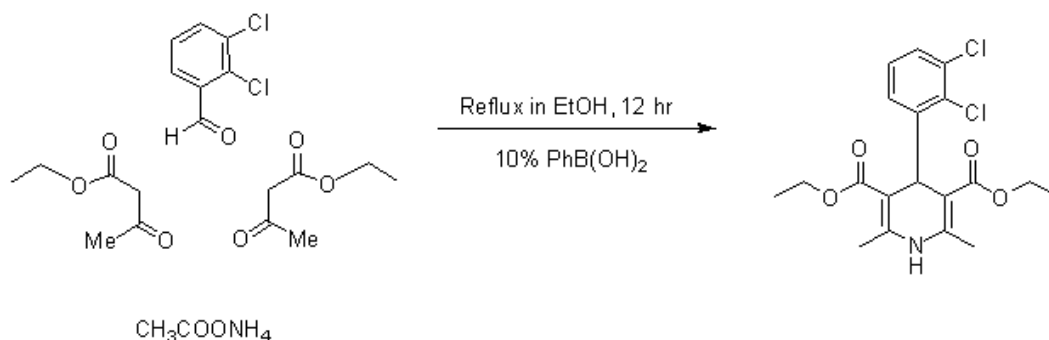


Figure 3.8: Reaction scheme for ZAL\_007

2,3-Dichlorobenzaldehyde (525 mg, 3 mmol), ethyl acetoacetate (781 mg, 759  $\mu\text{L}$ , 6 mmol), ammonium acetate (462 mg, 6 mmol) and  $\text{PhB}(\text{OH})_2$  (36 mg, 0.3 mmol, 10 mol%) were refluxed in EtOH (30 mL) for 12 hours. The reaction mixture was cooled

and the solvent removed by rotary evaporation. The product was dissolved in ethyl acetate ( $\sim 20$  mL) and poured into cold water ( $\sim 20$  mL). The product was extracted with further portions of EtOAc ( $2 \times \sim 20$  mL). The organic extract was washed with brine, dried ( $\text{Na}_2\text{SO}_4$ ) and filtered. The solvent was removed from the product by rotary evaporation and a recrystallisation from EtOH was attempted. However, this was unsuccessful as a viscous yellow oil was obtained that was found to be a mixture of products by TLC with  $R_f$  values of 0.46 and 0.66 (50% EtOAc/50% pet. ether). NMR and MS also confirmed that the oil was a mixture of compounds.

The mixture was separated by flash column chromatography. The column was primed with 100% pet. ether., and then eluted sequentially with 450 mL 10% (v/v) ethyl acetate in pet. ether, 20 mL 20% (v/v) ethyl acetate in pet. ether, and 100 mL 50% (v/v) ethyl acetate in pet. ether. A total of 33 fractions were isolated; fractions 1-8 containing the product with TLC  $R_f$  of 0.66 were combined (A), fractions 9-13 contained a mixture of products, and fractions 14-33 containing the product with TLC  $R_f$  of 0.46 were combined (C). Fractions A and C were dried *in vacuo* and samples analysed by NMR and MS. Fraction C was shown to be the desired product which had been successfully purified to yield a light-yellow solid (53%) with melting point onset at  $123.2^\circ\text{C}$  and peak at  $127.2^\circ\text{C}$ .

$^1\text{H}$  NMR (400 MHz,  $\text{d}_6\text{-DMSO}$ ):  $\delta$  1.07 (t, 6H,  $J=7.0$ ,  $2 \times \text{COOCH}_2\text{CH}_3$ ), 2.23 (s, 6H,  $\text{C}(\text{CH}_3)\text{NHC}(\text{CH}_3)$ ), 3.95 (qd, 4H,  $J_A=7.0$ ,  $J_B=3.2$ ,  $2 \times \text{COOCH}_2\text{CH}_3$ ), 5.31 (s, 1H,  $\text{C}(\text{COOCH}_2\text{CH}_3)\text{CH}(\text{R})\text{C}(\text{COOH}_2\text{CH}_3)$ ), 7.23 (t, 1H,  $J=7.8$ , -CCCICCHCHCH-), 7.30 (dd, 1H,  $J_A=7.8$ ,  $J_B=1.8$ , -CCCICCHCHCH-), 7.37 (dd, 1H,  $J_A=7.8$ ,  $J_B=1.8$ , -CCCICCHCHCH-), 8.86 (s, 1H, NH).  $^{13}\text{C}$  NMR (100 MHz,  $\text{d}_6\text{-DMSO}$ ):  $\delta$  14.08 ( $2 \times \text{COOCH}_2\text{CH}_3$ ), 18.11 ( $\text{RC}(\text{CH}_3)\text{NHC}(\text{CH}_3)\text{R}$ ), 38.04 ( $\text{ROC}=\text{OC}(\text{R}')\text{C}(\text{R}'')\text{C}(\text{R}')\text{C}=\text{OOR}$ ), 58.93 ( $\text{COOCH}_2\text{CH}_3$ ), 101.53 ( $\text{RC}(\text{CH}_3)\text{NHC}(\text{CH}_3)\text{R}$ ), 127.91, 128.03 and 129.46 (-CCCICCHCHCH-), 129.71 and 131.31 (-CCCICCHCHCH-), 145.62 (-CCCICCHCHCH-), 148.93 ( $2 \times \text{CC}=\text{OOR}$ ), 166.68 ( $2 \times \text{CC}=\text{OOR}$ ). HRMS (ESI+):  $m/z$   $[\text{M}+\text{H}]^+$  calcd for  $\text{C}_{19}\text{H}_{21}\text{Cl}_2\text{NO}_4$

396.0769, found 397.8366.

### 3.6.5 ZAL\_008 – 4-(2,3-dichlorophenyl)-2,6-dimethyl-1,4-dihydropyridine-3,5-dicarbonitrile

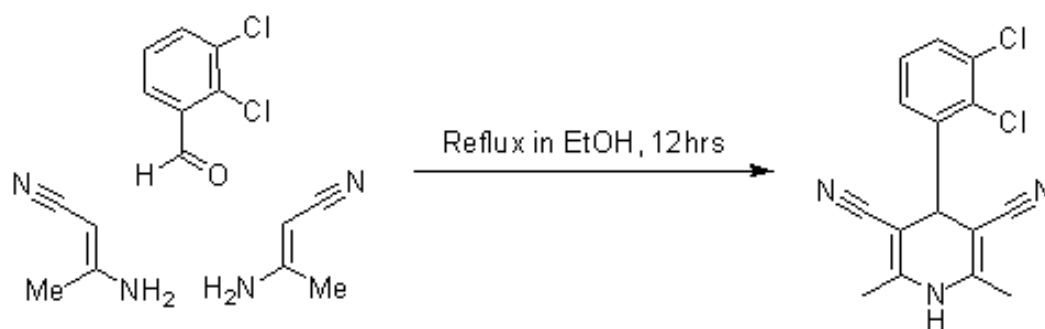


Figure 3.9: Reaction scheme for ZAL\_008

A mixture of 2,3-dichlorobenzaldehyde (525 mg, 3 mmol) and 3-aminocrotonitrile (781 mg, 6 mmol) were refluxed in ethanol (30 mL) for 12 hrs. TLC in 50% pet. ether: 50% ethyl acetate was used to monitor the reaction progress.

The reaction mixture was cooled and the solvent removed by rotary evaporation to obtain a solid. This was dissolved in ~ 30 mL ethyl acetate, and poured into cold water (~ 30 mL), prior to extraction via separation. Extraction was completed with a further 2 portions of EtOAc (~ 30 mL each). The combined organic extracts (which contained solid material) was then washed with brine. Further EtOAc (~ 25 mL) and DCM (~ 10 mL) was added to the organic extracts in an attempt to dissolve any remaining solids. TLC was carried out to confirm that the product was present in the organic phase, as there were still some solids present in the combined extracts. The solution was then dried over Na<sub>2</sub>SO<sub>4</sub> and then filtered, before being concentrated by rotary evaporation to yield a solid residue.

The product was suspended in 50% EtOAc: 50% pet. ether (~30 mL with gentle heating and sonication), and the suspension was left to settle for several hours. The supernatant was then removed, and the resultant solid was washed with EtOAc.



The product was then dried in vacuo. A white solid precipitate was yielded (59.7%) with melting point onset at 251.7°C and peak at 255.4°C.

$^1\text{H}$  NMR (400 MHz, d6-DMSO):  $\delta$  2.03 (s, 6H,  $2 \times \text{CH}_3$ ), 5.05 (s, 1H,  $\text{C}(\text{CN})\text{CHC}(\text{CN})$ ), 7.45 (m, 2H,  $-\text{CCCICCHCHCH}-$ ), 7.64 (dd, 1H,  $J_A=6.8$ ,  $J_B=2.8$ ,  $-\text{CC}(\text{Cl})\text{C}(\text{Cl})\text{CHCHCH}-$ ), 9.66 (s, 1H, NH).  $^{13}\text{C}$  NMR (100 MHz, d6-DMSO):  $\delta$  17.69 ( $2 \times \text{CH}_3$ ), 21.53 ( $2 \times \text{CCH}_3$ ), 81.11 ( $\text{NCC}(\text{R})\text{C}(\text{Ph})\text{C}(\text{R})\text{CN}$ ), 118.69 ( $\text{NCC}(\text{R})\text{C}(\text{Ph})\text{C}(\text{R})\text{CN}$ ), 128.99, 129.81 and 130.04 (Aromatic CH), 132.22 (Aromatic CCl), 143.081H ( $-\text{CCCICCHCHCH}-$ ), 147.76 ( $\text{NCC}(\text{R})\text{C}(\text{Ph})\text{C}(\text{R})\text{CN}$ ). m/z (+ve ES-MS) 320.9346 and 322.9304 ( $\text{M}+\text{H}_2\text{O}$ ).

### 3.6.6 ZAL\_009 – ethyl 5-cyano-2,6-dimethyl-4-phenyl-1,4-dihydropyridine-3-carboxylate

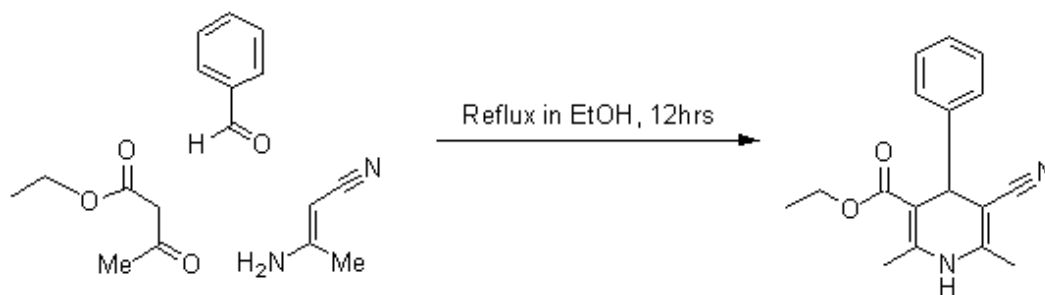


Figure 3.10: Reaction scheme for ZAL\_009

Benzaldehyde (212 mg, 204  $\mu\text{L}$ , 6 mmol), ethyl acetoacetate (781 mg, 759  $\mu\text{L}$ , 6 mmol) and 3-aminocrotonitrile (493 mg, 6 mmol) were refluxed in ethanol (45 mL) for 12 hours. The reaction mixture was cooled and concentrated *in vacuo*. The product was dissolved in ethyl acetate ( $\sim 30$  mL) and poured into cold water ( $\sim 25$  mL). The product was extracted with further portions of ethyl acetate ( $2 \times \sim 30$  mL). The organic extracts were washed with brine, dried ( $\text{Na}_2\text{SO}_4$ ) and filtered. TLC (50% EtOAc/50% pet. ether) showed that the organic extracts contained a mixture of compounds. Therefore, the material was purified using flash column chromatography. The fractions containing

the product were identified, and once they were combined, the solvent was removed by rotary evaporation, and the resultant light-yellow solid was dried in vacuo. Yield = 8%; melting point onset at 166.0°C and peak at 169.4°C.

$^1\text{H}$  NMR (400 MHz,  $\text{d}_6\text{-DMSO}$ ):  $\delta$  1.03 (t, 3H,  $\text{J}=7.0$ ,  $\text{COOCH}_2\text{CH}_3$ ), 2.02 (s, 3H,  $\text{NHC}(\text{CH}_3)\text{CCOOHCH}_2\text{CH}_3$ ), 2.27 (s, 3H,  $\text{NHC}(\text{CH}_3)\text{C}(\text{CN})$ ), 3.91 (qd, 2H,  $\text{J}_\text{A}=7.0$ ,  $\text{J}_\text{B}=2.8$ ,  $\text{COOCH}_2\text{CH}_3$ ), 4.45 (s, 1H,  $\text{C}(\text{COOCH}_2\text{CH}_3)\text{CH}(\text{R})\text{C}(\text{CN})$ ), 7.16 (d, 2H,  $\text{J}=7.6$ ,  $-\text{CCHCHCHCHCH}-$ ), 7.21 (dt, 1H,  $\text{J}_\text{A}=7.6$ ,  $\text{J}_\text{B}=1.4$ ,  $-\text{CCHCHCHCHCH}-$ ), 7.30 (t, 2H,  $\text{J}=7.4$ ,  $-\text{CCHCHCHCHCH}-$ ), 9.15 (s, 1H, NH).  $^{13}\text{C}$  NMR (100 MHz,  $\text{d}_6\text{-DMSO}$ ):  $\delta$  13.91 ( $\text{COOCH}_2\text{CH}_3$ ), 17.41 ( $\text{ROC}=\text{OC}(\text{R}')\text{C}(\text{CH}_3)\text{NH}$ ), 18.28 ( $\text{NC}(\text{R}')\text{C}(\text{CH}_3)\text{NH}$ ), 40.75 ( $\text{ROC}=\text{OC}(\text{R}')\text{C}(\text{Ph})\text{C}(\text{R}'')\text{CN}$ ), 59.07 ( $\text{COOCH}_2\text{CH}_3$ ), 99.82 ( $\text{C}(\text{CH}_3)\text{NHC}(\text{CH}_3)$ ), 126.68, 127.10 and 128.37 (Aromatic CH), 145.37 ( $\text{C}(\text{R})\text{CN}$ ), 146.30 ( $\text{C}(\text{R})\text{CN}$ ), 146.39 ( $-\text{CCHCHCHCHCH}-$ ), 147.45 ( $\text{CCOOC}_2\text{H}_5$ ), 166.48 ( $\text{CCOOC}_2\text{H}_5$ ).  $m/z$  (+ve ES-MS) 239.0427, 241.0355 and 242.0631 ( $\text{M}-\text{C}_2\text{H}_5\text{O}$ ).

### 3.6.7 ZAL\_010 – 2,6-dimethyl-4-phenyl-1,4-dihydropyridine-3,5-dicarbonitrile

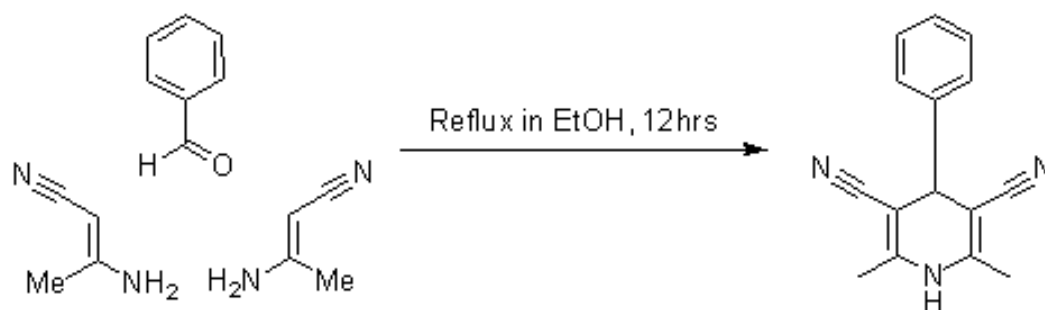


Figure 3.11: Reaction scheme for ZAL\_010

Benzaldehyde (212 mg, 204  $\mu\text{L}$ , 6 mmol) and 3-aminocrotonitrile (985 mg, 12 mmol) were refluxed in ethanol (45 mL) for 12 hours. The reaction mixture was cooled and concentrated *in vacuo*. The product was dissolved in ethyl acetate ( $\sim 30$  mL) and poured into cold water ( $\sim 25$  mL). The product was extracted with further portions

of ethyl acetate ( $2 \times \sim 30$  mL). The organic extracts were washed with brine, dried ( $\text{Na}_2\text{SO}_4$ ) and filtered. TLC (50% EtOAc/50% pet. ether) showed that the organic extracts contained a mixture of compounds. Therefore, the material was purified using flash column chromatography. The fractions containing the product were identified, and once they were combined, the solvent was removed by rotary evaporation, and the resultant white solid was dried in vacuo. Yield = 12%; melting point onset at  $95.9^\circ\text{C}$  and peak at  $104.4^\circ\text{C}$ .

$^1\text{H}$  NMR (400 MHz,  $\text{d}_6\text{-DMSO}$ ):  $\delta$  2.04 (s, 6H,  $2 \times \text{CH}_3$ ), 3.90 (s, 1H,  $\text{NH}$ ), 4.39 (s, 1H,  $\text{C}(\text{CN})\text{CHC}(\text{CN})$ ), 7.28 (d, 2H,  $J=7.6$ ,  $-\text{CCHCHCHCHCH}-$ ), 7.32 (d, 1H,  $J=7.2$ ,  $-\text{CCHCHCHCHCHCH}-$ ), 7.40 (t, 2H,  $J=7.4$ ,  $-\text{CCHCHCHCHCHCH}-$ ).  $^{13}\text{C}$  NMR (100 MHz,  $\text{d}_6\text{-DMSO}$ ):  $\delta$  17.72 ( $\text{C}(\text{CH}_3)\text{NHC}(\text{CH}_3)$ ), 18.85 ( $\text{C}(\text{CH}_3)\text{NHC}(\text{CH}_3)$ ), 40.96 ( $\text{NCC}(\text{R})\text{C}(\text{Ph})\text{C}(\text{R}')\text{CN}$ ), 119.21 ( $\text{NCC}(\text{R})\text{C}(\text{Ph})\text{C}(\text{R})\text{CN}$ ), 127.58, 127.61 and 128.77 (Aromatic CH), 146.67 ( $\text{NCC}(\text{R})\text{C}(\text{Ph})\text{C}(\text{R})\text{CN}$ ), 163.14 ( $-\text{CCHCHCHCHCHCH}-$ ). HRMS (ESI+):  $m/z$   $[\text{M}+\text{H}]^+$  calcd for  $\text{C}_{15}\text{H}_{13}\text{N}_3$  236.1188, found 236.1055.

### 3.6.8 ZAL\_011 – diethyl 4-(2,3-dichlorophenyl)-1,2,6-trimethyl-4H-pyridine-3,5-dicarboxylate

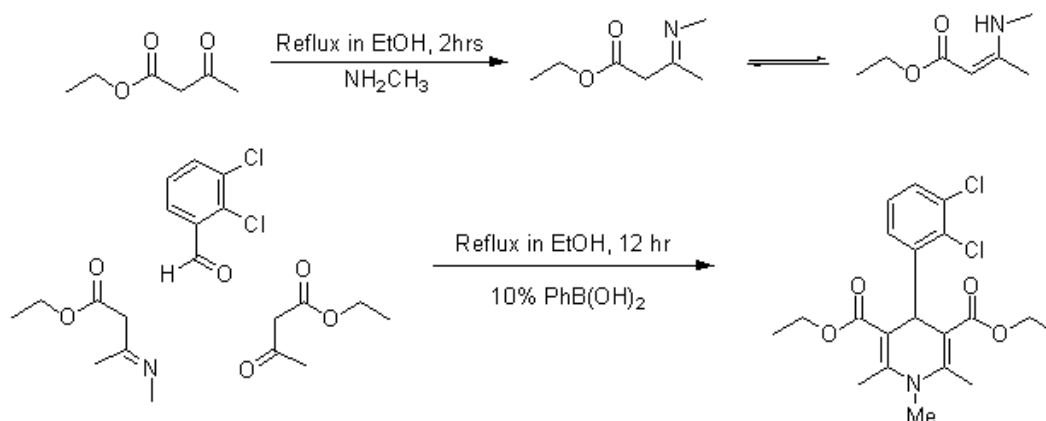


Figure 3.12: Reaction scheme for ZAL\_011

### Synthesis of (E)-ethyl 3-(methylimino)butanoate Intermediate

Ethyl acetoacetate (3.120 g, 3033  $\mu\text{L}$ , 24 mmol) and N-methylamine (2.150 g, 4976  $\mu\text{L}$  of 40% aqueous solution, 58 mmol) were stirred together in ethanol (45 mL) at room temperature for 30 minutes. The reaction mixture was concentrated *in vacuo*, and the product was then dissolved in ethyl acetate ( $\sim 30$  mL) before it was poured into cold water ( $\sim 25$  mL). The product was extracted with further portions of ethyl acetate ( $2 \times \sim 30$  mL). The organic extracts were washed with brine, dried ( $\text{Na}_2\text{SO}_4$ ) and filtered to yield the intermediate was yielded (2.72 g, 79.1%).

### Product Synthesis

**Without catalyst:** The intermediate (ethyl 3-(methylimino)butanoate, 1.385 g, 9.7 mmol), 2,3-dichlorobenzaldehyde (1.705 g, 9.7 mmol) and ethyl acetoacetate (1.265 g, 1229  $\mu\text{L}$ , 9.7 mmol) were refluxed in ethanol (100 mL) overnight. The reaction mixture was cooled to room temperature and concentrated *in vacuo*.

The residue was partitioned between EtOAc (30 mL) and cold  $\text{H}_2\text{O}$  (25 mL). The phases were separated and the aqueous phase was extracted twice with EtOAc ( $2 \times 30$  mL). The combined organic fractions were washed with brine, dried over  $\text{Na}_2\text{SO}_4$  and filtered. TLC (50% EtOAc/50% pet. ether) showed that the organic extracts contained a mixture of compounds. Therefore, the material was purified using flash column chromatography. The fractions containing the product were identified, and once they were combined, the solvent was removed by rotary evaporation, and the resultant yellow crystalline solid (0.50 g, 14.7%), with melting point onset at  $101.5^\circ\text{C}$  and peak at  $108.0^\circ\text{C}$ , was dried *in vacuo*.

**With catalyst:** The intermediate (ethyl 3-(methylimino)butanoate, 1.193 g, 8.3 mmol), 2,3-dichlorobenzaldehyde (1.459 g, 8.3 mmol), ethyl acetoacetate (1.080 g, 1049  $\mu\text{L}$ , 8.3 mmol) and  $\text{PhB}(\text{OH})_2$  catalyst (103 mg, 0.83 mmol, 0.10 mol%) were refluxed in ethanol (100 mL) overnight. The reaction mixture was cooled to room temperature

and the work-up was the same as for the uncatalysed reaction detailed above (1.25 g, 31.1%).

$^1\text{H}$  NMR (400 MHz, d6-DMSO):  $\delta$  1.23 (t, 6H,  $J=7.2$ ,  $2 \times \text{COOCH}_2\text{CH}_3$ ), 2.42 (s, 6H,  $\text{C}(\text{CH}_3)\text{N}(\text{Me})\text{C}(\text{CH}_3)$ ), 3.23 (s, 3H,  $\text{NCH}_3$ ), 4.12 (tt, 4H,  $J_A=12.8$ ,  $J_B=3.6$ ,  $2 \times \text{COOCH}_2\text{CH}_3$ ), 5.58 (s, 1H,  $\text{C}_2\text{H}_5\text{OC}=\text{OC}(\text{R})\text{CH}(\text{R}')\text{C}(\text{R})\text{C}=\text{OOC}_2\text{H}_5$ ), 7.05 (m, 2H,  $-\text{CCHCHCHCCICCI}-$ ), 7.24 (dd, 1H,  $J_A=7.4$ ,  $J_B=2.2$ ,  $-\text{CCHCHCHCHCCICCI}-$ ).  $^{13}\text{C}$  NMR (100 MHz, d6-DMSO):  $\delta$  14.08 ( $2 \times \text{COOCH}_2\text{CH}_3$ ), 16.07 ( $\text{C}(\text{CH}_3)\text{NHC}(\text{CH}_3)$ ), 33.73 ( $\text{NCH}_3$ ), 37.52 ( $\text{C}_2\text{H}_5\text{OC}=\text{OC}(\text{R})\text{CH}(\text{R}')\text{C}(\text{R})\text{C}=\text{OOC}_2\text{H}_5$ ), 59.44 ( $2 \times \text{COOCH}_2\text{CH}_3$ ), 104.25 ( $\text{C}(\text{CH}_3)\text{NHC}(\text{CH}_3)$ ), 128.26, 128.38 and 129.09 (Aromatic CH), 131.49 ( $-\text{CCHCHCHCHCCICCI}-$ ), 138.45 ( $-\text{CCHCHCHCHCCICCI}-$ ), 146.62 ( $-\text{CCHCHCHCHCCICCI}-$ ), 148.85 ( $2 \times \text{C}(\text{R})\text{C}=\text{OOC}_2\text{H}_5$ ), 167.15 ( $2 \times \text{C}(\text{R})\text{C}=\text{OOC}_2\text{H}_5$ ). HRMS (ESI+):  $m/z$   $[\text{M}+\text{H}]^+$  calcd for  $\text{C}_{20}\text{H}_{23}\text{Cl}_2\text{NO}_4$  412.1082, found 411.7990.

### 3.7 Results and Discussion

By comparing the results of the syntheses detailed above with the original list of analogue targets, it is possible to determine the overall level of success of the syntheses.

The first compound to be identified as a sythentic target was the aromatised felodipine analogue, in which the dihydropyridine is oxidised to produce a pyridine. The planned synthesis using CAN was a very straightforward one-pot method, which was successful on the first attempt. Using this method the pyridine product (ZAL\_001) was succesfully produced in high yields of up to 93%. A potential issue that may arise in subsequent experiments with this compound is that it is an oil at room temperature. However, it may be that after sufficient time this compound may crystallise, though this did not occur during the course of this study.

A partial oxidation of felodipine was also attempted, in which the same CAN reagent was used in conjunction with sodium bromate in acetonitrile with the aim of yielding two oxidation by-products. TLC was used to follow the progress of this synthesis, which again, was a straightforward, one-pot method. However, rather than TLC

revealing the evolution of three products (the pyridine and two oxidation by-products), five compounds were seen to be produced, all with very similar  $R_f$  values. It is apparent from the molecular structure of the felodipine that the five products seen on the TLC plate have arisen as a result of the asymmetry of the felodipine starting compound (see figure 3.2). Despite attempts at purification using flash column chromatography with a number of different solvent systems and solvent gradients, it proved very difficult to separate the products, especially as they formed in small amounts. It was thought that a potential solution that would facilitate an easier separation of the compounds in better yields, was to use a starting material with ester chains of the same length.

The diethyl ester analogue of felodipine was successfully obtained from a one-pot Hantzsch synthesis followed by purification by flash column chromatography as a light yellow solid in yields up to 53% (ZAL\_007). Whilst this yield was not particularly high, it is the author's opinion that this is largely due to losses during separation by flash chromatography, as TLC monitoring during the reaction indicated an exhaustion of the starting materials. Therefore, should this reaction be repeated with more care taken at the purification stage, the yield may be improved. As the diethyl ester analogue is a symmetrical analogue of felodipine, a portion of ZAL\_007 was taken forward for use in a repeat attempt to synthesise the oxidation by-products. Due to the symmetry of the starting compound, it was thought that this would yield only three products as opposed to the five that appeared to have been produced in the previous synthetic attempt from felodipine. Reaction monitoring by TLC showed only 3 products as predicted, but again the  $R_f$  values for the compounds were very close, and despite careful solvent choice and consideration of solvent gradients for flash column chromatography, it once again proved difficult to completely separate the compounds in meaningful yields. No further attempts to produce the oxidation by-products were made.

The N-methyl analogue was the next target that was identified, and synthesis of this compound was anticipated to be a facile and reasonably high-yielding reaction of felodipine first by deprotonation with potassium hydroxide and then alkylation with

methyl iodide in DMF. However, initial attempts at producing the N-methyl derivative via this method proved to be more tricky than expected, and the reason for this was believed to be due to the need for strictly anhydrous conditions, which were difficult to maintain. Whilst it was possible that the anhydrous conditions and therefore the yield might be improved with continued attempts using this method, it was considered more prudent to attempt an alternative method of synthesis. The Hantzsch dihydropyridine synthesis had already proved to work in the production of the diethyl ester ZAL\_007, and a modified version of this synthetic pathway was proposed in the synthesis of the N-methyl analogue, whereby the ammonium acetate is replaced with N-methylamine. Initially a one-pot synthesis was attempted, but it became apparent that side-reactions of the methylamine with the dichlorobenzaldehyde were occurring, which led to a reduction in the yield of the desired product, and also would have necessitated an additional purification step. Therefore, the reaction protocol was adapted so that the ethyl acetoacetate and N-methylamine were reacted first to produce an iminoester intermediate, which was isolated prior to addition of 2,3-dichlorobenzaldehyde to enable formation of the 1,4-dihydropyridine. Once the intermediate had been isolated, it was divided and taken forward in two separate concurrent reactions; one containing 0.10 mol% PhB(OH)<sub>2</sub> catalyst, and the other without the catalyst. The use of the Hantzsch reaction method was shown to be successful, and produced the N-methyl analogue ZAL\_011 in better yields. It was also shown that use of the catalyst was successful in aiding the progression of the reaction, as the reaction in which the catalyst was used yielded 31% product compared to 15% in the reaction without the catalyst. Because the N-methyl was produced using a two-step Hantzsch synthesis, rather than via the originally proposed method using potassium hydroxide and methyl iodide, ZAL\_011 differs from the target N-methyl compound in that the ester groups are the same length, as it was determined that synthesis of this product would be more straightforward.

The diethyl ester analogue, ZAL\_007 has already been shown to be successfully made using the Hantzsch dihydropyridine synthesis, and so the same method was used

to produce the des-chloro analogue which was the next target compound that had been identified. The one-pot synthesis was used, as there was no requirement to isolate an intermediate as was the case for the N-methyl analogue, and benzaldehyde was used instead of 2,3-dichlorobenzaldehyde. ZAL\_005 was produced in low yields of up to 17% as a yellow solid. It is thought that these low yields could partially be attributed to losses that occur during the recrystallisation stage, but due to the scale that the synthesis of this compound was carried out on, over 600 mg of the des-chloro ZAL\_005 material was produced, which was considered to be enough for subsequent experiments. Again, the ester chains in this compound were of the same length, unlike in felodipine, as this was a simpler approach that would prevent the formation of additional side-products during the Hantzsch synthesis.

The final compound on the list of synthetic targets was the nitrile ester compound. Again, this compound (ZAL\_006) was made using the one-pot Hantzsch dihydropyridine synthesis which had previously shown to be successful in producing the diethyl ester, and des-chloro analogues. However, instead of using two equivalents of ethyl acetoacetate in the synthesis, one molar equivalent of the ethyl acetoacetate was replaced with one molar equivalent of 3-aminocrotonitrile. This synthesis was more successful than that of ZAL\_005 as the light yellow solid resulting from this reaction was yielded in higher amounts of up to 38%, but again, it is believed that the yield of ZAL\_006 could be improved upon if losses incurred during recrystallisation were further minimised. Inspection of the reaction scheme indicated the possibility that a number of by-products could have been produced due to the presence of two different enolates in the reaction mixture, which would also explain the reduced yield of the desired product. However, TLC of the reaction mixture prior to work-up, and NMR of the recrystallised product, indicated that this was not the case.

It is possible to see from comparing the results of these syntheses with the original list of target analogues, that all of the compounds except the two oxidation by-products were successfully produced in some form. The aromatised (ZAL\_001), diethyl ester



(ZAL\_007) and nitrile ester (ZAL\_006) analogues all had the same molecular structure as the target compounds listed at the outset of the synthesis work. On the other hand, as a result of using the Hantzsch dihydropyridine synthesis, the N-methyl (ZAL\_011) and the des-chloro (ZAL\_005) analogues were both diethyl esters unlike the target molecules, which had been based directly on the asymmetrical felodipine compound. Despite some low-yielding reactions, the Hantzsch dihydropyridine synthesis was shown to be a facile method that led to the successful production of the products required; hence this method was used to synthesise three extra compounds that had not been identified in the original list of targets.

The first of these additional compounds to be synthesised was ZAL\_008, which was a dinitrile analogue of felodipine. This white solid was readily produced, and began to precipitate from the reaction mixture. This led to some issues with extraction of the compound from the reaction mixture as extra organic solvent was required to get the product into solution, and some of the solid was still present in the organic extracts so that when the mixture was dried, and then filtered it is very likely that a portion of the product was lost. Despite this, the compound was still recovered in yields of up to 60%.

The final two compounds to be synthesised were des-chloro versions of both the mono- and di-nitrile analogues. The des-chloro mono-nitrile compound (ZAL\_009), was a light yellow solid produced in a very low yield of 8%, and the dinitrile (ZAL\_010) was a white solid produced with a marginally better yield of 12%. Only one batch of each of these compounds was synthesised, but both were purified by flash column chromatography, and it is possible that the yield of both could be significantly improved by taking more care to prevent losses at this stage. Also, carrying out these reactions in two steps, whereby the aldehyde is initially reacted with one enolate, before the other reagents are added may reduce the potential for side reactions to occur, and thus improve the yields.

Table 3.1: Summary of the compounds synthesised.

Analogue	Total amount of compound available for subsequent experiments
ZAL_001	352 mg
ZAL_005	669 mg
ZAL_006	1269 mg
ZAL_007	385 mg
ZAL_008	870 mg
ZAL_009	142 mg
ZAL_010	156 mg
ZAL_011	1748 mg

### 3.8 Conclusions

Eight analogues of felodipine were successfully synthesised for use in experiments to investigate the influence of molecular structure on the formation of good solid dispersions as will be described in the following chapters. These analogues were synthesised with yields ranging from a poor 8% to a more successful 93%, leading to varying amounts of material available for use in subsequent chapters (see table 3.1). This is important to note, as the limited amounts of some compounds directly impacts on the number of experiments that can be carried out, and careful planning is needed to get the most out of each analogue.

### 3.9 Future work

In order to further investigate the effect of drug molecular structure on the successful formation of solid dispersions, there is almost an infinite number of modifications that can be made to the felodipine compound. However, the scope of any future work should initially be limited to the following suggestions.

As the reaction in which the 1,4-dihydropyridine was oxidised to the pyridine

ZAL\_001 using CAN was so successful, the first suggestion for future work would be to also carry out this oxidation on the other analogues that had been synthesised, as well as any additional analogues that may be produced. With the capacity of the nitrogen to be a hydrogen bond donor removed from all of the analogues, it may enable a better understanding of the influence of other functional group modifications on the intermolecular interactions between the polymer and drug compound in subsequent experiments.

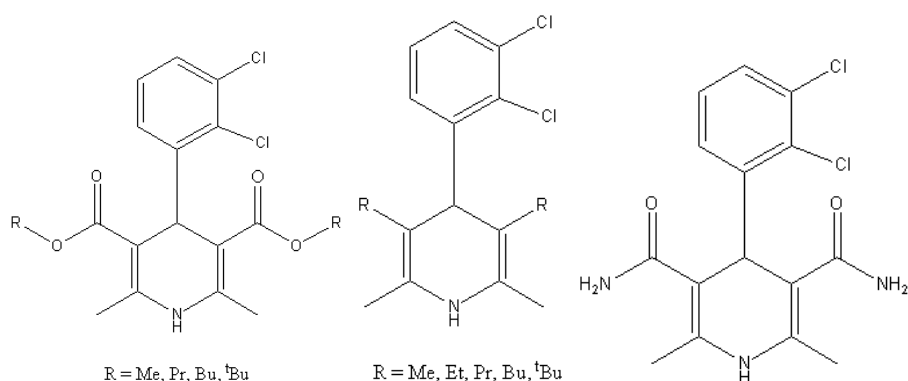


Figure 3.13: Potential targets in future syntheses of additional felodipine analogues, including a) analogues with modified ester chain length, b) analogues with alkyl chains of varying lengths instead of esters, and c) analogues with amide substituents.

The next adaptations to the felodipine molecule should be focussed around the side chains on carbons 3 and 5 of the dihydropyridine. The diethyl ester has already been produced in this work, but it may also be of value to synthesise the dimethyl ester. Furthermore, the alkyl chains could be lengthened to a propyl, butyl or tertiary butyl group (figure 3.13a). As well as altering the length of the ester side chains, it may also prove valuable to synthesise analogues which have alkyl chains without the preceding ester moieties (figure 3.13b). Whilst synthesis of these analogues using the one-pot Hantzsch dihydropyridine method would require the two side chains to be of equal length for greater chance of success, it may be possible to explore a 2-step synthetic pathway that would enable asymmetrical analogues to be made with several combinations of side

chains. The lengthened side chains would increase steric bulk around the drug molecule, and hence the effect of increased drug lipophilicity on solid dispersion formation could be investigated using these analogues. Similarly, lengthening the alkyl groups at carbons 2 and 6 of the DHP would also increase steric bulk. An additional series of analogues that may also be of interest are the amides that could be formed by gentle hydrolysis of the nitrile analogues ZAL\_006, ZAL\_008, ZAL\_009 and ZAL\_010 (figure 3.13c).

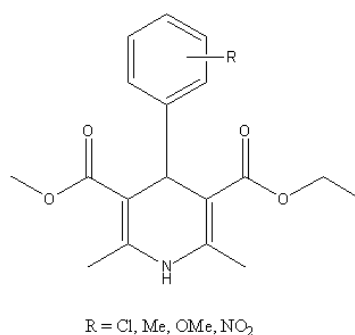


Figure 3.14: Potential targets in future syntheses of additional felodipine analogues in which the phenyl ring substituents have been changed or placed at different ring positions.

Another significant area of the felodipine molecule for modification is the substitutions on the phenyl ring. Compounds ZAL\_005, ZAL\_009 and ZAL\_010 have already been produced to explore the impact that removing the chlorine groups might have on the formation of solid dispersions with copovidone, however, no further alterations were made to the analogues in terms of either phenyl substituent position or functionality. Therefore it may be of relevance to synthesise analogues with methyl, methoxy or nitro substituents at different ring positions (figure 3.14). These analogues could be easily produced using the one-pot Hantzsch dihydropyridine synthesis using commercially available substituted benzaldehydes.

## **Chapter 4**

# **Solid State Analysis of Solid Dispersions**

### **4.1 Introduction**

As discussed in Chapter 1, the term solid dispersion can actually have several meanings in terms of the solid-state structure of the material. In this work, the aim was to produce fully amorphous material in which the drug compound is molecularly dispersed throughout the polymer; i.e. 'a solid solution'.

There are a number of potential methods for preparing amorphous solid dispersions as was highlighted in Chapter 1. However, because of the limited availability of drug compound, for this project the main focus has been on using a solvent casting method with an additional annealing step. In this method the drug compound and the polymer are co-dissolved in an appropriate solvent, which is then evaporated resulting in the formation of a coprecipitate containing both the drug and polymer. For the samples produced in this study, the production of a drug/polymer solution was often used as a vehicle to deposit the solid dispersion material in a suitable vessel or on a substrate, and the evaporation step in some instances of sample preparation may be too slow to ensure the material was amorphous. Therefore the samples were always annealed above

the melting points of the drug and polymer components, and quench cooled to room temperature. This step also served to ensure that there was essentially no solvent remaining in the sample that could act as a plasticiser, or in any other way influence the properties of what was assumed to be a two-component system. This method was also used to render samples of crystalline drug amorphous for control experiments.

A series of spray dried solid dispersion samples was also prepared for specific use in dissolution experiments detailed in Chapter 6. The preparation, and solid state analysis of the freshly prepared materials will be discussed in this chapter, and attempts will be made to compare the structure of the material produced using this method with film-cast samples.

The underlying hypothesis for the work in this thesis is that there are intermolecular interactions between the drug and polymer compounds in a solid dispersion that determine the properties and performance of that solid dispersion. Therefore, if this is true, it would seem to follow that the drug to polymer ratio of the solid dispersions would also directly correlate with their properties and performance. This is because there would be more or less of these intermolecular interactions depending on the relative amounts of the two components in the solid dispersion. To test this, the solid dispersions throughout this work have been produced with a range of drug loadings of 5% - 50% w/w.

This chapter will focus on the solid state analysis of freshly prepared solid dispersions of felodipine and the molecular analogues with copovidone, in a range of drug loadings. The aims of the work detailed in this chapter were to use a range of analytical methods to:

1. determine if solid dispersions formed were amorphous.
2. determine if any solid dispersions formed were molecular dispersions.

## 4.2 Materials

Felodipine (Batch 16101) was used as supplied by AstraZeneca. Copovidone (Kollidon VA64, Lot 85392236WO) was used as supplied by BASF (Ludwigshafen, Germany)[98]. Molecular analogues of Felodipine were used as synthesised in Chapter 3. All solvents were used as supplied by Fisher Scientific (Loughborough, UK)

### 4.2.1 Preparation of Solid Dispersion Samples

#### Film-Cast Felodipine Solid Dispersions

Solutions of 10% w/w felodipine/copovidone mixture were prepared in a solvent mixture of 80% Methanol: 20% Acetone v/v, with drug:polymer concentration ratios which varied from 5% w/w to 50% w/w Felodipine. The solvent was evaporated under ambient conditions, and the samples were then placed in a pre-heated oven at 155°C for 30 minutes and nitrogen was flowed over the samples. The samples were quench cooled to room temperature on removal from the oven. Samples were stored in a vacuum desiccator prior to analysis and all samples were analysed within 2 days of preparation.

#### Spray Dried Solid Dispersion Samples

Solid dispersions of felodipine in copovidone were produced by spray drying from a mutually compatible solvent system (80% Methanol: 20% Acetone v/v). Solutions of 10% w/w drug/polymer mixture were prepared for spray drying, with drug:polymer concentration ratios which varied from 5% w/w to 50% w/w Felodipine.

Spray drying was performed with a Büchi Mini Spray Dryer B-290 (Flawil, Switzerland), [4]). The drug/polymer solutions were spray dried using the following process parameters: the inlet temperature was 100°C, the aspirator and air flow were set at 100%; the pump speed was set to 30%. The spray dried solid dispersion material was isolated and dried in a vacuum-oven (Gallenkamp) at 40°C overnight. All samples were stored in a vacuum desiccator prior to use.

### **Felodipine Analogue Solid Dispersions**

The Felodipine analogue solid dispersions were prepared in the same way as the felodipine solid dispersions, except that chloroform was used as a solvent. This solvent was chosen as it was thought to be more likely that all of the analogue compounds would be more likely to completely dissolve in this solvent than the methanol/acetone mix used previously. Annealing temperatures were adjusted according to the melting point of the compound being studied. The samples were quench cooled to room temperature on removal from the oven. Samples were stored in a vacuum desiccator prior to analysis and all samples were analysed within a day of preparation.

#### **4.2.2 Preparation of Amorphous Drug, Copovidone, and Physical Mixture Samples**

Amorphous samples of Felodipine and the molecular analogues were also prepared for comparison to the solid dispersions. These samples were produced using the same methods detailed above, but during the solution formation step, no polymer was added. Conversely, samples of copovidone in which no drug compound was added were also prepared using the same method.

Physical mixture samples were also produced for comparative purposes in some analyses. These samples were prepared by blending drug and polymer powders in the desired ratio.

### **4.3 Methods of analysis**

#### **4.3.1 X-ray Powder Diffraction (XRPD)**

X-ray powder diffraction data were collected on a Bruker D4 Endeavor diffractometer in reflectance mode. Samples of solid dispersion were gently powdered with a pestle and mortar prior to analysis. The powder samples were then smeared onto zero-background silicon wafer sample holders. Each sample was exposed to  $\text{CuK}\alpha 1$  and 2 radiation with



an average wavelength of 1.5418 Å, for 0.03 s per 0.00570° 2θ increment (continuous scan mode) over the range 2° to 40° in theta-theta mode. The operating voltage was 40 kV and the operating current was 40 mA.

### 4.3.2 Pair Distribution Function Analysis (PDF)

#### Data Collection

X-ray powder diffraction data were collected on the Bruker D8 diffractometer, which has a Copper source generating X-rays with a wavelength of 1.5418 Å (Göbel mirrors used to provide parallel beam optics remove the  $k\beta$  leaving a beam with an average wavelength of  $k\alpha_1$  and  $k\alpha_2$ ) using a voltage of 40 kV and a filament emission of 40 mA. Samples were measured in reflection mode and the diffraction pattern collected using a scanning position-sensitive detector.

Data was collected by placing the material on a modified TTK sample holder with reduced background noise under vacuum (typically  $2.5 \times 10^{-2}$  mbar) using the Bruker TTK stage with vacuum attachment. Data acquisition parameters of 4-80° 2θ in steps of 0.007091° counting for 0.2 s/step were used for each sample.

A peak in the patterns at 6.6° 2θ is caused by the sample holder, this was removed in each case through subtraction of a blank run (i.e. an empty sample holder) which is measured first in each experiment at the beginning of each set of experiments.

#### Data Analysis

PDFs were generated from each X-ray diffraction pattern measured using the software PDFgetX2 [138]. Simulated traces of amorphous physical mixes were generated through a linear combination of the PDFs of the separate components to the formulation combined in the correct ratios to give a simulated PDF trace for a physical mixture of the two. This could then be compared to the observed traces to determine whether the materials produced were “phase separated” amorphous physical mixes or “molecularly dispersed”.

### 4.3.3 Differential Scanning Calorimetry (DSC)

#### Felodipine Samples and Felodipine/Copovidone Solid Dispersions

For DSC analysis 1.5-7 mg of material for testing was weighed directly into an aluminium sample pan, which was then hermetically sealed. Samples were analysed using a DSC2920 Differential Scanning Calorimeter coupled to a Refrigerated Cooling System (both TA Instruments, New Castle, DE, USA). An Indium sample was used to calibrate both the temperature and heat flow of the instrument prior to analysis of each set of samples. Additionally, a sapphire standard was used to calibrate for heat capacity measurement. The sample chamber was purged with nitrogen gas flowing at 50 mL/min. Samples were analysed in standard DSC mode. Each sample was heated from 20°C to 200°C at 10°C/min and then cooled back to 20°C at the same rate. This cycle was repeated three times for each sample. Data analysis was performed using TA Instruments Universal Analysis 2000 software v4.3A. The onset, peak and enthalpy ( $\Delta H_f$ ) of melting ( $T_m$ ) were determined from the initial heating cycle. Glass transition temperatures, and the associated change in specific heat capacity ( $\Delta C_P$ ) were calculated as an average of the three glass transition temperatures observed in the cooling sections of the temperature cycle.

#### Crystalline Analogue Samples

Material for testing (1.5-7 mg) was weighed directly into a 50  $\mu$ L aluminium sample pan and hermetically sealed. The sample was then analysed using a PerkinElmer Jade DSC (PerkinElmer, Massachusetts, USA). An Indium sample was used to calibrate both the temperature and heat flow of the instrument prior to analysis of each set of samples. Additionally, a sapphire standard was used to calibrate for heat capacity measurement. The sample chamber was purged with nitrogen gas flowing at 50 mL/min. Samples were analysed in standard DSC mode. Each sample was heated from 25°C to 300°C at 10°C/min and then cooled back to 25°C at the same rate. This cycle was repeated three times for each sample. Data analysis was performed using Pyris Thermal Analysis

software v8.0 (PerkinElmer, Massachusetts, USA). The onset, peak and enthalpy ( $\Delta H_f$ ) of melting ( $T_m$ ) were determined from the initial heating cycle. Glass transition temperatures were recorded from the cooling section of the third temperature cycle where this was possible. Some samples showed evidence of degradation at higher temperatures - in these cases, the glass transition temperature was taken from the last complete cooling cycle prior to degradation.

### **Amorphous Analogue and Analogue Solid Dispersion Samples**

For analysis of the solid dispersion samples containing the analogue compounds, 1.5-7 mg of material for testing was weighed directly into a standard aluminium sample pan. Samples were analysed using a Q1000 Differential Scanning Calorimeter coupled to a Refrigerated Cooling System (both TA Instruments, New Castle, DE, USA). An Indium sample was used to calibrate both the temperature and heat flow of the instrument prior to analysis of each set of samples. Additionally, a sapphire standard was used to calibrate for heat capacity measurement. The sample chamber was purged with nitrogen gas flowing at 50 mL/min. Samples were analysed in standard DSC mode. Samples were heated at 10°C/min from 0°C to either 140°C or 200°C, depending on the thermal profile of the analogue. Samples were then cooled back to 0°C at the same rate. This cycle was repeated three times for each sample. Data analysis was performed using TA Instruments Universal Analysis 2000 software v4.3A. Glass transition temperatures, and the associated change in specific heat capacity ( $\Delta C_p$ ) were calculated as an average of the three glass transition temperatures observed in the cooling sections of the temperature cycle.

#### **4.3.4 Helium Pycnometry**

The true density of amorphous felodipine and the analogues was required for producing Gordon-Taylor plots (see Chapter 2). Samples were prepared by dissolving the crystalline material in chloroform, and then flash evaporating the solvent over 15-20 min.

Helium pycnometry was carried out using a Micrometrics AccuPyc 1330 pycnometer with a 1 cm<sup>3</sup> sample cup.

Samples were analysed by XRPD after the pycnometry, to ensure that the measurements were for amorphous material. In cases where the material was subsequently shown to have been crystalline, an estimated amorphous density value of  $0.95 \times$  the crystalline density was used, as has been shown in a previous study [139].

#### **4.3.5 Optical Microscopy**

Spray dried material was placed on a glass microscope slide and immersed in paraffin oil, and “sandwiched” with a cover slide. The sample was then imaged by brightfield transmission microscopy using an inverse microscope (Olympus IX50 with Olympus TH4-200 lamp, both Olympus, Japan), with a colour video camera attached (JVC KY-F55B 3CCD, Japan) using Image Pro Plus software (version 7.0).

#### **4.3.6 Scanning Electron Microscopy (SEM)**

Spray dried material was imaged using SEM according to the following protocol. Samples were prepared on specimen stubs with a Carbon layer, and then coated with gold by a low vacuum sputter coater. The gold-coated samples were imaged using a Hitachi TM-1000 Tabletop Microscope, and the associated Hitachi TM-1000 software.

### **4.4 Results and Discussion**

#### **4.4.1 Copovidone**

Copovidone is an X-ray amorphous polymer, as shown in following diffractogram figures for reference. It was shown by DSC analysis to have a glass transition temperature at 96.44°C. This value is lower than the value of 108.1°C reported in the literature [42], but this is possibly due to the effect of moisture in the sample, which acts as a plasticizer. Loss of water was observed as a broad endotherm with onset 49.29°C and

peak of 97.46°C during the initial heating cycle of the DSC analysis. It is also possible that the value obtained here differs from the literature value due to a difference in the molecular weight distribution of the polymer. The true density ( $\rho$ ) of copovidone was determined using helium pycnometry, and was found to be 1.2026 g cm<sup>-3</sup>. This value corresponds well with values presented in the literature [42].

#### 4.4.2 Felodipine

##### Film Cast Samples

Felodipine was shown by XRPD to be easily rendered amorphous using the sample preparation method detailed above. Solid dispersion samples were also shown to be X-ray amorphous compared with the starting material (see Figure 4.1).

By DSC, crystalline felodipine was shown to have a  $T_g$  at 43.14°C with  $\Delta C_P$  of 0.2731 J g<sup>-1</sup> K<sup>-1</sup>, and  $T_m$  with onset at 143°C, peak at 147.93°C, and  $\Delta H_f$  of 26.28 kJ mol<sup>-1</sup>. The measured  $T_g$  and  $T_m$  are both in close agreement with data in the literature [56, 64]. Single glass transition temperatures were observed for each drug-polymer blend, indicating that the drug and polymer were intimately mixed at all the drug loadings tested. The true density ( $\rho$ ) of amorphous felodipine was found to be 1.3287 g cm<sup>-3</sup>; a value that agrees well with reported literature values [87], and was used to create Gordon-Taylor and Couchman-Karaszi plots (see Chapter 2). The single  $T_g$ s measured for felodipine/copovidone solid dispersions were shown to fit well with the Gordon-Taylor plot, confirming that felodipine and copovidone were miscible at the drug loadings tested (Figure 4.2).

In contrast to the DSC data, PDF analysis suggests that the solid dispersion samples are not true molecular dispersions, as the PDF traces for these materials closely matches the traces simulated for physical mixtures at the same drug loadings (Figure 4.3). However, no conclusions can be made about the size of any domains, as the PDF methodology used in this work is limited by low resolution. Nevertheless, there are few peaks in the PDF traces, indicating that there isn't much order left in the

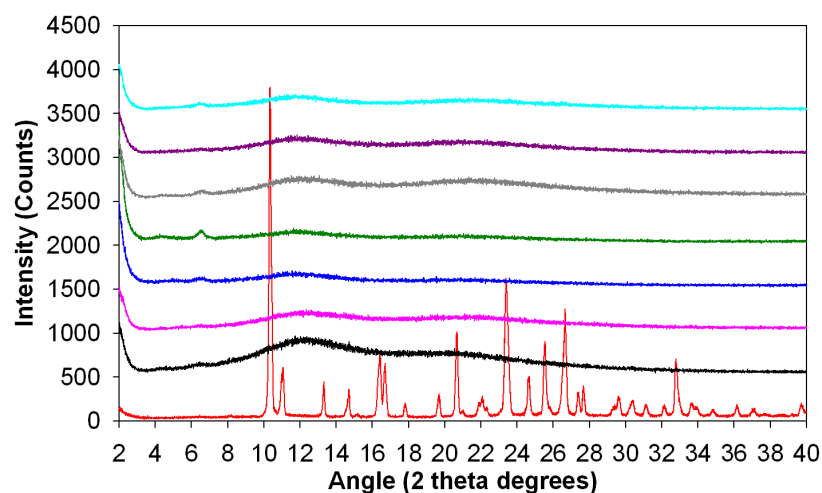


Figure 4.1: X-ray powder diffractograms of the film-cast felodipine/copovidone solid dispersions with drug loadings of 5% (pink), 10% (blue), 20% (green), 30% (grey), 40% (purple) and 50% (light blue). Diffractograms of crystalline felodipine (red) and copovidone (black) are also shown for comparison.

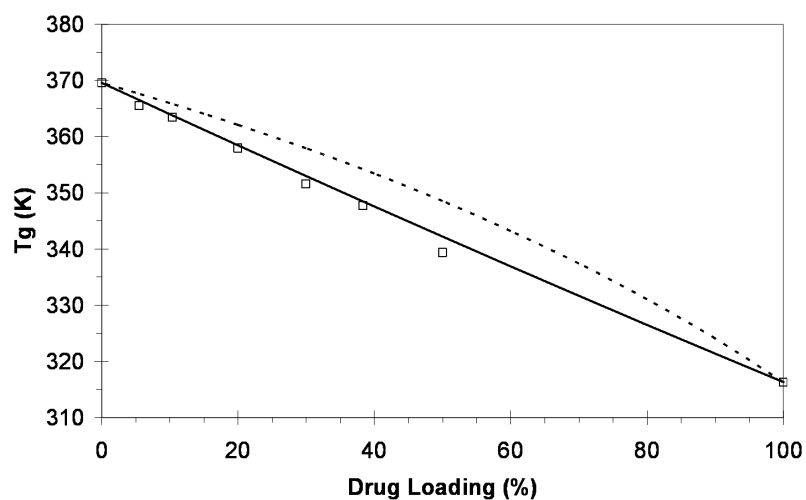
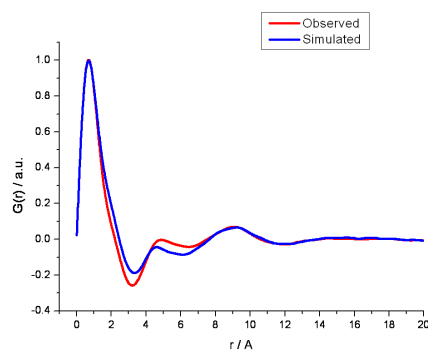
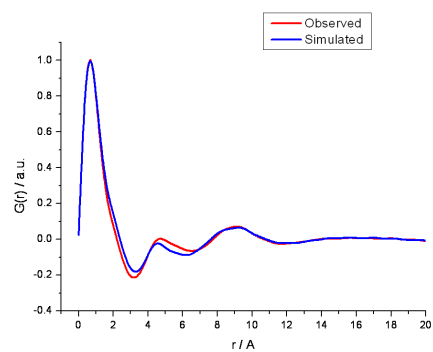


Figure 4.2:  $T_g$  of amorphous felodipine as a function of weight fraction drug. The solid line represents the fit to the Gordon-Taylor equation and the dashed line represents the fit to the Couchman-Karas equation.

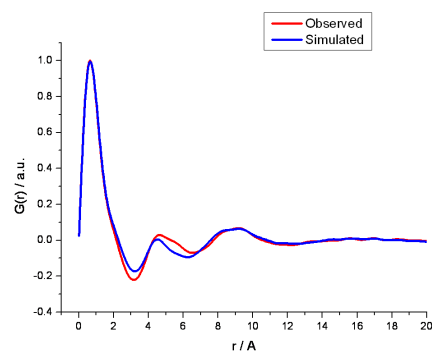
formulations, and therefore confirming that the systems are essentially amorphous. Also, the suggestion that the 5% drug-loaded formulation is phase separated is contradictory to the good dissolution performance of this formulation in Chapter 6 that indicates a solid solution has been formed. It could be that whilst the majority of the drug is dispersed as amorphous nanoparticles in the polymer (giving rise to the PDF trace), there is a small percentage of the drug that is molecularly dispersed (leading to the enhancement in dissolution).



(a) 15% drug loading



(b) 30% drug loading



(c) 50% drug loading

Figure 4.3: Comparison of the simulated traces of felodipine/copovidone amorphous physical mixes with the observed traces of the film-cast solid dispersions at drug loadings of a) 15%, b) 30% and c) 50%.



## Spray Dried Samples

Before use in dissolution experiments (Chapter 6), the spray dried materials were assessed with regards to their physical characteristics and solid-state properties. Firstly, the samples were examined by optical microscopy to determine the morphology of the spray dried particles, and as an initial check that no crystalline material was present. The images in Figure 4.4 show that there were no obvious signs of crystalline material in any of the spray dried samples. Additionally, it appears that the spray drying process has generally produced spherically-shaped particles. These particles seem more likely to form larger aggregates at higher drug loadings such as 30 and 50%.

Imaging of the spray dried material at higher magnifications by SEM supports the optical microscopy by showing the morphology of the particles to be mostly spherical. The spray dried particles also appear to be hollow, as shown by the fragmented particles circled in Figures 4.6b, 4.7b and 4.8b. The hollow nature of the particles is most likely to be due to solvent evaporation during the spray drying process as suggested previously in the literature [140, 141, 142, 143]. It was also noted that at higher drug loadings (i.e. 30 and 50%) the particles were smooth (see Figures 4.7 and 4.8), but as the polymer content increased to 85% the particles became more wrinkled (see figure 4.6), and the 5% drug-loaded particles had numerous sizeable indentations (see figure 4.5). Again, this is likely to be due to the solvent evaporation during the particle processing.

Crystallisation of the drug compound from the spray dried dispersions was not detected by SEM imaging, but to fully ensure that no crystalline material was present in the spray dried material, samples were subjected to analysis by XRPD. This is because whilst SEM is more sensitive than XRPD, it is also less statistically robust. Diffractograms of spray dried material at all four drug loadings showed the felodipine to have been successfully rendered amorphous (see Figure 4.9). There was some concern that the compaction process used for making the samples for the MRI flowcell experiments may induce crystallisation of the felodipine. Therefore, samples of the spray dried material after compaction were also analysed by XRPD, and were shown to have remained

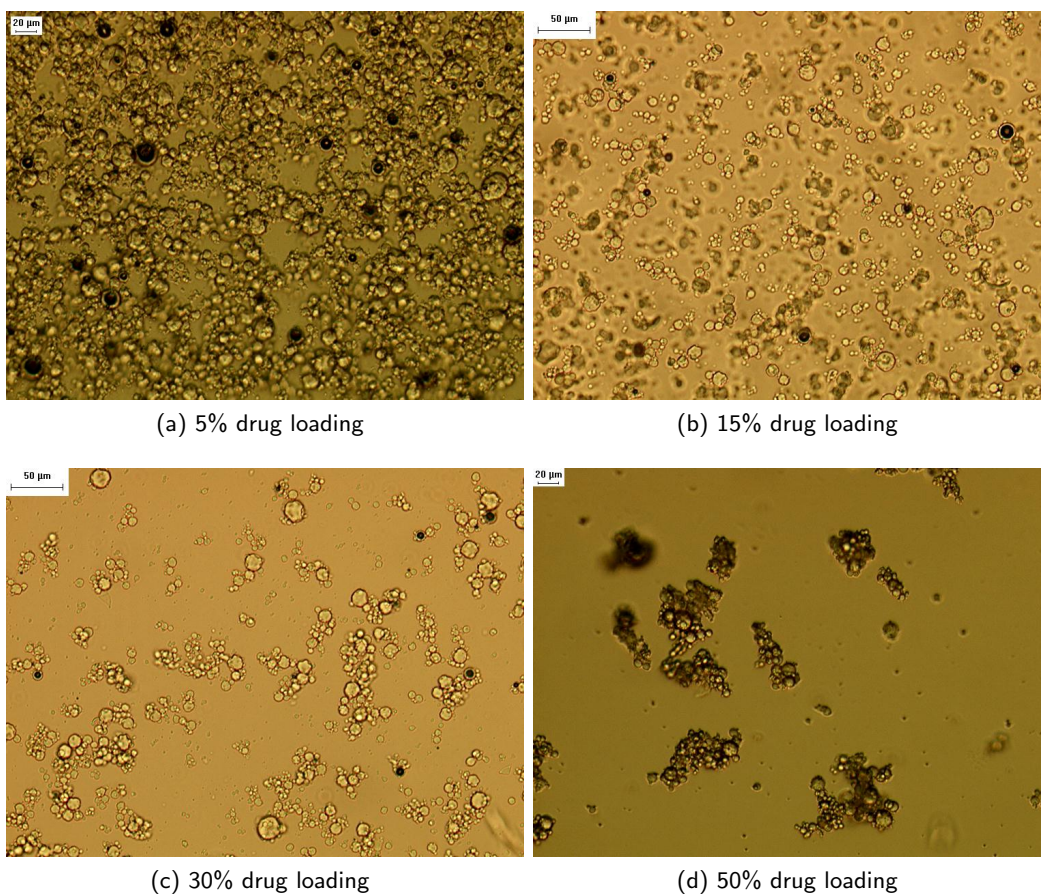


Figure 4.4: Images obtained by optical microscopy of spray dried solid dispersions with drug loadings of a) 5%, b) 15%, c) 30% and d) 50%. Scale bars for images a) and d) represent 20  $\mu\text{m}$  and for images b) and c) represent 50  $\mu\text{m}$ .

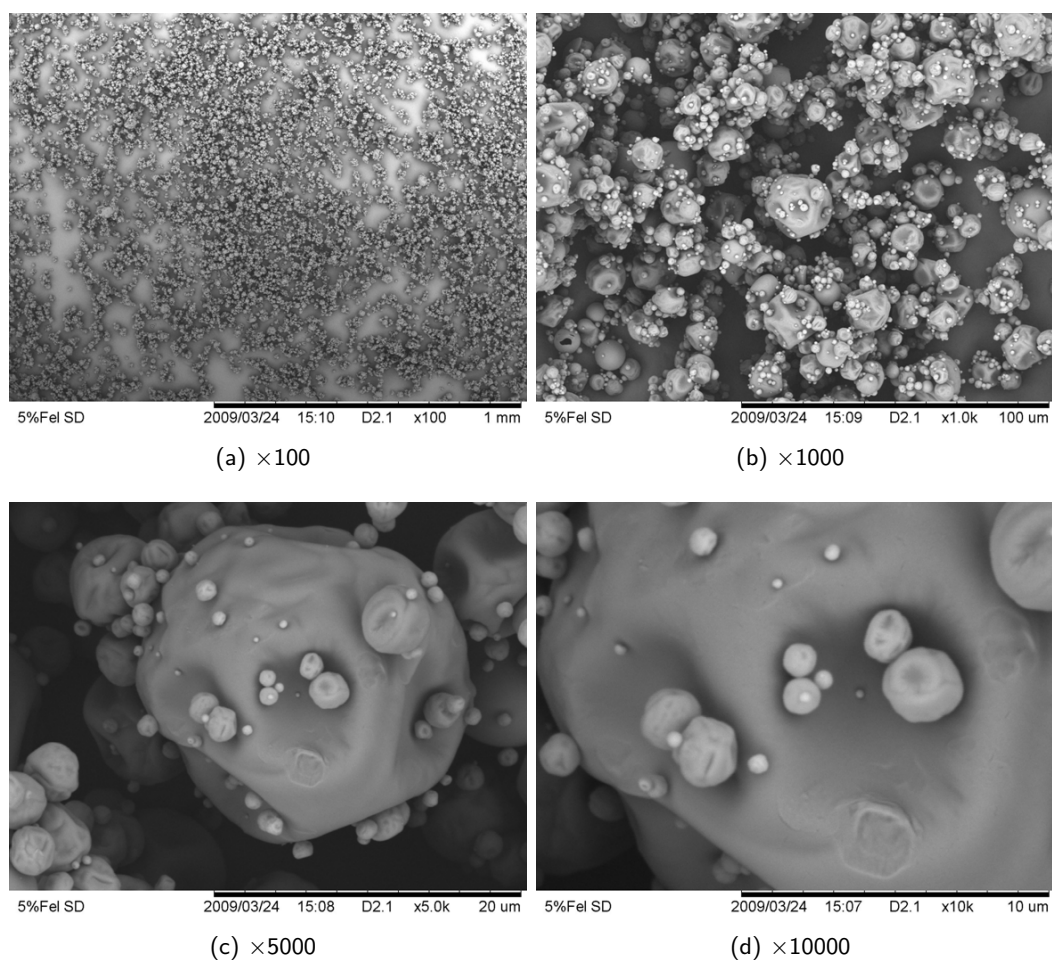


Figure 4.5: SEM images of the spray dried material containing 5% felodipine taken at a)  $\times 100$ , b)  $\times 1000$ , c)  $\times 5000$  and d)  $\times 10000$  magnifications.

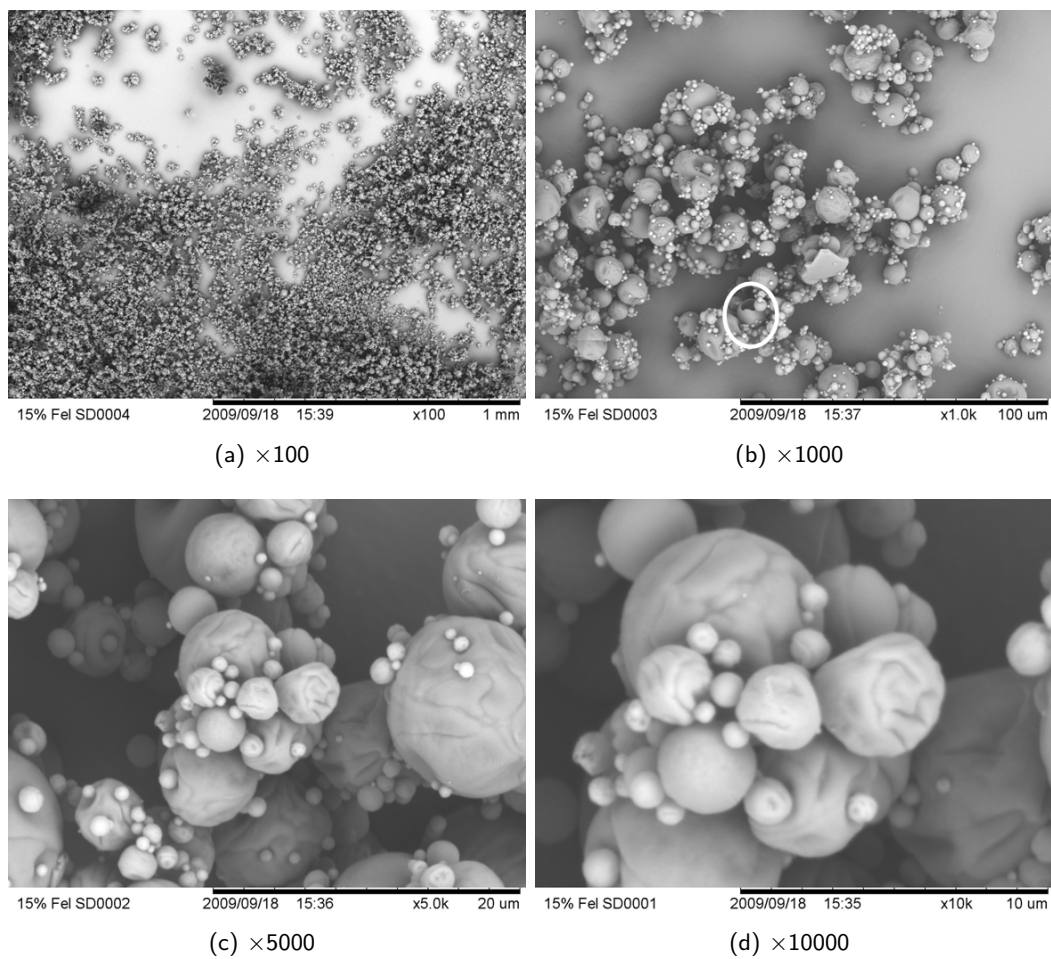


Figure 4.6: SEM images of the spray dried material containing 15% felodipine taken at a)  $\times 100$ , b)  $\times 1000$ , c)  $\times 5000$  and d)  $\times 10000$  magnifications. Circled in image b) is a fragmented hollow particle.

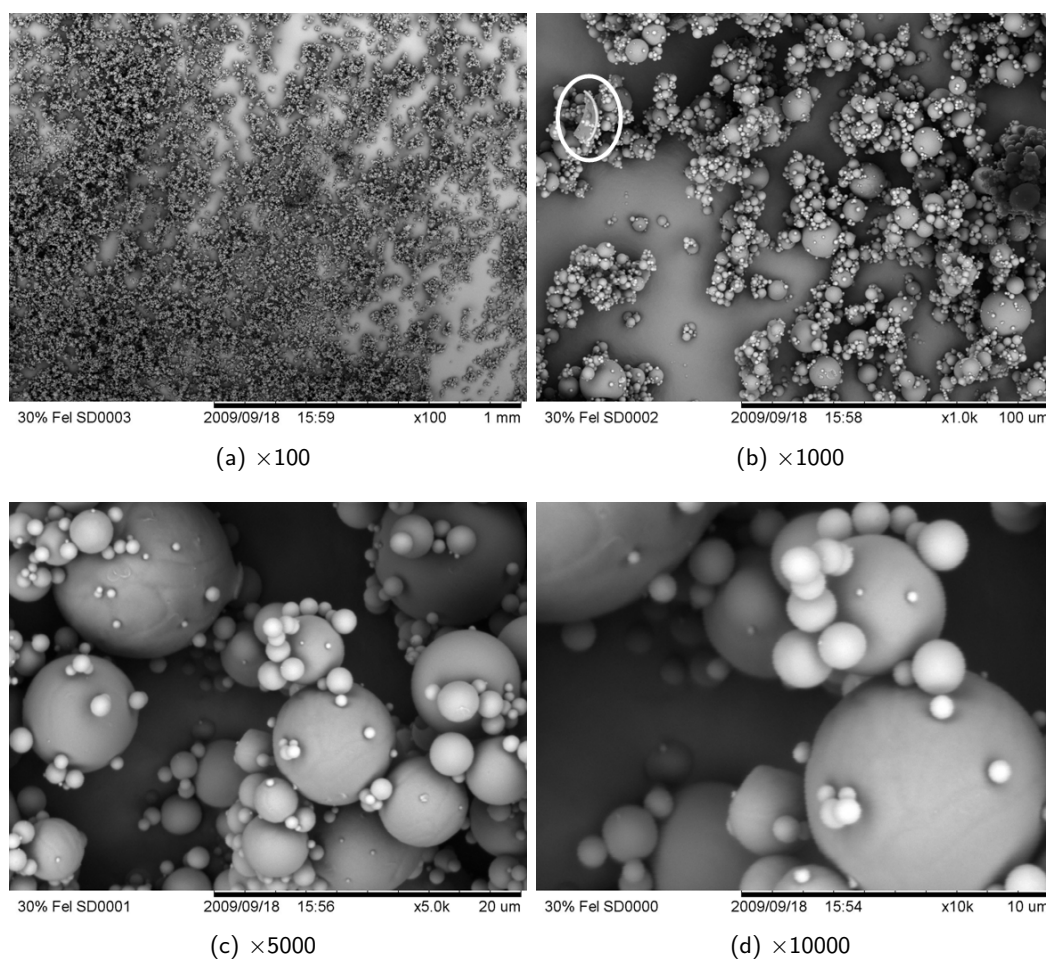


Figure 4.7: SEM images of the spray dried material containing 30% felodipine taken at a)  $\times 100$ , b)  $\times 1000$ , c)  $\times 5000$  and d)  $\times 10000$  magnifications. Circled in image b) is a fragmented hollow particle.

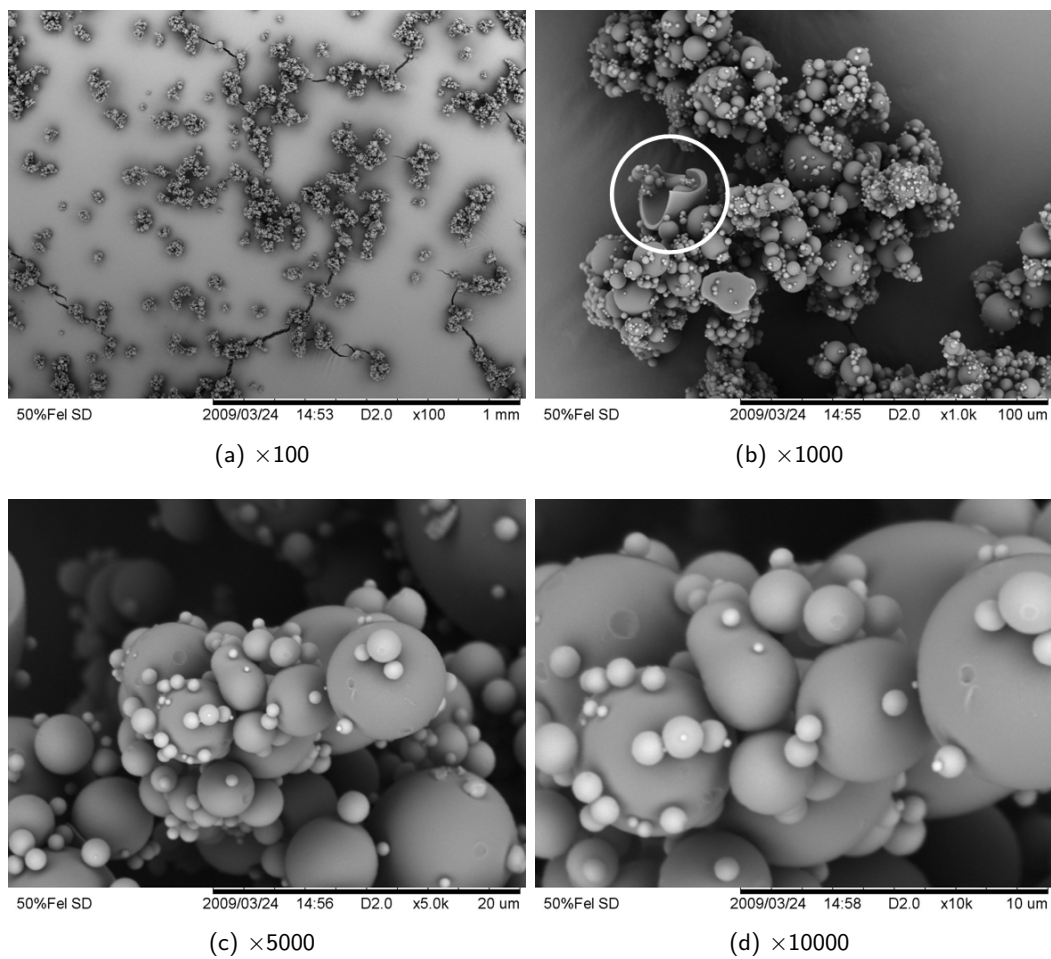


Figure 4.8: SEM images of the spray dried material containing 50% felodipine taken at a)  $\times 100$ , b)  $\times 1000$ , c)  $\times 5000$  and d)  $\times 10000$  magnifications. Circled in image b) is a fragmented hollow particle.

amorphous (see Figure 4.10).

PDF analysis was carried out on the spray dried material to determine if molecular dispersions had been produced. PDF analysis suggests that the spray dried materials are not molecular dispersions, as the PDF traces for these materials closely matches the traces simulated for physical mixtures at the same drug loadings (Figure 4.11). This data suggests that these samples are solid suspensions, though as discussed previously for the film-cast samples, the dissolution improvements also observed in Chapter 6 for this material indicates the formation of solid solutions. This discrepancy is likely due to there being a small percentage of drug that is molecularly dispersed, whilst the rest of the drug is present as amorphous nanoparticles in the polymer matrix.

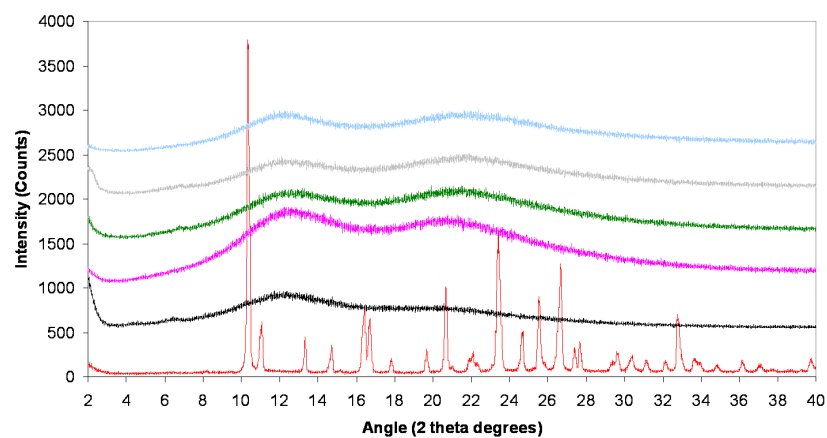


Figure 4.9: X-ray powder diffractograms of the spray dried felodipine/copovidone solid dispersions with drug loadings of 5% (pink), 15% (green), 30% (grey) and 50% (light blue). Diffractograms of crystalline felodipine (red) and copovidone (black) are also shown for comparison.

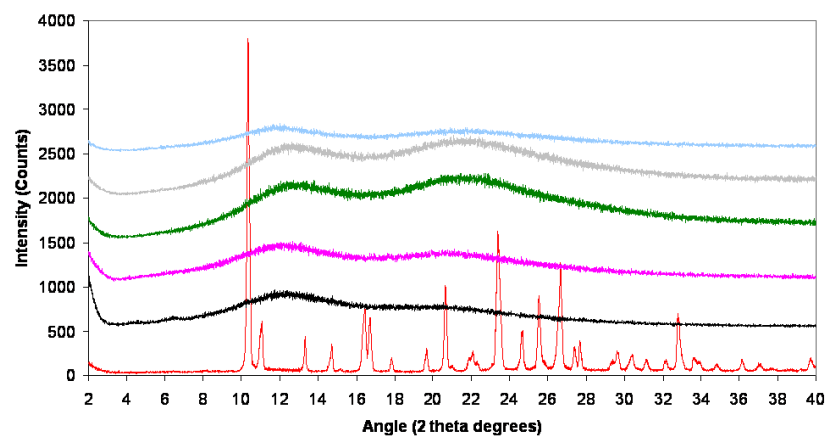
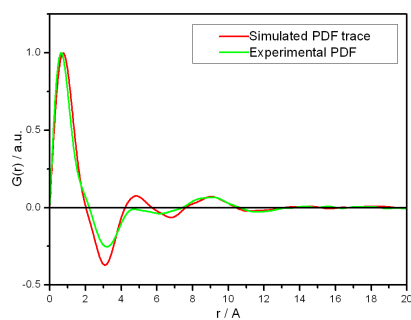
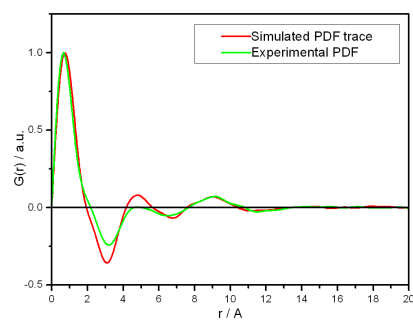


Figure 4.10: X-ray powder diffractograms of the compacted spray dried felodipine/copovidone solid dispersions with drug loadings of 5% (pink), 15% (green), 30% (grey) and 50% (light blue). Diffractograms of crystalline felodipine (red) and copovidone (black) are also shown for comparison.

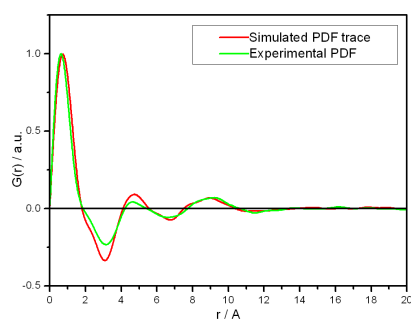




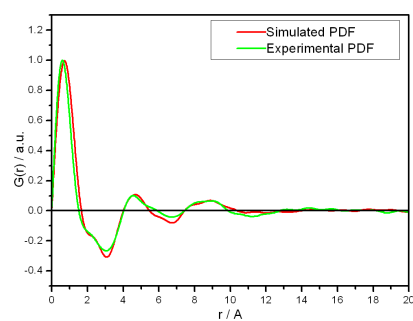
(a) 5% drug loading



(b) 15% drug loading



(c) 30% drug loading



(d) 50% drug loading

Figure 4.11: Comparison of the simulated traces of felodipine and copovidone amorphous physical mixes with the observed traces of the spray dried solid dispersions at drug loadings of a) 5%, b) 15%, c) 30% and d) 50%.

#### 4.4.3 ZAL\_001

ZAL\_001 was an oil, and hence was shown to be amorphous by XRPD. Because it was an oil, DSC analysis was not carried out on this sample, or its solid dispersions.

#### 4.4.4 ZAL\_005

A sample of ZAL\_005, was shown to be crystalline by XRPD (see Figure 4.12). By DSC, crystalline ZAL\_005 was shown to have a  $T_g$  at 12.74°C with  $\Delta C_P$  of 0.346 J g<sup>-1</sup> K<sup>-1</sup>, and  $T_m$  with onset at 101.5°C, peak at 107.2°C, and  $\Delta H_f$  of 38.53 kJ mol<sup>-1</sup>. ZAL\_005 was successfully rendered X-ray amorphous after preparation according to the method detailed above with an annealing step at 180°C. Solid dispersion samples of ZAL\_005 were also all found to be amorphous when annealed at 180°C (see Figure 4.12).

Single glass transition temperatures were observed for each drug-polymer blend, indicating that the drug and polymer were intimately mixed at all the drug loadings tested. The true density ( $\rho$ ) of crystalline ZAL\_005 was found to be 0.2059 g cm<sup>-3</sup>; and this value was used in a corrected form to create Gordon-Taylor and Couchman-Karasz plots (see Chapter 2). The single  $T_g$ s measured for ZAL\_005/copovidone solid dispersions lay between the Gordon-Taylor and Couchman-Karasz plots, suggesting that ZAL\_005 and copovidone were miscible at the drug loadings tested (Figure 4.13).

Most of the amorphous analogue compounds analysed by PDF, displayed ordering to a length scale of  $\sim 10$  Å (see Figure 4.14). By contrast, analysis of amorphous ZAL\_005 by PDF showed that it displayed ordering out to a longer length scale of  $\sim 15$  Å, which suggests that this compound may be more prone to recrystallisation than the other compounds analysed. PDF analysis of the solid dispersion samples suggests that they are not molecular dispersions, as the PDF traces for these materials closely matches the traces simulated for physical mixtures at the same drug loadings (see Figure 4.15). This suggests that this particular chemical modification of felodipine did not achieve the formation of a solid solution at 15%.

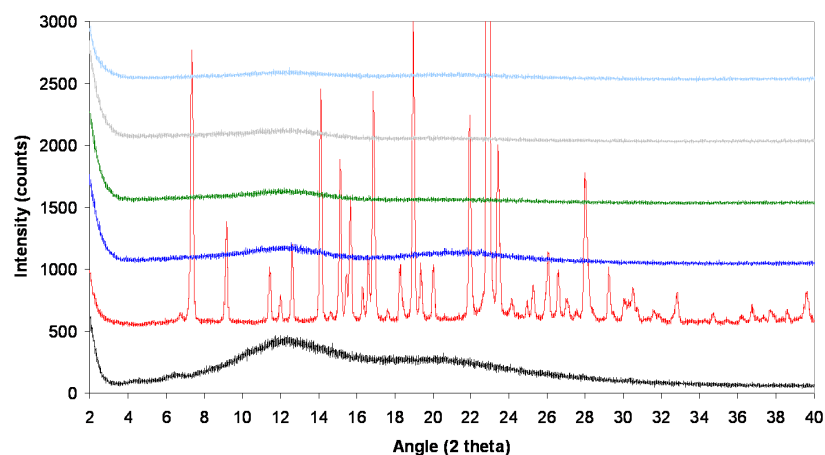


Figure 4.12: X-ray powder diffractograms of samples of crystalline ZAL\_005 (red), amorphous ZAL\_005 (dark blue), and solid dispersions of ZAL\_005 and copovidone with drug loadings of 15% (green), 30% (grey) and 50% (light blue). Copovidone is also shown for reference (black).

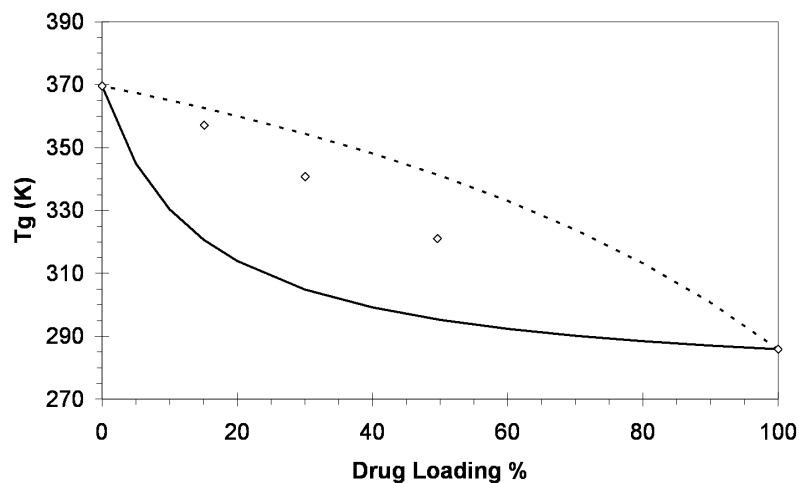


Figure 4.13:  $T_g$  of amorphous ZAL\_005 as a function of weight fraction drug. The solid line represents the fit to the Gordon-Taylor equation and the dashed line represents the fit to the Couchman-Karas equation.

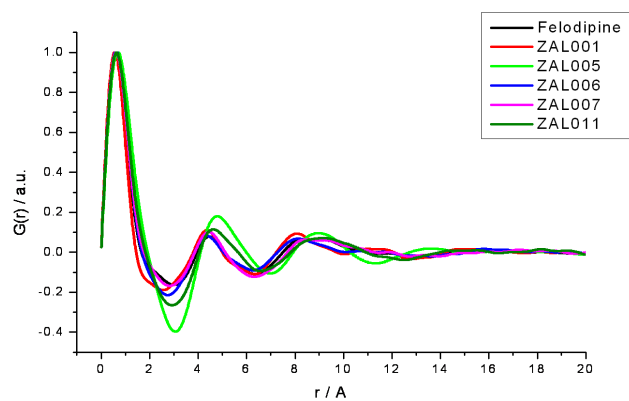


Figure 4.14: Comparison of the PDF traces generated for each of the amorphous felodipine analogues

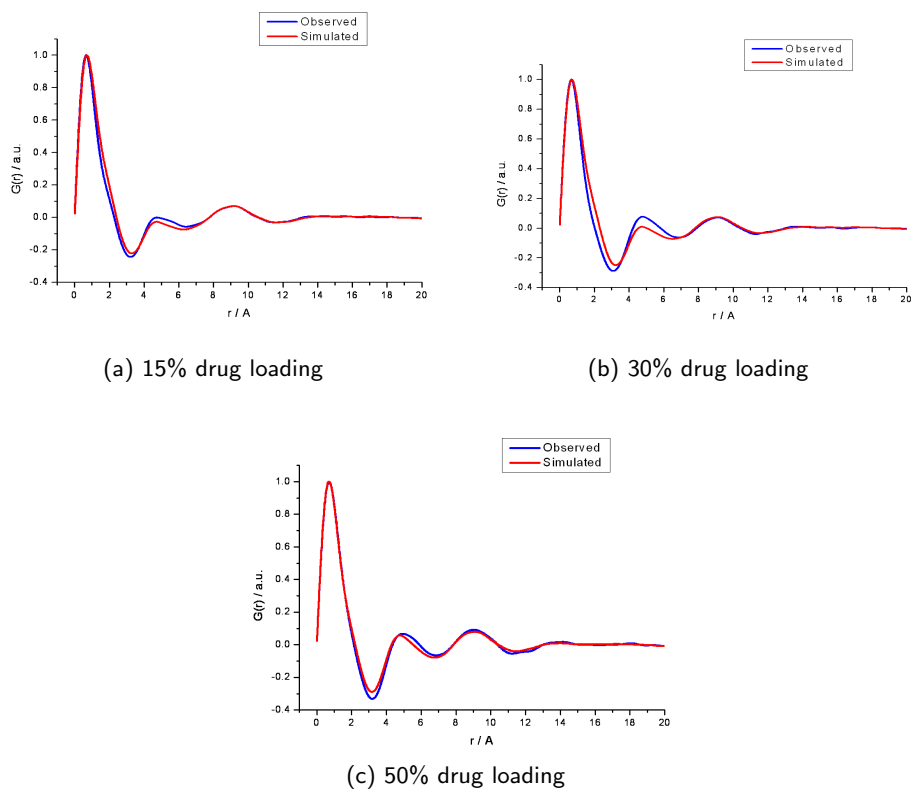


Figure 4.15: Comparison of the simulated traces of ZAL\_005 and copovidone amorphous physical mixes with the observed traces of the solid dispersion at drug loadings of a) 15%, b) 30% and c) 50%.

#### 4.4.5 ZAL\_006

XRPD analysis of ZAL\_006 showed it to be a crystalline solid (see Figure 4.16). By DSC, crystalline ZAL\_006 was shown to have a  $T_g$  at 55.38°C with  $\Delta C_P$  of 0.3642 J g<sup>-1</sup> K<sup>-1</sup>, and  $T_m$  with onset at 165.3°C, peak at 168.3°C, and  $\Delta H_f$  of 27.16 kJ mol<sup>-1</sup>. As a result of this information, amorphous and solid dispersion samples were produced with an annealing step at 180°C. The drug compound was shown to be successfully rendered amorphous using this method by XRPD, and solid dispersion samples were also shown to be X-ray amorphous (see Figure 4.16).

Single glass transition temperatures were observed for each drug-polymer blend, indicating that the drug and polymer were intimately mixed at all the drug loadings tested. The true density ( $\rho$ ) of amorphous ZAL\_006 was found to be 0.2374 g cm<sup>-3</sup>; and this value was used to create Gordon-Taylor and Couchman-Karaszc plots (see Chapter 2). The single  $T_g$ s measured for ZAL\_006/copovidone solid dispersions lay between the Gordon-Taylor and Couchman-Karaszc plots, suggesting that ZAL\_006 and copovidone were miscible at the drug loadings tested (Figure 4.17).

PDF analysis of the solid dispersion samples suggests that they are not molecular dispersions, as the PDF traces for these materials closely matches the traces simulated for physical mixtures at the same drug loadings (Figure 4.18).

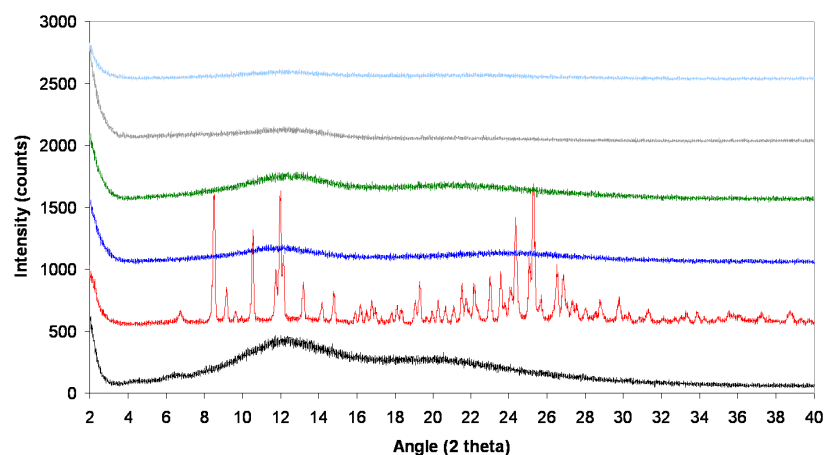


Figure 4.16: X-ray powder diffractograms of samples of crystalline ZAL\_006 (red), amorphous ZAL\_006 (dark blue), and solid dispersions of ZAL\_006 and copovidone with drug loadings of 15% (green), 30% (grey) and 50% (light blue). Copovidone is also shown for reference (black).

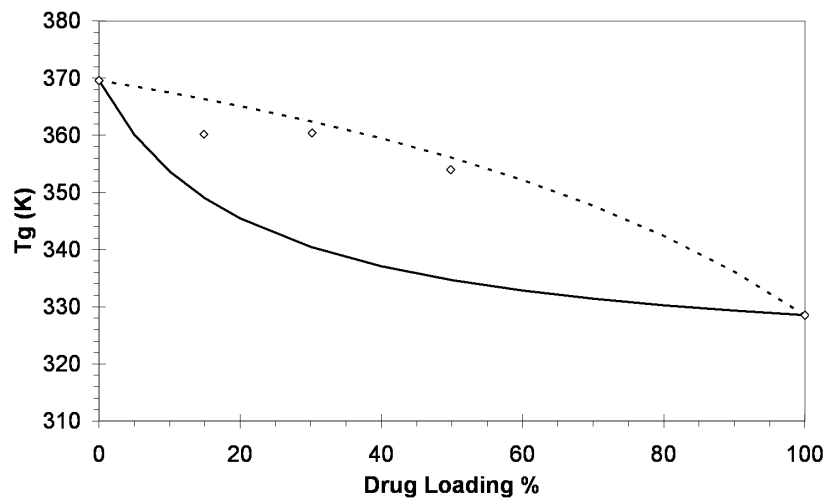
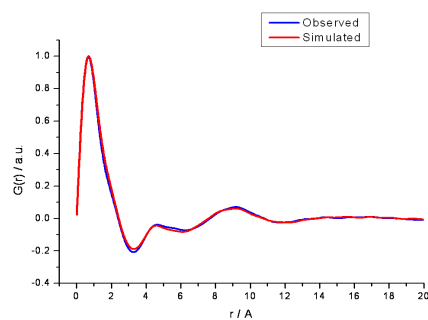
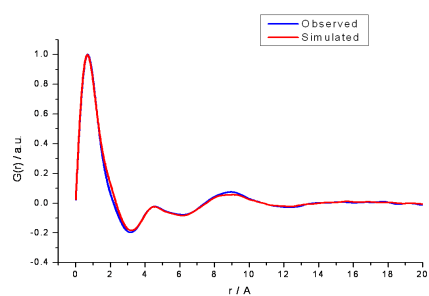


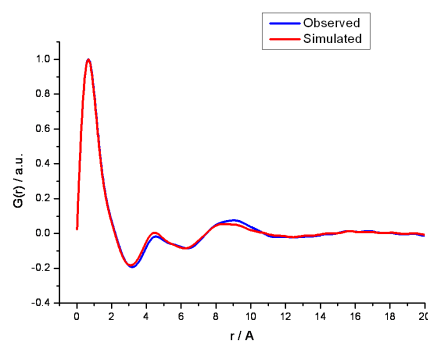
Figure 4.17:  $T_g$  of amorphous ZAL\_006 as a function of weight fraction drug. The solid line represents the fit to the Gordon-Taylor equation and the dashed line represents the fit to the Couchman-Karas equation.



(a) 15% drug loading



(b) 30% drug loading



(c) 50% drug loading

Figure 4.18: Comparison of the simulated traces of ZAL\_006 and copovidone amorphous physical mixes with the observed traces of the solid dispersion at drug loadings of a) 15%, b) 30% and c) 50%.

#### 4.4.6 ZAL\_007

ZAL\_007 material was analysed by XRPD and shown to be crystalline (see Figure 4.19). By DSC, crystalline ZAL\_007 was shown to have a  $T_g$  at 81.41°C with  $\Delta C_P$  of 0.2396 J g<sup>-1</sup> K<sup>-1</sup>, and  $T_m$  with onset at 123.2°C, peak at 127.2°C, and  $\Delta H_f$  of 19.84 kJ mol<sup>-1</sup>. As a result of the DSC data, it was decided that amorphous and solid dispersion samples of ZAL\_007 would be produced by annealing at 130°C. Analysis of these samples by XRPD showed that this annealing step successfully afforded amorphous material (see Figure 4.19).

Single glass transition temperatures were observed for each drug-polymer blend, indicating that the drug and polymer were intimately mixed at all the drug loadings tested. The true density ( $\rho$ ) of crystalline ZAL\_007 was found to be 0.1847 g cm<sup>-3</sup>; and this value was in a corrected form used to create Gordon-Taylor and Couchman-Karasch plots (see Chapter 2). The single  $T_g$ s measured for ZAL\_007/copovidone solid dispersions lay between the Gordon-Taylor and Couchman-Karasch plots, except at 50% drug loading, suggesting that ZAL\_007 and copovidone were miscible at the drug loadings of 15% and 30% (Figure 4.21).

Analysis of the solid dispersion samples by PDF suggests that they are not molecular dispersions, as the experimental PDF traces for these materials closely matches the traces simulated for physical mixtures at the same drug loadings (see Figure 4.20).



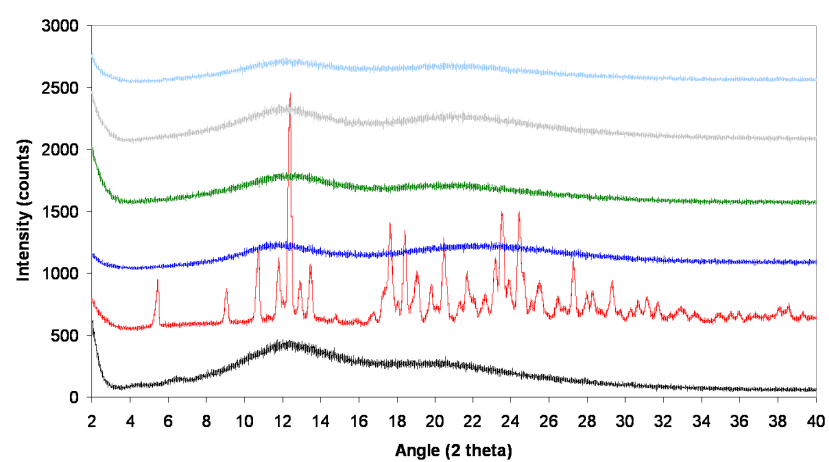
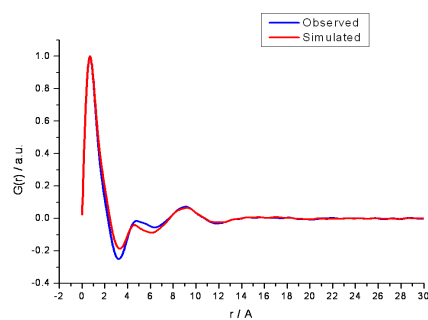
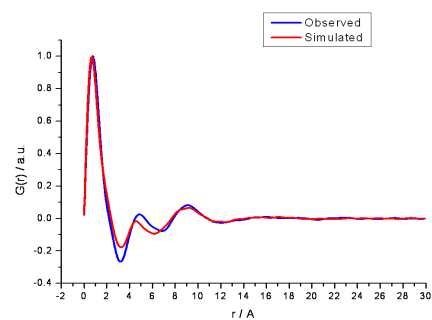


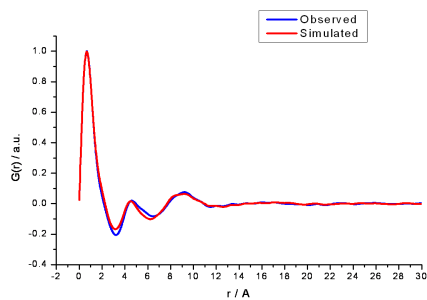
Figure 4.19: X-ray powder diffractograms of samples of crystalline ZAL\_007 (red), amorphous ZAL\_007 (dark blue), and solid dispersions of ZAL\_007 and copovidone with drug loadings of 15% (green), 30% (grey) and 50% (light blue). Copovidone is also shown for reference (black).



(a) 15% drug loading



(b) 30% drug loading



(c) 50% drug loading

Figure 4.20: Comparison of the simulated traces of ZAL\_007 and copovidone phase separated solid dispersion with the observed traces of the solid dispersion at drug loadings of a) 15%, b) 30% and c) 50%.

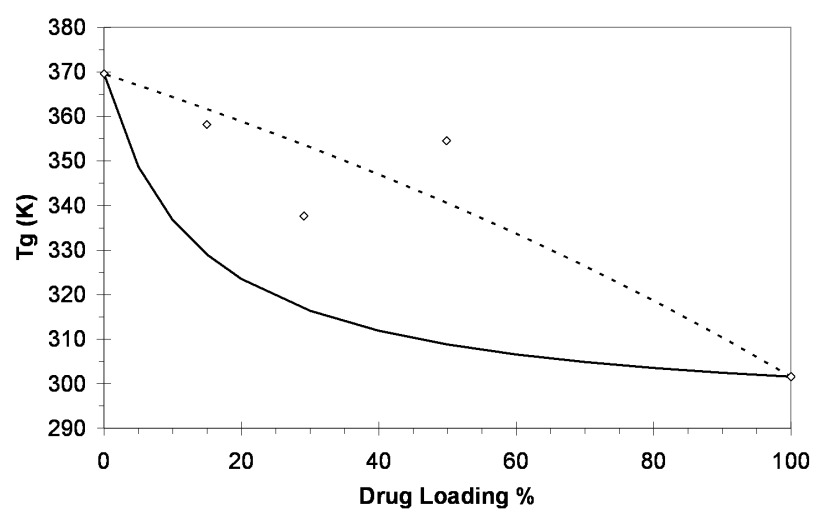


Figure 4.21:  $T_g$  of amorphous ZAL\_007 as a function of weight fraction drug. The solid line represents the fit to the Gordon-Taylor equation and the dashed line represents the fit to the Couchman-KarasZ equation.

#### 4.4.7 ZAL\_008

A sample of ZAL\_008, was shown by XRPD to be crystalline. By DSC, crystalline ZAL\_008 was shown to have a  $T_m$  with onset at 251.7°C, peak at 255.4°C, and  $\Delta H_f$  of 6.68 kJ mol<sup>-1</sup>, but a degradation endotherm was observed immediately after the melting endotherm. No  $T_g$  was observed in this sample. Degradation of the sample after melting made it difficult to prescribe a suitable annealing temperature for forming amorphous or solid dispersion samples of this material that would not be chemically degraded. An additional barrier to forming amorphous or solid dispersion samples of this compound was that an organic solvent that fully dissolved the compound at a suitable concentration, but was also volatile enough to be flash evaporated could not be identified. Therefore no further work was carried out using this compound during the course of the project described in this thesis.

This issues encountered with this compound highlights that one of the main pitfalls of high melting compounds is that they have poor solubility in processing solvents. As a result, this compound may be unable to be formulated as a solid dispersion using conventional approaches.

#### 4.4.8 ZAL\_009

A sample of ZAL\_009 as produced from the synthesis detailed in chapter 3 was analysed by XRPD, and was shown to be crystalline (see figure 4.22). By DSC, crystalline ZAL\_009 was shown to have a  $T_g$  at 31.29°C with  $\Delta C_P$  of 0.4966 J g<sup>-1</sup> K<sup>-1</sup>, and  $T_m$  with onset at 166.0°C, peak at 169.4°C., and  $\Delta H_f$  of 30.09 kJ mol<sup>-1</sup>. Therefore an annealing temperature of 180°C was proposed for the the formation of amorphous and solid dispersion samples of this compound. XRPD analysis of these samples showed that this sample preparation method successfully produced amorphous material (see Figure 4.22).

Single glass transition temperatures were observed for each drug-polymer blend, indicating that the drug and polymer were intimately mixed at all the drug loadings

tested. The true density ( $\rho$ ) of crystalline ZAL\_009 was found to be 0.0718 g cm<sup>-3</sup>; and this value was used in a corrected form to create Gordon-Taylor and Couchman-Karas plots (see Chapter 2). The single  $T_g$ s measured for ZAL\_009/copovidone solid dispersions all lay between the Gordon-Taylor and Couchman-Karas plots suggesting that ZAL\_009 and copovidone were miscible at all tested drug loadings (Figure 4.23).

PDF analysis was not carried out on solid dispersion samples of ZAL\_009 due to limitations in the amount of available material.

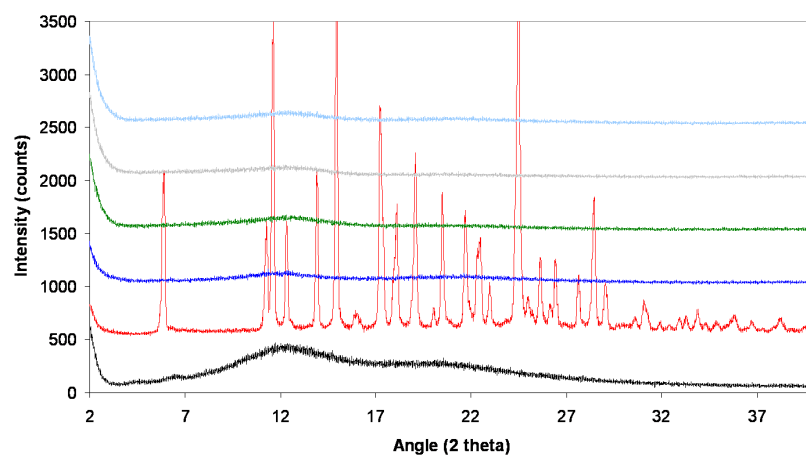


Figure 4.22: X-ray powder diffractograms of samples of crystalline ZAL\_009 (red), amorphous ZAL\_009 (dark blue), and solid dispersions of ZAL\_009 and copovidone with drug loadings of 15% (green), 30% (grey) and 50% (light blue). Copovidone is also shown for reference (black).

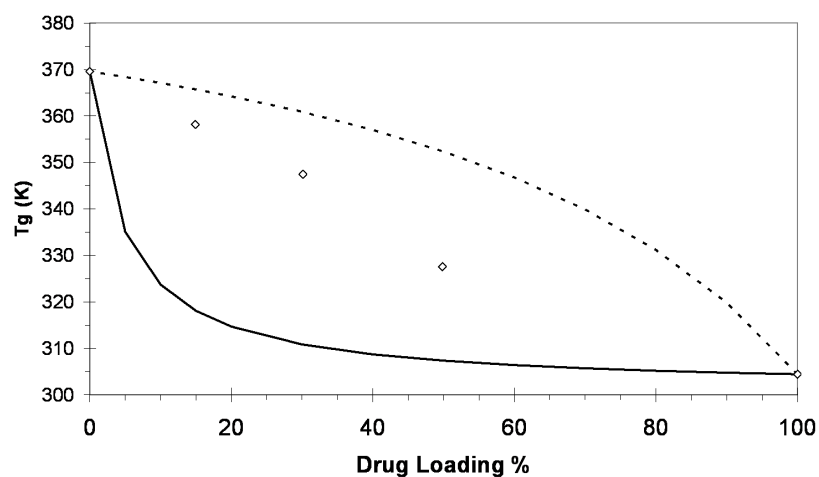


Figure 4.23:  $T_g$  of amorphous ZAL\_009 as a function of weight fraction drug. The solid line represents the fit to the Gordon-Taylor equation and the dashed line represents the fit to the Couchman-Karaszi equation.

#### 4.4.9 ZAL\_010

ZAL\_010 was analysed by XRPD, and found to be crystalline (see Figure 4.25). Initial DSC carried out with heating to 200°C showed a melting point around 100°C, and as a result of this, an annealing temperature of 130°C was suggested for the preparation of amorphous material. DSC analysis of the sample subjected to amorphisation did not contain any melting endotherms, and a  $T_g$  was identified in the cooling cycles at 76.80°C with  $\Delta C_P$  of 0.256 J g<sup>-1</sup> K<sup>-1</sup>, suggesting that the material was amorphous. However, later XRPD analysis of the sample subjected to amorphisation was shown to be crystalline, but of a different polymorphic form (referred to from here on as Form II - see Figure 4.25) to the original, synthesised material (referred to as Form I). Repeat DSC analysis of crystalline ZAL\_010 showed a  $T_m$  for Form I with onset at 95.9°C, peak at 104.4°C and  $\Delta H_f$  of 11.41 kJ mol<sup>-1</sup>, followed by a recrystallisation exotherm, (indicating formation of Form II material), with onset at 161.11°C and peak at 175.13°C. This was followed by a further  $T_m$  for Form II with onset at 288.21°C, peak at 289.89°C and  $\Delta H_f$  of 6.03 kJ mol<sup>-1</sup>. A  $T_g$  is evident on subsequent heating cycles at 174°C, and it is likely that this is in fact the 'true' amorphous  $T_g$ . As a result of these experiments, it seems that an annealing temperature above 300°C is required for the sample to be heated above all the phase transitions, but this temperature is not practical with regards to decomposition of the polymer.

Solid dispersion samples of ZAL\_010 had been prepared at the same time as the amorphous pure drug sample, and hence an annealing temperature of 130°C had been used in the preparation of these samples. By DSC analysis, these samples were all shown to be amorphous and displayed a single  $T_g$  (see Figure 4.24). The true density ( $\rho$ ) of crystalline Form I ZAL\_010 was found to be 0.0672 g cm<sup>-3</sup>; and this value was used in a corrected form to create Gordon-Taylor and Couchman-Karasz plots (see Chapter 2). The single  $T_g$ s measured for ZAL\_010/copovidone solid dispersions all lay between the Gordon-Taylor and Couchman-Karasz plots suggesting that ZAL\_010 and copovidone were miscible at all tested drug loadings (Figure 4.24). However, XRPD analysis of the

same samples indicated that whilst 15% and 30% drug loaded solid dispersions were amorphous, there was some evidence of Bragg peaks in the 50% drug loaded sample, which appeared to correspond to Form II ZAL\_010 (see Figure 4.25). This indicates that the samples were likely to have been partially phase separated at the time the DSC analysis had been carried out, but that this level had been below the detection limit of the DSC instrument (as discussed in Chapter 2). Unfortunately, there was not enough material available for PDF analysis to confirm this.



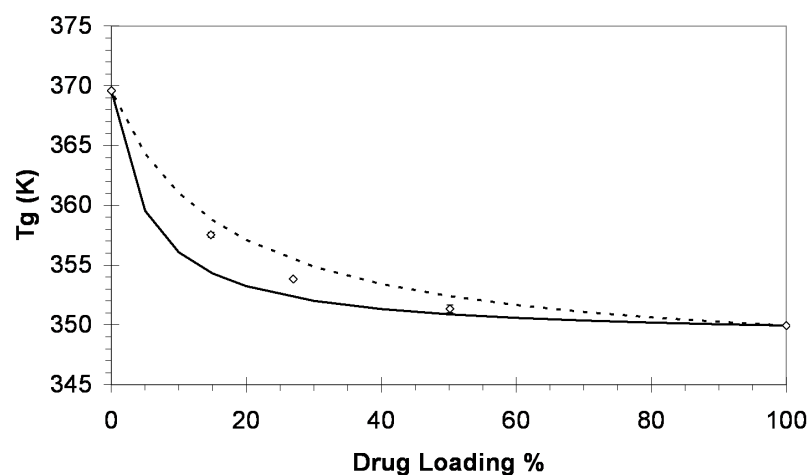


Figure 4.24:  $T_g$  of amorphous ZAL\_010 as a function of weight fraction drug. The solid line represents the fit to the Gordon-Taylor equation and the dashed line represents the fit to the Couchman-Karas equation.

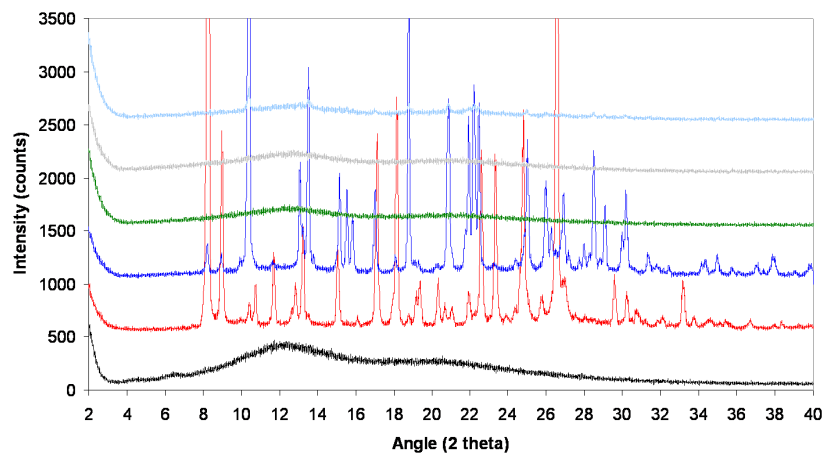


Figure 4.25: X-ray powder diffractograms of samples of crystalline ZAL\_010 (red), ZAL\_010 subjected to amorphisation (dark blue), and solid dispersions of ZAL\_010 and copovidone with drug loadings of 15% (green), 30% (grey) and 50% (light blue). Copovidone is also shown for reference (black).

#### 4.4.10 ZAL\_011

A sample of ZAL\_011 was analysed by XRPD and found to be crystalline (see Figure 4.26). By DSC, crystalline ZAL\_011 was shown to have a  $T_g$  at 70.82°C with  $\Delta C_P$  of 0.1912 J g<sup>-1</sup> K<sup>-1</sup>, and  $T_m$  with onset at 101.5°C, peak at 108.0°C, and  $\Delta H_f$  of 23.5 kJ mol<sup>-1</sup>. Therefore an annealing temperature of 130°C was proposed for the the formation of amorphous and solid dispersion samples of this compound. XRPD analysis of these samples showed that this sample preparation method successfully produced amorphous material (see Figure 4.26).

Single glass transition temperatures were observed for each drug-polymer blend, indicating that the drug and polymer were intimately mixed at all the drug loadings tested. The true density ( $\rho$ ) of crystalline ZAL\_011 was found to be 0.1995 g cm<sup>-3</sup>; and this value was used in a corrected form to create Gordon-Taylor and Couchman-Karaszc plots (see Chapter 2). The single  $T_g$ s measured for the solid dispersion with 15% drug loading lay on the Gordon-Taylor plot, but solid dispersion samples with higher loadings were below both the Gordon-Taylor and Couchman-Karaszc plots (Figure 4.27).

The experimental PDF traces for ZAL\_011 solid dispersion samples closely matches the traces simulated for physical mixtures at the same drug loadings, suggesting that they are not molecular dispersions (see Figure 4.28).

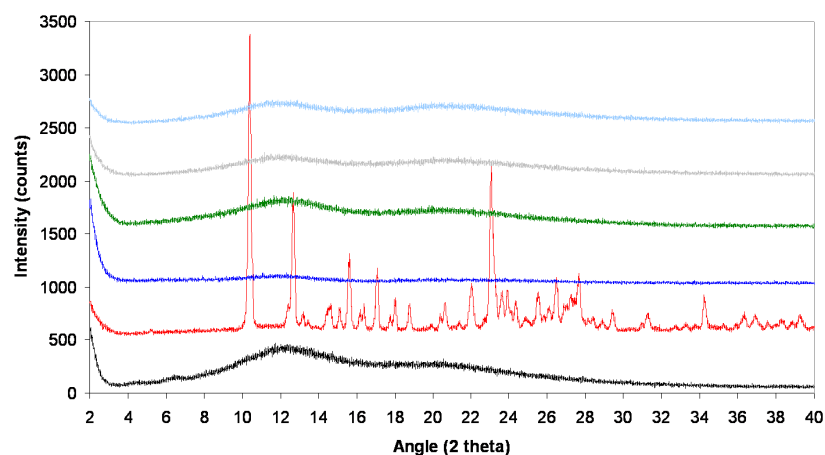


Figure 4.26: X-ray powder diffractograms of samples of crystalline ZAL\_011 (red), amorphous ZAL\_011 (dark blue), and solid dispersions of ZAL\_011 and copovidone with drug loadings of 15% (green), 30% (grey) and 50% (light blue). Copovidone is also shown for reference (black).

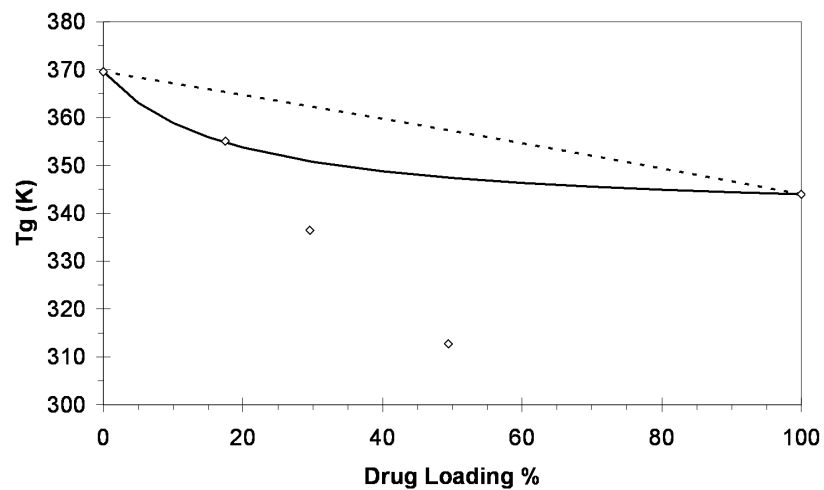


Figure 4.27:  $T_g$  of amorphous ZAL\_011 as a function of weight fraction drug. The solid line represents the fit to the Gordon-Taylor equation and the dashed line represents the fit to the Couchman-Karas equation.

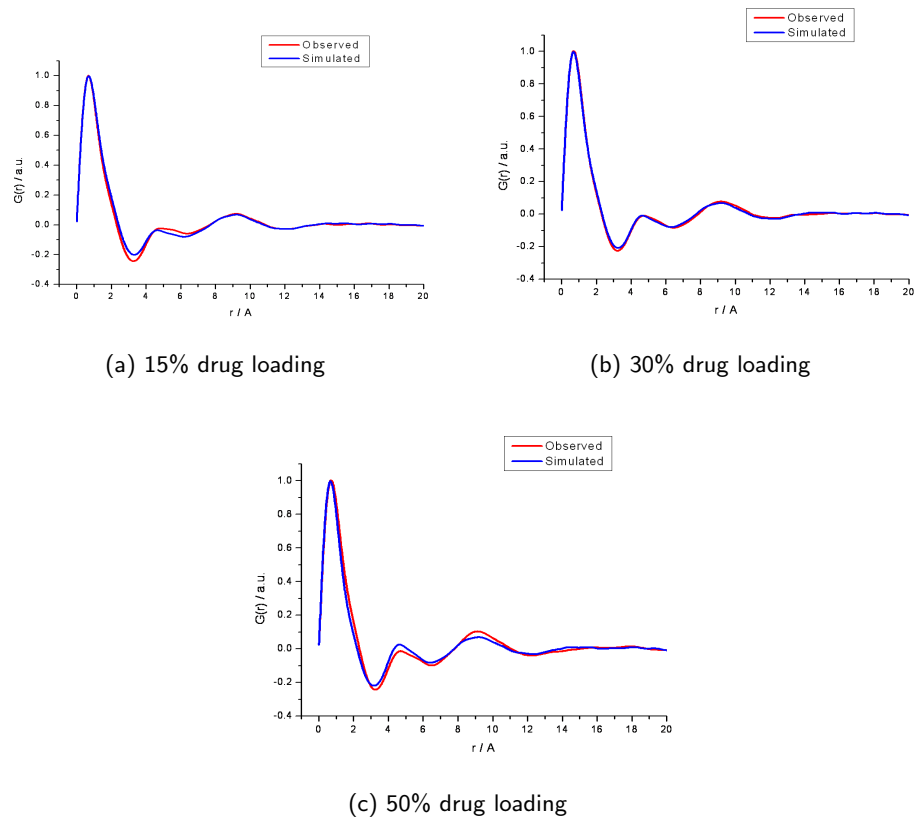


Figure 4.28: Comparison of the simulated traces of ZAL.011 and copovidone amorphous physical mixes with the observed traces of the solid dispersion at drug loadings of a) 15%, b) 30% and c) 50%.

## 4.5 Conclusions

From analysis of the molecular analogues by DSC analysis, it has been possible to identify a suitable annealing temperature to be used in the preparation of solid dispersion samples for the work detailed in the following chapters. XRPD analysis of samples produced using these prescribed annealing temperatures, shows that amorphous material can be successfully produced for most analogues.

Solid State analysis of ZAL\_001 was not possible as this compound is an oil. NMR analysis of this compound in Chapter 3 indicates that the oily nature of this compound is unlikely to be due to the presence of impurities in the material, and therefore that this compound is an oil must be related to the molecular structure of the compound. The only difference between this compound and felodipine (which is a crystalline solid) is that ZAL\_001 has an aromatised pyridine ring, compared with the dihydropyridine ring in felodipine, and this structural modification leaves ZAL\_001 without a hydrogen-bond donating group that can participate in the drug-drug intermolecular interactions present in the felodipine crystal structure [144]. ZAL\_001 will be used in following experiments, but when interpreting data for this compound it is important to bear in mind that it is liquid in ambient conditions, and that initial testing to determine extent of mixing has not been carried out on the solid dispersion samples.

ZAL\_008 was found to be practically insoluble in suitable organic solvents, which was likely to be due to its high melting point. This meant that formation of solid dispersion samples was not possible for this compound by solvent evaporation, and the degradation of the compound above the melting point indicated that processing by melt methods was also unlikely to be successful. These limitations mean that no further work will be carried out using ZAL\_008.

ZAL\_010 was shown to have a solid state profile that was complicated by the existence of two polymorphs. The analogue was shown to crystallise readily from two of the amorphous samples, which is likely to be because the samples were not annealed above the melting point of the Form II polymorph, and this may prove to be an issue in

later experiments.

PDF data indicated that all of the solid dispersions tested are phase separated in the drug loading range 15-50%, suggesting that solid solutions had not been formed for any of the analogues. It may be that at these loadings the amount of drug is above its super-saturation level in copovidone, and that at lower drug loadings the samples would be shown to be solid solutions.

## **4.6 Future work**

Firstly it would be useful to carry out PDF analysis on samples containing ZAL\_009 and ZAL\_010, as these analyses were not possible here due to restrictions on the amount of material available. Similarly, if more analogue material were available, it would be useful to test solid dispersions with a greater range of drug loadings.

FTIR analysis of the analogues and their solid dispersions could be useful in highlighting the presence of drug-drug and drug-polymer intermolecular hydrogen-bonding motifs, which could be used to explain the results from experiments in the following chapters.

## Chapter 5

# Physical Stability Testing of Felodipine-based Solid Dispersions

As solid dispersions are formulations of thermodynamically unstable amorphous material, their stability with respect to physical changes is a key consideration in their development. Exposure to particular environmental conditions may cause solid dispersions to undergo morphological changes such as polymer swelling, phase separation (de-mixing) or drug crystallisation. Any such changes can subsequently have a detrimental effect on the performance of the drug; for example, by affecting the release of the drug from the delivery system, or reducing the apparent drug solubility. The relative stability of a solid dispersion formulation is of particular relevance when one considers the lengthy shelf-lives that are desirable for a marketed drug, and the need for the dosage form to behave in the same way after storage as it would have done prior to storage. Therefore, in order for a solid dispersion to reach the market, it is of major importance to fully understand the potential for any physical changes to occur.

In this chapter we will look at the effect of environmental conditions on the physical stability of solid dispersions in two parts. The first part of this chapter will focus on the use of a laser light scattering technique, with the intention of investigating how the phase separation of solid dispersions can be initiated under specific environmental

conditions. This work focusses specifically on the solid dispersions of felodipine in copovidone. In the second part of this chapter, we will look at the crystallisation of the felodipine analogues that were synthesised in chapter 3 from their solid dispersions with copovidone under different storage conditions at a range of drug loadings using polarised light microscopy.

## **5.1 Light Scattering Studies of Felodipine/Copovidone Solid Dispersions**

### **5.1.1 Introduction**

#### **Phase Separation**

Phase separation is a term used to describe the collection of component molecules into domains, meaning that they are no longer evenly dispersed. This phenomenon is well-documented in the literature with respect to polymer blends (for example, see [145, 146, 147, 148, 149, 150]), and it is also of particular relevance to the field of solid dispersions, as phase separation could be considered to be a pre-cursor to crystallisation. This has been discussed in more detail in Chapter 1

It is clear that the crystallisation of the drug component from amorphous solid solutions cannot happen unless phase separation has first occurred. This is because several molecules of the compound are required to be within close proximity of each other in order for crystals to nucleate and grow. We have already discussed in chapters 1, 2 and 4, how systems that may appear by XRPD and DSC analysis to be molecularly disperse can in fact be shown to be more accurately described as a microparticles of drug in carrier, or solid suspensions. In such systems it could be considered that the drug and polymer components already exist in discrete domains, therefore fulfilling the true definition of a phase separated material; yet they are not necessarily termed so, particularly if the drug remains in the amorphous state. Therefore, perhaps a key question should be: "when do we consider phase separation to be a problem with respect to



crystallisation?" Afterall, it strikes the author that there may not be a defined boundary between molecular dispersions and solid suspensions, but that there is in fact a continuum from one state to the other. That is, there is no rule to say how many molecules of a substance must be near to each other, and how close they must be before a material is no longer considered a solid dispersion and becomes a phase separated system. It is most likely that the answer to this question lies both in the sensitivity of the analytical instruments used to detect structural changes in such materials, and continued observations showing that crystallisation occurs as a result of such changes. Therefore, for the remainder of this chapter we will use the term phase separation to refer to the process of a solid dispersion becoming less intimately mixed, rather than as a general descriptor of the physical state.

Ideally, once it has been decided that a drug will be formulated as a solid dispersion, the propensity for a solid dispersion to phase separate would be determined during the screening activities to identify a suitable polymer. This way, the time and costs associated with developing a formulation that is later shown to be unstable can be avoided. Or, at the very least, the early identification of such challenges would provide formulators with more time to develop strategies to successfully bring the product to market. In an attempt to address this, we set about developing a laser light scattering instrument as a means of detecting phase separation. If successful, this technique would lend itself to forming the basis of a high-throughput screening method to identify phase separation of solid dispersions during initial screening work. This is because laser light scattering is a relatively cheap method, and the data obtained from such methods gives a better statistical average over a larger area of the sample compared with microscopy. With further development, the film-cast samples used for screening activities could be presented to the light scattering instrument in their well-plates, thus meaning that more information could be obtained from small amounts of material. Also, whilst there is obviously no real substitute for human observations arising from years of experimental experience, the data acquired using this method could be automatically manipulated by

a computer to enable faster screening.

### **Development of the Laser Light Scattering Instrument**

As discussed in Chapter 1, phase separation occurs if the total free energy of separated phases is lower than the free energy of the mixed state (i.e. there is a 'miscibility gap') [71], and may be brought about by changes in, for example, temperature or humidity. The different domains of a phase separated material have slightly different optical properties (refractive index), and light passing through the sample will undergo Mie scattering if the domains are of a similar or larger size to the wavelength of the incident light [151]. In a static laser light scattering experiment, the intensity of the scattered light over a range of angles is measured, and this information can then be used to determine the size of the domains in the material. [151, 152, 153]. This technique has already been used in a number of studies to investigate phase separation in polymer blends [154, 155, 156], and in particular, the method used by Hashimoto et al in their 1984 work [155] seemed appropriate to emulate for the purposes of this study.

The light scattering system described by Hashimoto et al basically consists of a laser beam that is passed through the sample (which is held in a temperature controlled cell), and scattered by it. The scattered light is then projected onto a screen, and the resulting scattering pattern is in turn imaged using a video camera. From the scattering patterns the size of the phase separated domains ( $R_s$ ), and the interdomain distance ( $D_s$ ) were determined as shown in equations (5.1) and (5.2) respectively, where  $\lambda$  is the wavelength of the incident laser light, and  $\theta_m$  is the angle at which the intensity of the scattered light reaches a maximum [155].

$$4\pi(R_s/\lambda) \sin(\theta_m/2) = 5.765 \quad (5.1)$$

$$2D_s \sin(\theta_m/2) = \lambda \quad (5.2)$$

Generally speaking the scattering pattern projected onto the screen is due to

light scattered at an angle of  $\leq 35^\circ$  [153]. Therefore, if we use this as the value for  $\theta_m$  in equation 5.1, we can see that with a helium-neon laser with  $\lambda = 633$  nm, the smallest domain size that can be detected using this method is approximately 970 nm.

This method was attempted for detecting phase separation in solid dispersions, but the samples did not produce the well-defined scattering patterns observed by Hashimoto et al in their phase separated polymer blend systems, and so a more simple approach was attempted. It was reasoned that the more domains that appear, and the larger they become during the phase separation process, the more light will be scattered by the sample. It therefore followed, that this process would lead to an attenuation of the central incident light beam by the sample with increasing phase separation. Hence, the method that was developed involved measuring the intensity of the central laser light beam after it had passed through the sample, using a photodiode, in order to determine the level of beam attenuation with time. Using this approach would enable information regarding the kinetics of phase separation to be acquired.

### 5.1.2 Materials

#### Drop cast film samples

Solid Dispersions of felodipine (AstraZeneca) in copovidone (Kollidon VA64, BASF) were produced by casting from a mutually compatible solvent system (80% Methanol: 20% Acetone v/v). Solutions of the drug / polymer mixture with different concentrations were prepared and then drop-deposited onto clean, glass substrates, where the solvent was allowed to evaporate for 75 minutes. The samples were then placed in an oven under Nitrogen at  $30^\circ\text{C}$ , heated to  $155^\circ\text{C}$ , and held at that temperature for 30 minutes to anneal the sample. The samples were then quench cooled to room temperature. All samples were stored in a vacuum desiccator and analysed within 2 days of preparation. It was important to produce flat, featureless film samples, as any bubbles in the film, or an uneven surface to the film could lead to additional scattering of the laser light during the experiment.

### 5.1.3 Methods

#### Light Scattering Experimental

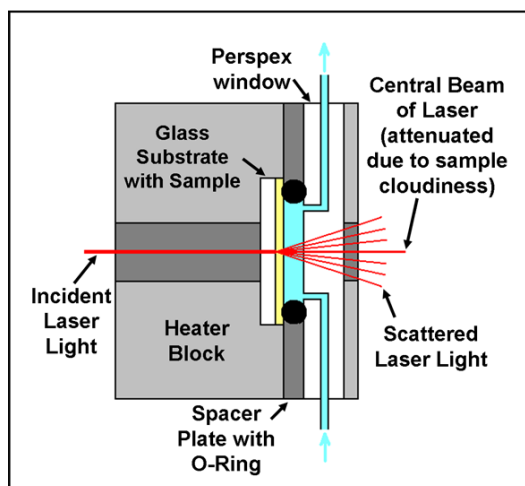


Figure 5.1: Schematic showing a cross-section of the temperature controlled sample cell used in the laser light scattering experiments.

Laser Light Scattering experiments, during which the intensity of light passing directly through the sample was measured, were carried out using a custom-built instrument. A Helium-Neon laser beam (Spectra Physics, Model 31005; power, 1.5 mW; wavelength,  $\lambda_0 = 633nm$ ) travels to a beam splitter. Part of the beam is diverted to a Reference Photodiode, whereas the rest of the beam passes through the sample (which is held in a temperature-controlled flow cell - see Figure 5.1), and then to another photodiode (see Figure 5.2). Changes in intensity are measured by obtaining a Transmission Coefficient, which enables any fluctuations in the intensity of the incident laser to be ratioed out:

$$\text{Transmission Coefficient} = \frac{\text{Sample Intensity}}{\text{Reference Intensity}} \quad (5.3)$$

The computer controlling the light scattering apparatus samples the light intensities measured by the photodiodes every 2-3 seconds as the experiment progresses.

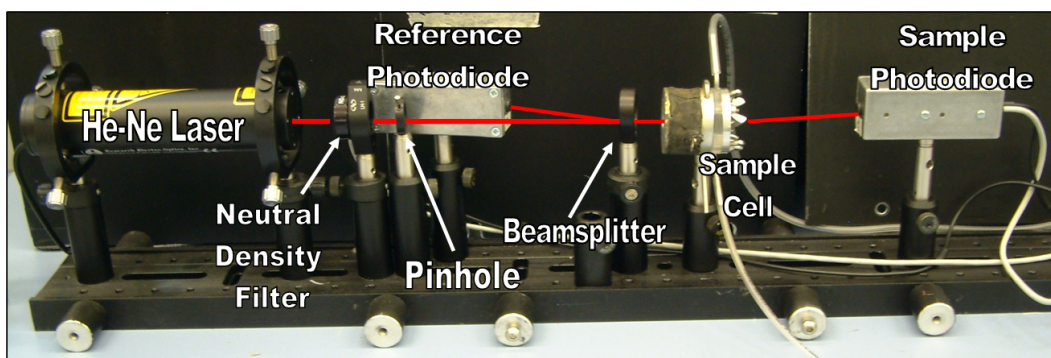


Figure 5.2: Photograph showing the experimental setup for the laser light scattering studies. The path of the laser beam is shown in red.

### Optical Microscopy

Optical microscopy was carried out on water-exposed film samples using an Olympus BX51M microscope in Brightfield mode. ImageProPlus software (version 5.0) was used for imaging.

### Atomic Force Microscopy (AFM)

Film samples were analysed before and after exposure to water by atomic force microscopy using an Asylum Research MFP-3D scanning probe microscope, with NSC16/AIBS tips (MikroMasch), and controlled using Igor Pro software (version 6.04). Samples were analysed in tapping mode, and topographic and phase information about each sample was collected.

#### 5.1.4 Results and Discussion

Initial tests performed using the felodipine / copovidone films showed that when a water droplet was placed on the sample, the film turned cloudy. When the water was removed from the film, the cloudiness remained for some time, indicating that the turbidity was present in the film itself, and not due to a saturated solution that had formed in the water droplet. This was also evident from the properties of the film which had changed

from having a hard, glassy texture to being swollen and gel-like. The same test was performed using a control sample containing 100% copovidone, but this sample did not turn cloudy. These observations suggested that the cloudiness could be due to the drug separating out from the dispersion.

To further investigate this phenomenon in a more quantitative manner, the samples were analysed using the light scattering apparatus. The analyses were performed at a range of temperatures encompassing 37°C, and at least four repeat analyses were performed for each drug loading at each temperature. From these experiments it became evident that the total time for the films to become completely opaque differed from sample to sample, depending on the concentration of the film and the temperature at which the experiment was carried out (see Figure 5.3).

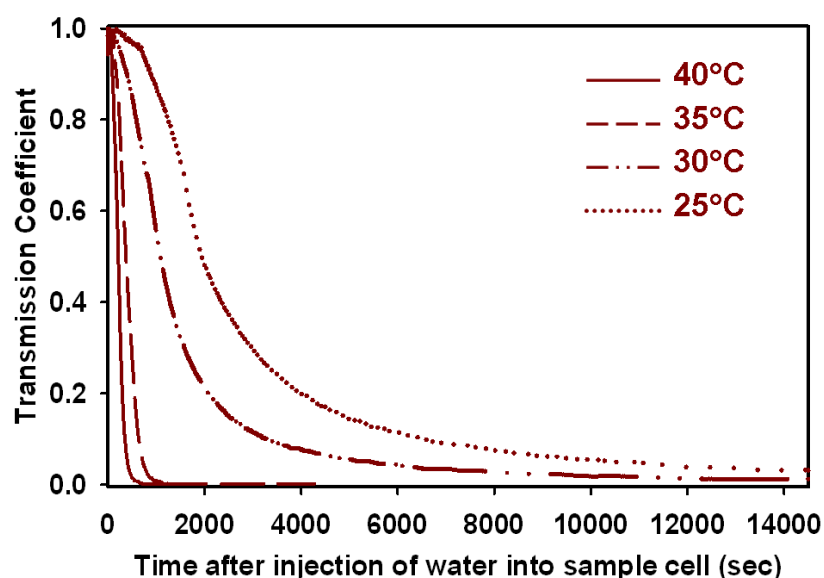


Figure 5.3: Graph showing changes in transmission coefficient after water is injected into the sample cell for solid dispersions containing 50% felodipine at four temperatures.

In order to better understand the effects of temperature and concentration on the changes in film turbidity, a number of transformations of the data were made. As the decrease in transmission coefficient appears to be exponential in nature, the natural

log of the transmission coefficient was taken for each plot, in order to produce a straight-line graph. This transformation produced plots which had two distinct regions; a region after water injection which is horizontal, and a second straight-line region with a negative gradient (see Figure 5.4). The first region could be considered as a time during which the nucleation of phase separated domains occurs ( $\tau_N$ ). The gradient of the second region could be considered as equal to the reciprocal of a time during which the phase separated domains grow ( $1/\tau_G$ ).

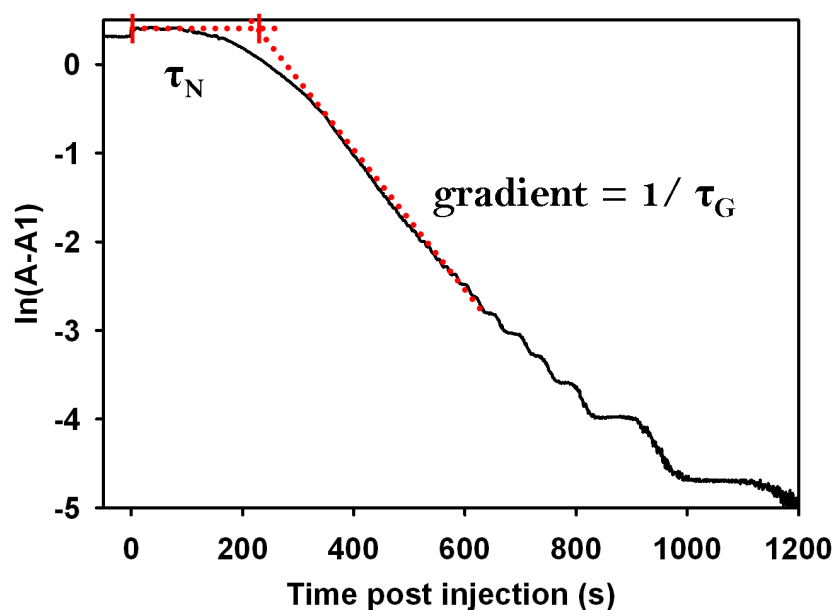


Figure 5.4: Semi-log plot of the light scattering data, showing how characteristic nucleation times ( $\tau_N$ ) and growth times ( $\tau_G$ ) can be determined for each sample.

Once determined, the  $\tau_N$  and  $1/\tau_G$  values were used to produce Arrhenius plots in order to establish any trends in the data (Figures 5.5 and 5.6). These plots indicate that the nucleation and growth rates for the turbidity are influenced by the temperature at which the experiment is carried out in a way that is consistent with the behaviour of thermally activated processes. More unexpectedly, it was found that nucleation and growth rates for the evolution of turbidity in the samples was lower for those containing higher concentrations of drug. Initially it was considered that this may have been

influenced by uptake of water into the samples, and so further analysis was carried out to determine what was happening to the samples during the experiment.

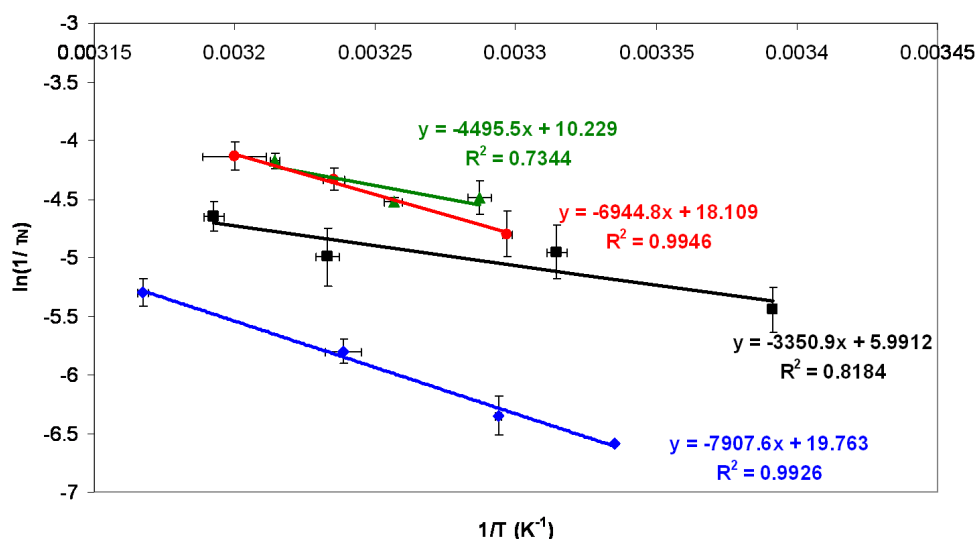


Figure 5.5: Arrhenius plots of  $\ln(1/\tau_N)$  against  $1/T$  for film cast solid dispersions with drug loadings of 50% (blue), 40% (black), 30% (green) and 20% (red).

In order to investigate the changes occurring in the film samples that may account for the increase in turbidity, further analysis was carried out on them using several techniques. Firstly, material was recovered from films that had been exposed to water and then been left to dry, and this was subjected to analysis by XRPD. If the turbidity was indeed due to phase separation, it seemed logical to suggest that this might lead to the crystallisation of felodipine from the samples. However, the samples were found to be X-ray amorphous, indicating that if crystallisation had begun to occur, it was at levels undetectable by XRPD, i.e. typically less than 2% of the sample [105].

The films were then observed during exposure to water with brightfield optical microscopy. The films prior to water exposure were shown to be smooth and glassy, with no notable features (Figure 5.7a). Within a minute of the water droplet being placed on the film, cracks in the film can be seen to appear (Figure 5.7b), from which the film seems to raise away from the substrate (Figure 5.7c). After the water droplet has



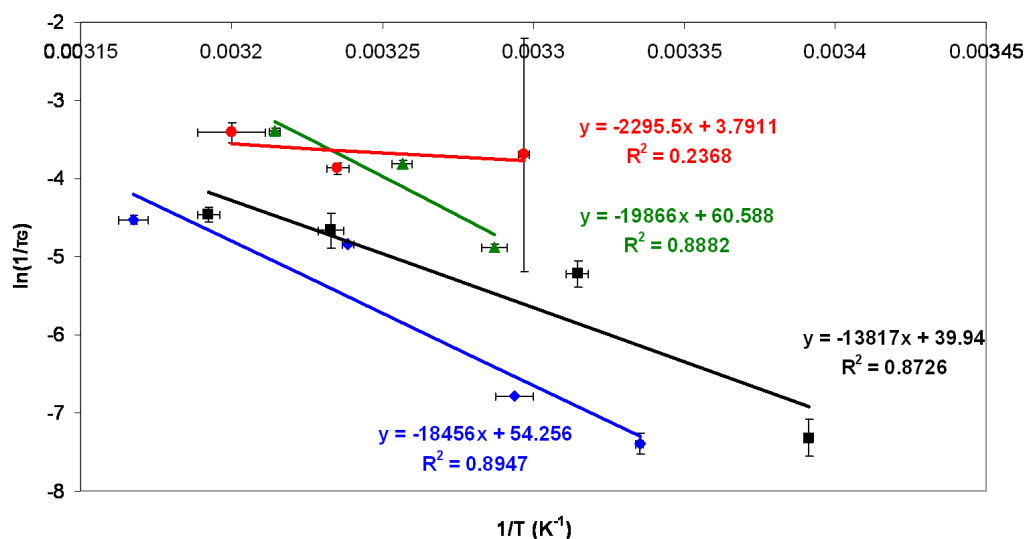


Figure 5.6: Arrhenius plots of  $\ln(1/\tau_G)$  against  $1/T$  for film cast solid dispersions with drug loadings of 50% (blue), 40% (black), 30% (green) and 20% (red).

dried, the film can be seen to be mostly smooth and glassy again, but with some cracks remaining where the film appears to have buckled away from the substrate (Figure 5.7d). The cracks present in the film when wet, and the associated buckling of the film, were of a scale which would go some way to explaining the increase in the amount of laser light scattered by, and hence the attenuation of the laser beam passing through the samples.

Atomic force microscopy experiments were also carried out on samples both pre- and post-water exposure. Tapping mode AFM was used to analyse the samples, as this method would enable phase information as well as topological information to be gathered from the sample. If phase separation was the cause of the increased turbidity (and hence increased light scattering), then the different domains of the phase separated material will have different phase information associated with them. AFM of the samples prior to water exposure showed them to be homogenous, and mostly smooth as any height variations across the samples were very small (Figure 5.8), and this supports the optical microscopy data. This can be seen in Figure 5.9a where variations in film height are to the order of hundreds of picometres. After exposure to water, a greater variation in

the topographies of the samples is observed, which is of the order of several nanometres (Figure 5.9b). However, this topographical change does not appear to be accompanied by significant changes in phase across the samples which would be consistent with a theory of phase separation. It was also noted from AFM experiments that films with higher polymer concentration appear to show greater changes in surface structure.

Following the experiments detailed above, the turbidity and topographical changes in the samples on exposure to water appears to be most consistent with polymer swelling of the film. This swelling causes the films to buckle and crack away from the sample substrate as shown by optical microscopy, and this has an effect on the topography across the whole of the film surface, as shown by AFM. The observation that films with higher polymer loadings appear to show greater changes in surface structure also supports the idea that polymer swelling in the presence of water is more likely. The theory that the turbidity is caused by phase separation is not supported by optical microscopy or AFM, neither of which shows evidence of the formation of distinct phase separated domains. Additionally, XRPD does not provide evidence that the materials are phase separated or that the felodipine has crystallised out from the films.

### **5.1.5 Conclusions - Light Scattering Work**

Glassy, transparent solid dispersion films of felodipine in copovidone were shown in these experiments to become increasingly opaque upon contact with water. This study has shown that the laser light scattering method detailed here can be used to detect and monitor changes in film turbidity caused by morphological changes on micron length scales. It was shown that the rate at which the solid dispersion films became turbid was dependant on the drug loading and the temperature at which the experiment was carried out. This turbidity was initially believed to be due to phase separation of the solid dispersion films, however, the Arrhenius plots indicated that nucleation and growth of turbidity in the films was slower in films containing more felodipine, and hence suggested that the opacity of the films was caused by water

uptake by the samples. Microscopic techniques showed that the turbidity in the films is most likely caused by surface structure modifications caused by polymer swelling.

Laser light scattering is a technique that has the potential to form the basis of a high-throughput method for the detection of morphological changes in solid dispersion, due to its simple design, low costs and the ability to analyse samples under a range of environmental conditions. However, this technique does have some limitations - the most crucial of which is that whilst this technique can be used to detect changes in a sample, it cannot tell us what causes those changes. This was highlighted with the experiments detailed in this chapter, in which it was shown that morphological changes in the sample were not due to phase separation as had originally been suspected, but were instead due to polymer swelling. Despite this, the polymer swelling process was successfully monitored using the light scattering technique, and it was possible to show how the kinetics of the polymer swelling process were dependent on the temperature at which the experiment was conducted, and the polymer-loading of the solid dispersion. Polymer swelling is also of particular interest to the pharmaceutical industry, as it can impact upon the release of drug from a formulation during dissolution, as we will see in Chapter 6. It is believed that if attempts to develop a system that could provide further structural information about the changes in the samples had been more successful (for example, regarding the length scales at which the changes were occurring), it may be possible to better distinguish between different types of morphological changes such as polymer swelling and phase separation.

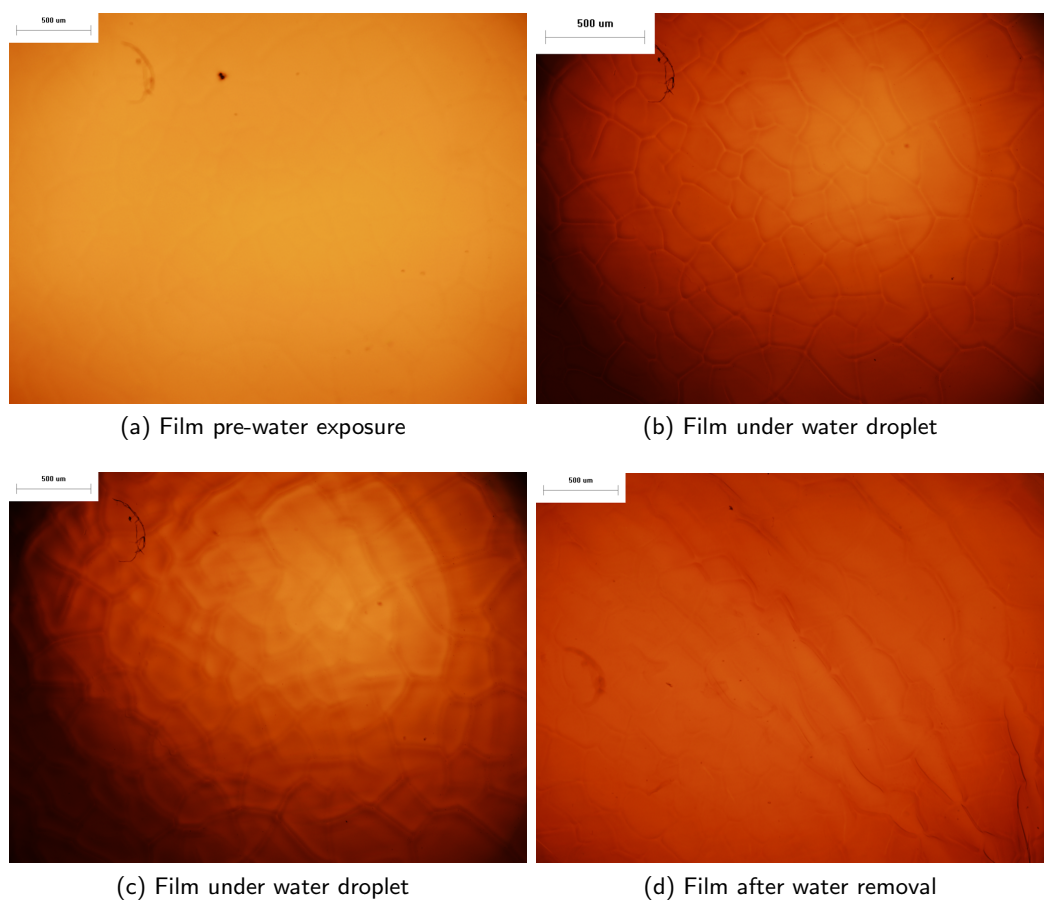


Figure 5.7: Brightfield optical microscopy images of a 10% felodipine-loaded film prior to water exposure (a), during water exposure (b & c) and after removal of the water droplet (d). All images were taken at  $\times 5$  magnification and scale bars represent 500  $\mu\text{m}$ .

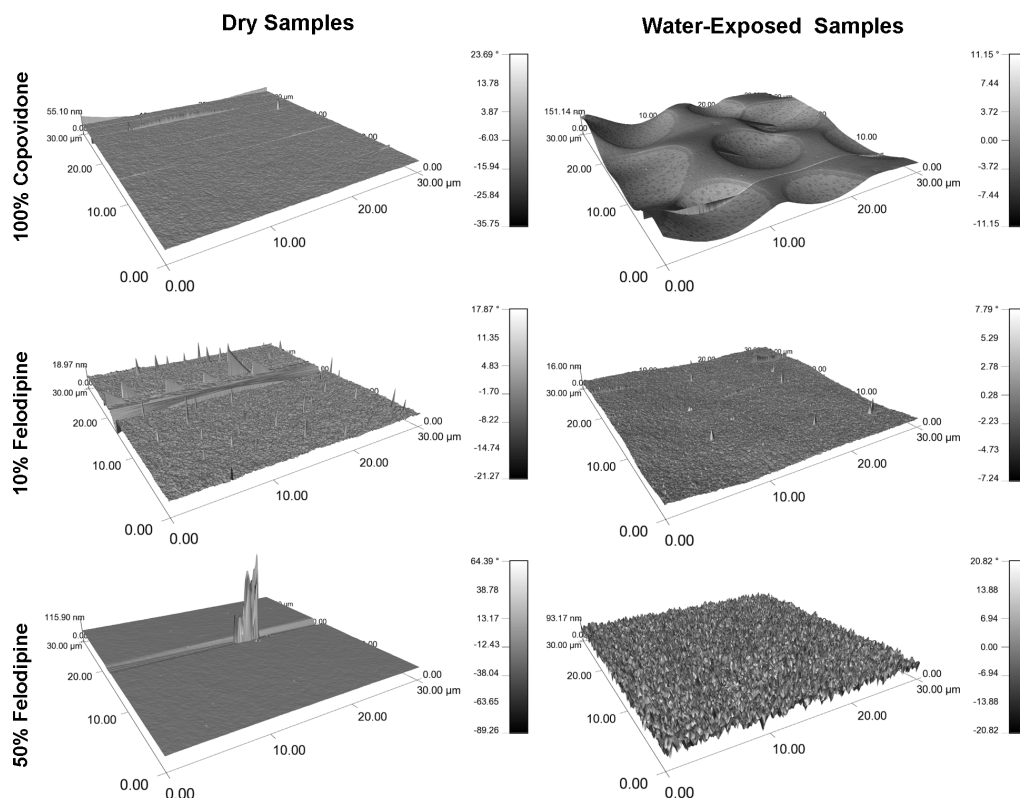


Figure 5.8: Topographies of Felodipine/Copovidone films as imaged using AFM prior to and after exposure to water. Phase data is shown overlaid on the topographies, with shadings as indicated by the individual scale bars. Images on the left are samples pre-water exposure and images on the right are of samples after exposure to water. Images are of samples with 0% (top images), 10% (middle images) and 50% (bottom images) felodipine-loadings.

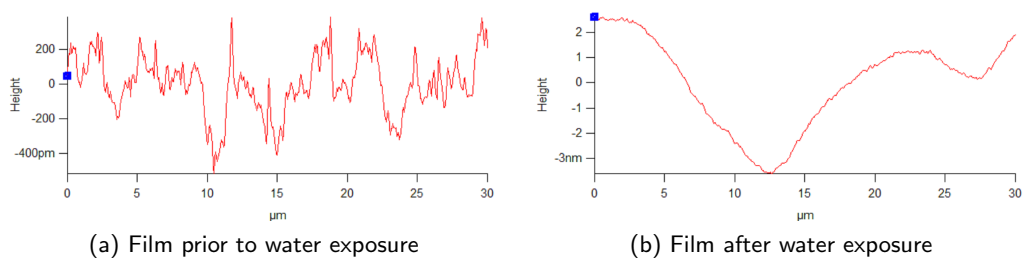


Figure 5.9: Graphs showing the topography of 10% felodipine loaded films a) pre- and b) post-water exposure along a cross-section of the samples, as determined by AFM.

## 5.2 Polarised Light Microscopy Studies of Felodipine-based Solid Dispersions

### 5.2.1 Introduction

Drug crystallisation from amorphous solid dispersions has been the subject of a large number of papers in the literature, as physical instability with respect to crystallisation poses one of the biggest obstacles to their successful formulation and marketing. In previous studies it has been suggested that intermolecular interactions between the drug and polymer components are key to explaining the relative stability of some solid dispersions compared to the pure amorphous form. For example, Taylor and Zografi identified that in solid dispersions of indomethacin with PVP, the polymer carbonyl group forms hydrogen bonds with the carboxylic acid moiety of the drug [100]. This intermolecular interaction was later shown to stabilise these solid dispersions with respect to crystallisation by preventing the dimerization of the drug which was known to act as a nucleation point in its crystallisation [157]. Khougaz and Clas also suggested that the inhibition of crystallisation of compound MK-0591 from solid dispersions with PVP and PVP/VA was due to the formation of an ion-dipole interaction between the PVP carbonyl group and the  $\text{COO}^- \text{Na}^+$  moiety of the drug [158]. Vasanthavada et al added weight to the argument that the formation of drug-polymer interactions leads to improved physical stability of solid dispersions with respect to phase separation and crystallisation when they found that solid dispersions of indoprofen, which has a proton donating group, was miscible with PVP, unlike griseofulvin, which did not contain any proton donating groups [59]. Shibata et al carried out a broader study that investigated the physical stability of several drug compounds when they were formulated as solid dispersions with PVP-CL, and found that the amorphous state was maintained for at least 6 months for drugs containing hydrogen-bond donor groups, irrespective of their melting points or molecular weights. Once again, it was suggested that in these compounds a hydrogen-bond was formed between the drug and the carbonyl group of the polymer. Conversely,

the amorphous state was not maintained in the drug compounds without hydrogen-bond donating groups. Additionally the type and number of hydrogen-bond donating groups in the drugs was not shown to have an effect on solid dispersion formation in this study [48].

Of particular influence on the work detailed here, are the studies carried out by Lynne Taylor's group. One series of experiments investigated inhibition of felodipine crystallisation by three different polymers; PVP, HPMC and HPMCAS. It was found that all three polymers were effective in inhibiting crystallisation in the absence of moisture, and a correlation between the nucleation rate and the  $T_g$  of either the drug or polymer, or the strength of the drug-polymer hydrogen-bonds could not be determined. Therefore, it was suggested that the kinetic barrier to crystal nucleation was increased proportionally with polymer loading [87]. Analysis of the same systems after storage in the presence of moisture showed that a decrease in  $T_g$  of the solid dispersions occurred due to the absorption of more water by the samples as a result of the addition of the hydrophilic polymer. This indicates an increase in molecular mobility and would suggest a greater propensity for drug crystallisation, but the nucleation rate of felodipine was still found to be lower in the solid dispersion samples than the pure drug samples [56]. More recently, it was shown that crystallisation of felodipine from bulk solid dispersions stored in humid conditions was more rapid when relative humidity levels were greater than 75%. Moreover, it was shown that crystallisation of felodipine from PVP was faster than from HPMCAS, and this was attributed to PVP absorbing more water than HPMCAS. Crystallisation of felodipine was shown to reach a kinetic plateau, whereby a fraction of the drug remained amorphous even after 500 days or more [60]. Another series of studies compared the tendency of two structurally related 1,4-dihydropyridine calcium channel blockers to crystallise from solid dispersions with PVP. The first study, carried out in the absence of moisture, concluded that the tendency for nifedipine to crystallise more readily from solid dispersions with PVP than felodipine could not be predicted from parameters commonly measured by DSC such as  $T_g$  and molecular mobility, as

these values were virtually the same for the two drug compounds tested. Instead, it was concluded that the tendency for the drug to crystallise from the solid dispersion was related to the readiness of the pure substance to crystallise from the amorphous form [91]. A subsequent study, in which the same samples were stored in humid conditions suggested the reason for nifedipine to crystallise more readily than felodipine was because it exhibits a higher level of supersaturation in the polymer, and also takes up more water, which acts as an anti-solvent [93]. The following study aims to build upon the work by Lynne Taylor's group by providing further insight into how the molecular structure of felodipine impacts on the physical stability of its solid dispersions.

This study, set out to further test the hypothesis that strong intermolecular bonds between drug and polymer molecules in a solid dispersion lead to increased physical stability with respect to crystallisation. It could be considered that these drug-polymer interactions might aid physical stability in two ways. Firstly, that the interactions act to complex the drug to the amorphous polymer, and hence, 'fix' the drug molecules in an amorphous arrangement. Secondly, these intermolecular bonds may serve to block the functional groups involved in competing drug-drug interactions that would potentially otherwise lead to drug crystallisation. It was also proposed that the disruption of competing drug-drug intermolecular bonding motifs that would lead to crystallisation of the API, could occur through engineering the drug molecule in such a way as to make any drug-drug interactions weaker or less likely to form. Therefore, the aim of these experiments was to use observations of the ability of copovidone to inhibit the crystallisation of the felodipine molecular analogues synthesised in chapter 3 to further understand what molecular interactions might lead to the formation of physically stable solid dispersions. The crystallisation of the analogues formulated as solid dispersions was observed over time when stored under a range of environmental conditions, and compared to the performance of felodipine in the same tests. As studies in the literature have already shown that hydrogen bond formation between the drug and the PVP carbonyl leads to improved physical stability of the solid dispersion, it was our hypothesis that removal of



the hydrogen-bond donor NH group from felodipine would lead to rapid crystallisation of the drug. Further to this we were interested to determine the effects of changing other felodipine functional groups on the ability of copovidone to inhibit crystallisation of the drug.

## Experimental Design

A key concern in the design of these experiments was that only very limited amounts of material were available for some of the analogue compounds (in some cases only 100 mg) and this placed constraints on which analytical techniques could be used for sample monitoring and the number of storage conditions used during the experiments, as well as the number of repeat samples that could be produced. In previous studies, measurements of sample  $T_g$  by DSC provided the means for testing [157], but using this method would require a minimum of 20 mg of material for just one set of samples (with drug loadings of 100%, 50%, 30% and 15%), with no repeat analysis, held under only one set of storage conditions for 5 experimental timepoints. Additionally, the DSC run for a single sample could take upwards of 30 mins, meaning that an absolute maximum of 48 samples could be analysed in a 24 hour period (not taking into account sample preparation time, and assuming that the instrument had an autosampler). The combination of all these factors indicated that analysis of the samples by DSC was not a viable option.

Raman mapping initially seemed like a suitable alternative to DSC analysis, however this method was discounted for two reasons: firstly on account of the amount of time required to map a single well in the plate, and secondly because some of the compounds fluoresced. Therefore, polarised light microscopy was selected as the most suitable method for analysing the well-plates.

Polarised light microscopy was chosen for several reasons. Firstly, the process of taking an image of a sample is quick and easy, particularly if the microscope is equipped with a motorised X,Y stage that can be programmed to automatically 'read' the well-

plate. Microscopy is also a cheap and simple analytical method, which makes it ideal for analysing a large number of samples. Using cross-polarised light to analyse the samples means that crystals will be spotted as soon as they are above the lower size limit for detection. The resolution  $d$ , of a microscope is given by:

$$d = \lambda/2NA \quad (5.4)$$

where the wavelength of the incident light ( $\lambda$ ) is usually assumed to be 550 nm (the wavelength of green visible light), and NA refers to the numerical aperture of the objective in use. The highest practical NA when imaging in air is usually 0.95, and this would result in a resolution of 290 nm.

Although imaging a single well in a plate is a quick process, analysis of all the samples is still a time-consuming process due to the number of them. As a result of this, and the fact that the well plates would be removed from their storage conditions during the analysis, it was determined that the shortest time interval between analyses would be 1 day. Therefore, it was scheduled for the well plates to be analysed after storage for 1 day, 2 days, 1 week and then weekly thereafter for 7 weeks.

## 5.2.2 Materials

### Preparation of well-plates

Solid Dispersions of felodipine (AstraZeneca) or molecular analogue (See Chapter 3) in copovidone (Kollidon VA64, BASF) were produced by casting from chloroform (Fischer Scientific).

Wells in the well-plates were known to have a capacity of 400  $\mu\text{L}$ , and it was determined that there should be approximately 1 mg of material in each well in order to detect the crystallisation. Therefore, a solution was prepared for each of the analogue compounds (including felodipine) and copovidone with a concentration of 2.5 mg/mL. Using a multi-channelled pipettor, different ratios of the analogue and polymer solutions were dispensed into the well plates such that 400  $\mu\text{L}$  of solution in total was

placed in each well, so that solid dispersions of 100%, 50%, 30% and 15% drug loading were present in each plate in duplicate (see Figure 5.10). The solvent was flash evaporated from the well plates, which were then placed immediately in a pre-heated oven under a nitrogen flow for 30 minutes. The samples were then quench cooled to room temperature.

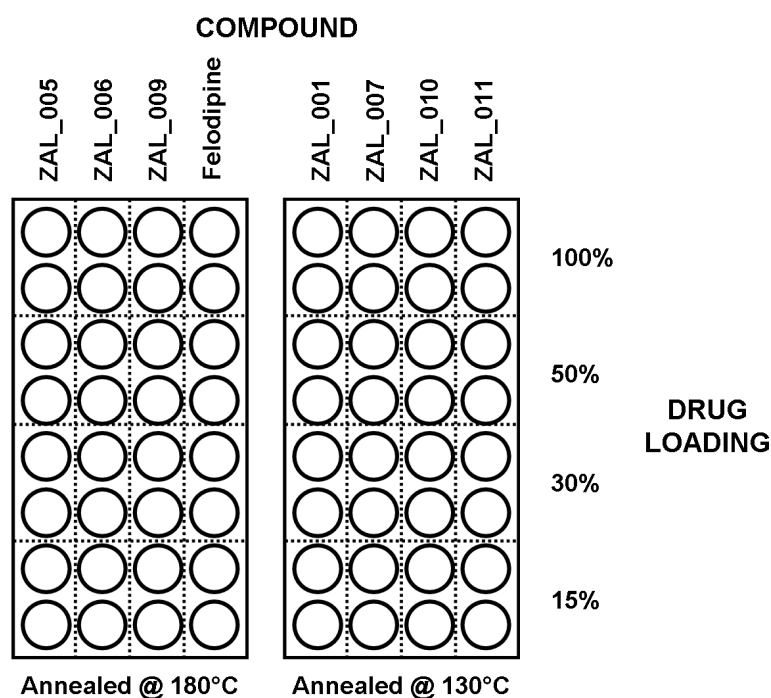


Figure 5.10: A schematic to show the layout of samples in well plates for crystallisation studies. Each well plate was prepared in triplicate to enable storage in three different stability testing rooms.

As a result of DSC experiments in Chapter 4, it was determined that different compounds required their solid dispersions to be annealed at different temperatures. To aid in sample preparation, two annealing temperatures were used, and the samples were prepared in separate well-plates accordingly. Felodipine, ZAL\_005, ZAL\_006 and ZAL\_009 were annealed at 180°C, and ZAL\_001, ZAL\_007, ZAL\_010 and ZAL\_011 were annealed at 130°C. Each well plate was produced in triplicate to enable storage of the

samples under three different environmental conditions.

The well plates took a day to prepare, and so they were stored overnight in sealed containers with desiccant in a fridge at 5°C, prior to initial analysis by polarized light microscopy.

### **5.2.3 Methods**

#### **Polarized Light Microscopy**

Crystallization of the drug compounds from their respective solid dispersions was followed by polarized light microscopy. An Olympus IX50 Inverted Microscope (Tokyo, Japan), equipped with motorised X,Y,Z stage (H107PIX model, Prior Scientific, Fulbourn, UK), and camera (JVC KY-F55B 3-CCD, Yokohama, Japan) was used. Images were taken at 2x magnification using Image Pro Plus version 7.0 software (Media Cybernetics, Inc., Maryland, USA). Samples were analyzed using polarized light with an analyzer (model IX-LWPO, Olympus, Tokyo, Japan) set to 90° with respect to the polarizer.

#### **Storage and sampling**

The well plates were first imaged by polarized light microscopy prior to storage in environmentally-controlled stability testing rooms. Due to the time-consuming nature of this analysis, and the fact that the well plates would be removed from their storage conditions during this time, it was determined that the shortest time interval between analyses would be 1 day. Therefore, it was scheduled for the well plates to be analysed after storage for 1 day, 2 days, 1 week and then weekly thereafter.

The well-plates were stored in stability rooms with conditions of 25°C/60% Relative Humidity (RH) and 40°C/75% RH, and in an oven set at 40°C. The well-plates stored in the stability rooms were stored in open boxes, and the plates stored in the oven were stored in an air-tight tin containing desiccant, to ensure 0% RH for those samples.

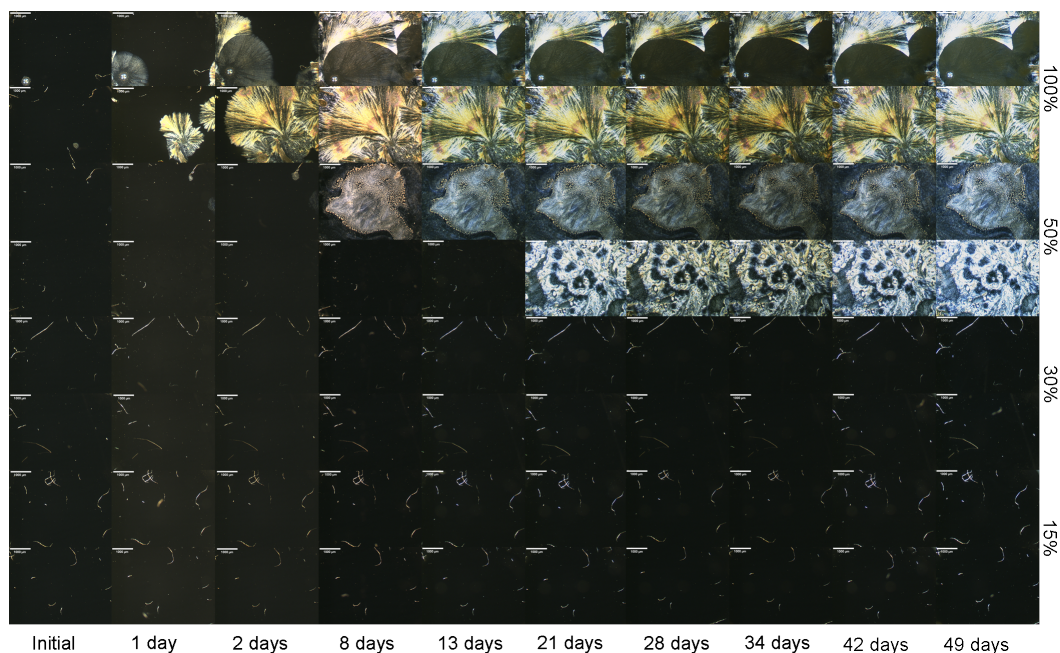


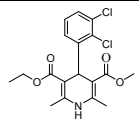
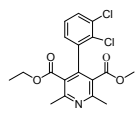
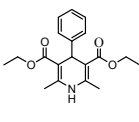
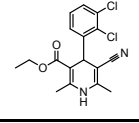
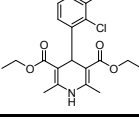
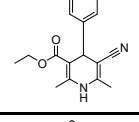
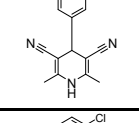
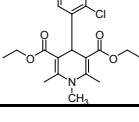
Figure 5.11: Example grid of images obtained from crystallisation experiments. This example shows the images obtained for solid dispersions of ZAL\_011 with ranging drug loadings stored at 25°C/60% Relative Humidity over 7 weeks.

#### 5.2.4 Results and Discussion

The images obtained from the well-plate crystallisation experiments were arranged in grids like the example shown in Figure 5.11 in order to better observe trends in crystallisation with respect to time, drug-loading and storage conditions. The grids are organised with 10 images in the horizontal direction; one image for each sampling timepoint, and eight images vertically; two images, one below the other, for each of four drug loadings. Each analogue has three image grids associated with it - one for each storage condition. All of the images obtained from these experiments can be seen in Appendix A, and the results of these experiments are summarised in Table 5.1.

Firstly, an assessment of the felodipine samples shows that whilst the 100% drug material crystallised rapidly after storage in all three conditions, solid dispersion formation with copovidone was able to successfully prevent the nucleation of any crystals

Table 5.1: Table summarising the results of the well-plate crystallisation experiments. Duplicate samples were tested, and both results for each condition are detailed in the table. The numbers indicate the sampling day on which evidence of crystallisation was first seen for that sample; 0 denotes that crystals were seen during the initial analysis carried out prior to storage of the well-plate; '-' denotes that no evidence of crystallisation was observed for this sample for the duration of the experiment (49 days).

Storage Conditions		25°C/60%RH				40°C/75%RH				40°C/0%RH			
% Drug Loading		100	50	30	15	100	50	30	15	100	50	30	15
	Felodipine	1	-	-	-	1	-	-	-	1	-	-	-
		21	-	-	-	1	-	-	-	0	-	-	-
	ZAL_001	-	-	-	-	-	-	-	-	-	-	-	-
		-	-	-	-	-	-	-	-	-	-	-	-
	ZAL_005	0	-	-	-	0	1	1	1	1	-	-	-
		0	-	-	-	0	1	1	1	1	-	-	-
	ZAL_006	-	-	-	-	0	-	-	-	1	-	-	-
		-	-	-	-	0	-	-	-	8	-	-	-
	ZAL_007	1	-	-	-	1	-	-	-	8	-	-	-
		1	-	-	-	1	-	-	-	1	-	-	-
	ZAL_009	1	-	-	-	1	1	2	8	1	-	-	-
		1	-	-	-	1	0	2	34	1	-	-	-
	ZAL_010	0	0	0	0	0	0	0	1	0	-	-	-
		0	0	0	0	0	0	0	1	0	-	-	-
	ZAL_011	0	0	-	-	0	0	49	-	0	-	-	-
		0	21	-	-	0	2	8	13	8	-	-	-

at all three drug-loadings. This supports previous work by Konno and Taylor, which showed that the crystallization of felodipine could be inhibited when formulated as a solid dispersion with either PVP or HPMC [87].

Upon assessment of the crystallisation behaviour of the solid dispersions containing the felodipine analogues, ZAL\_001 in particular stands out, as no crystals are observed for this compound at any drug loadings under any conditions. Based simply on the hypothesis that intermolecular interactions between the drug and polymer in a solid dispersion influence its physical stability, this compound was originally expected to perform less well than felodipine due to the lack of the secondary amine hydrogen-bond donor. However, the absence of crystallisation in samples containing this compound is simply explained when we are reminded from observations detailed in chapters 3 and 4 that this compound is an oil at room temperature, and for this reason would not be expected to crystallise.

If we move on to analyse the crystallisation of the remaining analogues, it can be seen that there is an overall trend for the relative humidity at which the samples are stored to have a greater impact on the rate of crystal nucleation and growth than temperature. This can be seen for 100% samples of compounds ZAL\_005, ZAL\_006 and ZAL\_007, which all crystallise at earlier timepoints when stored at 40°C/75%RH compared with samples stored 40°C/0%RH. Also, it can be seen that solid dispersion samples of ZAL\_010 and ZAL\_011 that crystallise out when stored at 25°C/60% RH and 40°C/75% RH, do not crystallise when stored at 40°C/0% RH. It is well known that in general amorphous materials are more hygroscopic than their crystalline counterparts [159, 160], and also that the presence of water can cause the plasticization (i.e. the lowering of the  $T_g$ ) of both the polymer and drug [161, 162]. Therefore, it can be seen how the combination of these two factors during the storage of the samples at 25°C/60% RH and 40°C/75% RH, leads to an enhancement of molecular mobility, and with time, the crystallisation of the drug.

The 100% drug sample of the des chloro diethyl ester analogue, ZAL\_005, was

shown to crystallise early on in the study under all conditions. This correlates with the results of the PDF experiments detailed in chapter 4, which suggested that due to the ordering of this compound to a greater length scale than the other analogues in the amorphous state, recrystallisation would occur more readily. The solid dispersions containing ZAL\_005 did not crystallise when stored at 25°C/60% RH or 40°C/0% RH, but in contrast, all of the solid dispersions stored at 40°C/75% RH (regardless of the level of drug loading) crystallised after just one day.

ZAL\_007 (the diethyl ester analogue) is structurally the most similar analogue to ZAL\_005, in that the only difference between these two molecules is the presence of the chlorine substituents on the phenyl ring of ZAL\_007 which are absent in ZAL\_005. Therefore, we may conclude that any discrepancies in performance between these two compounds during the stability tests are likely to be due to these molecular differences. Whilst the samples of 100% ZAL\_007 crystallised at an early timepoint under all storage conditions, none of the solid dispersion samples gave indications of crystallisation, even under the accelerated conditions of 40°C/75% RH. As the only molecular difference between ZAL\_005 and ZAL\_007 is the chlorine substituents on the phenyl ring, it may be supposed that either the presence of the chlorine atoms contribute to drug-polymer interactions, or, that the lack of chlorine atoms is more favourable to the crystallisation of the compound. It has previously been shown that in the felodipine crystal lattice, the plane of the phenyl ring bisects the dihydropyridine (DHP) of another felodipine molecule [144]. If an ortho-substituent is present on the phenyl ring, as in the case of felodipine, it must be oriented so that this substituent points away from the DHP due to the steric strain that might otherwise be imposed on the 3,5-diester groups. Therefore, it seems logical to suggest that if the phenyl ring does not have any substituents (as in the case of ZAL\_005) there is no energy barrier resulting from steric strain that would hinder the phenyl ring bisecting the adjacent DHP, and hence explaining why such a compound may crystallise more readily (see Figure 5.12). Additionally, the 3,5-diester groups are shielded by the ortho-substituents on the phenyl (as in the case of felodipine and



ZAL\_007), meaning that they are less accessible for drug-drug hydrogen-bonding [144], and therefore such compounds would be less likely to crystallise.

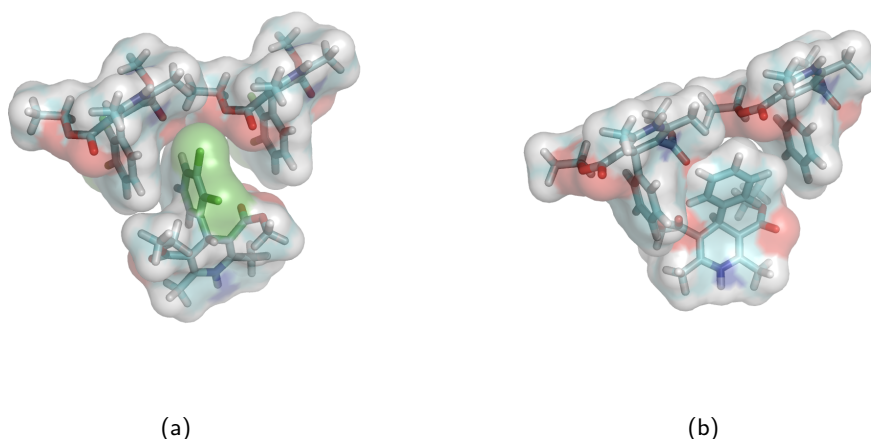


Figure 5.12: Images showing how entropy of crystallisation is lower for chlorine substituted analogues (a) compared with analogues without chlorine substituents (b) due to the restriction for only  $\pi$  face-to-face stacking, compared with the additional possibility of  $\pi$  edge-to-face interactions when there are no chlorine substituents.

ZAL\_007 also has a very similar molecular structure to felodipine, in that the two compounds only differ by one carbon unit on one of the ester chains. Despite this difference, felodipine and ZAL\_007 performed in a very similar manner with respect to crystallisation, and therefore we can suggest that the extra carbon unit in ZAL\_007 has very little affect on intermolecular interactions with copovidone.

ZAL\_011 is also similar to the diethyl ester analogue, ZAL\_007, and differs only in the addition of a methyl group on the nitrogen of the DHP. Despite this small change, the performance of ZAL\_011 was much poorer than ZAL\_007, as not only did the pure drug crystallise immediately under all three storage conditions, but also, all of the solid dispersions stored at 40°C/75% RH, and the 50% drug-loaded dispersions stored at 25°C/60% RH crystallised before the study concluded. These results indicate that, as predicted, the secondary amine in felodipine is key to the formation of physically

stable solid dispersions, and this is because it participates in hydrogen-bonding with the carbonyls present in the vinylpyrrolidone rings of copovidone, as shown previously by Konno and Taylor for felodipine/PVP systems[87]. In considering the influence of intermolecular interactions on the formation of stable solid dispersions, it should not be forgotten that this process is competing against the process of drug crystallisation, which is itself directed in many ways by the formation of intermolecular bonds. It is well documented that the amine in felodipine is involved in hydrogen bonding with the carbonyls of other felodipine molecules in its pure state, in both crystalline and amorphous forms [163, 91]. For the analogue ZAL\_011, the hydrogen bond donating amine has been blocked, and therefore the ability for the molecule to hydrogen bond with itself in this way is lost. Nevertheless ZAL\_011 crystallises more readily than ZAL\_007, and this suggests that the free energy difference between the amorphous and crystalline states of ZAL\_011 is greater than for ZAL\_007. This must indicate that there are intermolecular interactions that occur between molecules of ZAL\_011 other than the hydrogen bonds between the amine and carbonyl in order to drive crystallisation of the pure drug.

ZAL\_006, the mono nitrile compound, was the only analogue for which the pure drug did not crystallise at 25°C/60% RH. However, at other storage conditions the 100% drug samples crystallised at an early timepoint. The solid dispersion samples did not show any evidence of crystallisation under any of the conditions tested. It may be that the replacement of one of the strong hydrogen-bond accepting ester carbonyls with a weaker hydrogen bond acceptor in the form of a nitrile has resulted in less difference between the free energies of the crystalline and amorphous forms of this compound. This would mean that amorphous felodipine or ZAL\_007 are more likely to crystallise than ZAL\_006, as their crystalline forms will have a lower energy potential than the crystalline form of ZAL\_006. Additionally, the ability for ZAL\_006 to hydrogen bond with copovidone is not lost by the presence of the nitrile group, and so the solid dispersion samples are more stable than the pure drug samples, which would explain why they do

not crystallise.

Moving on to compare ZAL\_006 with the des-chloro mononitrile compound, ZAL\_009, it is once again evident that the presence of chlorine substituents on the phenyl ring leads to the formation of more stable solid dispersions. This is because not only had the samples of pure ZAL\_009 readily crystallised under all storage conditions, but also all of the solid dispersion samples stored at 40°C/75% RH had crystallised by the end of the experiment. Also, comparison of ZAL\_009 with the des-chloro diethyl ester, ZAL\_005, further supports the theory that the weaker nature of the nitrile as a hydrogen bond acceptor than the carbonyl reduces the difference in free energy between the crystalline and amorphous forms, as the ZAL\_009 solid dispersion samples take longer to crystallise at 40°C/75% RH than the ZAL\_005 solid dispersions.

Swapping the remaining ester group on ZAL\_009 for an additional nitrile leads to analogue ZAL\_010, which also lacks the presence of chlorine substituents on the phenyl ring. ZAL\_010 was found to be the least stable of all the analogues with respect to crystallisation, as not only was crystalline material detected in all samples of pure ZAL\_010 prior to storage, but crystallinity was also observed in most of the solid dispersion samples stored at 25°C/60% RH and 40°C/75% RH prior to their storage.

The plates due to be stored at 40°C/0% RH were held under the same conditions in the same place as the other two plates prior to being placed in the stability rooms, and so the absence of crystals in the solid dispersion samples in this plate prior to storage is difficult to understand. However, one suggestion may be that nanocrystalline material that was too small for detection by polarised light microscopy formed in the plate destined for storage at 40°C/0% RH, but that once this plate was placed in storage, these nanocrystallites did not sufficiently grow any further to enable their detection.

### **5.2.5 Conclusions - Well-plate crystallisation experiments**

These experiments have identified trends in crystallisation tendency with respect to the molecular structure of the drug compound. It has been shown that blocking the

amide group of felodipine prevents the formation of hydrogen bonds between the drug and polymer that are required to maintain drug amorphicity. Additionally, the absence of chlorine substituents on the phenyl group leads to more rapid crystallisation of the drug as drug-drug interactions are strengthened in two ways: Firstly, because there is no steric hindrance to the phenyl ring bisecting the DHP in the crystal lattice; and secondly, because there is no shielding of the diester carbonyls, thus making drug-drug hydrogen bonding more favourable. The substitution of one of the ester groups with a nitrile group also appeared to lead to the formation of more physically stable solid dispersions. These experiments have shown how important it is to study the drug molecule as a whole, and investigate the variety of both drug-polymer and competing drug-drug intermolecular bonding interactions that can occur in order to understand the physical stability of a solid dispersion.

### **5.3 Future Work**

It is the author's opinion that with further investigation the laser light scattering approach could eventually be successfully developed to detect phase separation in film solid dispersion samples, as has already been shown to be possible for polymer blends. In order to do this the next step would be to identify a system that is known to phase separate, and use this as a model to refine the technique. The sample cell of the light scattering instrument could also be used to enable experiments under humid conditions, and it would be of particular interest to determine whether or not such experiments could be undertaken without the risk of water vapour at high relative humidities scattering the light in addition to the sample. If it could be shown that such experiments are practical, experiments on the felodipine/copovidone solid dispersions under such conditions might be used to further support the data obtained from the well-plate crystallisation experiments by highlighting changes that occur prior to crystallisation in samples stored under humid conditions.

In the case of the well-plate crystallisation experiments, it is clear that the amount

of available analogue material was the limiting factor in the scope of the experiments that could be carried out. However, there are a number of improvements that could be made to the experimental protocol if these experiments were to be repeated. Firstly, it appeared that in many cases if the compound crystallised out, it did so within a week, and that analysis of a sample at a particular timepoint would show the well to be completely filled with crystals when at the previous timepoint there had been no evidence of crystal nucleation. Therefore there may be a better time-resolution to the data if sampling occurred at more frequent timepoints, particularly during the initial two weeks of the study. With these additional timepoints, it may have been possible (provided that the sample wells were imaged in exactly the same region at each timepoint) to determine crystal nucleation and growth rates for the analogues as demonstrated in the literature [87, 56, 93]. If unlimited amounts of analogue material were available, it also follows that solid dispersions with a wider range of drug loadings could be tested during storage under additional conditions, to provide a more detailed understanding of the differences between the analogues and their crystallisation mechanisms.

If both the laser light scattering and well-plate crystallisation experiments were further developed in the ways outlined above, future work would ideally involve combining the two approaches to provide a high-throughput screening method for detecting (and understanding) the onset of phase separation and ultimately crystallisation.

## Chapter 6

# Dissolution Performance of Felodipine-based Solid Dispersions

### 6.1 Introduction

As discussed in Chapter 1, it is important for a drug compound to have a good dissolution profile and acceptable aqueous solubility levels, as this in turn influences the amount of drug available for absorption from the GI tract into the systemic circulation [164]. Therefore, it is imperative that poorly soluble APIs formulated as solid dispersions demonstrate an enhanced dissolution profile compared with the free drug. In most cases, this means faster initial dissolution rates, and higher solution concentrations achieved and maintained for longer for drugs formulated as solid dispersions.

Despite the large number of reports in the literature of dissolution enhancement as a result of solid dispersion formation, the mechanisms by which dissolution enhancement occurs are still not fully understood, and there are several theories as to the release mechanism of the drug from the solid dispersion during dissolution, as explained in Chapter 1.

It is well known that amorphous compounds have a solubility advantage over more stable crystalline forms [78], and this is because the lattice energies associated

with dissolving crystalline material are not present and do not need to be overcome during the dissolution of amorphous materials. However, the actual measurement of the 'true' solubility of an amorphous form is often challenging because precipitation and crystallisation are likely to occur before the amorphous solubility is reached. Because of the challenges associated with experimentally determining amorphous solubility, *in silico* models have been developed to calculate this [165, 166, 167, 168]. Determining the amorphous solubility of a drug is important for understanding the dissolution mechanisms and physical structure of solid dispersions.

As has previously been alluded to in previous chapters, the physical structure of a solid dispersion may have a significant impact on its dissolution profile. For example, a molecular-level solid solution would be expected to exhibit better dissolution properties than an equivalent solid suspension, due to reduction of the particles to their smallest size [55]. Also, whilst incorporation of the drug into a polymer matrix is often a means to stabilise the drug with respect to crystallisation, the polymer can also act to solubilise the drug.

In this chapter, felodipine/copovidone solid dispersions will continue to be used as a model system to interrogate the dissolution mechanism. Previous studies have shown that the dissolution of felodipine can be enhanced when formulated as a solid dispersion with PVP or HPMC [69, 88, 92, 94], but there appear to be no previous reports in the literature about the dissolution enhancement of felodipine in formulations with copovidone. The dissolution performance of solid dispersions containing the felodipine analogues will then be investigated, and attempts will be made to relate dissolution performance to the molecular structure of the analogue.

In Chapter 2 it was discussed that a variety of dissolution testing methods are available to formulation scientists, and that each method has advantages and disadvantages. In this study a combination of two dissolution methods will be used in attempts to further elucidate the mechanisms responsible for the dissolution enhancement of felodipine from solid dispersions. Firstly, the micro-dissolution method, which was used for the

analysis of the majority of samples, is a technique which can be carried out using just milligram quantities of material [169]. This enables formulation scientists to gain an understanding of whether formulating a drug as a solid dispersion will produce a dissolution enhancement at an earlier stage of drug development, when there may be only small quantities of drug compound available for testing. Dissolution testing with smaller sample sizes is made possible with the use of fibre optic UV probes which negate the need for continued removal of sample aliquots from the dissolution media, and therefore allow for smaller dissolution vessels to be used. For this reason, the micro-dissolution technique was ideal for use in this study, as limited quantities of analogue material were available for testing. Additionally, the automated and frequent analysis made possible by the use of the fibre optic probes, meant that 'high resolution' dissolution profiles could be obtained.

"MRI dissolution" uses a flow-cell located within a magnetic resonance imager to enable the non-invasive study of dissolution processes under a controlled liquid flow. MRI has been used in previous studies to monitor water ingress into solid dosage forms [170], but the measurements are usually made using a low volume of static water as the dissolution medium. Because of this restriction it can be difficult to relate physical processes such as water ingress, to the dissolution monitored in separate tests (e.g. using USP I or II apparatus). Other studies which have sought to overcome this restriction by performing MRI experiments on controlled release dosage forms located within USP IV or other apparatus, in which the dissolution media flows past the tablet or capsule [171, 172, 173]. In this study we have adopted a novel integrated measurement strategy in which the UV absorbance of the re-circulating dissolution media from a USP IV-style flow-cell is continuously recorded during imaging. Through simultaneous measurements this enables changes in the dissolution profile to be directly related to the physical changes occurring to the dosage form.



## 6.2 Materials

### Spray Dried Micro-dissolution Samples

For micro-dissolution testing, samples of spray dried material (see Chapter 4) were weighed directly into the vials, such that the mass of drug was kept constant (2 mg), and the maximum achievable felodipine concentration was 100  $\mu\text{g/mL}$  in all experiments, corresponding to  $100 \times$  the crystalline solubility of felodipine [88].

### Compact Samples for MRI-flowcell

For analysis using the MRI-flow cell, the spray dried formulations (see Chapter 4) were compacted. Unlike the micro-dissolution experiments, the same total mass of spray dried formulation (500 mg) was used to produce each compact, and therefore with the changes in drug:polymer ratio, there were different masses of drug in each compact, corresponding to maximum felodipine concentrations of 50-500  $\mu\text{g/mL}$ . Monolithic compacts with dimensions of  $7.5 \times 3.0 \times 20$  mm were formed using a die in an IR press with 2000 kg pressure.

### 6.2.1 Preparation of Solid Dispersion Films

#### Solid Dispersions Containing Felodipine

Solid dispersion films containing felodipine were prepared by solvent-casting directly into the 20 mL vials. Samples were prepared such that the mass of drug was kept constant (2 mg), and the maximum achievable felodipine concentration was 100  $\mu\text{g/mL}$  in all experiments, corresponding to  $100 \times$  the crystalline solubility of felodipine [88].

Solutions containing both felodipine and copovidone were produced such that the concentration of felodipine in solution was fixed at 4 mg/mL, and the mass of copovidone was adjusted to ensure the correct drug:polymer ratio for each sample. Casting solutions were prepared in 80% methanol: 20% acetone v/v solvent mix. A 500  $\mu\text{L}$  aliquot of the solution was pipetted into the dissolution vial, so that the mass

of felodipine in each vial was constant at 2 mg. (For 5% drug-loaded samples, 1 mL of 2 mg/mL felodipine solution was used instead, as the copovidone was not soluble in such a small volume.) Where possible, the volume of solution was kept close to 500  $\mu$ L to ensure the formation of uniform films from which the solvent could be rapidly evaporated. The sample vials containing drug/polymer solution were inserted into a pre-heated vial holder on a stirrer hotplate at 60-70°C for 10-15 minutes until the solvent had evaporated (checked visually). The samples were then annealed at 155°C for 30 mins prior to use.

### **Solid Dispersions Containing Analogue Compounds**

Only compounds ZAL\_001, ZAL\_005, ZAL\_006, ZAL\_007 and ZAL\_011 were subjected to dissolution testing as there were insufficient quantities of the other analogue compounds. Due to the limited amount of available analogue material, the dissolution tests for these compounds were carried out in smaller vials which had a capacity of 2.5 mL.

Again, samples were prepared such that the maximum achievable solubility of each compound was  $100 \times$  the solubility of the crystalline compound. Because the solubility of the compounds had not been measured, predicted solubilities were used (see below for details), and multiplied by 2 to account for the raised temperature of the experiments compared with the prediction. The mass of analogue in each vial was kept constant for each series of experiments (see Table 6.1).

Samples were prepared by solvent-casting directly into the vials using the same method described above, except that chloroform was used as the solvent, and annealing was carried out at a temperature appropriate for the drug compound (see Chapter 5).

## **6.2.2 Pure Drug and Physical Mixture Samples**

### **Felodipine Samples**

To obtain the dissolution profile of pure crystalline felodipine by micro-dissolution, approximately 2 mg of the drug was dispensed directly into the 20 mL dissolution vessel.

Amorphous felodipine samples were also prepared for micro-dissolution testing. These samples were prepared by solvent-casting 500  $\mu\text{L}$  of a 4 mg/mL solution prepared in 80% methanol: 20% acetone v/v solvent mix directly into the vial. The solvent was flash evaporated as detailed above, and the samples were then annealed at 155°C for 30 min prior to use.

In order to assess the impact of copovidone on the dissolution and solubility of crystalline felodipine, physical mixtures were prepared by directly weighing  $\sim 2$  mg felodipine and the required quantity of copovidone to give the required composition (15 or 50% w/w felodipine).

### **Felodipine Analogues**

Pure drug and physical mixtures containing the felodipine analogues were prepared using the same method as for felodipine, except for the following:

- the solvent used for casting amorphous samples was chloroform,
- the dissolution vessels had a volume of 2.5 mL,
- the mass of drug in the vial determined by the predicted solubility of the particular analogue (see Table 6.1),
- the annealing temperature depended on the compound (see Chapter 5).

### **6.2.3 Dissolution Media**

Blank Fasted-state Simulated Intestinal Fluid (FasSIF) was used as prepared by AstraZeneca, Alderley Park Media Preparation Lab according to the following method:

1.74 g NaOH pellets, 19.77 g  $\text{NaH}_2\text{PO}_4 \bullet \text{H}_2\text{O}$  (or 17.19 g  $\text{NaH}_2\text{PO}_4$  anhydrous) and 30.93 g NaCl are dissolved in 5 litres of deionized water. The pH is adjusted with 1N NaOH or 1N HCl to exactly pH 6.5 using a pH meter calibrated over the range pH 4 to 7.

Dissolution tests of amorphous drug samples were also carried out using blank FasSIF media which contained pre-dissolved copovidone at 2% w/v. These samples are referred to as having been tested in 'doped media'.

## **6.3 Methods**

### **6.3.1 Solubility Prediction**

Aqueous solubilities, used to calculate the mass of each analogue used in the dissolution tests, were predicted using AstraZeneca in-house C-Lab software based on AstraZeneca library compounds. These values correspond to the predicted molar solubility of the compound in aqueous buffer at pH 7.4, and the data used to build the model comes from solid solubility measurements, rather than DMSO solubility (see Table 6.1).

#### **Amorphous Solubility Prediction**

Amorphous solubility was calculated *In Silico* using the computational methods detailed by Lüder et al [168], based upon their previous work [165, 166, 167] (see Table 6.1). The charges of each of the components (i.e. the drug and the water) are taken into account in this statistical model via the Lennard-Jones potential approximations. Then, a statistical algorithm (Monte Carlo method) explores the possible metastable states of the system and ascertains their relative likelihood to appear. Through the results of these computations, it is possible to predict the likely solubility of the amorphous drug in water.

### **6.3.2 Dissolution Methods**

#### **Micro-dissolution**

Dissolution testing was carried out on the mg scale using  $\mu$ Diss™ stirrer blocks (pION Inc., Woburn, MA, USA) connected to a water bath (Julabo F34 with Julabo ME

Table 6.1: Summary of the predicted crystalline and amorphous solubilities for the felodipine analogues tested in this chapter, and the mass of analogue used in micro-dissolution tests.

Analogue	Crystalline Solubility Prediction (pH 7.4, µg/mL)	Mass of Analogue per 2.5 mL Dissolution Vial (mg)	Amorphous Solubility Prediction (mol/dm <sup>-3</sup> )	Amorphous Solubility Prediction (µg/mL)
ZAL_001	1.37	0.75	2.91E-06	1112
ZAL_005	3.84	2.00	5.68E-06	1871
ZAL_006	2.31	1.25	1.40E-05	4917
ZAL_007	0.86	0.50	9.30E-07	370
ZAL_011	1.88	1.00	4.27E-07	176

control unit), and with Fibre Optic UV detectors (Rainbow Dynamic Dissolution Monitor System)(see Figure 6.1).

The fibre optic UV probes (5 mm pathlength) were calibrated for measurement of wavelengths within the range of 200-380 nm prior to use with a standard of the compound being tested. The  $\mu$ -Diss™ software (pION, Woburn, MA, USA) was used to collect and analyse the UV/Vis absorbance data. UV/Vis spectra were recorded according to the following schedule:

200 spectra with 5 sec intervals followed by  
 50 spectra with 30 sec intervals followed by  
 19 spectra with 1 min intervals followed by  
 84 spectra with 5 min intervals.  
 (total = 8hrs of spectra collection)

Additional spectra were recorded with 30 minute intervals if required.

The concentrations of dissolved drug were determined using the 2nd derivative (to reduce particulate effects) of the UV absorbance in a suitable range for the particular compound being tested (see Table 6.2). All experiments were performed in duplicate at 37°C. Felodipine experiments were carried out in 20 mL of media, with a cross-shaped magnetic follower stirring at 300 rpm. Experiments with felodipine analogues

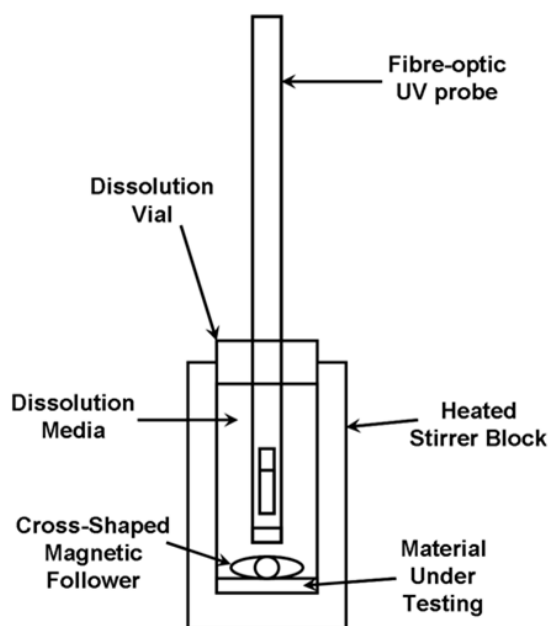


Figure 6.1: Schematic of a single  $\mu$ Diss vessel.

were carried out in 2.5 mL of media, with a disc-shaped magnetic follower stirring at 300 rpm.

Table 6.2: Summary of the UV absorption ranges used to determine the solution concentrations of drug in the micro-dissolution experiments.

Compound	UV Absorbance Range (nm)
Felodipine	300-380
ZAL_001	260-310
ZAL_005	290-380
ZAL_006	290-380
ZAL_007	290-380
ZAL_011	250-380

### High-Performance Liquid Chromatography (HPLC)

Samples for analysis by HPLC were prepared as follows: 300  $\mu$ L of solution of interest was centrifuged at 14000 rpm for 10 minutes and 200  $\mu$ L of the supernatant was transferred

Table 6.3: The HPLC method, mobile phase gradient used for analysing the drug content of dissolution samples.

Minutes	% A	% B
0	90	10
0.3	90	10
3.3	10	90
4.0	10	90
4.1	90	10

into a second eppendorf, and centrifuged again at 14000 rpm for a further 10 minute period. An aliquot of 100  $\mu$ L of acetonitrile was dispensed into a HPLC vial with an insert, and to the acetonitrile, 100  $\mu$ L of the double-centrifuged supernatant was added.

HPLC analysis was carried out using a Phenomenex Luna 5u C8 (2) 100 A column in a Hewlett Packard instrument. The mobile phases used were: A = 100% water + 0.1% Tetrafluoroacetic acid (TFA) B = 100% Acetonitrile + 0.1% TFA

The mobile phase was changed during the sample run according to the gradient detailed in Table 6.3.

The detection wavelength was adjusted depending on the compound (see Table 6.2). The column was maintained at 40°C, with a flow rate of 1.5 mL/min. The sample injection volume was 5  $\mu$ L.

This method is checked with 100% standard set at 100  $\mu$ g/ml. Standards were made up to give a nominal composition of 50/50 acetonitrile /water.

Solution concentrations were determined using the area under the chromatographic peak for the compound under test with reference to a calibration solution of known concentration.

### **MRI Flow-cell**

The compacts were fixed inside a USP 4-type flow-cell (see Figure 6.2) constructed from 20 mm internal diameter glass tubing, through which 500 mL of blank FasSIF dissolution

medium was circulated at a flow rate of  $15 \text{ mL min}^{-1}$ . The extent of dissolution was determined by continuous sampling of the medium using a 10 mm UV flow cell and measuring the absorbance at 350 nm.

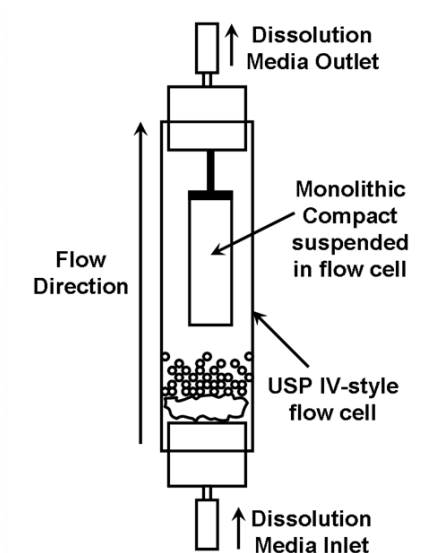


Figure 6.2: Schematic of the USP IV-style flow cell used in the MRI experiments.

The flow-cell was placed in the probe of a 400 MHz Bruker Advance NMR spectrometer (see Figure 6.3). Data acquisition and processing was performed using ParaVision software v4.0. Magnetic resonance images were acquired using a standard single spin-echo multi-slice protocol to produce  $16 \times 1$  mm thick horizontal and vertical slices with a 1 mm slice separation. The field of view was 2.5 cm and split into a 2D matrix of  $256 \times 256$  pixels giving an in-plane resolution of 0.0098 cm/pixel. The effective echo time was 8 ms and the repetition time was 1 s. No correction for T2 relaxation was applied to images; the repetition rate was chosen to give good contrast between the hydrated gel layer and the buffer. Experiment time for acquisition of 16 slices was 4 mins 16 s. The extent of hydration and gelation was followed by measuring the dimensions of a single horizontal slice through the monolith (see Figure 6.4) as a function of time.



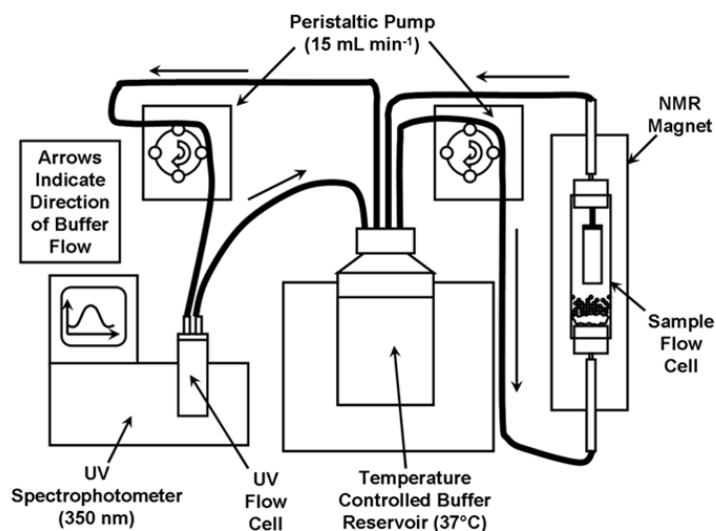


Figure 6.3: Schematic of the MRI flow-cell system with in-line UV monitoring.

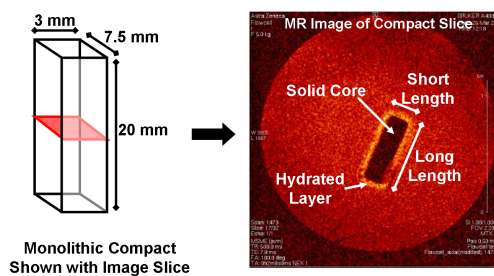


Figure 6.4: Diagram showing the monolithic compact and an example cross-sectional image obtained by MRI.

### 6.3.3 Complimentary Measurement Techniques

#### XRPD

X-ray powder diffraction data were collected on a Bruker D4 Endeavor diffractometer in reflectance mode. Compacts were gently powdered in a mortar and pestle prior to analysis. The powder samples were then smeared onto zero-background silicon wafer sample holders. Each sample was exposed to  $\text{CuK}\alpha 1$  and 2 radiation with an average wavelength of  $1.5418 \text{ \AA}$ , for  $0.03 \text{ s}$  per  $0.00570^\circ 2\theta$  increment (continuous scan mode)

over the range  $2^{\circ}$  to  $40^{\circ}$  in theta-theta mode. The operating voltage was 40 kV and the operating current was 40 mA.

## 6.4 Results and Discussion

### 6.4.1 Felodipine Dissolution

#### Micro-dissolution - Film-Cast and Spray Dried Samples

A summary of all the results from the micro-dissolution experiments on felodipine samples can be found in Table 6.4. Crystalline felodipine demonstrated a poor dissolution profile with an 8-hour solubility level of  $0.41 \mu\text{g mL}^{-1}$ , which was similar to the value obtained by Karavas et al [88]. The amorphous felodipine material demonstrated an improvement in initial dissolution rate, and gave a peak solubility level of  $0.90 \mu\text{g mL}^{-1}$ , this level was not maintained, and the 8-hour solubility of the material was found to be the same as for crystalline felodipine material. The initial dissolution rate and maximum solution concentration of amorphous felodipine in media containing pre-dissolved polymer were both almost a factor of 10 greater than for the amorphous sample. In addition, the 8-hour solubility of the amorphous felodipine in doped media was higher than that of either of the pure drug samples at  $2.82 \mu\text{g/mL}$ .

When crystalline felodipine was formulated as a physical mixture with copovidone, improvements in the initial dissolution rate and the equilibrium solubility level, compared to the crystalline felodipine, were observed across all drug loadings (Figure 6.5). It was also noted that the maximum solution concentration of the crystalline felodipine was maintained in the presence of the copovidone, rather than the felodipine precipitating out of solution as had been observed with the amorphous material. It was also interesting to observe that the maximum solubility for all of the physical mixture samples was higher than that observed for the amorphous felodipine samples, but of a similar order to the amorphous felodipine sample in doped media. However, the maximum solution concentration of the amorphous samples in doped media was higher than

Table 6.4: Summary of the data from micro-dissolution experiments carried out on samples containing Felodipine. Data are reported as mean values  $\pm$  standard error. All equilibrium solubility values were determined from the micro-dissolution data at 8 hours. <sup>a</sup> Equilibrium solution concentration values could not be determined for the 5% drug-loaded film-cast samples as the solution concentration did not drop to equilibrium levels within the 8 hour experimental time frame.

Type of Sample	Drug Loading (%)	Initial Dissolution Rate ( $\mu\text{g/mL/s}$ )	Maximum Solution Concentration ( $\mu\text{g/mL}$ )	Maximum % Drug in Solution	Equilibrium Solution Concentration ( $\mu\text{g/mL}$ )
Crystalline Drug	100	$0.00006 \pm 0.00004$	$0.4625 \pm 0.0000$	$0.3602 \pm 0.0125$	$0.4116 \pm 0.0328$
Amorphous Drug	100	$0.00070 \pm 0.00000$	$0.8956 \pm 0.0727$	$0.8513 \pm 0.0691$	$0.4179 \pm 0.0488$
Amorphous Drug (doped media)	100	$0.00640 \pm 0.00030$	$9.8659 \pm 0.6466$	$9.9355 \pm 0.6511$	$2.8230 \pm 0.0549$
Physical Mix	50	$0.00013 \pm 0.00007$	$2.0776 \pm 0.0377$	$1.9654 \pm 0.3594$	$3.2727 \pm 0.0022$
	30	$0.00050 \pm 0.00020$	$2.6891 \pm 0.1503$	$2.4102 \pm 0.3666$	$1.9525 \pm 0.1349$
	15	$0.00055 \pm 0.00025$	$2.0661 \pm 0.2853$	$2.0956 \pm 0.0375$	$2.5742 \pm 0.2541$
	5	$0.00115 \pm 0.00015$	$3.3671 \pm 0.2084$	$3.0137 \pm 0.0247$	$1.9082 \pm 0.2320$
Spray Dried Solid Dispersion	50	$0.00540 \pm 0.00020$	$2.0183 \pm 0.0497$	$1.8771 \pm 0.0166$	$1.1422 \pm 0.0516$
	30	$0.08395 \pm 0.00615$	$15.2839 \pm 1.7234$	$15.0360 \pm 0.8661$	$8.5749 \pm 1.3406$
	15	$0.78750 \pm 0.00110$	$62.9972 \pm 7.8371$	$60.8053 \pm 7.1738$	$8.7845 \pm 0.9077$
	5	$1.45770 \pm 0.12070$	$96.2895 \pm 0.1061$	$96.0888 \pm 1.1645$	$7.2674 \pm 2.4249$
Film Cast Solid Dispersion	50	$0.03335 \pm 0.00015$	$10.9307 \pm 0.7522$	$11.0411 \pm 0.7598$	$3.1317 \pm 0.2316$
	30	$0.18455 \pm 0.02905$	$14.0418 \pm 2.0766$	$14.1764 \pm 2.0965$	$4.8818 \pm 0.1612$
	15	$0.50520 \pm 0.07200$	$30.5059 \pm 3.0126$	$29.9960 \pm 2.9622$	$6.9572 \pm 0.1860$
	5	$1.57130 \pm 0.00000$	$105.1862 \pm 5.5062$	$102.5206 \pm 5.3667$	<sup>a</sup>

for the physical mixtures, due to the amorphicity of the drug in these samples. This was despite the initial dissolution rate for all loadings of the physical mixtures being less than for the amorphous felodipine (except the 5% felodipine physical mixture which had an initial dissolution rate of  $1.15 \times 10^{-3} \mu\text{g mL}^{-1} \text{s}^{-1}$ ). These results both indicate that the amorphous felodipine is crystallizing on contact with the aqueous media and preventing the theoretical amorphous solubility to be reached, and that copovidone has a solubilising effect on crystalline felodipine.

The dissolution profile of felodipine was significantly enhanced when it was formulated as a solid dispersion with copovidone (see Figures 6.6 and 6.7). The initial

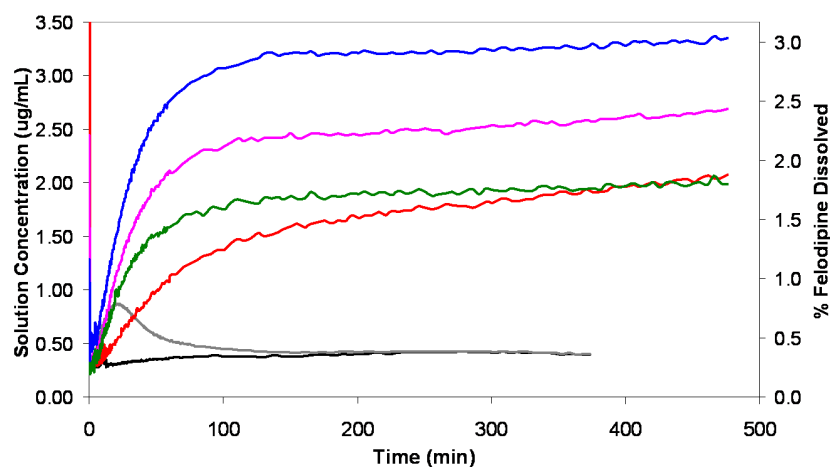


Figure 6.5: Dissolution profiles from micro-dissolution experiments of crystalline felodipine (black plot), amorphous felodipine (grey plot) and physical mixtures of crystalline felodipine with copovidone at drug loadings of 50% (red plot), 30% (pink plot), 15% (green plot) and 5% (blue plot). Mean data is plotted (n=2).

dissolution rates for both the spray-dried and film-cast materials were shown to be much higher than for the pure drug or physical mixes; and although the maximum solution concentrations were not maintained, they were also shown to be much higher than for either the pure felodipine or the physical mixes (see Table 6.4). Of particular interest was the observation that the performance of the solid dispersion formulations appears to be highly dependant on the drug loading, with the solid dispersions containing less drug exhibiting higher initial dissolution rates (Figure 6.8), higher maximum solution concentrations (Figure 6.9) and maintaining the maximum solution concentration for longer. The initial dissolution rate and maximum solution concentration are highly correlated, as shown in Figure 6.10, and this suggests that dissolution is driven by solubility. However, it was noted that the maximum solution concentration for the 50% drug loaded solid dispersions ( $2.02 \mu\text{g mL}^{-1}$ ) was no higher than the level achieved for the equivalent physical mixture ( $2.08 \mu\text{g mL}^{-1}$ ). It was also observed that upon precipitation of the drug from solution for the solid dispersions, the concentration of drug in solution tended towards similar plateau levels measured for the physical mixtures, which again supports

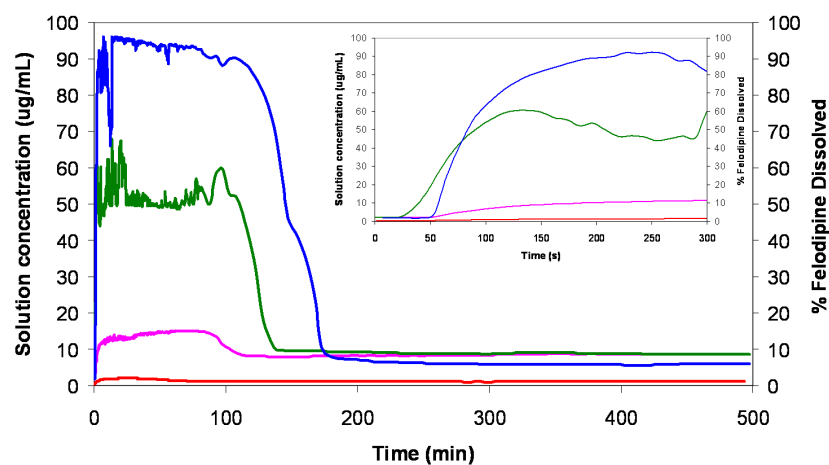


Figure 6.6: Dissolution profiles from micro-dissolution experiments of spray-dried solid dispersions of felodipine with copovidone at drug loadings of 50% (red plot), 30% (pink plot), 15% (green plot) and 5% (blue plot). Inset shows the first 5 minutes of the experiment in detail. Mean data is plotted (n=2).

other reports in the literature that indicate that the felodipine crystallizes from the solid dispersions [88, 94], and it is in fact the aqueous solubility level of the crystalline drug (influenced by dissolved polymer) that is observed.

It was noted that different extents of release were observed between the samples prepared by the two methods for 15% and 50% drug-loaded solid dispersions. The spray dried sample loaded with 15% drug performed better than its film-cast counterpart, and this suggests that in this sample a higher percentage of the drug is molecularly dispersed within the polymer. This may be a kinetic effect due to more rapid evaporation of the solvent during spray drying. It was also observed that the 50% spray dried sample achieved a much lower maximum solution concentration than its film-cast counterpart, and it may be that this material was contaminated with residual crystalline material.

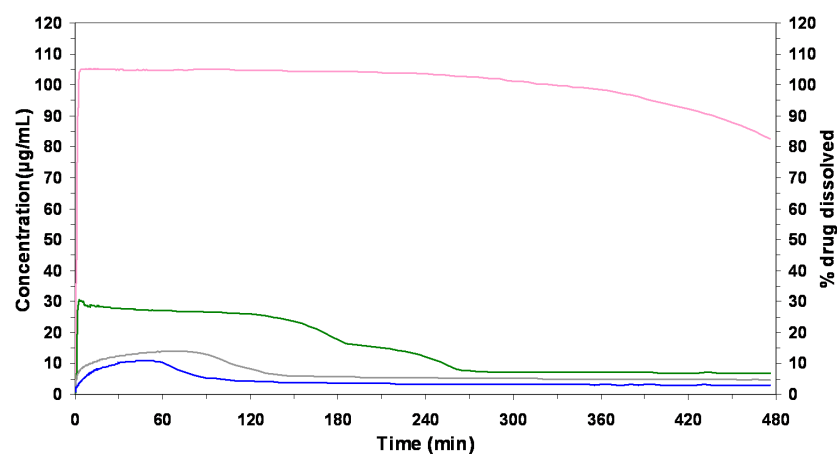


Figure 6.7: Dissolution profiles from micro-dissolution experiments of film-cast solid dispersions of felodipine with copovidone at drug loadings of 50% (blue), 30% (grey), 15% (green) and 5% (pink). Mean data is plotted (n=2).

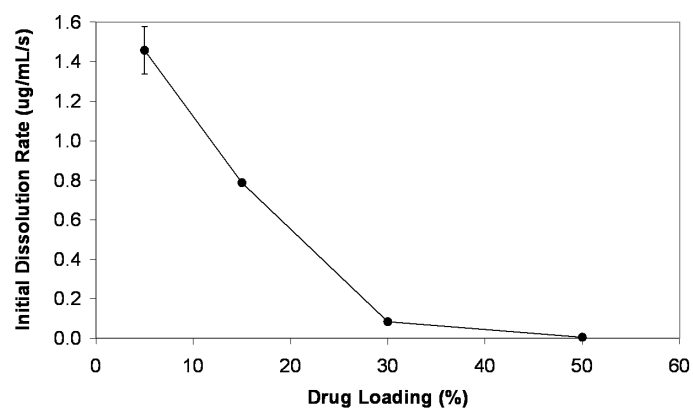


Figure 6.8: The initial dissolution rate of the film-cast dried solid dispersion samples as determined from micro-dissolution experiments plotted against drug loading. Mean data is plotted (n=2) and error bars represent the std error.

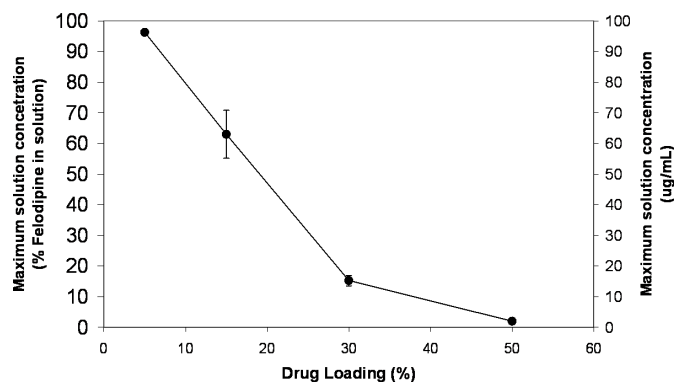


Figure 6.9: The maximum solution concentration of the film-cast solid dispersion samples as determined from micro-dissolution experiments plotted against drug loading. Mean data is plotted ( $n=2$ ) and error bars represent the std error.

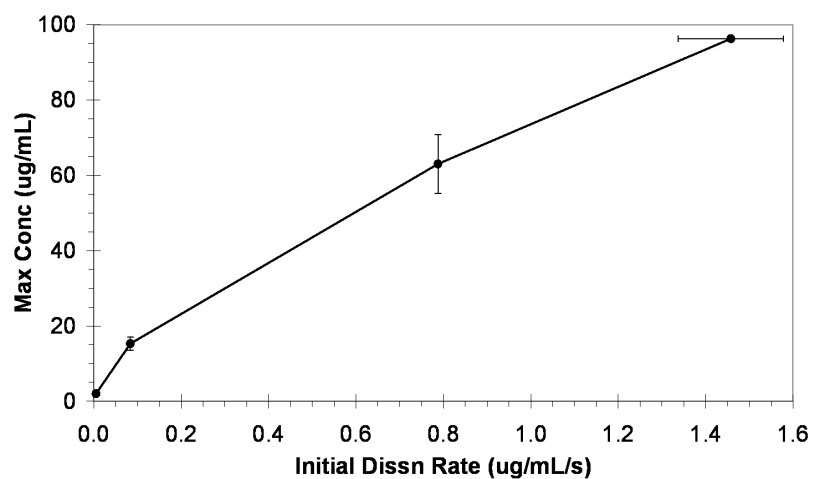


Figure 6.10: The maximum solution concentration of the film-cast solid dispersions plotted against the initial dissolution rate. Mean data measured from micro-dissolution experiments is plotted ( $n=2$ ) and error bars represent the std error.

### MRI-flowcell Dissolution Experiments - Spray Dried Compacts

The dynamic environment of the flow cell located within the MRI scanner better represents the conditions present in standard dissolution tests, compared with the static cells used in MRI experiments detailed elsewhere in the literature. Therefore, MRI experiments as detailed above were conducted on compacts of the solid dispersion material in order to gain a better understanding of the dissolution of bulk material, the effect of compaction on the material dissolution of the material, and to better understand the mechanisms which lead to the dissolution profiles seen in the micro-dissolution experiments. By linking the flow cell to a UV-vis spectrophotometer, we were able to record a dissolution profile at the same time as monitoring the physical form of the compact.

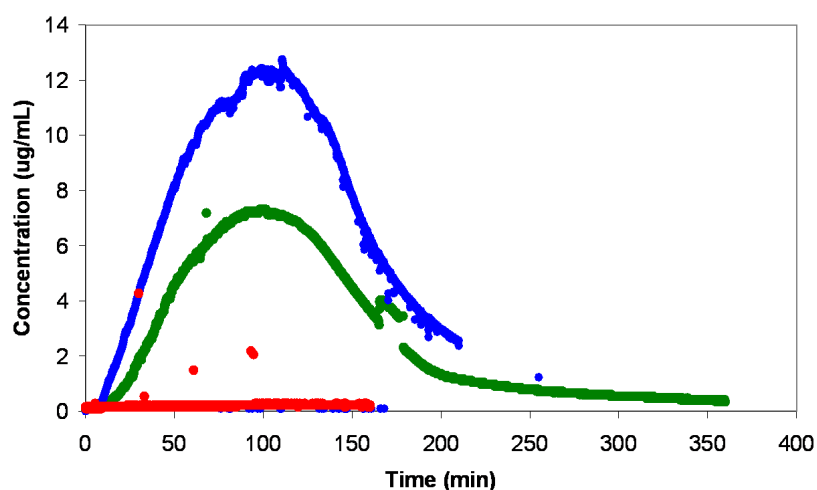


Figure 6.11: Dissolution profiles for spray-dried solid dispersions of felodipine with copovidone at drug loadings of 50% (red plot), 15% (green plot) and 5% (blue plot), as recorded by UV spectrophotometry in MRI experiments. 30% drug loaded sample not shown as the concentration levels were below the detection level of the UV spectrophotometer.

One of the findings of the MRI flow-cell experiments was the observation of a clear divide in dissolution behaviour between the samples with low drug loading (5% and 15% felodipine) and higher drug loadings (30% and 50% felodipine). This is most clear



from the UV spectrophotometry, in which the levels of drug released from the 30% and 50% drug-loaded compacts were below the level of detection for the instrument. This was in comparison to the 15% loaded compact which reached a maximum solubility level of  $7.31 \mu\text{g mL}^{-1}$  from an initial dissolution rate of  $2.2 \times 10^{-3} \mu\text{g mL}^{-1} \text{s}^{-1}$ , and the 5% loaded compact which reached a maximum solubility of  $12.75 \text{ g mL}^{-1}$  from an initial dissolution rate of  $3.2 \times 10^{-3} \mu\text{g mL}^{-1} \text{s}^{-1}$  (see Figure 6.11 and Table 6.5).

Table 6.5: Summary of the data from MRI-flowcell dissolution experiments carried out on samples containing Felodipine. <sup>a</sup> Only data for 5% and 15% drug loaded samples is shown as the levels of drug released from the 30% and 50% drug-loaded compacts were below the level of detection for the UV/Vis instrument.

Type of Sample	Drug Loading (%) <sup>a</sup>	Initial Dissolution Rate ( $\mu\text{g/mL/s}$ )	Maximum Solution Concentration ( $\mu\text{g/mL}$ )	Maximum % Drug in Solution
Spray Dried Solid Dispersion	15	0.0022	7.3101	5.1549
	5	0.0032	12.7532	24.2990

Analysis of the dissolution profiles obtained from the MRI-flow cell experiments corresponded with the data obtained in the micro-dissolution experiments, in that it showed a clear correlation with drug loading. However, the maximum percentages of felodipine dissolved were found to be significantly lower in the flow-cell experiments than in the corresponding micro-dissolution experiments, and the maximum solution concentration was maintained for a shorter duration. For the 5% loaded samples, the drug release peaked at  $96.29 \mu\text{g mL}^{-1}$  in the micro-dissolution experiments, compared to  $12.75 \mu\text{g mL}^{-1}$  for the MRI compact sample. The initial dissolution rate was also found to be lower for the compact samples analysed in the MRI-flow cell experiments ( $2.2 \times 10^{-3} \mu\text{g mL}^{-1} \text{s}^{-1}$  for 15% felodipine loaded compact compared with  $0.79 \mu\text{g mL}^{-1} \text{s}^{-1}$  for the samples with same loading in the micro-dissolution experiments).

These differences between the MRI-flowcell and micro-dissolution experiments may be due to a number of factors. Firstly, it is important not to ignore the fact that

the fibre-optic probes are closer to the source of dissolving drug in the micro-dissolution experiments than the UV flow cell is to the compact in the MRI experiment, and this may lead to a time-lag in measuring changes in the solution concentration, leaving more time for the drug to crystallise in the MRI-flowcell. Additionally, if crystallisation and precipitation of the drug from solution is a continuous process, as has been suggested elsewhere in the literature, there may be an introduction of errors associated with the equilibration of the solution concentration between measurements, and there may have been some deposition of precipitated drug on the inside of the connecting tubes between the flow cell and the UV spectrophotometer. However, these reasons alone do not appear significant enough to explain the observed differences. The main reason for these differences between the UV measurements from the two experiments is likely to be due to a change in dissolution mechanism for the compacts of spray dried material. The effect of compaction would lead to the spray dried particles being compressed and packed more closely, thus inhibiting water ingress into the compact compared with the free-flowing powder, and hence could be a key explanation for the lower levels of drug detected in solution in the MRI experiments.

Following the MR images obtained from these experiments, it can be seen that the dimensions of the compacts change with time (Figure 6.12). When these changes in dimension were plotted against time (Figure 6.13), it is clear that a distinction can be made between the 5% and 15% drug loaded compacts, and the 30% and 50% drug loaded compacts. The 5% and 15% drug loaded compacts demonstrate the same linear rate of change in their dimensions of  $-0.02 \text{ mm s}^{-1}$ , which corresponds to erosion of the compact. The 5% and 15% drug loaded compacts had both dissolved entirely after 120 mins. Conversely, the 50% drug loaded compact appears to swell as it is hydrated, demonstrating increases in dimensions of 1.25 mm for the long side and 2.09 mm for the short side of the cross-section, and shows no evidence of erosion.

The 50% drug loaded compact was still shown by the MR images to be completely intact after 52 hours. The experiment was stopped at this time, and the compact was

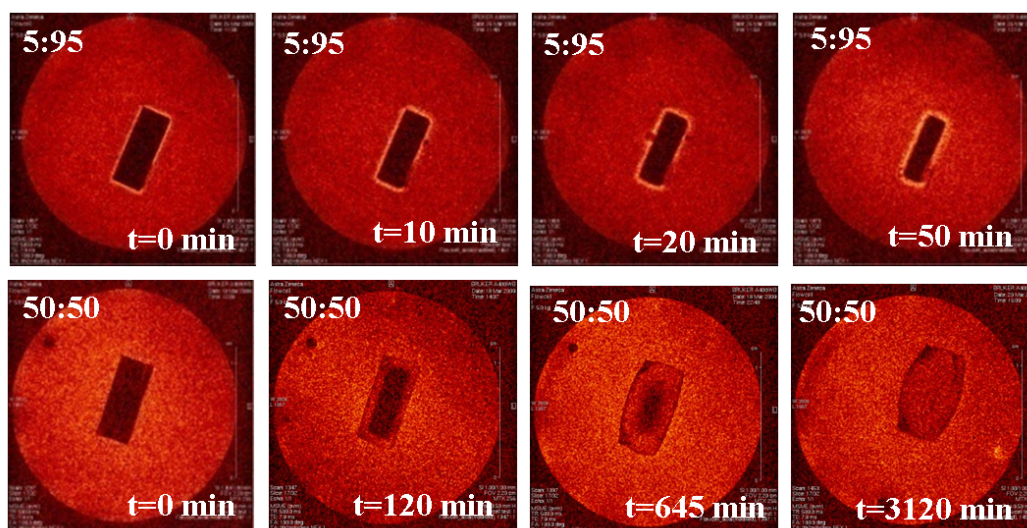


Figure 6.12: Example MR images of the 5% (top row) and 50% (bottom row) drug-loaded compacts at a range of time points.

recovered from the flowcell. Similarly, the undissolved core of the 30% drug loaded compact was also recovered from the flowcell after 24 hours. These compacts were analysed by XRPD and the drug in these compacts was shown to have crystallised (see Figure 6.14). The crystallisation of the drug in these two samples is likely to be via solid-to-solid transitions on exposure to the aqueous dissolution media, as identified by Alonzo et al [94], and this is likely to be one of the main contributing factors in the swelling behaviour of these samples. From the MRI-flow cell experiments, there appears to be a marked distinction between the lower loaded samples (5 and 15%) and the higher drug loaded samples (30 and 50%) both in terms of the dissolution profiles and the physical changes to the samples during the dissolution, thus indicating that there are different processes dominating the dissolution mechanisms.

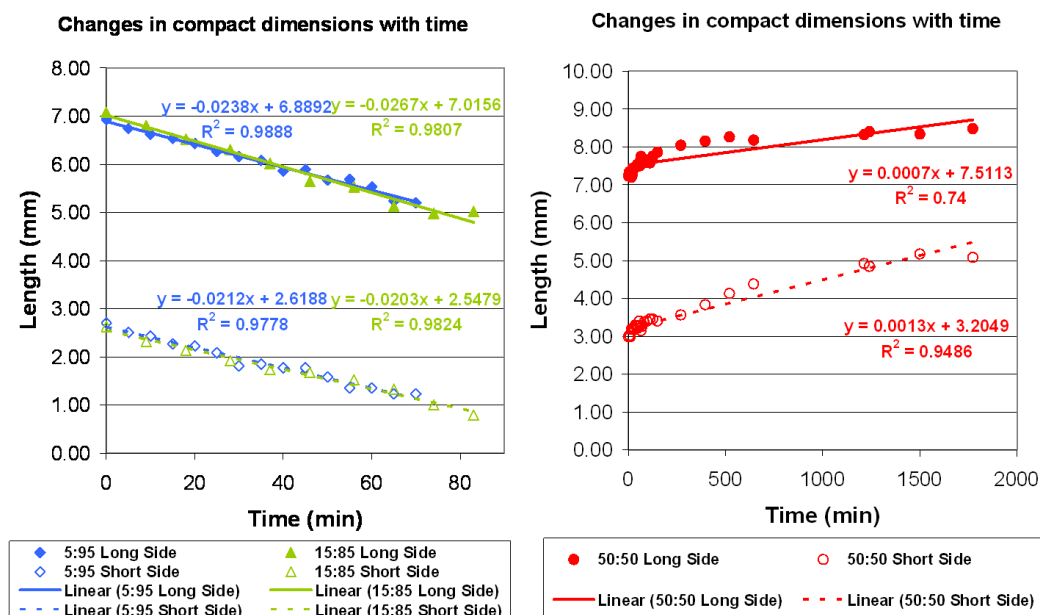


Figure 6.13: Graphs to show the changes in the dimensions of the compacts in the MRI experiments with time.

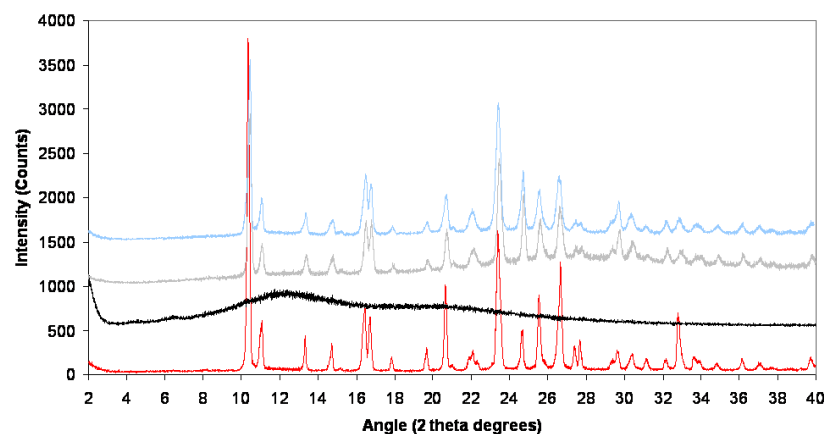


Figure 6.14: X-ray powder diffractograms of the compacted spray dried felodipine/copovidone solid dispersions recovered from the MRI flow-cell experiments. The samples with drug loadings of 30% (grey) and 50% (light blue) are shown. Diffractograms of crystalline felodipine (red) and copovidone (black) are also shown for comparison.

### Suggestion of a Dissolution Mechanism

By drawing upon key observations of the dissolution data presented here, a mechanism can be suggested for the dissolution of felodipine from solid dispersions with copovidone.

The dissolution profiles for the physical mixture samples shows that copovidone has a solubilising effect on crystalline felodipine. If we assume that a 1:1 complex is formed between the drug and the monomer units in the polymer, a binding constant,  $K_{11}$ , can be calculated using equation 6.1:

$$S_t = S_0 + \frac{(K_{11}S_0L_t)}{(1 + K_{11}S_0)} \quad (6.1)$$

where  $S_0$  is the solubility of the crystalline drug in the absence of ligand (which in this case is the polymer),  $S_t$  is the solubility of the drug in the presence of the ligand, and  $L_t$  is the concentration of the ligand [174]. The binding constant calculated from the physical mixture micro-dissolution data for felodipine and copovidone is  $154.5 \text{ M}^{-1}$  (see Figure 6.15). If this binding constant is used in the same equation to determine the influence of copovidone on the amorphous solubility of felodipine, it predicts that whilst the effect is not negligible, it does not explain the solution concentrations observed in the dissolution experiments. This is supported by observations that even in the presence of the relatively high-polymer-concentration doped media, dissolution of the amorphous drug film did not exceed the literature value for amorphous solubility of felodipine in the absence of polymer.

If the solubilising effect of copovidone on felodipine is not significant, this suggests that observations of concentrations of felodipine in solution above the amorphous solubility, such as from 5% and 15% spray dried powders, is due to a significant proportion of the drug being molecularly dispersed in the polymer. This would enable the drug to be rapidly released into solution following the dissolution of the porous spray dried powder, resulting in solution concentrations of the drug in excess of the amorphous solubility.

Assuming that the maximum solution concentration levels observed in the micro-

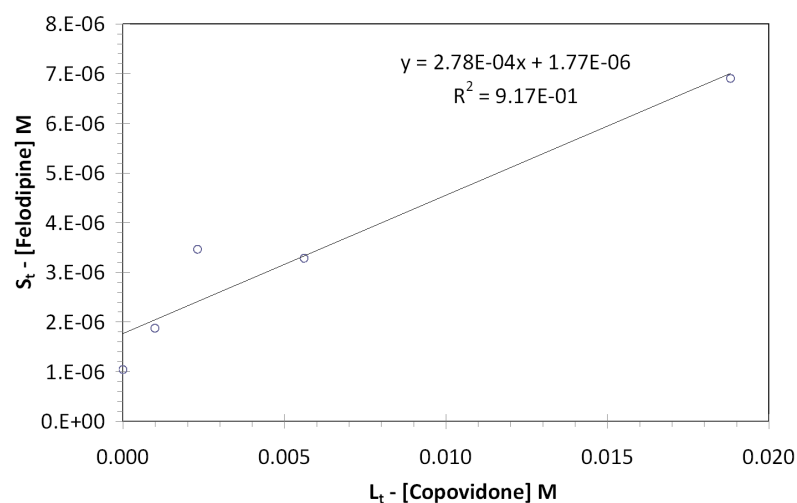


Figure 6.15: A plot of the aqueous solubility of felodipine in the presence of copovidone ( $S_t$ ) against the concentration of the ligand copovidone ( $L_t$ ). The linear fit from this graph can be used to determine the binding constant ( $K_{11}$ ) for felodipine and copovidone.

dissolution experiments of film-cast samples correlate with the amount of drug molecularly dispersed in the solid dispersions, it then follows that the solubility of felodipine in copovidone is approximately 5% w/w. This would lead to 100% dissolution of felodipine from a 5% drug-loaded solid dispersion, 33% dissolution from a 15% loaded dispersion, 17% from a 30% loaded dispersion and 10% dissolution from a solid dispersion with a drug loading of 50%. Reference to Figure 6.7 shows that these values are very close to the maxima in the dissolution profiles. The low solubility of felodipine in copovidone is also consistent with concentrations reported for solutions of felodipine in the structurally similar polymer, PVP [75]. The extent of drug dissolution enhancement from solid dispersions may therefore be limited in cases where the drug has low solubility in the polymer, and this consequently means that higher (more practical) drug-loaded solid dispersions cannot significantly improve drug bioavailability.

Taking into account these factors, and additional observations from the MRI experiments, the suggested mechanism of felodipine release from these solid dispersion

samples is as follows:

- Erosion, driven by the aqueous solubility of the polymer, initiates and continues the dissolution of the compact (as observed by MRI).
- A boundary layer, in which there is a higher local concentration of drug, is formed adjacent to the slowly dissolving compact.
- Super-saturation of the drug in the boundary layer drives the formation of amorphous nanoparticles and reduces the solution concentration of drug below the level predicted by the analysis of the erosion.
- The dissolution profile of the 5% drug-loaded compact peaks around the literature value for the amorphous solubility of the drug [75], suggesting the presence of amorphous particles. These act as a thermodynamic sink for the dissolving material and limit the maximum solution concentration to the amorphous solubility of the drug.
- Nucleation of crystalline material occurs. As the maximum solution concentration for the 5% formulation approximates to the amorphous solubility, the crystallisation process must have minimal contributions for this formulation. However, as samples with higher drug loadings do not reach the amorphous solubility, this suggests that crystallisation is a competing process from early in the dissolution process.
- At 30% and 50% drug-loadings there is a switch from the erosion-driven process to a swelling-dominated mechanism. The influence of crystalline drug on the dissolution of the drug occurs from an earlier stage

It is believed that the mechanism outlined here can be used as a basis to develop a model to describe the release of drug compounds from amorphous solid dispersions, that could potentially be applied to other drug/polymer systems [175].

#### 6.4.2 Analogue Dissolution and Solubility - Micro-dissolution

The dissolution profiles for the analogue samples are shown in tables below, and numerical data derived from the analogue dissolution experiments is summarised in tables in Appendix B.

ZAL\_001 is the aromatic felodipine analogue that is an oil at room temperature. As a crystalline form of this compound had not been produced, all of the samples containing this compound were amorphous, and as such were expected to demonstrate better aqueous dissolution than felodipine. Although all of the samples would be amorphous, solid dispersion samples were still prepared by film-casting for comparison with the drug in its native form, in order to determine if the film casting process had an impact on the performance of the drug.

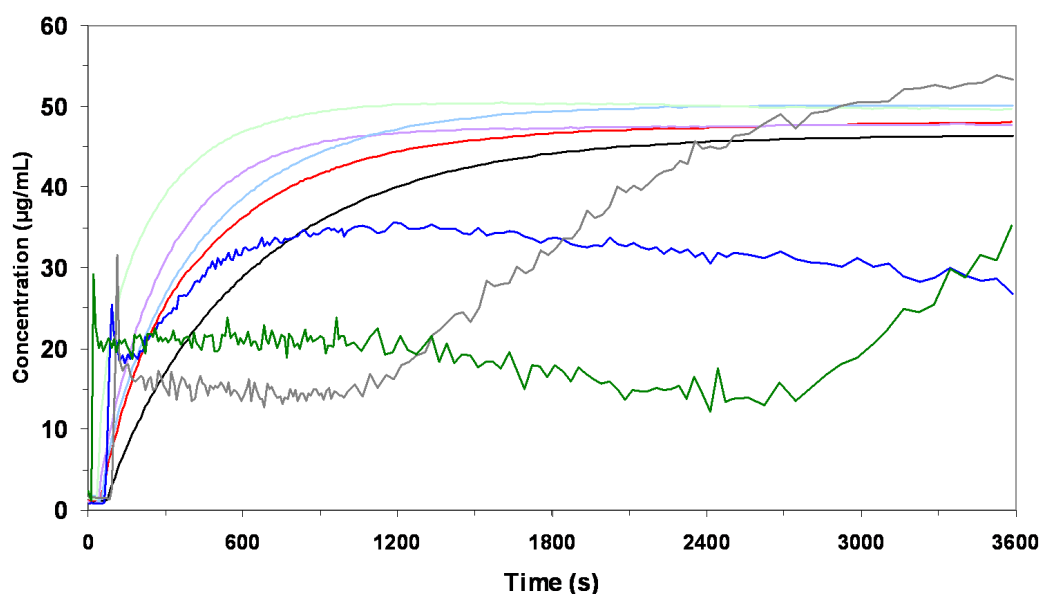


Figure 6.16: Mean dissolution profiles of samples of ZAL\_001 and the corresponding physical mixture and solid dispersion samples (n=2). Profiles for the pure (unprocessed) drug (black), film-cast drug (red) and film-cast drug in media containing 2% w/v copovidone (purple) are shown alongside profiles for physical mixture samples loaded with 15% (light blue) and 50% drug (light green), as well as film-cast solid dispersion samples with drug-loadings of 15% (dark blue), 30% (grey) and 50% (dark green).



As predicted, this compound had a much higher maximum solution concentration ( $5.87 \mu\text{g mL}^{-1}$ ) than crystalline felodipine and also amorphous felodipine. There was virtually no difference between the two pure drug samples, despite the different sample preparation methods. The addition of copovidone to the dissolution media, led to a small increase in the dissolution rate of the drug ( $0.25 \times 10^{-3} \mu\text{g mL}^{-1} \text{s}^{-1}$ ) compared to the equivalent film cast sample dissolved in the absence of dissolved copovidone ( $0.15 \times 10^{-3} \mu\text{g mL}^{-1} \text{s}^{-1}$ ), but did not significantly enhance either the maximum or equilibrium solution concentrations. The physical mixture samples also exhibited small increases in the initial dissolution rate and maximum and equilibrium solution concentrations in a drug-loading dependent manner. These results indicate that copovidone has a solubilising effect on the drug, but the increases in solubility as a result of this effect are very small compared with the baseline values obtained for the pure drug compounds. The dissolution profiles of the solid dispersion samples were somewhat erratic (see Figure 6.16, and a theory for this is that some form of degradation may have occurred to the drug during sample preparation that has adversely effected the dissolution behaviour of the drug compound.

It can be seen that the maximum solution concentration does not scale with the initial dissolution rate when these variables are plotted against each other for each drug loading (see Figure 6.17), and this suggests that the dissolution of the drug does not benefit from the addition of polymer. This result is not surprising considering that this analogue is a liquid. It is interesting to note that the maximum solution concentration of this compound does not reach the predicted amorphous solubility ( $1112 \mu\text{g/mL}$ ) despite the compound being liquid, and this suggests that the amorphous solubility calculation has over-estimated the amorphous solubility. It is possible that the amorphous solubility calculations for the other analogues have similarly been over-estimated, but nevertheless, this calculation can still give an indication of the ranking of the solubilities that can be expected for the analogues.

Dissolution profiles of the samples containing the des chloro diethyl ester, ZAL\_005

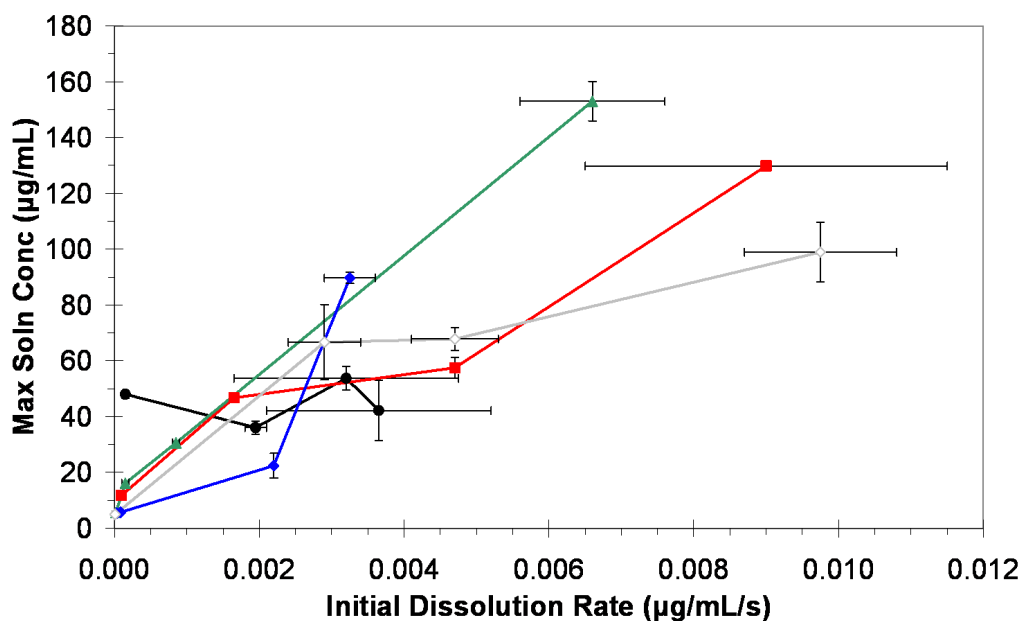


Figure 6.17: Plots of maximum solution concentration against initial dissolution rate for felodipine analogues ZAL\_001 (black), ZAL\_005 (red), ZAL\_006 (green), ZAL\_007 (blue) and ZAL\_011 (grey). Mean data ( $n=2$ ) is plotted and error bars represent the standard error.

are shown in Figure 6.18 and the data from these experiments is detailed in Table B.2. The crystalline solubility of this compound was low at  $0.8 \mu\text{g/mL}$ , and following the crystallisation experiments detailed in Chapter 5 it was expected that the amorphous drug would crystallise very rapidly during the dissolution experiments, and exhibit an equilibrium solubility equal to that of the crystalline sample. However, whilst the maximum solution concentration of  $11.71 \mu\text{g/mL}$  could not be maintained, the sample did not revert to the crystalline solubility, but was maintained at  $1.7 \mu\text{g/mL}$  - twice the equilibrium solution concentration for the crystalline sample. This may be due to the crystallisation of the drug as a different polymorphic form.

The amorphous solubility was calculated at  $1871 \mu\text{g/mL}$  for ZAL\_005, and again, none of the samples achieved this level. However, from the plot in Figure 6.17 it can be seen that the maximum solution concentration increases with increased initial dissolution

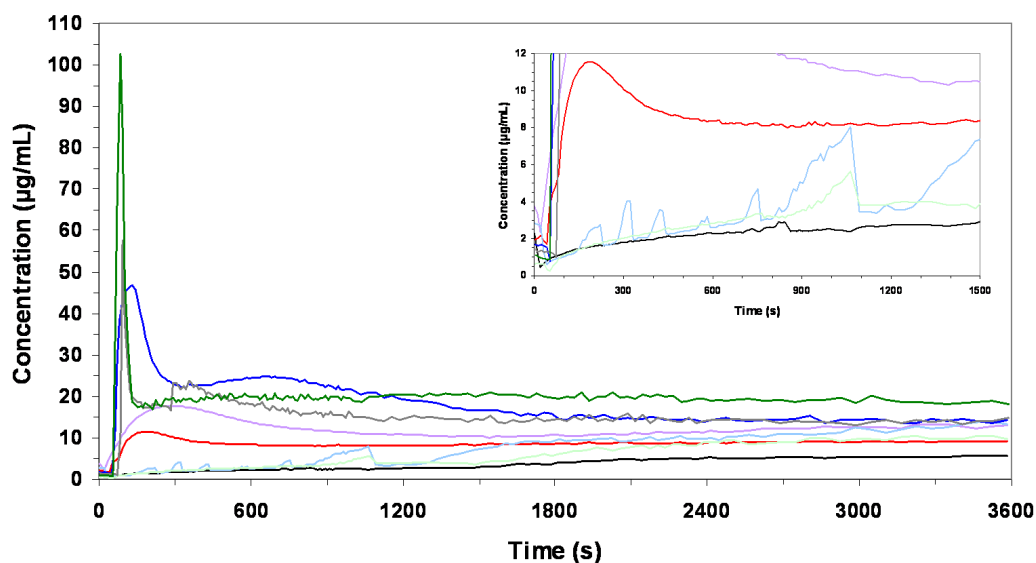


Figure 6.18: Mean dissolution profiles of samples of ZAL\_005 and the corresponding physical mixture and solid dispersion samples (n=2). Profiles for the crystalline drug (black), amorphous drug (red) and amorphous drug in media containing 2% w/v copovidone (purple) are shown alongside profiles for physical mixture samples loaded with 15% (light blue) and 50% drug (light green), as well as film-cast solid dispersion samples with drug-loadings of 15% (dark blue), 30% (grey) and 50% (dark green). The inset shows a zoomed-in area of the graph.

rate, indicating that dissolution is driven by the solubility of the drug.

Dissolution profiles of the samples containing the mono nitrile ester, ZAL\_006 are shown in Figure 6.19 and the data from these experiments is detailed in Table B.3. The amorphous solubility was predicted to be 4917  $\mu\text{g}/\text{mL}$  for this analogue - the highest value of the analogues that underwent dissolution testing, and in Figure 6.17 it can be seen that this compound also achieves the highest maximum solution concentration of the analogues tested for the 15% drug loaded sample. Again, this suggests that whilst the amorphous solubility has been over-estimated, it is still a useful tool to compare the performance of analogous compounds relative to each other.

Dissolution profiles of the samples containing the diethyl ester, ZAL\_007 are shown in Figure 6.20 and the data from these experiments is detailed in Table B.4.

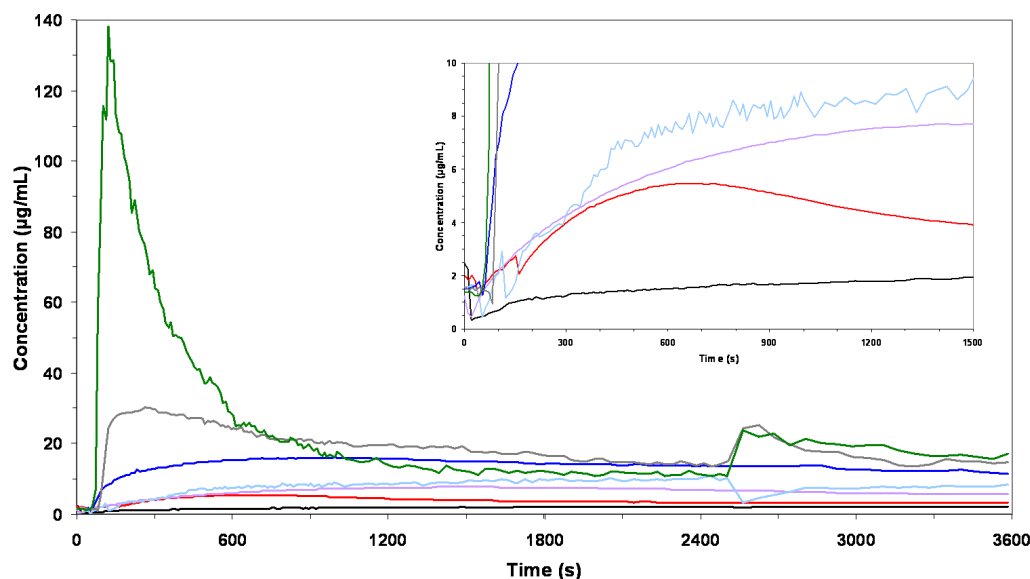


Figure 6.19: Mean dissolution profiles of samples of ZAL\_006 and the corresponding physical mixture and solid dispersion samples. Profiles for the crystalline drug (black), amorphous drug (red) and amorphous drug in media containing 2% w/v copovidone (purple) are shown alongside profiles for a physical mixture sample loaded with 15% drug (light blue), as well as film-cast solid dispersion samples with drug-loadings of 15% (dark blue), 30% (grey) and 50% (dark green). The inset shows a zoomed-in area of the graph.

The amorphous solubility was predicted to be 370  $\mu\text{g/mL}$  for this analogue. In Figure 6.17 it can be seen that for this compound the maximum solution concentration and initial dissolution rate are correlated, again suggesting that dissolution is driven by solubility. However, the solid dispersions generally have lower initial dissolution rates and maximum solution concentrations than the equivalent drug-loaded samples for the other analogues. ZAL\_005 and ZAL\_007 differ only by the presence of chlorine substituents on the phenyl ring, but ZAL\_005 samples have better dissolution profiles than ZAL\_007 samples - a ranking that is supported by the predicted amorphous solubility values. Similarly ZAL\_007 and ZAL\_006 only differ by the substitution of an ester side-chain for a nitrile group, but again, ZAL\_006 samples have better dissolution profiles than ZAL\_007 samples - a ranking again supported by the predicted amorphous solubility values. This

suggests that the nitrile group has improved the intrinsic solubility of the compound.

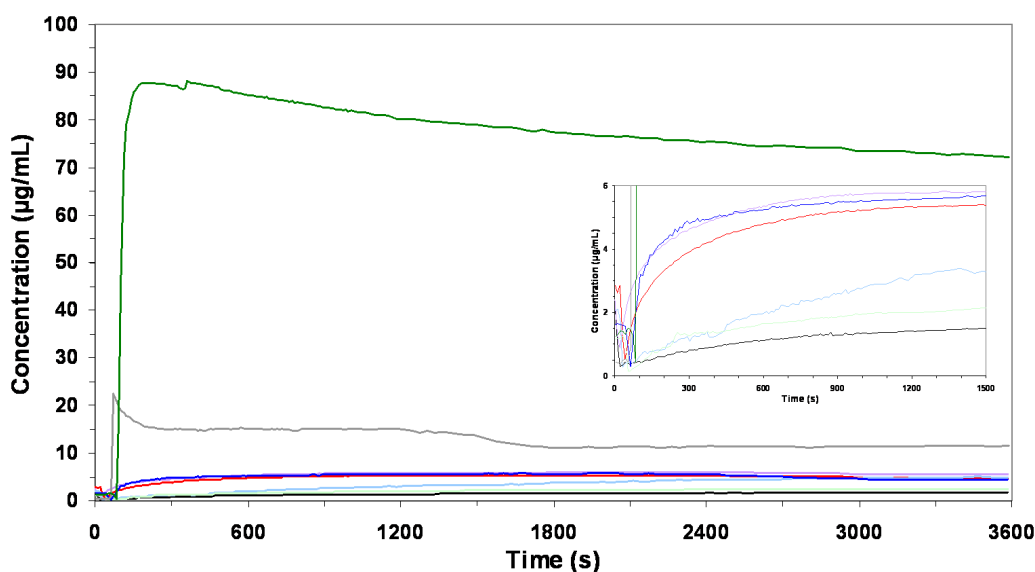


Figure 6.20: Mean dissolution profiles of samples of ZAL\_007 and the corresponding physical mixture and solid dispersion samples. Profiles for the crystalline drug (black), amorphous drug (red) and amorphous drug in media containing 2% w/v copovidone (purple) are shown alongside profiles for physical mixture samples loaded with 15% (light blue) and 50% drug (light green), as well as film-cast solid dispersion samples with drug-loadings of 15% (dark blue), 30% (grey) and 50% (dark green). The inset shows a zoomed-in area of the graph.

Dissolution profiles of the samples containing the diethyl ester, ZAL\_011 are shown in Figure 6.21 and the data from these experiments is detailed in Table B.5. The amorphous solubility was predicted to be 176  $\mu\text{g/mL}$  for this analogue - the lowest of the analogues tested. In Figure 6.17 it can be seen that for this compound the maximum solution concentration and initial dissolution rate are again correlated, suggesting that dissolution is driven by solubility. The maximum solution concentration of ZAL\_011 is lower than for ZAL\_005 or ZAL\_006, but higher than for ZAL\_007. However, in general, samples of ZAL\_011 achieve higher initial dissolution rates than for equivalent ZAL\_005, ZAL\_006 and ZAL\_007 solid dispersions. ZAL\_011 is the N-methyl analogue, and it may be that the better initial dissolution rates are due to blocking the hydrogen

bond donating amine, leading to a reduction in crystalline lattice enthalpy, and hence improving dissolution. It is also interesting to note that whilst the maximum solution concentration does not reach the predicted amorphous solubility for any of the analogue solid dispersions, the 15% drug loaded sample of ZAL\_011 achieves a maximum solution concentration closest to the amorphous solubility prediction.

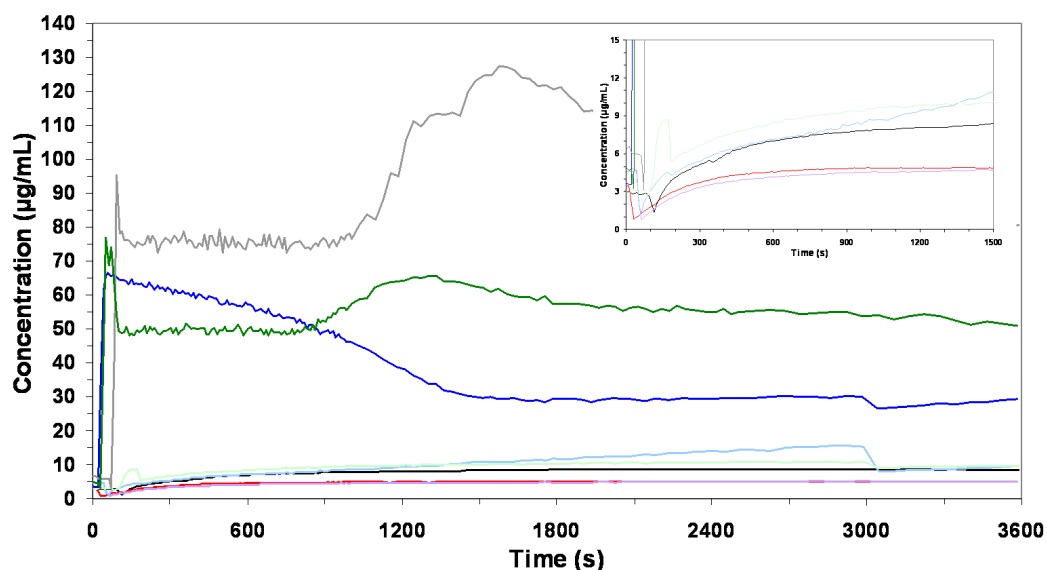


Figure 6.21: Mean dissolution profiles of samples of ZAL\_011 and the corresponding physical mixture and solid dispersion samples. Profiles for the crystalline drug (black), amorphous drug (red) and amorphous drug in media containing 2% w/v copovidone (purple) are shown alongside profiles for physical mixture samples loaded with 15% (light blue) and 50% drug (light green), as well as film-cast solid dispersion samples with drug-loadings of 15% (dark blue), 30% (grey) and 50% (dark green). The inset shows a zoomed-in area of the graph.

## 6.5 Conclusions

In this chapter it has been shown that it is important to select a dissolution testing method that is appropriate for the aim of the experiments being carried out. The MRI flow-cell instrument was ideal for providing additional information about the physical

changes to the sample during the experiment that could be used to aid suggestions for dissolution mechanisms. On the other hand, the micro-dissolution instrument was ideal for providing as much information about the dissolution behaviour of a compound as possible with the minimum amount of sample.

Across all of the dissolution experiments detailed in this chapter, it has become clear that in general, the dissolution performance of a solid dispersion is inversely proportional to the drug loading of the solid dispersion. Whilst the polymer may have a solubilising effect on the drug, which is enhanced at higher polymer loadings, it was shown for felodipine solid dispersions that this was effect was negligible. Instead, the dissolution enhancement resulted mainly from the proportion of drug that was molecularly dispersed in the polymer, and although his proportion did not change with lower drug loadings, it was a greater percentage of the drug incorporated in the solid dispersion, meaning that maximum solution concentrations closer to 100% dissolution were achieved for lower drug loaded samples. These observations enabled a dissolution mechanism for solid dispersion systems to be suggested.

With the spray dried samples it was seen that the compacted samples achieved a lower initial dissolution rate and maximum solution concentration compared with the free-flowing powder tested in the micro-dissolution experiments. This highlights the need to carefully consider the formulation of solid dispersion materials as tablets, and contemplate the need for other excipients such as disintegrants to be incorporated in the dosage form to ensure that the potential of the formulation can be realised.

For the analogue samples, it was shown that whilst amorphous solubility predictions tended to over-estimate the amorphous solubility, the values obtained still provided a measure by which the performance of the analogues could be ranked. It was also suggested that the presence of the N-methyl group in ZAL\_011 and the nitrile group in ZAL\_006 enhanced the dissolution performance.

## **6.6 Future work**

The first priority for future work would be to carry out dissolution analysis on the analogues for which there was limited material, so that further correlations between drug molecular structure and dissolution performance can be determined. Additionally, the dissolution testing of solid dispersions with a wider range of drug-loadings may provide a better indication of the dissolution mechanism for the analogue compounds.

If more material were available, it would also be interesting to carry out dissolution testing on samples that had previously been subjected to storage in physical stability testing experiments, as this would provide a better understanding of both the physical stability and dissolution performance of the analogues.



## **Chapter 7**

# **Molecular Descriptors of Felodipine Analogues and Correlation With Measured Properties**

### **7.1 Introduction**

The overall aim of this thesis, as outlined in Chapter 1, was to study the correlation between the molecular structure of a family of drug compounds and the performance of their respective solid dispersions. In Chapter 5 it was found that blocking the amine hydrogen bond donating group in felodipine led to less physically stable solid dispersions, which supported the findings from other work in the literature. However, it was also seen that the absence of chlorine substituents on the felodipine phenyl ring decreased the stability of the analogue with respect to crystallisation, and that the nature of the dihydropyridine substituents at positions 3 and 5 also impacted upon the physical stability of the analogue solid dispersions. In Chapter 6 it was appeared that blocking the

felodipine amine, and presence of a nitrile group led to an increased dissolution rate. In this chapter, we will look to see if it is possible to quantitatively correlate the performance of the analogue solid dispersions in the crystallisation screen and dissolution tests, with molecular descriptors calculated *in silico*, as well as physical properties.

If it is possible to identify trends between molecular descriptors and experimental data using a large enough test dataset, this approach could become invaluable to pharmaceutical companies seeking to formulate compounds as solid dispersions for a number of reasons. If a particular trend can be reliably identified, this knowledge could be used to narrow the design space for the molecular structure of a drug compound which will have both the desired pharmacological effect, and a greater chance of successful formulation as a solid dispersion. This would result in a more economical and targeted approach to drug discovery, whereby attrition of candidate drugs may be reduced, and actively engineered to form a high performance formulation with a specific solid dispersion excipient. As a result, this would reduce spending on unviable drug candidates, and lead to a greater number of poorly soluble compounds reaching the market.

## 7.2 Methods

### 7.2.1 In Silico Calculations

#### Calculations of $pK_a$ values

$pK_a$  values were calculated for the felodipine analogues using ACD software and  $pK_a$  database (ACD labs version 12.01, Advanced Chemistry Development, Inc).

#### Amorphous Solubility Prediction

Amorphous solubility was calculated *In Silico* using the computational methods detailed by Lüder et al [168], based upon their previous work [165, 166, 167].

## C-Lab

Molecular descriptors were calculated using C-Lab (AstraZeneca) software. The results of these calculations are shown in Appendix B. Most of these descriptors are calculated based on quantum mechanics.

### 7.2.2 Thermal Properties

Correlations were also investigated between the thermal properties of the analogue compounds (as determined in Chapter 4) and the performances of their solid dispersions in crystallisation and dissolution experiments. The reduced temperature  $T_r$ , which is the  $T_g/T_m$  ratio, was also calculated.

### 7.2.3 Scoring Analogue Performance

The process of identifying correlations between the experimental data and the molecular and physicochemical descriptors of the drug analogues, is facilitated by scoring the performance of the compounds in each of the experiments with numerical values. This score must be devised in such a way as to capture all the data obtained from all samples in that particular experiment, and also in such a way that it takes into account the performance of the solid dispersions relative to the drug compound alone, or physical mixture samples. The scoring systems devised and used in this study are described below.

#### Scoring the Performance of the Analogues in the Crystallisation Experiments

As detailed in Chapter 5, the images obtained from the crystallisation experiments were arranged in grids (see Figure 7.1). Through examination of the images and understanding of the most desirable outcome in terms of crystallisation inhibition for drug use, two rules were identified to aid the objective analysis of the images:

1. Crystals seen at earlier timepoints were less desirable than those seen after longer

storage times, and indicated that the polymer was less able to inhibit crystallisation for that analogue under the conditions of storage.

2. Crystals were more likely to appear at higher drug loadings due to the relative absence of crystallisation-inhibiting polymer. Crystals seen at 15% drug-loadings were deemed less desirable than crystals seen at 50% (and in fact it was assumed that in most cases the drug would crystallise out in the 100% samples)

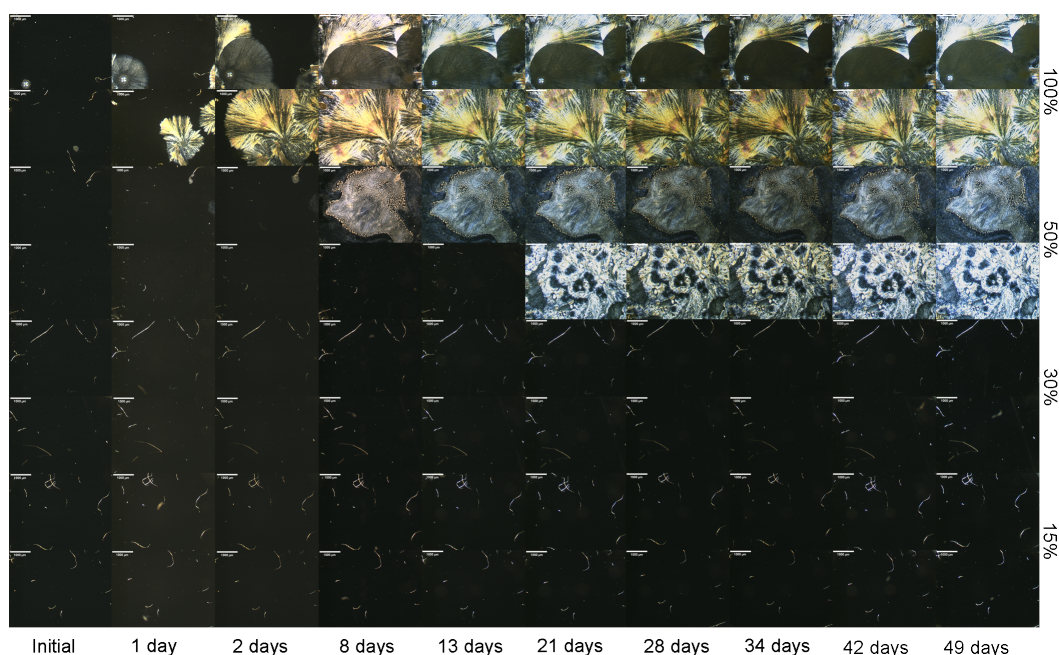


Figure 7.1: Example grid of images obtained from crystallisation experiments. This example shows the images obtained for solid dispersions of ZAL\_011 with ranging drug loadings stored at 25°C/60% RH over 7 weeks.

From these rules it can be seen that crystals observed in the bottom-left corner of the grid are much less desirable than crystals observed in the top-right corner, with gradations between these two extreme states that form along diagonals running downwards from left to right. The number of images along each diagonal that contain crystals is then multiplied by a ranking assigned to the diagonal according to the gradations described above (see Figure 7.2), thus leading to a series of scores being obtained

for each image grid. The scores from each diagonal are added to give a score for the entire grid, and in turn the three grid scores for each compound (one for each storage condition) are added together to give a score for the compound. Using this scoring system a compound will have a score between 0 and 1680, where the higher the score, the worse the compound has performed with respect to crystallisation.

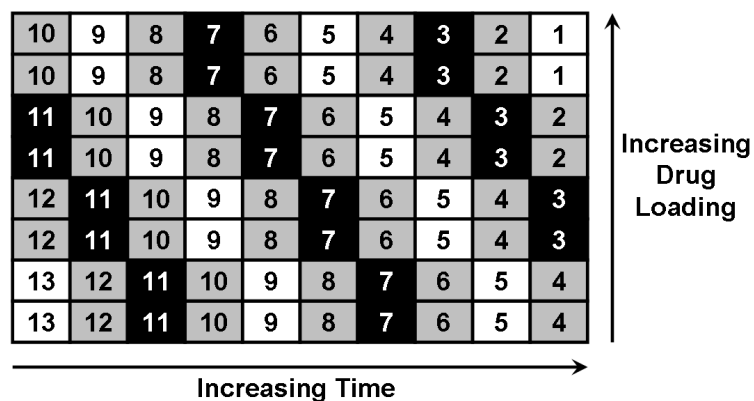


Figure 7.2: A schematic to demonstrate the system used to score the performance of compounds in the crystallisation study carried out in Chapter 5. The 10x8 image grids are scored along diagonals such that the number of images containing crystals along each diagonal is counted, and this number is multiplied by the weighted ranking assigned to that diagonal.

To further illustrate how the scoring system described above can be applied to provide a score for each analogue, the calculations for the grid in Figure 5.11 are shown in Table 7.1. The score for this example grid is 184, and when this is added to the scores of 299 for samples stored at 40°C/75% RH and 83 for samples stored at 40°C/0% RH, an overall score of 570 is obtained for compound ZAL\_011. The total scores obtained for each analogue using this method are shown in Table 7.2.

Table 7.1: The scoring system for crystallisation images obtained in chapter 5 applied to the image grid in figure 5.11 for ZAL\_011 stored at 25°C/60% Relative Humidity over 7 weeks.

Diagonal	Number of images containing crystals in diagonal	No. of images × Diagonal weight-ing
1	2	2
2	4	8
3	4	12
4	4	16
5	4	20
6	4	24
7	3	21
8	3	24
9	3	27
10	3	30
11	0	0
12	0	0
13	0	0
Total	34	184

Table 7.2: Summary of the scores determined for each analogue from the crystallisation screening experiment.

Compound	Score from Crystallisation Screen
Felodipine	250
ZAL_001	0
ZAL_005	721
ZAL_006	174
ZAL_007	253
ZAL_009	557
ZAL_010	1204
ZAL_011	570

### Scoring the performance of the analogues in the micro-dissolution experiments

In order to score the dissolution performance of the solid dispersion samples relative to the parent crystalline analogue compounds as determined in Chapter 6, the following integration methodology using the Area Under the Curves (AUC) was utilised. Using this approach meant that information regarding the initial dissolution rate, the maximum dissolved drug concentration achieved and the 1 hour equilibrium dissolved drug concentration would all be represented by the number obtained.

Firstly, the area under the first hour of the dissolution profile curves was determined for each dissolution sample using the trapezium rule (Equation 7.1), where  $A$  is the area under the curve,  $t$  represents the time in seconds, and  $c$  is the concentration in  $\mu\text{g/mL}$ .

$$A = \sum_{n=1}^N \left( \frac{c_n + c_{n+1}}{2} \right) (t_{n+1} - t_n) \quad (7.1)$$

Because  $n = 2$  for the dissolution experiments in Chapter 6, the mean of the two AUC values was determined (see Table 7.3 for these values). The AUC values for the solid dispersion samples ( $A_n$ ) were normalized with respect to the crystalline pure drug sample ( $A_0$ ), and then 1 was subtracted from these ratios to provide values which represented the improvement in dissolution performance compared with the crystalline pure drug sample. The normalized AUC values ( $\frac{A_n}{A_0} - 1$ ) were then plotted against the drug loading of the solid dispersion (see Figure 7.3). The AUC of this subsequent plot was determined, again using the trapezium rule (Equation 7.2), where  $Z$  is the area of the new plot, and  $L$  is the percentage drug loading of the solid dispersion.

$$Z = \sum_{n=0}^N \left( \frac{A_{N-n} + A_{N-n-1}}{2} \right) (L_{N-n} - L_{N-n-1}) \quad (7.2)$$

$Z$  was then used as a final score to represent the performance of the solid dispersions of each felodipine analogue (see Table 7.4).

Table 7.3: Summary of the Area under the Curve (AUC) values obtained from the dissolution data for solid dispersions of each analogue tested after 60 minutes. Data for 100% drug loaded samples refers to the crystalline form (except for ZAL\_001, where this data refers to the oil sample). Data are reported as mean dimensionless scores  $\pm$  standard error.

Drug Loading (%)	Felodipine AUC <sub>60</sub>	ZAL_001 AUC <sub>60</sub>	ZAL_005 AUC <sub>60</sub>	ZAL_006 AUC <sub>60</sub>	ZAL_007 AUC <sub>60</sub>	ZAL_011 AUC <sub>60</sub>
100	1159 $\pm$ 91	137730 $\pm$ 2499	13534 $\pm$ 4557	6515 $\pm$ 204	5128 $\pm$ 602	27952 $\pm$ 2048
50	32248 $\pm$ 2134	109792 $\pm$ 8388	64475 $\pm$ 265	48889 $\pm$ 449	18148 $\pm$ 423	134577 $\pm$ 27329
30	42048 $\pm$ 4543	115059 $\pm$ 6120	54450 $\pm$ 2225	66329 $\pm$ 9204	45616 <sup>a</sup>	163629 $\pm$ 3922
15	98252 $\pm$ 7335	70238 $\pm$ 10786	71449 $\pm$ 4275	82030 $\pm$ 8873	273372 $\pm$ 5306	196549 $\pm$ 23745

Table 7.4: Summary of the scores determined for each analogue from the dissolution data. Scores are determined by calculating the AUC for a graph in which the AUC values for each drug loading have been plotted, and normalised with respect to the 100% crystalline sample. Data are reported as mean values  $\pm$  standard error.

Felodipine Analogue	Dissolution Score
Felodipine	2184 $\pm$ 199
ZAL_001	-14 $\pm$ 1
ZAL_005	217 $\pm$ 73
ZAL_006	475 $\pm$ 40
ZAL_007	619 $\pm$ 74
ZAL_011	264 $\pm$ 42



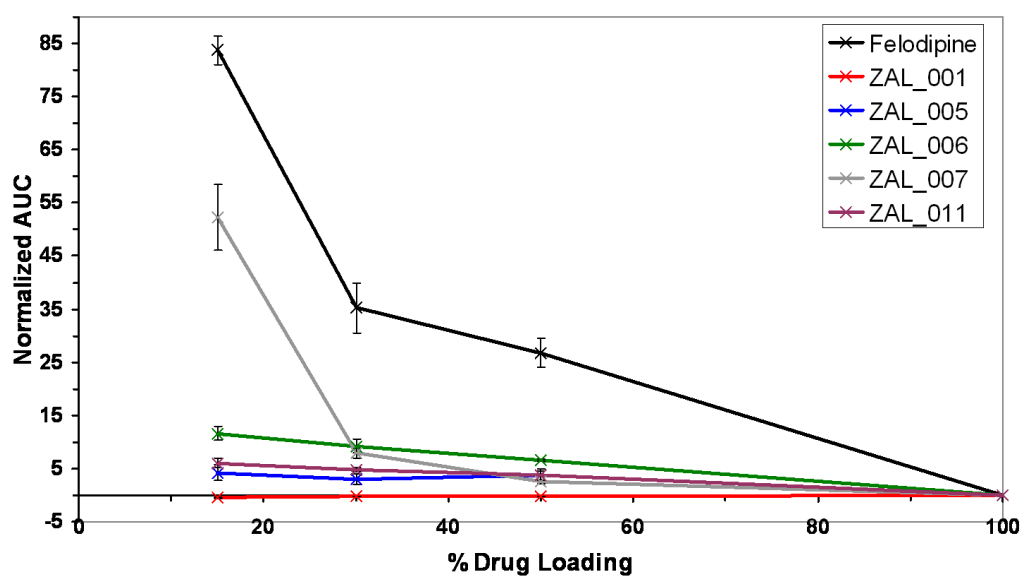


Figure 7.3: Plots of  $AUC_{60}$  against % drug Loading for each felodipine analogue analysed by micro-dissolution. Mean values are plotted ( $n=2$ ) and error bars represent the standard error. The area under each of these plots ( $Z$ ) is used to score the dissolution performance of each analogue.

#### 7.2.4 Determining correlations between modelled and experimental datasets

In order to determine if there were any correlations between the molecular descriptors predicted using clab, and the experimental data obtained from the micro-dissolution and crystallisation experiments, the Pearson correlation coefficient,  $r$ , was calculated between the datasets of interest ( $x$  and  $y$ ) (equation 7.3).

$$r = \frac{\Sigma(x - \bar{x})(y - \bar{y})}{\sqrt{\Sigma(x - \bar{x})^2 \Sigma(y - \bar{y})^2}} \quad (7.3)$$

Using the Pearson correlation coefficient yields a score of between -1.0 and 1.0 inclusive to describe the extent of a linear relationship between the two data sets. The value of the score indicates the noisiness of the relationship, whereby a score of 0.0 denotes that there is no correlation, and the closer the score is to 1.0 or -1.0, the stronger the correlation is. The sign of the score indicates the whether the relationship has a positive or negative correlation. The sample sizes in these experiments is small (9 structural analogues, 8 of which were used in crystallisation studies, and 5 in dissolution testing), and so correlation coefficients were required at least to be less than -0.8, or greater than 0.8 to be considered statistically relevant for linear relationships [176].

There are three main assumptions in the calculation of the Pearson correlation coefficient:

1. there is a linear relationship between the two variables;
2. both variables consist of continuous data;
3. each variable is approximately normally distributed.

It is not unreasonable to suggest that some of the datasets may have a correlation that is not linear, but perhaps exponential or polynomial in nature, and these will give Pearson correlation coefficients with absolute values lower than 0.8, despite potentially having a good fit to a non-linear trendline. It was for this reason that comparisons which yielded a correlation coefficient with an absolute value greater than 0.6 were then plotted as a scatter graph to visualise the relationship. If appropriate, a trendline (linear

or otherwise) was fitted to the data, and least square regression analysis ( $R^2$ ) was carried out to determine how well the trendline fits to the data.

### 7.3 Results and Discussion

The Pearson correlation coefficient was calculated between all experimental and calculated descriptors, and the cells with a correlation coefficient with an absolute value greater than 0.6 were highlighted (see Appendix C for data and correlation calculations). Of initial interest was to determine if a correlation existed between the two sets of experimentally determined data; that is the scores determined from the micro-dissolution data and the crystallisation screen experiments. The correlation coefficient for these sets of data was very low at just -0.13, and plotting the points clarified that there was no discernible trend (see Figure 7.4).

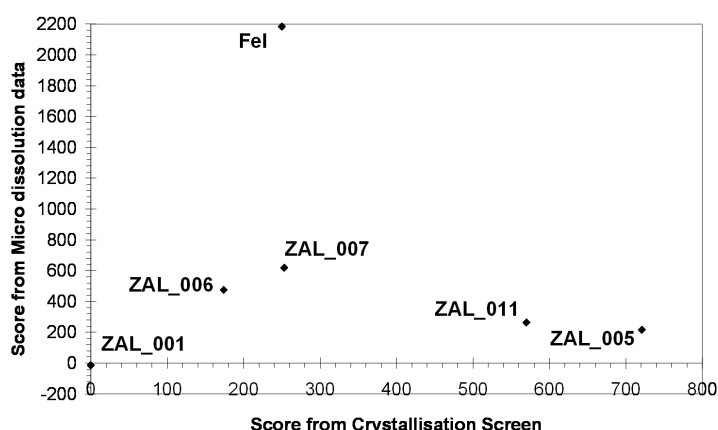


Figure 7.4: Scores determined from micro dissolution data plotted against scores determined from the crystallisation screening experiments. The linear trendline is shown with its equation and  $R^2$  value, indicating that it is a poor fit.

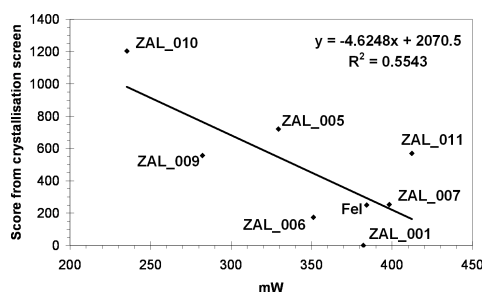
Strong correlations between the micro dissolution scores and other molecular descriptors were also sought, but as there are only 6 data points from the dissolution experiments, the correlation coefficient would have to have an absolute value greater than 1 to be statistically significant, which is not possible. Therefore, it would be

prudent to obtain micro-dissolution data for more of the analogue compounds before correlations can be calculated with this data.

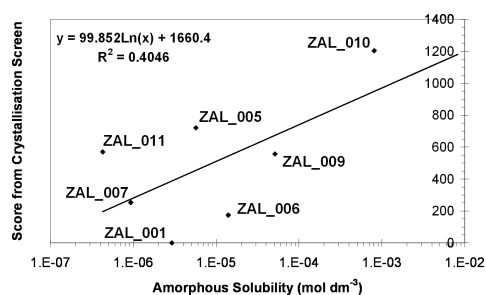
Next, strong correlations were sought between the scores from the crystallisation screens and the calculated molecular descriptors. In total, out of the 81 descriptors tested, 27 had a Pearson correlation coefficient with an absolute value greater than 0.6. Of these, 14 descriptors had a correlation coefficient absolute value above 0.7, and only one variable scored above an absolute value of 0.8 - the score required for a relationship to be considered statistically significant. Examination of the datasets indicated that many of the descriptors had a very coarse spread of data. With so few unique values of one particular descriptor, we essentially have even fewer useful data points, and as such the data is not sufficient to draw any firm conclusions or trends for these descriptors. Therefore, if we disregard the data sets without a broad range of unique data values, the number of descriptors with an absolute correlation above 0.6 is reduced to 18. Several of the correlations were with quantum mechanic molecular descriptors, which do not have an intuitive physical interpretation. Nevertheless, consistently strong correlations with such descriptors could still be useful in the development of a screening tool for identifying drug compounds for solid dispersion formulation.

The plots for some of the more physically intuitive correlations with absolute Pearson correlation coefficients above 0.7 are shown in Figures 7.5, and it can be seen that the  $R^2$  value for the trendline for most of these graphs is  $\geq 0.5$ .

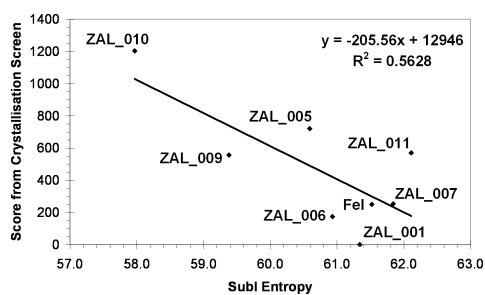
It is interesting to note that the placement of the data points follows a similar pattern in these graphs. Using the crystallisation score vs. molecular weight (MW) graph as an example we can see that analogues with the same chemical moieties are grouped together (Figure 7.6). For example, analogues which have the chlorine substituents on the phenyl ring are all located in the bottom right hand corner of the plot graph, whereas those without the chlorine substituents are in the top left corner of the graph. Similarly, compounds appear to be grouped depending on the nature of the dihydropyridine substituents. Graphs in Figures 7.5a, 7.5c and 7.5d closely follow this pattern, and the



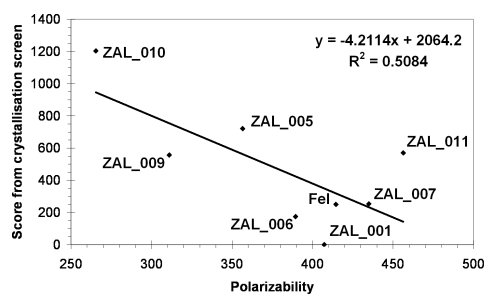
(a)



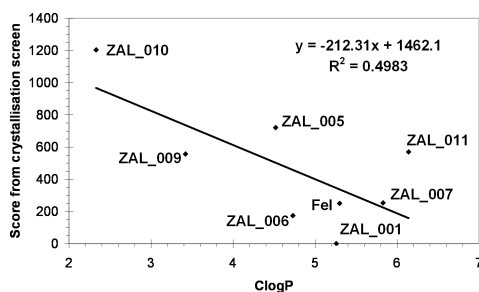
(b)



(c)



(d)



(e)

Figure 7.5: Graphs in which the scores obtained from the crystallisation screen are plotted against a) molecular weight (MW), b) amorphous solubility, c) Entropy of Sublimation, d) Polarizability and e) log P. For each plot, the trendline is shown with its equation and  $R^2$  value.

position of points in Figure 7.5b is a mirror image of those in Figure 7.6. From the patterns highlighted, it seems that the substituents of the phenyl group have the strongest influence on the stability of a solid dispersion with respect to crystallisation compared to the DHP substituents. From the graphs in Figure 7.5, we could perhaps also suggest that felodipine analogues with a high mW, Entropy of Sublimation and polarizability, all form solid dispersions with improved stability against crystallisation. However, the values of some of these descriptors may be weighted according to their substituents. For example, chlorine atoms have a higher atomic weight than carbon, hydrogen, oxygen or nitrogen atoms, and so their incorporation into a molecular structure will affect the molecular weight more than other structural changes. Also, C-Cl bonds are more polar than C-O or C-N bonds, and so their inclusion is also likely to increase the polarizability of a compound. Once again, it seems that it would be prudent to test additional analogue compounds for two reasons. Firstly, this would improve the statistical significance of the correlation coefficient, as well as the  $R^2$  value of the trendline. Secondly, the incorporation in the graphs of more analogues with greater structural variety may better highlight any effects the substituents may have on the molecular descriptors.

Whilst the  $R^2$  value for the correlation between the crystallisation score and log P was low, this trend is particularly noteworthy. The octanol/water partition coefficient (log P) is the ratio of concentrations of un-ionized compound between the two solvents (Equation (7.4)), and is used as a measure of the lipophilicity of a compound [177].

$$\log P_{oct/wat} = \log \left( \frac{[solute]_{octanol}}{[solute]_{water}} \right) \quad (7.4)$$

Log P is an important pharmaceutical descriptor, as it gives an indication of the ability of the compound to pass through lipophilic biological membranes - such as during gastrointestinal absorption, as well as the aqueous solubility of the drug. The higher the log P value for a compound, the more lipophilic, and the less water soluble it tends to be [178]. As discussed in Chapter 1, increasing numbers of drugs in development are lipophilic, and accordingly these would be expected to have higher log P values. The

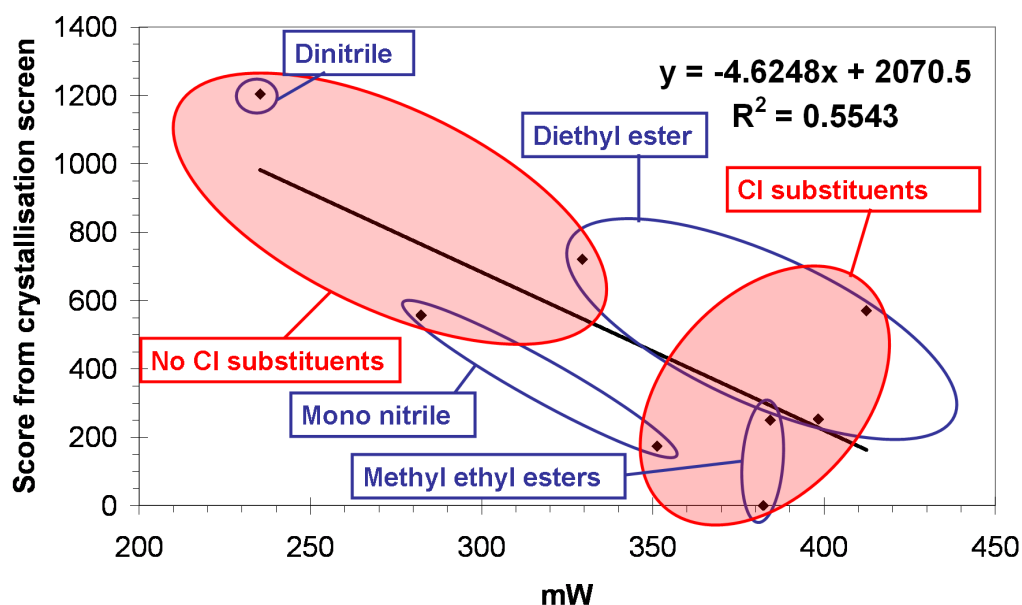


Figure 7.6: Copy of the plot of crystallisation screen score vs. molecular weight, with overlays to show regions where different molecular structures dominate. Red circles highlight phenyl substituents, blue circles highlight DHP substituents.

trend shown in Figure 7.5e is that the crystallisation of analogues with a higher log P values is better inhibited when formulated as a solid dispersion: a trend that does not appear to have been identified previously in the literature. This trend is particularly noteworthy, as it is more likely that compounds nominated for formulation as solid dispersions will have higher log P values, and indicates that, in so far as stabilising the amorphous form, solid dispersions may be a suitable answer for the formulation of poorly soluble compounds. In order to further assess the usefulness of solid dispersions as a method to improve the aqueous solubility of the analogue compounds, it would be desirable to carry out dissolution testing on more compounds, and identify if a similar trend exists between the results of these experiments and calculated log P values.

As well as identifying strong correlations between the crystallisation scores and several molecular descriptors, it was also interesting to note some of the molecular descriptors that did not have a correlation with the crystallisation score. For example,

perhaps the most surprising observation was that correlations between the crystallisation scores and any of the molecular descriptors pertaining to hydrogen bonding capability were not higher (Pearson correlation coefficients were 0.261 for hydrogen-bond-donor dispersion, -0.596 for hydrogen-bond-acceptor dispersion and -0.583 for hydrogen-bond strength). This could be for one of two reasons: Firstly, that the hydrogen bonding capability of an analogue only plays a relatively small part in the stabilisation of a compound with respect to crystallisation compared with other intermolecular interactions, and therefore the effect is not strongly correlated. On the other hand, it may be that inclusion of additional data points would lead to identification of a stronger correlation.

In the literature it has been suggested that compounds that cannot form hydrogen-bonds with the carrier may still form stable solid dispersions if both components have high dipole moments [75]. Therefore, it was anticipated that a strong correlation between the dipole moment and score from the crystallisation screen would be observed. However, the Pearson correlation coefficient for these variables was only 0.178. This may be because most of the compounds are able to hydrogen bond with copovidone via the amine group, and therefore the dipole moment has less of an influence.

It was also surprising that more and better correlations were not observed between the thermal descriptors and the crystallisation scores. The highest correlation observed was with the analogue  $T_m$ , which had a Pearson correlation coefficient of -0.636, a trendline was not fitted to the plotted data because it was thought that the data would fit better to a polynomial trendline (see Figure 7.7).  $\Delta C_P$ , a measure of the fragility of the amorphous glass of the analogue and  $T_r$ , which were also expected to have good correlations with the crystallisation score, gave Pearson correlation coefficients of -0.085 and 0.311 respectively.



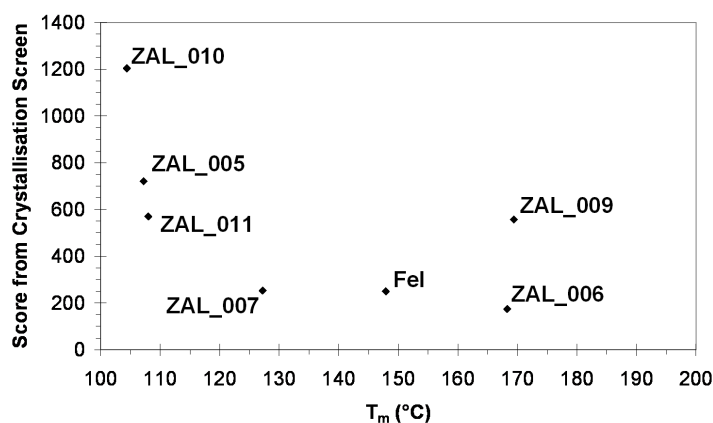


Figure 7.7: Graph in which the scores obtained from the crystallisation screen are plotted against  $T_m$ .

## 7.4 Conclusions

In this chapter we have identified some trends between the performance of solid dispersions containing felodipine analogues, and their molecular descriptors. We have also seen that inherent in some of these trends is a pattern relating to the molecular structures of the analogues, and it appears that the presence of chlorine substituents on the phenyl ring have the strongest influence on these trends. It was expected that removal or blocking of the hydrogen bond donating amine group in the dihydropyridine ring of the analogue compounds would heavily impact on the performance of the solid dispersions, but this was shown not to be as crucial to solid dispersion performance as predicted. However, it may be that not enough of the analogue compounds had this modification to accurately reflect the impact that this change may have.

Perhaps the most interesting correlation observed in this chapter was that between the crystallisation score and log P, as this trend suggests that more poorly water-soluble compounds will be more likely to form physically stable solid dispersions. Additionally it was shown that compounds with lower MW, entropy of sublimation and polarizability were less likely to form solid dispersions that were stable to crystallisa-

tion. However, it is important to note that the trends observed in this chapter are only relevant in relation to solid dispersions of felodipine analogues in copovidone. To determine general rules that could be applied to all solid dispersion systems, would require testing on analogues of a wider range of drugs as well as analysis of several different pharmaceutically relevant polymers.

It is also important to realise that none of the correlations observed were strictly statistically significant due to the small sample sizes, and therefore, it is important to test additional analogues. Carrying out further experiments on a greater range of analogues would also enable a better understanding of how the molecular structure influences the performance of the solid dispersions.

## **7.5 Future Work**

Carrying out the micro dissolution tests on the compounds not originally tested (i.e. ZAL\_009 and ZAL\_010) should be the first priority of any future work. These additional points may better highlight any correlations between datasets. It may also be necessary to refine the method used for scoring the performance of the analogue solid dispersions in the dissolution tests, so that the scoring system is more sensitive to subtle differences in the dissolution profiles.

For a more thorough assessment as to whether any trends exist between molecular descriptors and experimental results from both dissolution and crystallisation studies, it would be prudent to synthesise and test additional analogue compounds which have a greater structural diversity. It was also noted in the conclusions that the results presented here are only relevant to felodipine analogues dispersed in copovidone, and therefore it would be of particular interest to carry out the same experiments on solid dispersions in which a different polymer, such as PVP or HPMC, has been used. This may identify the effect of the polymer molecular structure on the solid dispersion performance, and would also show if the same or different drug molecular descriptors are relevant in understanding the performance of solid dispersions which use different carriers.

With an enlarged sample size, it might be of interest to employ some more sophisticated statistical analysis tools to better identify any correlations between molecular descriptors and experimental results. For example, principal component analysis could help to identify when several factors of molecular structure contribute concurrently to improve the performance of a solid dispersion. It may also be of use to develop scoring strategies for data from other experiments, and identify if correlations exist between the molecular descriptors and performance in other tests.

## Chapter 8

# Conclusions and Future Work

### 8.1 Conclusions

The aim of the work in this thesis was to investigate the influence of molecular structure on the properties and performance of solid dispersions, and then use this data to identify trends between molecular and physicochemical descriptors and the performance of the solid dispersions, which could then be used as the basis for a high-throughput screening method to identify drug molecules that can be more successfully formulated as solid dispersions.

In order to do this, a testing protocol was developed, using felodipine/copovidone solid dispersions as a model system. In Chapter 4 it was shown that amorphous solid dispersions of felodipine in copovidone with a single  $T_g$  were successfully formed, however PDF analysis suggested that the systems tested were not completely miscible. A laser light scattering instrument was developed in Chapter 5 for detecting morphological changes in solid dispersion films. Using this apparatus, it was shown that polymer swelling occurred in felodipine/copovidone solid dispersion films when exposed to water. Finally, dissolution experiments in Chapter 6 were carried out using both a small-scale micro-dissolution apparatus, and an integrated MRI flowcell system for testing of bulk samples. The data from both techniques was used to suggest a mechanism for the disso-

lution of solid dispersions. Using these experiments as a starting point, the methodology for testing a series of analogues was developed.

A series of eight analogues based on felodipine were successfully synthesised in Chapter 3 with a range of yields, requiring that experiments were carefully planned to fully utilise the available material. In subsequent experiments, solid dispersions containing these analogues (including felodipine) were tested to identify the effect of drug molecular structure on their properties and performance. To the author's knowledge, there is no prior evidence in the literature of this type of approach, whereby each drug molecule in the series differs by only one functional group, being used in order to further understand the contribution of each group on the properties and performance of solid dispersions. In Chapter 4 it was shown that amorphous solid dispersions with single  $T_g$  were successfully formed for six of the synthesised analogues. PDF analysis was carried out on solid dispersions of four of these analogues, and as with the felodipine samples, the results of this technique suggested that none of the systems tested was completely miscible at the drug loadings analysed. In Chapter 5, the ability of copovidone to inhibit drug crystallisation in the solid dispersion was tested. Literature evidence shows that hydrogen bonding between the amine of felodipine and the carbonyl of the polymer pyrrolidone ring is central to explaining the physical stability of this solid dispersion. This was supported by the data in Chapter 5 that showed an analogue with an N-methyl group (and therefore unable to act as a hydrogen bond donor) crystallised rapidly from its respective solid dispersions. Additionally, it was shown that analogues without chlorine substituents on the phenyl ring crystallised more readily from their solid dispersions than those with substituted phenyls, and similarly, changing the functional groups on carbons 3 and 5 of the DHP also impacted on the crystallisation of the analogue from its solid dispersions. These observations suggest that additional intermolecular interactions other than hydrogen bonding must be important in the formation of stable solid dispersions. In Chapter 6 it was suggested that blocking the felodipine amine, and presence of a nitrile group led to an increased dissolution rate.

In Chapter 7, correlations were calculated between molecular and physicochemical descriptors (including thermal properties from Chapter 4) for the analogues, and crystallisation and dissolution performance data for their respective solid dispersions with copovidone from Chapters 5 and 6. It was the intention that identification of strong correlations between descriptors and performance can be used to direct the synthesis of drug molecules that will be more likely to be successfully formulated as solid dispersions. For this particular series of analogues it was shown that compounds were more likely to crystallise from solid dispersions with copovidone if they had a low log P, low  $M_r$  and low polarizability. Prior to these experiments, it was thought that the number or dispersion of hydrogen bonding groups, and the dipole moment would correlate strongly with the performance of the compound in a solid dispersion, but for this system, no correlations were observed for these particular descriptors.

In summary, a number of testing methodologies have been used in this thesis to provide further understanding of the solid state structure, physical stability, and dissolution performance of solid dispersions containing analogues of felodipine and copovidone. From the results of these experiments, a number of general observations have been made regarding the influence of drug molecular structure on the performance of the solid dispersions. Subsequently, a screening method can be derived from the correlations between compound descriptors and the data from these experimental observations in order to identify analogous drug compounds that are likely to form solid dispersions with copovidone that have favourable properties. With further experimental data, the methodology detailed herein for identifying correlations could be expanded to develop a database of a broader library of drug compounds, from which APIs suitable for development as solid dispersions with a number of polymers could be identified.

## 8.2 Future Work

The development of the API screening tool would benefit from the testing of more analogues (including other commercially available dihydropyridine drugs) using the same

methodology, so that more statistically relevant correlations are observed. In order to fully validate the screening method, it should then be used to suggest the molecular structure of an analogue that will be expected to perform well as a solid dispersion based on the observed correlations, and this compound should be tested according to the same protocol as the analogues in the test-set.

The work detailed in this thesis has focussed on felodipine-based solid dispersions, and so the observations regarding drug molecular structure are likely to be specific to this particular series of analogues. Therefore, it would be of interest to test compounds from other analogue series. Similarly, as all of the systems tested in this thesis use copovidone as the carrier, correlations with drug structure are specific for this polymer. Therefore, testing with other amorphous polymers, such as PVP and HPMC, would extend the dataset so that the screening tool could be used to predict successful solid dispersion formulation for a wider range of systems.

The evaluation of solid dispersions in this work has been based on the physical stability and dissolution performance of solid dispersions. However, as alluded to in Chapter 1, there are additional requirements that a solid dispersion must fulfill: not least, that it should have good *in vivo* activity. Therefore, further development of the screening technique described in this work should involve the inclusion of *in vivo* performance descriptors.

## Appendix A

# Images from Well-plate Crystallisation Study

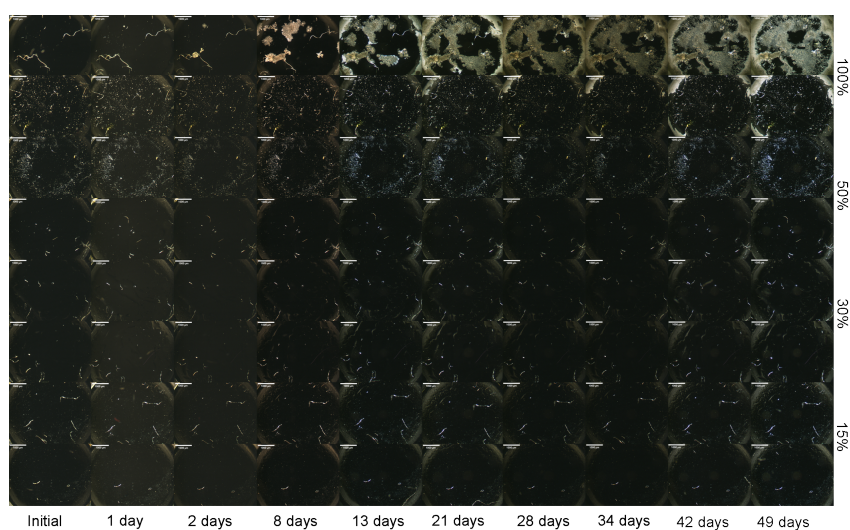


Figure A.1: Grid of images obtained from crystallisation experiments. This grid contains images obtained for solid dispersions of felodipine with ranging drug loadings stored at 25°C/60% Relative Humidity over 7 weeks.



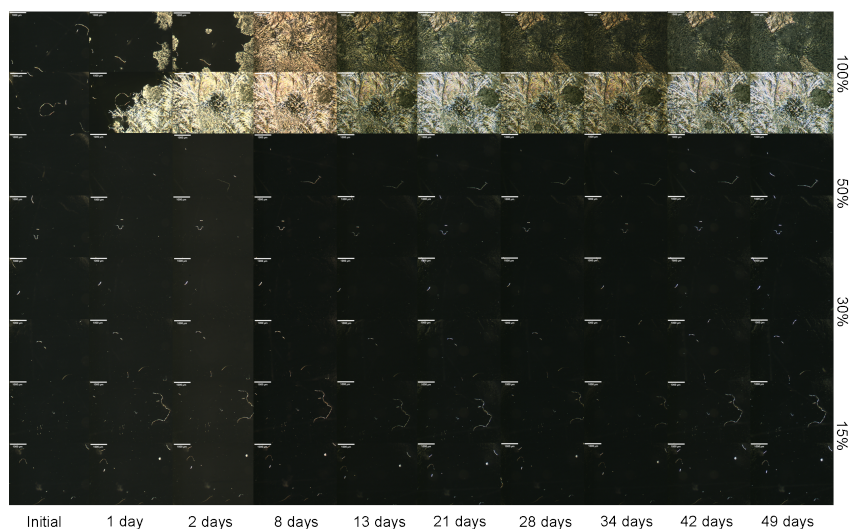


Figure A.2: Grid of images obtained from crystallisation experiments. This grid contains images obtained for solid dispersions of felodipine with ranging drug loadings stored at 40°C/75% Relative Humidity over 7 weeks.

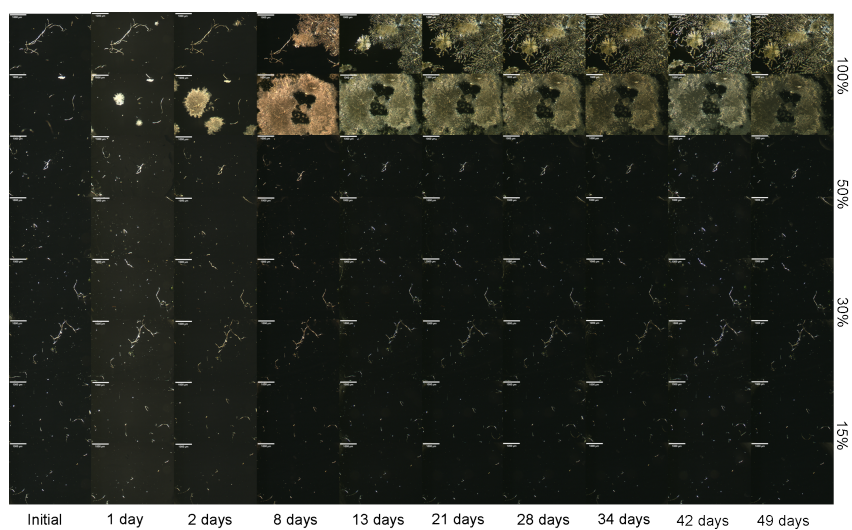


Figure A.3: Grid of images obtained from crystallisation experiments. This grid contains images obtained for solid dispersions of felodipine with ranging drug loadings stored at 40°C/0% Relative Humidity over 7 weeks.

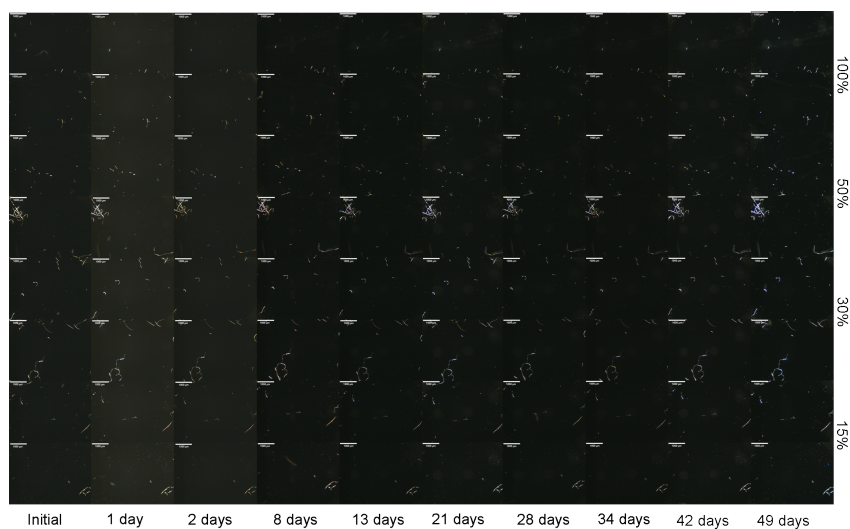


Figure A.4: Grid of images obtained from crystallisation experiments. This grid contains images obtained for solid dispersions of ZAL\_001 with ranging drug loadings stored at 25°C/60% Relative Humidity over 7 weeks.

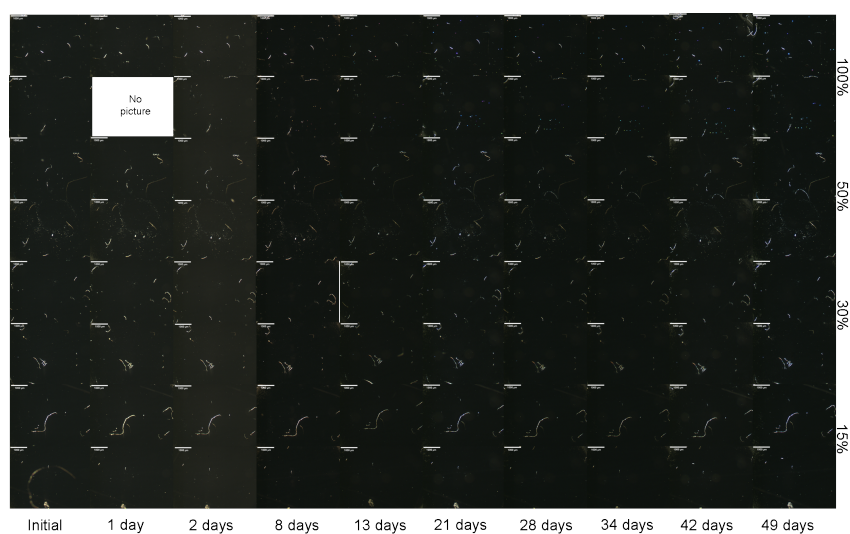


Figure A.5: Grid of images obtained from crystallisation experiments. This grid contains images obtained for solid dispersions of ZAL\_001 with ranging drug loadings stored at 40°C/75% Relative Humidity over 7 weeks.

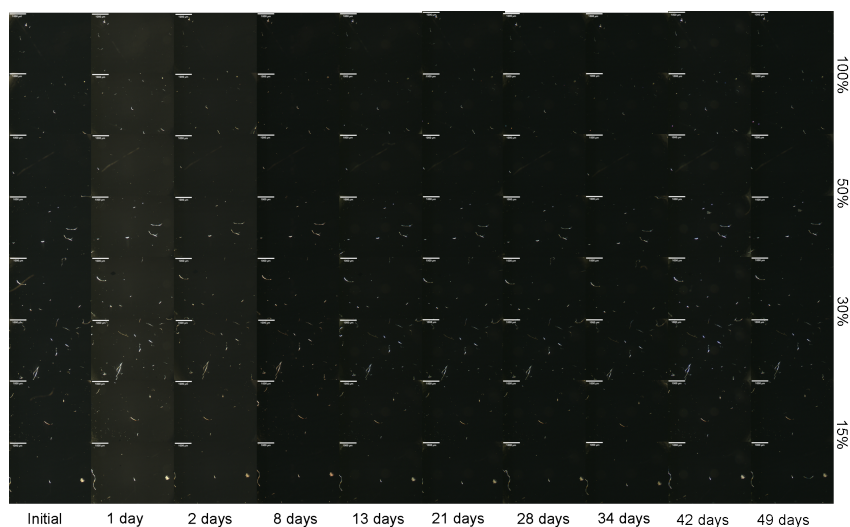


Figure A.6: Grid of images obtained from crystallisation experiments. This grid contains images obtained for solid dispersions of ZAL\_001 with ranging drug loadings stored at 40°C/0% Relative Humidity over 7 weeks.

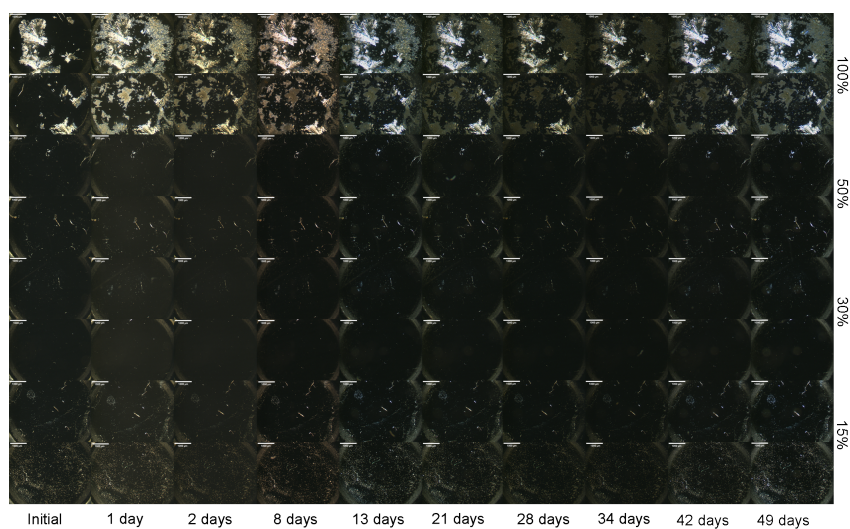


Figure A.7: Grid of images obtained from crystallisation experiments. This grid contains images obtained for solid dispersions of ZAL\_005 with ranging drug loadings stored at 25°C/60% Relative Humidity over 7 weeks.



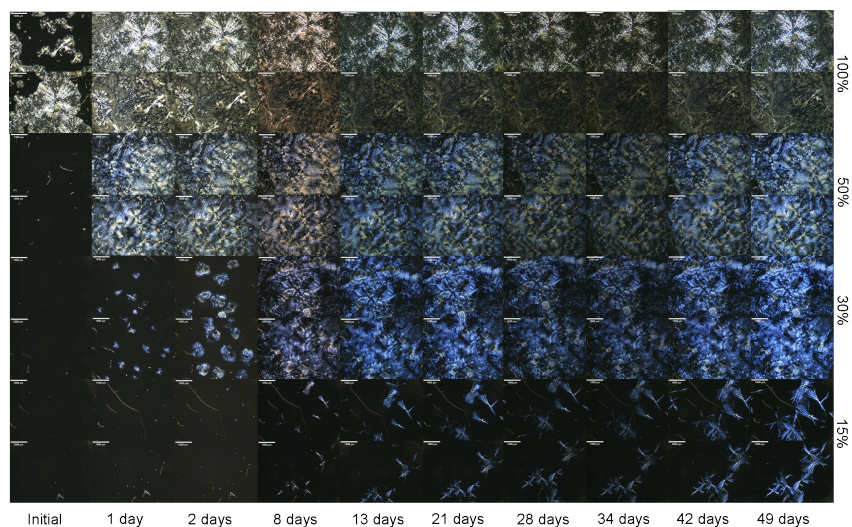


Figure A.8: Grid of images obtained from crystallisation experiments. This grid contains images obtained for solid dispersions of ZAL\_005 with ranging drug loadings stored at 40°C/75% Relative Humidity over 7 weeks.

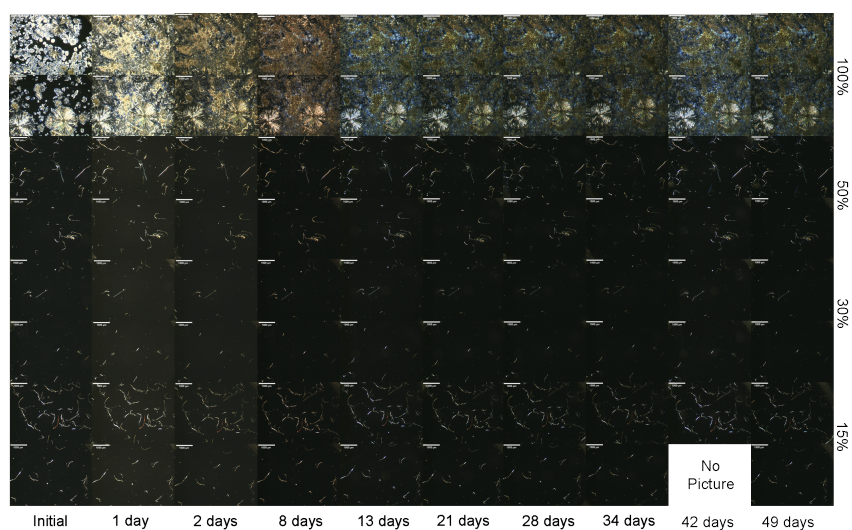


Figure A.9: Grid of images obtained from crystallisation experiments. This grid contains images obtained for solid dispersions of ZAL\_005 with ranging drug loadings stored at 40°C/0% Relative Humidity over 7 weeks.

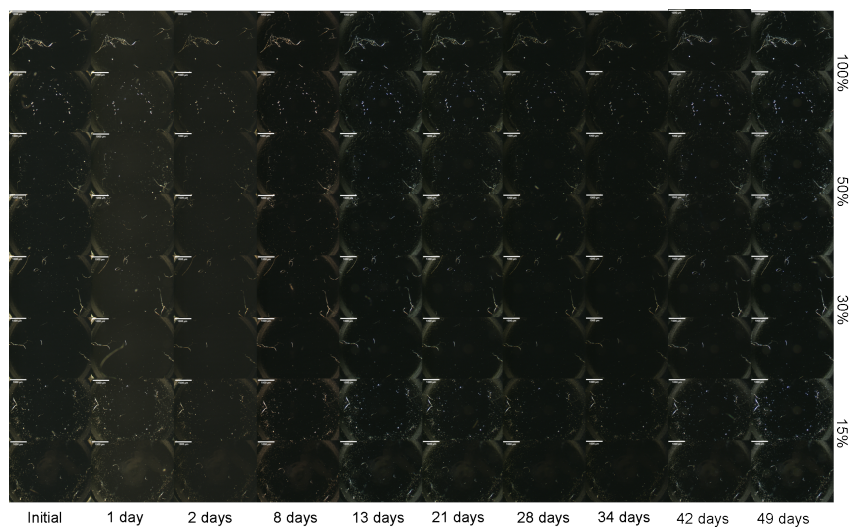


Figure A.10: Grid of images obtained from crystallisation experiments. This grid contains images obtained for solid dispersions of ZAL\_006 with ranging drug loadings stored at 25°C/60% Relative Humidity over 7 weeks.

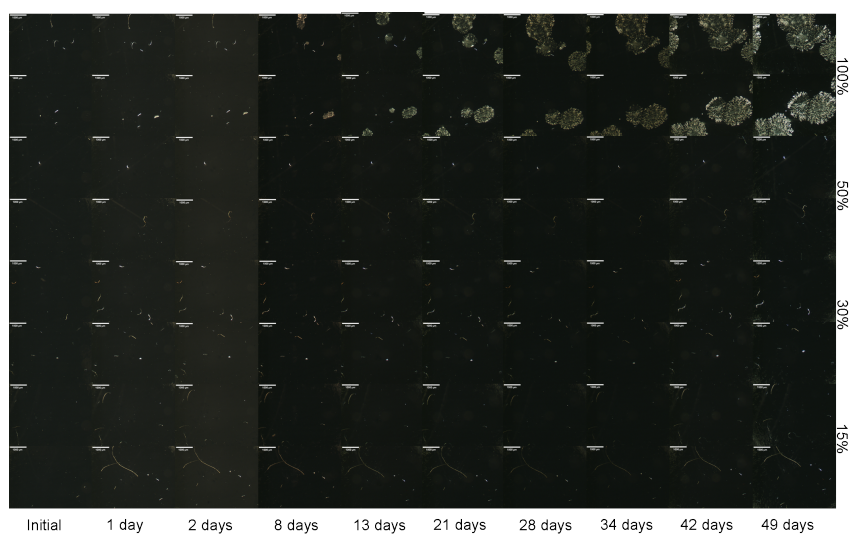


Figure A.11: Grid of images obtained from crystallisation experiments. This grid contains images obtained for solid dispersions of ZAL\_006 with ranging drug loadings stored at 40°C/75% Relative Humidity over 7 weeks.

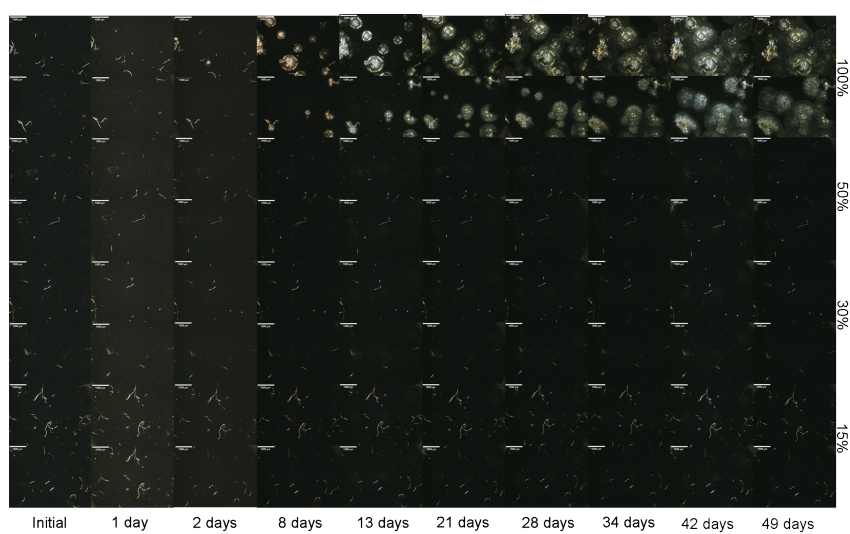


Figure A.12: Grid of images obtained from crystallisation experiments. This grid contains images obtained for solid dispersions of ZAL\_006 with ranging drug loadings stored at 40°C/0% Relative Humidity over 7 weeks.



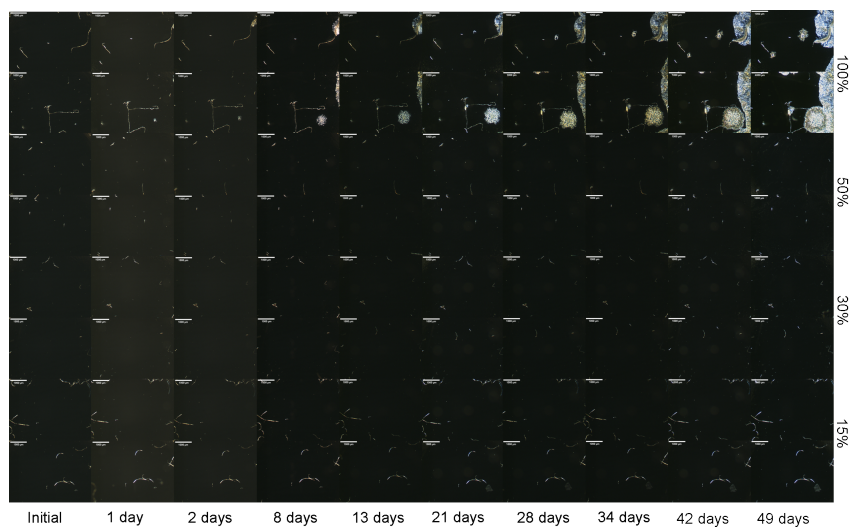


Figure A.13: Grid of images obtained from crystallisation experiments. This grid contains images obtained for solid dispersions of ZAL\_007 with ranging drug loadings stored at 25°C/60% Relative Humidity over 7 weeks.

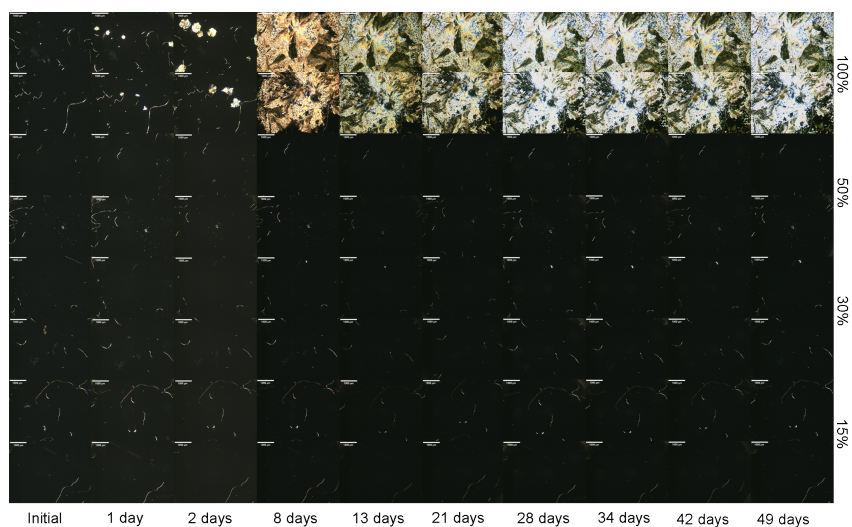


Figure A.14: Grid of images obtained from crystallisation experiments. This grid contains images obtained for solid dispersions of ZAL\_007 with ranging drug loadings stored at 40°C/75% Relative Humidity over 7 weeks.

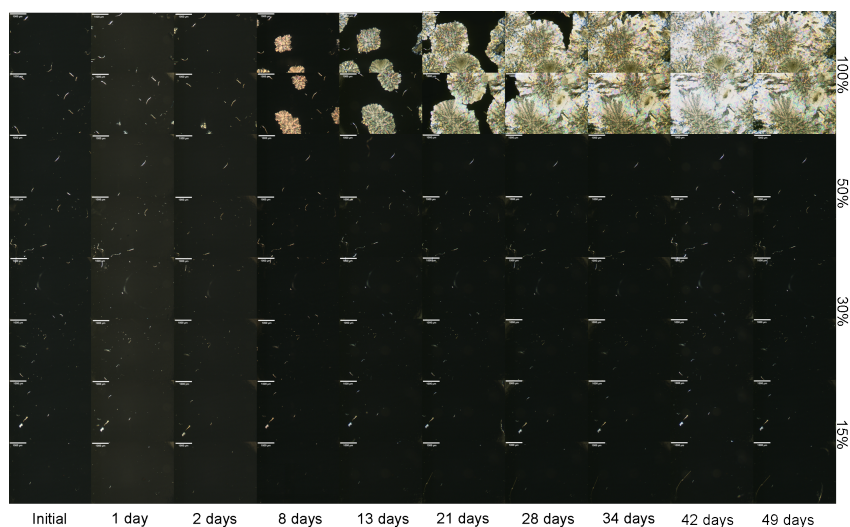


Figure A.15: Grid of images obtained from crystallisation experiments. This grid contains images obtained for solid dispersions of ZAL\_007 with ranging drug loadings stored at 40°C/0% Relative Humidity over 7 weeks.

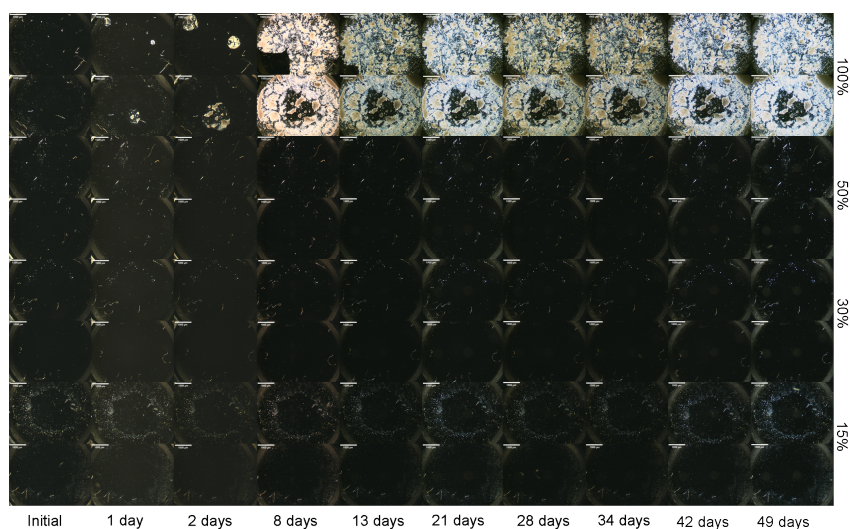


Figure A.16: Grid of images obtained from crystallisation experiments. This grid contains images obtained for solid dispersions of ZAL\_009 with ranging drug loadings stored at 25°C/60% Relative Humidity over 7 weeks.



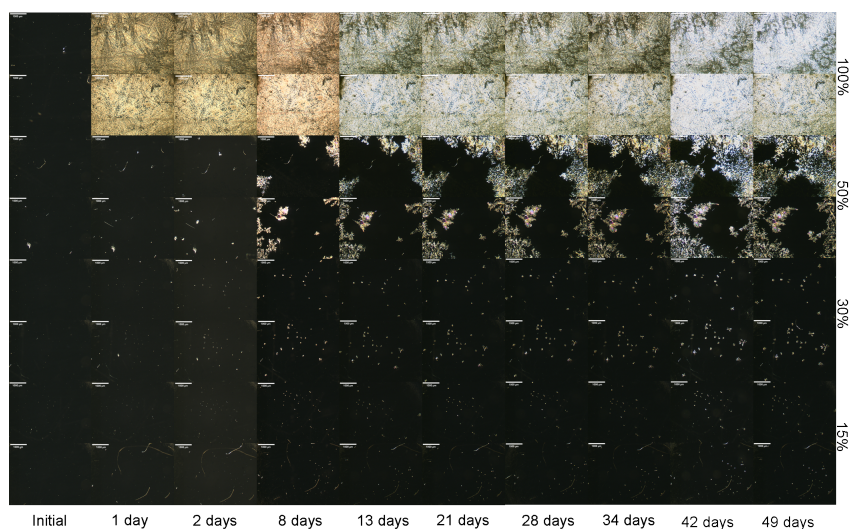


Figure A.17: Grid of images obtained from crystallisation experiments. This grid contains images obtained for solid dispersions of ZAL\_009 with ranging drug loadings stored at 40°C/75% Relative Humidity over 7 weeks.

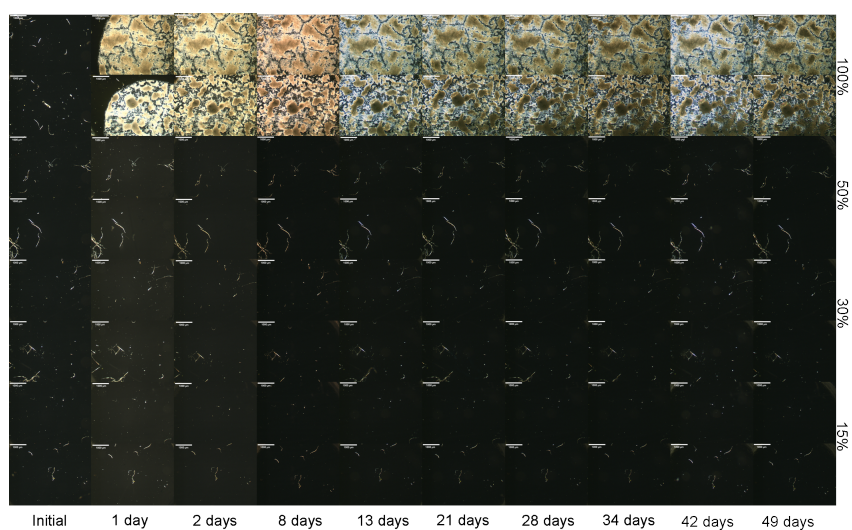


Figure A.18: Grid of images obtained from crystallisation experiments. This grid contains images obtained for solid dispersions of ZAL\_009 with ranging drug loadings stored at 40°C/0% Relative Humidity over 7 weeks.

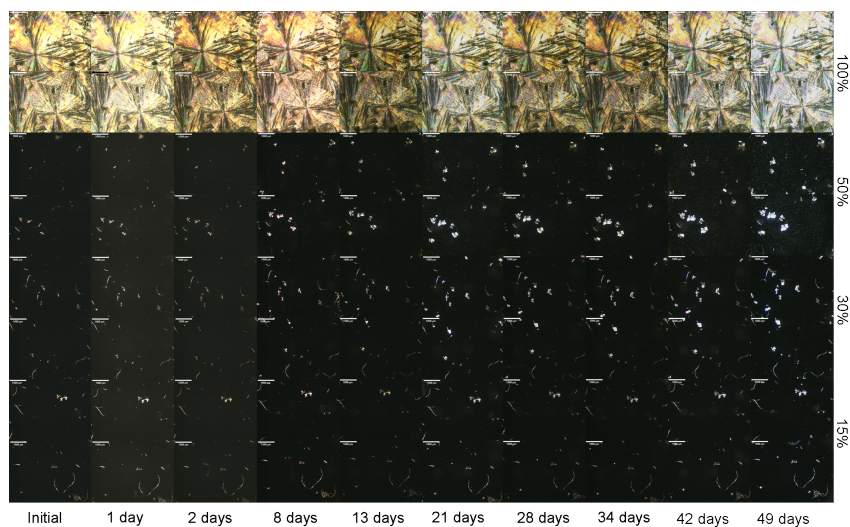


Figure A.19: Grid of images obtained from crystallisation experiments. This grid contains images obtained for solid dispersions of ZAL\_010 with ranging drug loadings stored at 25°C/60% Relative Humidity over 7 weeks.

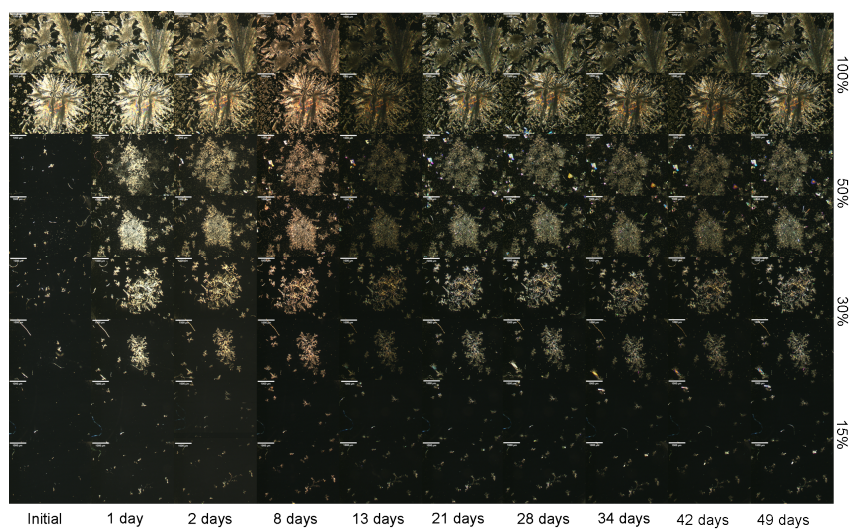


Figure A.20: Grid of images obtained from crystallisation experiments. This grid contains images obtained for solid dispersions of ZAL\_010 with ranging drug loadings stored at 40°C/75% Relative Humidity over 7 weeks.

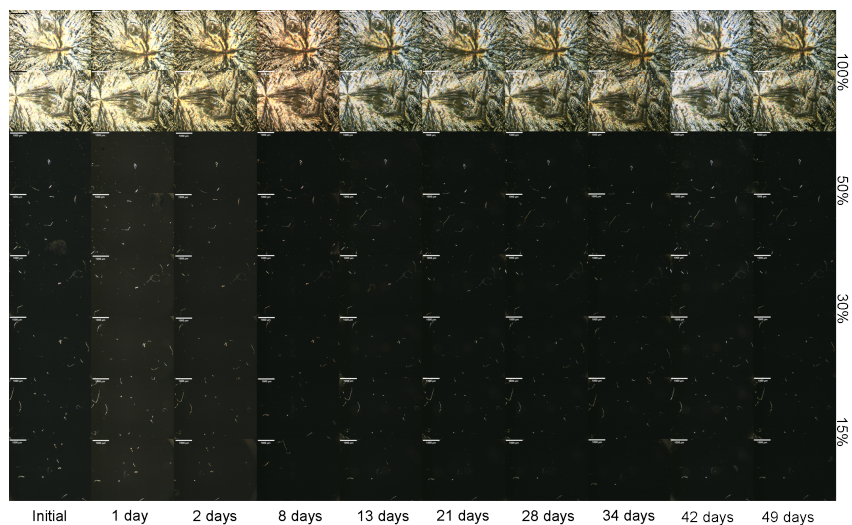


Figure A.21: Grid of images obtained from crystallisation experiments. This grid contains images obtained for solid dispersions of ZAL\_010 with ranging drug loadings stored at 40°C/0% Relative Humidity over 7 weeks.

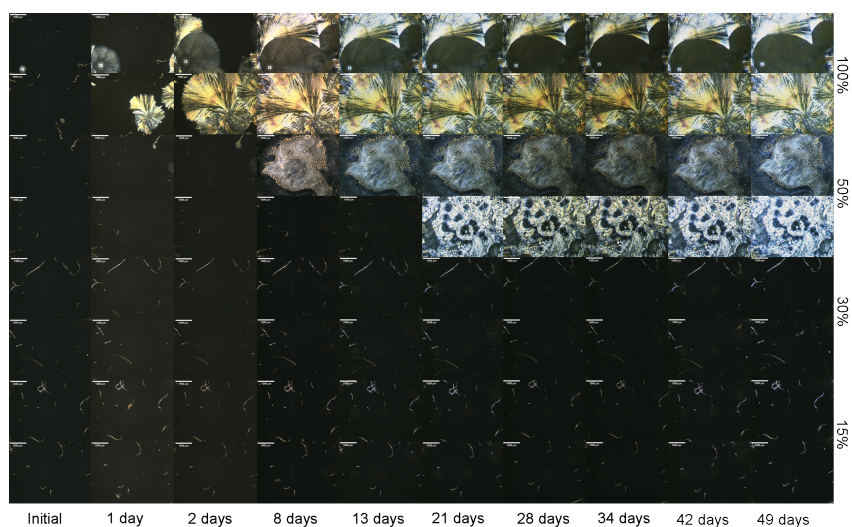


Figure A.22: Grid of images obtained from crystallisation experiments. This grid contains images obtained for solid dispersions of ZAL\_011 with ranging drug loadings stored at 25°C/60% Relative Humidity over 7 weeks.



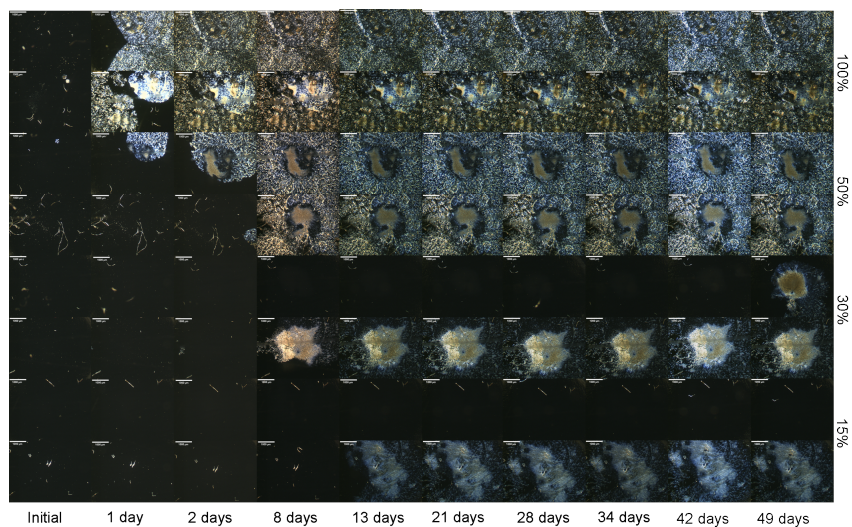


Figure A.23: Grid of images obtained from crystallisation experiments. This grid contains images obtained for solid dispersions of ZAL\_011 with ranging drug loadings stored at 40°C/75% Relative Humidity over 7 weeks.

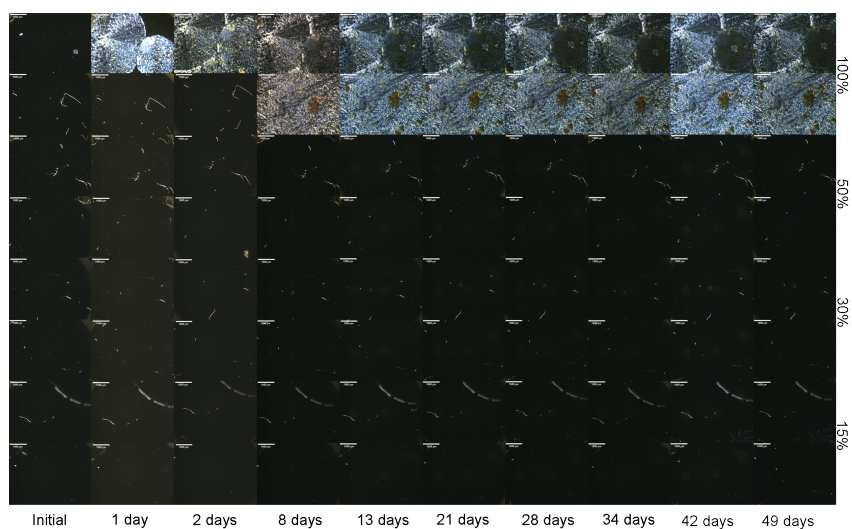


Figure A.24: Grid of images obtained from crystallisation experiments. This grid contains images obtained for solid dispersions of ZAL\_011 with ranging drug loadings stored at 40°C/0% Relative Humidity over 7 weeks.

## Appendix B

# Analogue Dissolution Results

Table B.1: Table summarising the data from dissolution experiments carried out on samples containing analogue ZAL.001. Data are reported as mean values  $\pm$  standard error. <sup>a</sup> Analysis of the crystalline form of this compound was not possible as it is an oil. For these samples the oil was dispensed directly into sample vials without any further preparation. <sup>b</sup> The equilibrium solubility determined by HPLC after 18 hours. <sup>c</sup> The equilibrium solubility determined by HPLC after 15 hours.

Type of Sample	Drug Loading (%)	Initial Dissolution Rate ( $\times 10^{-3}$ $\mu\text{g/mL/s}$ )	Maximum Solution Concentration ( $\mu\text{g/mL}$ )	Maximum % Drug in Solution	Equilibrium Solution Concentration ( $\mu\text{g/mL}$ )
Drug <sup>a</sup>	100	$0.09 \pm 0.00$	$47.28 \pm 0.63$	$5.87 \pm 0.19$	$15.7 \pm 0.2^b$
Film Cast Drug	100	$0.15 \pm 0.05$	$48.03 \pm 0.18$	$6.03 \pm 0.03$	$17.7 \pm 0.1^c$
Film Cast Drug (doped media)	100	$0.25 \pm 0.05$	$47.78 \pm 0.13$	$6.00 \pm 0.01$	$18.5 \pm 0.6^c$
Physical Mix	50	$0.20 \pm 0.00$	$50.27 \pm 0.06$	$6.35 \pm 0.63$	$18.5 \pm 0.7^b$
	15	$0.55 \pm 0.05$	$51.69 \pm 0.09$	$6.38 \pm 0.52$	$20.7 \pm 0.6^b$
Solid Dispersion	50	$1.95 \pm 0.15$	$36.08 \pm 2.32$	$4.93 \pm 0.32$	$20.3 \pm 0.1^c$
	30	$3.20 \pm 0.70$	$53.78 \pm 4.32$	$7.10 \pm 0.57$	$21.6 \pm 0.0^c$
	15	$3.65 \pm 1.55$	$42.21 \pm 10.94$	$5.26 \pm 1.36$	$25.1 \pm 0.9^c$

Table B.2: Table summarising the data from dissolution experiments carried out on samples containing analogue ZAL\_005. Data are reported as mean values  $\pm$  standard error. <sup>a</sup> Equilibrium solubility values are obtained by HPLC after 18 hours. <sup>b</sup> Equilibrium solubility values are obtained by HPLC after 48 hours.

Type of Sample	Drug Loading (%)	Initial Dissolution Rate ( $\times 10^{-3}$ $\mu\text{g/mL/s}$ )	Maximum Solution Concentration ( $\mu\text{g/mL}$ )	Maximum % Drug in Solution	Equilibrium Solution Concentration ( $\mu\text{g/mL}$ )
Crystalline Drug	100	$0.051 \pm 0.049$	$5.68 \pm 2.67$	$0.27 \pm 0.13$	$0.8 \pm 0.0^a$
Amorphous Drug	100	$0.095 \pm 0.005$	$11.71 \pm 0.44$	$0.59 \pm 0.02$	$1.7 \pm 0.2^b$
Amorphous Drug (doped media)	100	$0.100 \pm 0.000$	$17.78 \pm 1.47$	$0.89 \pm 0.07$	$2.3 \pm 0.0^b$
Physical Mix	50	$0.006 \pm 0.001$	$14.60 \pm 1.53$	$0.71 \pm 0.07$	$2.0 \pm 0.3^a$
	15	$0.007 \pm 0.003$	$11.04 \pm 2.71$	$0.55 \pm 0.12$	$3.5 \pm 0.6^a$
Solid Dispersion	50	$1.650 \pm 0.050$	$46.77 \pm 1.65$	$2.38 \pm 0.08$	$1.5 \pm 0.2^b$
	30	$4.700 \pm 0.000$	$57.52 \pm 3.67$	$2.83 \pm 0.18$	$1.3 \pm 0.2^b$
	15	$9.000 \pm 2.500$	$129.82 \pm 1.63$	$6.68 \pm 0.09$	$5.2 \pm 0.4^a$

Table B.3: Table summarising the data from dissolution experiments carried out on samples containing analogue ZAL\_006. Data are reported as mean values  $\pm$  standard error. <sup>a</sup> Initial dissolution rates could not be determined for these samples due to the irregularity of the data. <sup>b</sup> Equilibrium solubility values are obtained by HPLC after 18 hours. <sup>c</sup> Equilibrium solubility values are obtained by HPLC after 48 hours.

Type of Sample	Drug Loading (%)	Initial Dissolution Rate ( $\times 10^{-3}$ $\mu\text{g/mL/s}$ )	Maximum Solution Concentration ( $\mu\text{g/mL}$ )	Maximum % Drug in Solution	Equilibrium Solution Concentration ( $\mu\text{g/mL}$ )
Crystalline Drug	100	$0.203 \pm 0.198$	$3.01 \pm 0.86$	$0.24 \pm 0.08$	$0.4 \pm 0.0^b$
Amorphous Drug	100	$0.020 \pm 0.000$	$5.55 \pm 0.47$	$0.44 \pm 0.04$	$0.3 \pm 0.1^c$
Amorphous Drug (doped media)	100	$0.015 \pm 0.005$	$7.82 \pm 0.55$	$0.62 \pm 0.05$	$0.3 \pm 0.0^c$
Physical Mix	50	<sup>a</sup>	$10.95 \pm 0.70$	$0.82 \pm 0.04$	$0.8 \pm 0.0^b$
Solid Dispersion	50	$0.150 \pm 0.050$	$16.17 \pm 0.30$	$1.28 \pm 0.03$	$0.7 \pm 0.2^c$
	30	$0.850 \pm 0.050$	$30.66 \pm 0.55$	$2.35 \pm 0.05$	$1.0 \pm 0.0^b$
	15	$6.600 \pm 1.000$	$153.02 \pm 7.08$	$12.20 \pm 0.57$	$1.8 \pm 0.1^b$

Table B.4: Table summarising the data from dissolution experiments carried out on samples containing analogue ZAL\_007. Data are reported as mean values  $\pm$  standard error. <sup>a</sup> Only n=1 for this sample. <sup>b</sup> Equilibrium solubility values are obtained by HPLC after 18 hours. <sup>c</sup> Equilibrium solubility values are obtained by HPLC after 48 hours.

Type of Sample	Drug Loading (%)	Initial Dissolution Rate ( $\times 10^{-6}$ $\mu\text{g/mL/s}$ )	Maximum Solution Concentration ( $\mu\text{g/mL}$ )	Maximum % Drug in Solution	Equilibrium Solution Concentration ( $\mu\text{g/mL}$ )
Crystalline Drug	100	1.4 $\pm$ 0.6	2.37 $\pm$ 0.51	0.45 $\pm$ 0.09	<1 <sup>b</sup>
Amorphous Drug	100	35.0 $\pm$ 5.0	5.46 $\pm$ 0.02	1.09 $\pm$ 0.01	<1 <sup>c</sup>
Amorphous Drug (doped media)	100	50.0 $\pm$ 0.0	6.46 $\pm$ 0.06	1.29 $\pm$ 0.02	<1 <sup>c</sup>
Physical Mix	50	4.5 $\pm$ 0.5	5.23 $\pm$ 1.31	0.98 $\pm$ 0.15	<1 <sup>b</sup>
	15	8.5 $\pm$ 1.5	2.46 $\pm$ 1.86	0.47 $\pm$ 0.36	<1 <sup>b</sup>
Solid Dispersion	50	85.0 $\pm$ 15.0	5.74 $\pm$ 0.04	1.15 $\pm$ 0.01	<1 <sup>c</sup>
	30	2200.0 <sup>a</sup>	22.45 <sup>a</sup>	4.40 <sup>a</sup>	<1 <sup>a,b</sup>
	15	3250.0 $\pm$ 350.0	89.79 $\pm$ 1.99	16.95 $\pm$ 0.38	<1 <sup>c</sup>

Table B.5: Table summarising the data from dissolution experiments carried out on samples containing analogue ZAL\_011. Data are reported as mean values  $\pm$  standard error. All equilibrium solubility values are obtained by HPLC after 18 hours.

Type of Sample	Drug Loading (%)	Initial Dissolution Rate ( $\times 10^{-3}$ $\mu\text{g/mL/s}$ )	Maximum Solution Concentration ( $\mu\text{g/mL}$ )	Maximum % Drug in Solution	Equilibrium Solution Concentration ( $\mu\text{g/mL}$ )
Crystalline Drug	100	0.04 $\pm$ 0.01	8.80 $\pm$ 0.54	0.85 $\pm$ 0.06	0.0 $\pm$ 0.0
Amorphous Drug	100	0.01 $\pm$ 0.00	5.05 $\pm$ 0.00	0.47 $\pm$ 0.00	0.0 $\pm$ 0.0
Amorphous Drug (doped media)	100	0.02 $\pm$ 0.01	5.44 $\pm$ 0.64	0.50 $\pm$ 0.06	0.0 $\pm$ 0.0
Physical Mix	50	0.05 $\pm$ 0.02	15.62 $\pm$ 6.64	1.55 $\pm$ 0.69	0.0 $\pm$ 0.0
	15	0.14 $\pm$ 0.07	11.78 $\pm$ 0.16	1.10 $\pm$ 0.02	0.0 $\pm$ 0.0
Solid Dispersion	50	2.90 $\pm$ 0.50	66.67 $\pm$ 13.50	6.56 $\pm$ 1.33	0.5 $\pm$ 0.5
	30	4.70 $\pm$ 0.60	67.81 $\pm$ 4.11	6.33 $\pm$ 0.39	0.8 $\pm$ 0.8
	15	9.75 $\pm$ 1.05	98.95 $\pm$ 10.65	10.00 $\pm$ 1.08	1.4 $\pm$ 0.0

## Appendix C

# Calculated Molecular Descriptors and Correlations

Molecule Name	Xstal Screen Score	Dissn Score	Amorph Sol (mol dm <sup>-3</sup> )	Delta H Tm	Delta Hf Tm	pKa	Tg	Tm	Tg/Tm	Tm/Tg	Delta Cp	ClogP	ACDlogP	ACDlogD pH7.4	ACDlogD pH6.5
ZAL_007	253	619	9.30E-07	50.09	19.84	5.626	81.41	127.2	0.64	1.56	0.2396	5.83	5.36	5.36	5.36
ZAL_001	0	-14	2.91E-06			5.215						5.26	4.45	4.45	4.45
ZAL_011	570	264	4.27E-07	57.03	23.50	5.826	70.82	108.0	0.66	1.52	0.1912	6.14	4.40	4.40	4.40
ZAL_005	721	217	5.68E-06	177.10	38.53	5.626	12.74	107.2	0.12	8.41	0.3460	4.52	4.30	4.30	4.30
ZAL_006	174	475	1.40E-05	77.38	27.16	5.626	55.38	168.3	0.33	3.04	0.3642	4.73	3.60	3.60	3.60
ZAL_009	557		5.12E-05	106.33	30.09	5.626	31.29	169.4	0.18	5.41	0.4966	3.42	2.53	2.53	2.53
ZAL_008			8.19E-03	16.88	6.68	5.626		255.4				3.64	3.21	3.21	3.21
ZAL_010	1204		8.07E-04	48.36	11.41	5.626	76.80	104.4	0.74	1.36	0.2560	2.33	2.14	2.14	2.14
Felodipine	250	2184		68.44	26.26	5.626	43.14	147.9	0.29	3.43	0.2731	5.30	4.83	4.83	4.83
Xstal Screen Score vs. X		-0.128	0.784	0.095	-0.340	0.466	0.046	-0.636	0.311	0.034	-0.085	-0.706	-0.652	-0.652	-0.652
Dissn Score vs. X			0.195	-0.310	-0.200	0.238	-0.066	0.445	-0.192	-0.149	-0.084	0.050	0.342	0.342	0.342

Molecule Name	Xstal Screen Score	Dissn Score	MW	VOL	RotBond	RingCount	NPSA	HBD	HBA	PSA	Ion Class	Lipinski score	IP	EA	Hardness	Electronegativity
ZAL_007	253	619	398.3	317.8	5	2	369.5	1	5	68.7	Neutral	1	5.14	3.91	0.62	4.52
ZAL_001	0	-14	382.2	303.0	4	2	340.6	0	5	64.4	Neutral	1	6.75	3.21	1.77	4.98
ZAL_011	570	264	412.3	331.6	5	2	406.4	0	5	55.3	Neutral	1	4.99	4.01	0.49	4.50
ZAL_005	721	217	329.4	290.3	5	2	336.6	1	5	68.7	Neutral	0	4.99	3.23	0.88	4.11
ZAL_006	174	475	351.2	280.2	4	2	318.1	1	4	60.3	Neutral	0	5.54	3.34	1.10	4.44
ZAL_009	557		282.3	252.3	4	2	285.1	1	4	60.3	Neutral	0	5.37	2.49	1.44	3.93
ZAL_008			304.2	240.9	3	2	266.6	1	3	52.0	Neutral	0	5.94	3.02	1.46	4.48
ZAL_010	1204		235.3	212.8	3	2	233.7	1	3	52.0	Neutral	0	5.78	3.05	1.36	4.42
Felodipine	250	2184	384.3	302.8	4	2	346.9	1	5	68.7	Neutral	1	5.15	3.39	0.88	4.27
Xstal Screen Score vs. X		-0.128	-0.745	-0.664	-0.313		-0.563	0.292	-0.630	-0.581		-0.553	-0.273	-0.250	-0.051	-0.443
Dissn Score vs. X			0.151	-0.029	-0.355		-0.073	0.487	0.092	0.399		0.271	-0.355	-0.027	-0.255	-0.425



Molecule Name	Xstal Screen Score	Dissn Score	SCF_E	R2tak	qHC	qHN	qHO	SumqH	qCsp2	qCsp3	SumqC	qOsp2	qOsp3	SumqO	qNsp2	qNsp3	SumqN
ZAL_007	253	619	-2003	10070	0.21	0.36	0.00	2.63	0.91	0.77	0.11	-0.56	-0.48	-2.06	0.00	-0.55	-0.55
ZAL_001	0	-14	-1962	8607	0.19	0.00	0.00	2.23	0.98	0.33	0.52	-0.54	-0.49	-1.95	-0.73	0.00	-0.73
ZAL_011	570	264	-2042	10790	0.19	0.00	0.00	2.63	0.95	0.55	-0.36	-0.57	-0.50	-2.06	0.00	-0.07	-0.07
ZAL_005	721	217	-1088	8083	0.19	0.34	0.00	2.68	0.95	0.65	-0.13	-0.58	-0.47	-2.06	0.00	-0.49	-0.49
ZAL_006	174	475	-1829	8132	0.23	0.35	0.00	2.38	0.89	0.46	-0.27	-0.56	-0.49	-1.05	0.00	-0.49	-0.96
ZAL_009	557		-914	6005	0.21	0.35	0.00	2.45	0.90	0.56	-0.44	-0.56	-0.46	-1.02	0.00	-0.50	-0.99
ZAL_008			-1655	6317	0.23	0.37	0.00	2.05	0.51	0.48	-0.47	0.00	0.00	0.00	0.00	-0.56	-1.48
ZAL_010	1204		-740	4270	0.22	0.36	0.00	2.23	0.47	0.49	-0.78	0.00	0.00	0.00	0.00	-0.51	-1.45
Felodipine	250	2184	-1963	9242	0.20	0.35	0.00	2.50	1.00	0.87	0.16	-0.57	-0.49	-1.97	0.00	-0.56	-0.56
Xstal Screen Score vs. X		-0.128	0.799	-0.641	0.144	0.297		-0.024	-0.783	-0.011	-0.836	0.750	0.799	0.614	0.493	-0.286	-0.392
Dissn Score vs. X			-0.241	0.110	0.150	0.492		0.100	0.414	0.771	0.109	-0.306	-0.112	-0.051	0.393	-0.567	-0.032

Molecule Name	Xstal Screen Score	Dissn Score	SumqF	SumqS	SumqCI	SumqBr	Dipole Moment	SAS_H	SAS_C	SAS_N	SAS_O	SAS_F	SAS_CI	SAS_S	SAS_Br
ZAL_007	253	619	0.00	0.00	-0.13	0.00	5.60	317.7	126.1	1.95	43.85	0	90.66	0	0
ZAL_001	0	-14	0.00	0.00	-0.08	0.00	1.60	280.5	118.9	11.39	54.64	0	96.76	0	0
ZAL_011	570	264	0.00	0.00	-0.14	0.00	5.78	320.0	137.0	0.41	45.24	0	91.44	0	0
ZAL_005	721	217	0.00	0.00	0.00	0.00	3.20	366.7	143.3	2.05	46.73	0	0.00	0	0
ZAL_006	174	475	0.00	0.00	-0.10	0.00	9.34	242.8	111.8	46.90	27.12	0	107.70	0	0
ZAL_009	557		0.00	0.00	0.00	0.00	7.05	289.2	130.5	48.95	29.50	0	0.00	0	0
ZAL_008			0.00	0.00	-0.10	0.00	9.20	160.7	109.6	92.67	0.00	0	110.10	0	0
ZAL_010	1204		0.00	0.00	0.00	0.00	6.72	206.7	130.5	96.47	0.00	0	0.00	0	0
Felodipine	250	2184	0.00	0.00	-0.13	0.00	5.65	291.2	128.4	2.05	44.05	0	99.88	0	0
Xstal Screen Score vs. X		-0.128			0.640		0.178	-0.205	0.616	0.603	-0.713		-0.797		
Dissn Score vs. X					-0.412		0.285	-0.163	-0.013	-0.167	-0.161		0.279		

Molecule Name	Xstal Screen Score	Dissn Score	Polarizability	HBD dispersion	HBA dispersion	HB strength	Coul_HBD	Coul_HBA	vdw_HBD	vdw_HBA	AromAlif	DGcd	DGsolvH2O	DGsolvOct	DGcdOct
ZAL_007	253	619	435.0	0.70	-0.99	268.60	-8.12	279.00	-0.06	-2.22	20.83	2.03	-8.84	-17.61	-7.71
ZAL_001	0	-14	407.3	0.00	-3.32	227.50	0.00	229.60	0.00	-2.05	32.56	-1.19	-12.03	-17.37	-7.51
ZAL_011	570	264	456.4	0.00	-0.71	245.20	0.00	247.40	0.00	-2.22	19.61	1.78	-7.91	-16.94	-8.12
ZAL_005	721	217	356.6	0.70	-1.07	264.80	-7.79	274.90	-0.06	-2.22	20.83	2.61	-8.36	-18.35	-8.36
ZAL_006	174	475	389.4	0.70	-10.19	177.50	-8.00	186.90	-0.06	-1.36	23.08	-7.75	-20.09	-15.43	-4.20
ZAL_009	557		311.0	0.70	-10.64	175.80	-7.97	185.20	-0.06	-1.36	23.08	-7.51	-19.53	-15.60	-4.66
ZAL_008			344.2	0.66	-19.46	88.45	-8.40	97.41	-0.06	-0.50	26.67	-17.57	-28.93	-10.85	-0.51
ZAL_010	1204		265.4	0.66	-20.26	87.00	-8.12	95.68	-0.06	-0.50	26.67	-17.65	-28.34	-10.63	-0.90
Felodipine	250	2184	414.6	0.70	-1.04	259.20	-7.99	269.40	-0.06	-2.22	22.22	1.80	-9.71	-17.88	-7.40
Xstal Screen Score vs. X		-0.128	-0.713	0.261	-0.596	-0.583	-0.293	-0.573	-0.292	0.597	-0.181	-0.563	-0.510	0.679	0.555
Dissn Score vs. X			0.122	0.487	0.184	0.258	-0.492	0.309	-0.487	-0.173	-0.276	0.191	0.100	-0.208	0.042

Molecule Name	Xstal Screen Score	Dissn Score	RawLogP	Molradii	CohesiveE	SublEntropy	BO_HC	BO_HN	BO_HO	BO_Csp2	BO_Csp3	BO_Nsp2	BO_Nsp3	BO_Osp2	BO_Osp3
ZAL_007	253	619	6.44	6.80	-97.67	81.84	0.23	0.28	0	0.46	0.76	0.00	0.58	0.36	0.13
ZAL_001	0	-14	3.92	6.69	-89.09	61.34	0.23	0.00	0	0.29	0.99	0.56	0.00	0.37	0.14
ZAL_011	570	264	6.62	6.88	-102.70	62.11	0.23	0.00	0	0.46	0.75	0.00	0.50	0.36	0.13
ZAL_005	721	217	7.34	6.67	-92.66	60.59	0.22	0.28	0	0.44	0.73	0.00	0.58	0.36	0.13
ZAL_006	174	475	-3.42	6.53	-79.48	60.93	0.23	0.28	0	0.46	0.72	0.00	0.58	0.38	0.13
ZAL_009	557		-2.88	6.30	-74.47	59.38	0.23	0.28	0	0.46	0.72	0.00	0.58	0.37	0.14
ZAL_008			-13.27	6.14	-61.29	59.88	0.25	0.28	0	0.47	0.72	0.00	0.58	0.00	0.00
ZAL_010	1204		-13.00	5.88	-56.28	57.97	0.24	0.28	0	0.47	0.72	0.00	0.58	0.00	0.00
Felodipine	250	2184	5.99	6.71	-92.66	61.52	0.23	0.28	0	0.46	0.76	0.00	0.58	0.36	0.13
Xstal Screen Score vs. X		-0.128	-0.559	-0.688	0.574	-0.750	0.338	0.292		0.506	-0.563	-0.493	0.482	-0.794	-0.789
Dissn Score vs. X			0.121	-0.012	-0.019	0.164	0.251	0.487		0.430	-0.309	-0.393	0.432	-0.282	-0.393

# Bibliography

- [1] Christian Leuner and Jennifer Dressman. Improving drug solubility for oral delivery using solid dispersions. *Eur. J. Pharm. Biopharm.*, 50:47–60, 2000.
- [2] Win Loung Chiou and Sidney Riegelman. Pharmaceutical applications of solid dispersion systems. *J. Pharm. Sci.*, 60(9):1281–1302, 1971.
- [3] Duncan Q.M. Craig. The mechanisms of drug release from solid dispersions in water-soluble polymers. *Int. J. Pharm*, 231:131–144, 2002.
- [4] Büchi, Flawil, Switzerland. *Büchi Mini Spray Dryer B-290 Operating Manual*.
- [5] Lesley E. Smart and Elaine A. Moore. *Solid State Chemistry*. Taylor & Francis, 3rd edition, 2005. ISBN: 0-7487-7516-1.
- [6] Simon Bates, George Zografi, David Engers, Kenneth Morris, Kieran Crowley, and Ann Newman. Analysis of amorphous and nanocrystalline solids from their x-ray diffraction patterns. *Pharm. Res.*, 23(10):2333–2349, 2006.
- [7] Alexander T Florence and David Attwood. *Physicochemical Principles of Pharmacy*, chapter 9: Drug Absorption and routes of administration, pages 329–391. Pharmaceutical Press, London, 4th edition, 2006.
- [8] Center for Drug Evaluation & Research (CDER) U.S. Department of Health & Human Services, Food & Drug Administration. Guidance for industry: Waiver of

in vivo bioavailability and bioequivalence studies for immediate-release solid oral dosage forms based on a biopharmaceutics classification system, August 2000.

- [9] Gordon L. Amidon, Hans Lennernäs, Vinod P. Shah, and John R. Crison. A theoretical basis for a biopharmaceutics drug classification: The correlation of *in Vitro* drug product dissolution and *in Vivo* bioavailability. *Pharm. Res.*, 12(3): 413–420, 1995.
- [10] Christopher A. Lipinski, Franco Lombardo, Beryl W. Dominy, and Paul J. Feeney. Experimental and computational approaches to estimate solubility and permeability in drug discovery and development settings. *Adv. Drug Del. Rev.*, 46:3–26, 2001.
- [11] Toshihide Takagi, Chandrasekharan Ramachandran, Marival Bermejo, Shinji Yamashita, Lawrence X. Yu, and Gordon L. Amidon. A provisional biopharmaceutical classification of the top 200 oral drug products in the United States, Great Britain, Spain and Japan. *Mol. Pharm.*, 3(6):631–643, 2006.
- [12] Shoufeng Li, Handan He, Lakshman J. Parthiban, Hequn Yin, and Abu T.M. Serajuddin. IV-IVC considerations in the development of immediate-release oral dosage form. *J. Pharm. Sci.*, 94:1396–1417, 2005.
- [13] Robert A. Lipper. E pluribus product. *Modern Drug Discovery*, 2:55–60, 1999.
- [14] Valentino J. Stella and Kwame W. Nti-Addae. Prodrug strategies to overcome poor water solubility. *Adv. Drug Del. Rev.*, 59:677–694, 2007.
- [15] Kuei-Meng Wu. A new classification of prodrugs: regulatory perspectives. *Pharmaceuticals*, 2:77–81, 2009.
- [16] Sudhakar D. Garad. How to improve the bioavailability of poorly soluble drugs. *Am. Pharm. Rev.*, pages 80–93, 2004.

- [17] Eino Nelson. Solution rate of theophylline salts and effects from oral administration. *J. Am. Pharm. Assoc. (Sci. Ed.)*, 46(10):607–614, 1957.
- [18] Eino Nelson. Comparative dissolution rates of weak acids and their sodium salts. *J. Am. Pharm. Assoc. (Sci. Ed.)*, 47(4):297–299, 1958.
- [19] Abu T. M. Serajuddin. Salt formation to improve drug solubility. *Adv. Drug Del. Rev.*, 59:603–616, 2007.
- [20] Michael J. Bowker. A procedure for salt selection and optimization. In P. Heinrich Stahl and Camille G. Wermuth, editors, *Handbook of Pharmaceutical Salts: Properties, Selection and Use*, chapter 7, pages 161–189. VHCA, Zürich and Wiley-VCH, Weinheim., 2002.
- [21] N. Blagden, M. de Matas, P.T. Gavan, and P. York. Crystal engineering of active pharmaceutical ingredients to improve solubility and dissolution rates. *Adv. Drug Del. Rev.*, 59:617–630, 2007.
- [22] David J. Berry, Colin C. Seaton, William Clegg, Ross W. Harrington, Simon J. Coles, Peter N. Horton, Michael B. Hursthouse, Richard Storey, William Jones, Tomislav Friščić, and Nicholas Blagdon. Applying hot-stage microscopy to co-crystal screening: A study of nicotinamide with seven active pharmaceutical ingredients. *Cryst. Growth Des.*, 8(5):1697–1712, 2008.
- [23] Ning Shan and Michael J. Zaworotko. The role of cocrystals in pharmaceutical science. *Drug Discovery Today*, 13(13):440–446, 2008.
- [24] Nate Schultheiss and Ann Newman. Pharmaceutical cocrystals and their physicochemical properties. *Cryst. Growth Des.*, 9(6):2950–2967, 2009.
- [25] David J. W. Grant. Theory and origin of polymorphism. In Harry G. Brittain, editor, *Polymorphism in Pharmaceutical Solids*, volume 95 of *Drugs and the Pharmaceutical Sciences*, chapter 1, pages 1–33. Marcel Dekker, Inc., New York, 1999.

- [26] W.C. McCrone. *Physics and Chemistry of the Organic Solid State*, volume 2, pages 725–767. Interscience, London, 1965.
- [27] Bruno C. Hancock, Evgenyi Y. Shalaev, and Sheri L. Shamblin. Polyamorphism: a pharmaceutical science perspective. *J. Pharm. Pharmacol.*, 54:1151–1152, 2002.
- [28] Bruno C. Hancock and George Zografi. Characteristics and significance of the amorphous state in pharmaceutical systems. *J. Pharm. Sci.*, 86(1):1–12, 1997.
- [29] Kieran J. Crowley and George Zografi. Water vapor absorption into amorphous hydrophobic drug/poly(vinylpyrrolidone) dispersions. *J. Pharm. Sci.*, 91(10):2150–2165, 2002.
- [30] Panayiotis P. Constantinides. Lipid microemulsions for improving drug dissolution and oral absorption: Physical and biopharmaceutical aspects. *Pharm. Res.*, 12(11):1561–1572, 1995.
- [31] Abu T.M. Serajuddin. Development of lipid-based drug delivery systems for poorly water-soluble drugs as viable oral dosage forms - present status and future prospects. *Am. Pharm. Rev.*, March/April:34–42, 2008.
- [32] A. Meinzer, E. Mueller, and J. Vonderscher. Microemulsion - a suitable galenic approach for the absorption enhancement of low soluble compounds? *BT Gattefosse*, 88:21–26, 1995.
- [33] Arthur A. Noyes and Willis R. Whitney. The rate of solution of solid substances in their own solutions. *J. Am. Chem. Soc.*, 19:930–934, 1897.
- [34] Harry G. Brittain and Eugene F. Fiese. Effects of pharmaceutical processing on drug polymorphs and solvates. In Harry G. Brittain, editor, *Polymorphism in Pharmaceutical Solids*, volume 95 of *Drugs and the Pharmaceutical Sciences*, chapter 8, pages 331–361. Marcel Dekker, Inc., New York, 1999.

- [35] Abu T.M. Serajuddin. Solid dispersion of poorly water-soluble drugs: Early promises, subsequent problems, and recent breakthroughs. *J. Pharm. Sci.*, 88 (10):1058–1066, 1999.
- [36] Keiji Sekiguchi and Noboru Obi. Studies on absorption of eutectic mixture. i. a comparison of the behaviour of eutectic mixture of sulfathiazole and that of ordinary sulfathiazole in man. *Chem. Pharm. Bull.*, 9:866–872, 1961.
- [37] Arthur H. Goldberg, Milo Gibaldi, and Joseph L. Kanig. Increasing dissolution rates and gastrointestinal absorption of drugs via solid solutions and eutectic mixtures II: Experimental evaluation of a eutectic mixture: Urea-acetaminophen system. *J. Pharm. Sci.*, 55:482–487, 1966.
- [38] James L. Ford. The current status of solid dispersions. *Pharm. Acta. Helv.*, 61 (3):69–88, 1986.
- [39] Arthur H. Goldberg, Milo Gibaldi, and Joseph L. Kanig. Increasing dissolution rates and gastrointestinal absorption of drugs via solid solutions and eutectic mixtures I: Theoretical considerations and discussion of the literature. *J. Pharm. Sci.*, 54:1145–1148, 1965.
- [40] National Archives and Records Administration. Code of federal regulations, 21CFR182,184. [http://www.access.gpo.gov/nara/cfr/waisidx\\_09/21cfrv3\\_09.html](http://www.access.gpo.gov/nara/cfr/waisidx_09/21cfrv3_09.html), October 2010. Updated annually - for all revisions see <http://www.access.gpo.gov/nara/cfr/cfr-table-search.html>.
- [41] M. Langer, M. Höltje, N.A. Urbanetz, B.Brandt, H.-D. Höltje, and B.C. Lippold. Investigations on the predictability of the formation of glassy solid solutions of drugs in sugar alcohols. *Int. J. Pharm.*, 252:167–179, 2003.
- [42] Karel Six, Geert Verreck, Jef Peeters, Marcus Brewster, and Guy Van den Mooter. Increased physical stability and improved dissolution properties of itraconazole, a

class II drug, by solid dispersions that combine fast- and slow-dissolving polymers. *J. Pharm. Sci.*, 93(1):124–131, 2004.

- [43] George Z. Papageorgiou, Dimitrios Bikiaris, Feras I. Kanaze, Evangelos Karavas, Anagnostis Stergiou, and Emmanouil Georgarakis. Tailoring the release rates of fluconazole using solid dispersions in polymer blends. *Drug Dev. Ind. Pharm.*, 34: 336–346, 2008.
- [44] Sandrien Janssens, Jan Van Humbeeck, and Guy Van den Mooter. Evaluation of solid dispersions by co-spray drying itraconazole with inutec SP1, a polymeric surfactant, in combination with PVPVA 64. *Eur. J. Pharm. Biopharm.*, 70:500–505, 2008.
- [45] Alazar N. Ghebremeskel, Chandra Vemavarapu, and Mayur Lodaya. Use of surfactants as plasticizers in preparing solid dispersions of poorly soluble API: Selection of polymer-surfactant combinations using solubility parameters and testing the processability. *Int. J. Pharm.*, 328:119–129, 2007.
- [46] Carsten Timpe. Drug solubilization strategies: Applying nanoparticulate formulation and solid dispersion approaches in drug development. *Am. Pharm. Rev.*, January/February:12–21, 2010.
- [47] Jean-Luc Dubois and James L. Ford. Similarities in the release rates of different drugs from polyethylene glycol 6000 solid dispersions. *J. Pharm. Pharmacol.*, 37: 494–496, 1985.
- [48] Yusuke Shibata, Makiko Fujii, Makiko Kokudai, Shinobu Noda, Hideko Okada, Masuo Kondoh, and Yoshiteru Watanabe. Effect of characteristics of compounds on maintenance of an amorphous state in solid dispersion with crospovidone. *J. Pharm. Sci.*, 96(6):1537–1547, 2006.
- [49] Rina Chokshi and Hossein Zia. Hot-melt extrusion technique: A review. *Iranian J. Pharm. Res.*, 3:3–16, 2004.

- [50] Fernando A. Alvarez-Núñez and Mark R. Leonard. Formulation of a poorly soluble drug using hot melt extrusion: The amorphous state as an alternative. *Am. Pharm. Rev.*, July/August:88–92, 2004.
- [51] Dave A. Miller, Jason T. McConville, Wei Yang, and James W. McGinity Robert O. Williams III. Hot-melt extrusion for enhanced delivery of drug particles. *J. Pharm. Sci.*, 96(2):361–376, 2007.
- [52] Gavin P. Andrews, David S. Jones, Osama Abu Diak, Daniel N. Margetson, and Mark S. McAlister. Hot-melt extrusion: an emerging drug delivery technology. *Pharm. Tech. Eur.*, 21(1), 2009.
- [53] Michael A. Repka. Hot-melt extrusion. *Am. Pharm. Rev.*, September/October: 18–27, 2009.
- [54] Caroline Bruce, Kurt A. Fegely, Ali R. Rajabi-Siahboomi, and James W. McGinity. Crystal growth formation in melt extrudates. *Int. J. Pharm*, 341:162–172, 2007.
- [55] K. Nollenberger, A. Gryczke, Ch. Meier, J. Dressman, M.U. Schmidt, and S. Brühne. Pair distribution function X-Ray analysis explains dissolution characteristics of felodipine melt extrusion products. *J. Pharm. Sci.*, 98(4):1476–1486, 2009.
- [56] Hajime Konno and Lynne S. Taylor. Ability of different polymers to inhibit the crystallization of amorphous felodipine in the presence of moisture. *Pharm. Res.*, 25(4):969–978, 2008.
- [57] Alfred C.F. Rumondor, Igor Ivanisevic, Simon Bates, David E. Alonzo, and Lynne S. Taylor. Evaluation of drug-polymer miscibility in amorphous solid dispersion systems. *Pharm. Res.*, 26(11):2523–2534, 2009.
- [58] Shan-Yang Lin, Chao-Ming Liao, Ging-Ho Hsiue, and Run-Chu Liang. Study of a theophylline-eudragit L mixture using a combined system of microscopic Fourier-



transform infrared spectroscopy and differential scanning calorimetry. *Thermochimica Acta*, 245:153–166, 1995.

- [59] Madhav Vasanthavada, Wei-Qin Tong, Yatindra Joshi, and M. Serpil Kislalioglu. Phase behaviour of amorphous molecular dispersions II: Role of hydrogen bonding in solid solubility and phase separation kinetics. *Pharm. Res.*, 22(3):440–448, 2005.
- [60] Alfred C.F. Rumondor, Lindsay A. Stanford, and Lynne S. Taylor. Effects of polymer type and storage relative humidity on the kinetics of felodipine crystallization from amorphous solid dispersions. *Pharm. Res.*, 26(12):2599–2606, 2009.
- [61] Justin D. Moser, Jennifer Broyles, Lina Liu, Elise Miller, and Michael Wang. Enhancing bioavailability of poorly soluble drugs using spray dried solid dispersions. part I. *Am. Pharm. Rev.*, September/October:68–73, 2008.
- [62] Erika Broman, Cynthia Khoo, and Lynne S. Taylor. A comparison of alternative polymer excipients and processing methods for making solid dispersions of a poorly water soluble drug. *Int. J. Pharm.*, 222:139–151, 2001.
- [63] Markus Vogt, Klaus Kunath, and Jennifer B. Dressman. Dissolution improvement of four poorly water soluble drugs by cogrinding with commonly used excipients. *Eur. J. Pharm. Biopharm.*, 68:330–337, 2008.
- [64] Eun-Jung Kim, Myung-Kwan Chun, Jae-Sang Jang, In-Hwa Lee, Kyeo-Re Lee, and Hoo-Kyun Choi. Preparation of a solid dispersion of felodipine using a solvent wetting method. *Eur. J. Pharm. Biopharm.*, 64:200–205, 2006.
- [65] Mariarosa Moneghini, Barbara Bellich, Pietro Baxa, and Francesco Princivale. Microwave generated solid dispersions containing ibuprofen. *Int. J. Pharm.*, In Press, 2008.

- [66] F.I. Kanaze, E. Kokkalou, I. Niopas, M. Georgarakis, A. Stergiou, and D. Bikiaris. Dissolution enhancement of flavonoids by solid dispersion in PVP and PEG matrices: a comparative study. *J. Appl. Polym. Sci.*, 102(1):460–471, 2006.
- [67] Manfred Gordon and James S. Taylor. Ideal copolymers and the second-order transitions of synthetic rubbers. I. non-crystalline copolymers. *J. Appl. Chem.*, 2(9):493–500, 1952.
- [68] Ann Newman, David Engers, Simon Bates, Igor Ivanisevic, Ron C. Kelly, and George Zografi. Characterization of amorphous API:polymer mixtures using X-Ray powder diffraction. *J. Pharm. Sci.*, 97(11):4840–4856, 2008.
- [69] Evangelos Karavas, Emmanuel Georgarakis, Michael P. Sigalas, Konstantinos Avgoustakis, and Dimitrios Bikiaris. Investigation of the release mechanism of a sparingly water-soluble drug from solid dispersions in hydrophilic carriers based on physical state of drug, particle size distribution and drug-polymer interactions. *Eur. J. Pharm. Biopharm.*, 66:334–347, 2007.
- [70] Gert Strobl. *The Physics of Polymers: Concepts for Understanding Their Structures and Behaviour*. Springer-Verlag, Berlin, 2nd edition, 1997.
- [71] Richard A.L. Jones. *Soft Condensed Matter*. Oxford Master Series in Condensed Matter Physics. Oxford University Press, Oxford, 2002.
- [72] Patrick J. Marsac, Sheri L. Shamblin, and Lynne S. Taylor. Theoretical and practical approaches for prediction of drug-polymer miscibility and solubility. *Pharm. Res.*, 23(10):2417–2426, 2006.
- [73] P.J. Flory. *Principles of Polymer Chemistry*. Cornell University Press, Ithaca, 1953.
- [74] David J. Greenhalgh, Adrian C. Williams, Peter Timmins, and Peter York. Solubility parameters as predictors of miscibility in solid dispersions. *J. Pharm. Sci.*, 88(11):1182–1190, 1999.

- [75] Patrick J. Marsac, Tonglei Li, and Lynne S. Taylor. Estimation of drug-polymer miscibility and solubility in amorphous solid dispersions using experimentally determined interaction parameters. *Pharm. Res.*, 26(1):139–151, 2009.
- [76] Seung-Uk Yoo, Steven L. Krill, Zeren Wang, and Chitra Telang. Miscibility/stability considerations in binary solid dispersion systems composed of functional excipients towards the design of multi-component amorphous systems. *J. Pharm. Sci.*, 98(12):4711–4723, 2009.
- [77] Makiko Fujii, Junko Hasegawa, Hideaki Kitajima, and Mitsuo Matsumoto. The solid dispersion of benzodiazepams with phosphatidylcholine. the effect of substituents of benzodiazepins on the formation of solid dispersions. *Chem. Pharm. Bull.*, 39(11):3013–3017, 1991.
- [78] Bruno C. Hancock and Michael Parks. What is the true solubility advantage for amorphous pharmaceuticals? *Pharm. Res.*, 17(4):397–404, 2000.
- [79] O.I. Corrigan. Mechanisms of dissolution of fast release solid dispersions. *Drug Dev. Ind. Pharm.*, 11(2-3):697–724, 1985.
- [80] O.I. Corrigan. Retardation of polymeric carrier dissolution by dispersed drugs: factors influencing the dissolution of solid dispersions containing polyethylene glycols. *Drug Dev. Ind. Pharm.*, 12(11-13):1777–1793, 1986.
- [81] D.Q.M. Craig and J.M. Newton. The dissolution of nortriptyline HCl from polyethylene glycol solid dispersions. *Int. J. Pharm*, 78:175–182, 1992.
- [82] Eva Sjökvist Saers and Duncan Q.M. Craig. An investigation into the mechanisms of dissolution of alkyl p-aminobenzoates from polyethylene glycol solid dispersions. *Int. J. Pharm.*, 83:211–219, 1992.
- [83] Siriporn Okonogi and Satit Puttipipatkachorn. Dissolution improvement of high drug-loaded solid dispersion. *AAPS Pharm. Sci. Tech.*, 7(2):E1–E6, 2006.

- [84] Devalina Law, Eric A. Schmitt, Kennan C. Marsh, Elizabeth A. Everitt, Weili Wang, James J. Fort, Steven I. Krill, and Yihong Qiu. Ritonavir-PEG 8000 amorphous solid dispersions: *In Vitro* and *In Vivo* evaluations. *J. Pharm. Sci.*, 93(3): 563–570, 2004.
- [85] Bassam M. Tashtoush, Zubaida S. Al-Qashi, and Naji M. Najib. In vitro and in vivo evaluation of glibenclamide in solid dispersion systems. *Drug Dev. Ind. Pharm.*, 30(6):601–607, 2004.
- [86] Madhuri Newa, Krishna Bhandari, Dong Xun Li, Tae-Hyub Kwon, Jung Ae Kim, Bong Kyu Yoo, Jong Soo Woo, Won Seok Lyoo, Chul Soon Yong, and Han Gon Choi. Preparation, characterization and in vivo evaluation of ibuprofen binary solid dispersions with poloxamer 188. *Int. J. Pharm*, 343:228–237, 2007.
- [87] Hajime Konno and Lynne S. Taylor. Influence of different polymers on the crystallization tendency of molecularly dispersed amorphous felodipine. *J. Pharm. Sci.*, 95(12):2692–2705, 2006.
- [88] Evangelos Karavas, Georgios Ktistis, Aristotelis Xenakis, and Emmanouel Georgarakis. Effect of hydrogen bonding interactions on the release mechanism of felodipine from nanodispersions with polyvinylpyrrolidone. *Eur. J. Pharm. Biopharm.*, 63:103–114, 2006.
- [89] *British National Formulary 59, March 2010*. BMJ Group, London and Pharmaceutical Press, London, 2010.
- [90] E.K. Anderberg, M. Bisrat, and C. Nyström. Physicochemical aspects of drug release. VII. the effect of surfactant concentration and drug particle size on solubility and dissolution rate of felodipine, a sparingly soluble drug. *Int. J. Pharm*, 47:67–77, 1988.

- [91] Patrick J. Marsac, Hajime Konno, and Lynne S. Taylor. A comparison of the physical stability of amorphous felodipine and nifedipine systems. *Pharm. Res.*, 23(10):2306–2316, 2006.
- [92] Hajime Konno, Tetsurou Handa, David E. Alonzo, and Lynne S. Taylor. Effect of polymer type on the dissolution profile of amorphous solid dispersions containing felodipine. *Eur. J. Pharm. Biopharm.*, 70:493–499, 2008.
- [93] Patrick J. Marsac, Hajime Konno, Alfred C.F. Rumondor, and Lynne S. Taylor. Recrystallization of nifedipine and felodipine from amorphous molecular level solid dispersions containing poly(vinylpyrrolidone) and sorbed water. *Pharm. Res.*, 25(3):647–656, 2008.
- [94] David E. Alonzo, Geoff G.Z. Zhang, Deliang Zhou, Yi Gao, and Lynne S. Taylor. Understanding the behavior of amorphous pharmaceutical systems during dissolution. *Pharm. Res.*, 27(4):608–618, 2010.
- [95] J. Kerč, S. Srčič, M. Mohar, and J. Šmid Korbar. Some physicochemical properties of glassy felodipine. *Int. J. Pharm.*, 68:25–33, 1991.
- [96] S. Srčič, J. Kerč, U. Urleb, I. Zupančič, G. Lahajnar, B. Kofler, and J. Šmid Korbar. Investigation of felodipine polymorphism and its glassy state. *Int. J. Pharm.*, 87:1–10, 1992.
- [97] Andrijana Trojak, Klemen Kocevar, Igor Musevic, and Stane Srcic. Investigation of the felodipine glassy state by atomic force microscopy. *Int. J. Pharm.*, 218:145–151, 2001.
- [98] BASF, BASF SE, Care Chemicals Division, Pharma Ingredients and Services, 67117 Limburgerhof. *Technical Information: Kollidon ®VA 64, Kollidon VA 64 Fine*, emp 050602e-05 edition, June 2008.

- [99] O.I. Corrigan, E.M. Holohan, and M.R. Reilly. Physicochemical properties of indomethacin and related compounds co-spray dried with polyvinylpyrrolidone. *Drug Dev. Ind. Pharm.*, 11(2-3):677–695, 1985.
- [100] Lynne S. Taylor and George Zografi. Spectroscopic characterization of interactions between PVP and indomethacin in amorphous molecular dispersions. *Pharm. Res.*, 14(12):1691–1698, 1997.
- [101] Susumu Hasegawa, Takeshi Hamaura, Naho Furuyama, Akira Kusai, Etsuo Yonemochi, and Katsuhide Terada. Effects of water content in physical mixture and heating temperature on crystallinity of troglitazone-PVP K30 solid dispersions prepared by closed melting method. *Int. J. Pharm*, 302:103–112, 2005.
- [102] Michael Tobyn, Jonathan Brown, Andrew B. Dennis, Michael Fakes, Qi Gao, John Gamble, Yaroslav Z. Khimyak, Gary McGeorge, Chhaya Patel, Wayne Sinclair, Peter Timmins, and Shawn Yin. Amorphous drug-PVP dispersions: Application of theoretical, thermal and spectroscopic analytical techniques to the study of a molecule with intermolecular bonds in both the crystalline and pure amorphous state. *J. Pharm. Sci*, 98(9):3456–3468, 2009.
- [103] Atsutoshi Ito, Tomoyuki Watanabe, Shuichi Yada, Takeshi Hamaura, Hiroaki Nakagami, Kenjiro Higashi, Kunikazu Moribe, and Keiji Yamamoto. Prediction of recrystallization behaviour of troglitazone/polyvinylpyrrolidone solid dispersion by solid-state NMR. *Int. J. Pharm*, 2009.
- [104] Harry G. Brittain. Methods for the characterization of polymorphs and solvates. In Harry G. Brittain, editor, *Polymorphism in Pharmaceutical Solids*, volume 95 of *Drugs in the Pharmaceutical Sciences*, chapter 6, pages 227–278. Marcel Dekker, Inc., New York, 1999.
- [105] H.P. Klug and L.E. Alexander. *X-ray diffraction procedures for polycrystalline and amorphous materials*. Wiley, New York, 1974. 524-525 pp.

- [106] Robert E. Dinnebier and Simon J.L. Billinge, editors. *Powder diffraction: theory and practice*. Royal Society of Chemistry, Cambridge, 2008.
- [107] S.J.L. Billinge and M.F. Thorpe. *Local structure from diffraction*. New York: Plenum Press, 1998.
- [108] Simon J.L. Billinge and M.G. Kanatzidis. Beyond crystallography: the study of disorder, nanocrystallinity and crystallographically challenged materials with pair distribution functions. *Chem. Commun.*, pages 749–760, 2004.
- [109] Simon Bates, Ron C. Kelly, Igor Ivanisevic, Paul Schields, George Zografi, and Ann W. Newman. Assessment of defects and amorphous structure produced in raffinose pentahydrate upon dehydration. *J. Pharm. Sci.*, 95(5):1418–1433, 2007.
- [110] Hans Adam Schneider. Conformational entropy contributions to the glass temperature of blends of miscible polymers. *J. Res. Natl. Inst. Stand. Technol.*, 102(2):229–248, 1997.
- [111] P.R. Couchman and F.E. Karasz. A classical thermodynamic discussion on the effect of composition on glass-transition temperatures. *Macromol.*, 11:117–119, 1978.
- [112] Steven P. Stodghill. Thermal analysis - a review of techniques and applications in the pharmaceutical sciences. *Am. Pharm. Rev.*, March 2010:29–36, 2010.
- [113] Savile Bradbury. *An Introduction to the Optical Microscope*. Number 01 in Royal Microscopical Society Microscopy Handbooks. Oxford University Press, Oxford, 1984.
- [114] N.H. Hartshorne and A. Stuart. *Crystals and the Polarising Microscope*. Edward Arnold (Publishers) Ltd., London, 4th edition, 1970.
- [115] Kazuto Okimoto, Masatoshi Miyake, Rinta Ibuki, Mituru Yasumura, Norio Ohnishi, and Tasuku Nakai. Dissolution mechanism and rate of solid dispersion

- particles of nilvadipine with hydroxypropylmethylcellulose. *Int. J. Pharm*, 159: 85–93, 1997.
- [116] Evangelos Karavas, Manolis Georgarakis, Aristides Docoslis, and Dimitrios Bikiaris. Combining SEM, TEM and micro-raman techniques to differetiate between amorphous molecular level dispersions and nanodispersions of a poorly water-soluble drug within a polymer matrix. *Int. J. Pharm*, 340:76–83, 2007.
- [117] Carina Dahlberg, Anna Millqvist-Fureby, and Michael Schuleit. Surface composition and contact angle relationships for differently prepared solid dispersions. *Eur. J. Pharm. Biopharm.*, 70:478–485, 2008.
- [118] Ron Reifenberger and Arvind Raman. ME 597/PHYS 570: Fundamentals of atomic force microscopy (fall 2009), Sep 2009. URL <http://nanohub.org/resources/7320>.
- [119] R. Lal and S.A. John. Biological applications of atomic force microscopy. *Am. J. Physiol.*, 266:C1–C21, 1994.
- [120] A. Ikai. ATM and AFM of bio/organic molecules and structures. *Surf. Sc. R.*, 26: 261–332, 1996.
- [121] Alexander T Florence and David Attwood. *Physicochemical Principles of Pharmacy*, chapter 12: *In vitro* assessment of dosage forms, pages 463–478. Pharmaceutical Press, London, 4th edition, 2006.
- [122] Tanya Tadey and Geoffrey Carr. Dissolution testing for solid oral dosage forms. *Pharmaceutical Formulation and Quality*, 2009.
- [123] Shirzad Azarmi, Wilson Roa, and Raimer Lobenberg. Current perspectives in dissolution testing of conventional and novel dosage forms. *Int. J. Pharm*, 328: 12–21, 2007.



- [124] Ronald H. Böcker and F. Peter Guengerich. Oxidation of 4-Aryl- and 4-Alkyl-Substituted 2,6-Dimethyl-3,5-bis(alkoxycarbonyl)-1,4-dihydropyridines by human liver microsomes and immunochemical evidence for the involvement of a form of cytochrome P-450. *J. Med. Chem.*, 29:1596–1603, 1986.
- [125] Tadao Shibamura, Masaru Iwanami, Masaharu Fujimoto, Toichi Takenaka, and Masuo Murakami. Synthesis of the metabolites of 2-(n-benzyl-n-methylamino)ethyl methyl 2,6-dimethyl-4-(*m*-nitrophenyl)-1,4-dihydropyridine-3,5-dicarboxylate hydrochloride (nicardipine hydrochloride, YC-93). *Chem. Pharm. Bull.*, 28(9):2609–2613, 1980.
- [126] Jürg Pfister. Rapid, high-yield oxidation of hantzsch-type 1,4-dihydropyridines with ceric ammonium nitrate. *Synthesis*, page 689, 1990.
- [127] Tse-Lok Ho. Cerium (IV) oxidation of hydroquinones and sulfides with a dual oxidant system. *Synth. Commun.*, 9(4):237–239, 1979.
- [128] Leonid Metsger and Shmuel Bittner. Autocatalytic oxidation of ethers with sodium bromate. *Tetrahedron*, 56:1905–1910, 2000.
- [129] Paolo Cozzi, Germano Carganico, Domenico Fusar, Mauro Grossoni, Maria Menichincheri, Vittorio Pinciroli, Roberto Tonani, Fabrizio Vaghi, and Patricia Salvati. Imidazol-1-yl and pyridin-3-yl derivatives of 4-phenyl-1,4-dihydropyridines combining  $\text{Ca}^{2+}$  antagonism and thromboxane  $A_2$  synthase inhibition. *J. Med. Chem.*, 36:2964–2972, 1993.
- [130] Bo Lamm and Roger Simonsson. Synthesis of the enantiomers of felodipine and determination of their absolute configuration. *Tet. Lett.*, 30(46):6423–6426, 1989.
- [131] A. Hantzsch. Condensationsprodukte aus aldehydammoniak und ketonartigen verbindungen. *Berichte der deutschen chemischen Gesellschaft*, 14(2):1637–1638, July 1881.

- [132] Process for the preparation of 4-substituted-1,4-dihydropyridines, 1993.
- [133] Jonathan Clayden, Nick Greeves, Stuart Warren, and Peter Wothers. *Organic Chemistry*, chapter 44, pages 1185–1218. Oxford University Press, Oxford., 2001.
- [134] Abdelmadjid Debache, Raouf Boulcina, Ali Belfaitah, Salah Rhouati, and Bertrand Carboni. One-pot synthesis of 1,4-dihydropyridines via a phenylboronic acid catalyzed hantzsch three-component reaction. *Syn. Lett.*, 4:509–512, 2008.
- [135] Koji Ohsumi, Kazuo Ohishi, Yoshihiro Morinaga, Ryusuke Nakagawa, Yasuyo Suga, Takaaki Sekiyama, Yukio Akiyama, Takashi Tsuji, and Takashi Tsuruo. N-Alkylated 1,4-Dihydropyridines: New agents to overcome multidrug resistance. *Chem. Pharm. Bull.*, 43(5):818–828, 1995.
- [136] W.C. Still, M. Kahn, and A. Mitra. Rapid chromatographic technique for preparative separations with moderate resolution. *J. Org. Chem.*, 43:2923–2925, 1978.
- [137] Jihyun Jung, Laehee Kim, Chang Sik Lee, Yoon Hwan Cho, Seung-Ho Ahn, and Yoongho Lim. Spectral assignments and reference data: Total assignment of the  $^1\text{H}$  and  $^{13}\text{C}$  NMR data for felodipine and its derivatives. *Magn. Reson. Chem.*, 39:406–410, 2001.
- [138] Xiangyun Qiu, Jeroen W. Thompson, and Simon J.L. Billinge. PDFgetX2: a GUI-driven program to obtain the pair distribution function from x-ray powder diffraction data. *J. Appl. Cryst.*, 37:678, 2004.
- [139] Ilse Weuts, Frederic Van Dycke, Jody Voorspoels, Steve De Cort, Sigrid Stokbroekx, Ruud Leemans, Marcus E. Brewster, Dawei Xu, Brigitte Segmuller, Ya Tsz A. Turner, Clive J. Roberts, Martyn C. Davies, Sheng Qi, Duncan Q.M. Craig, and Mike Reading. Physicochemical properties of the amorphous drug, cast films and spray dried powders to predict formulation probability of success for solid dispersions: Etravirine. *J. Pharm. Sci.*, pages 1–15, 2010.

- [140] Keith Alexander and C. Judson King. Factors governing surface morphology of spray-dried amorphous substances. *Drying Technology*, 3(3):321–348, 1985.
- [141] D.E. Walton and C.J. Mumford. Spray dried products - characterization of particle morphology. *Trans IChemE, Part A*, 77:21–38, 1999.
- [142] D.E. Walton and C.J. Mumford. The morphology of spray-dried particles: The effect of process variables upon the morphology of spray-dried particles. *Trans IChemE, Part A*, 77:442–460, 1999.
- [143] D.E. Walton. The morphology of spray-dried particles a qualitative view. *Drying Technology*, 18(9):1943–1986, 2000.
- [144] Rune Fosshem. Crystal structure of the dihydropyridine  $\text{Ca}^{+2}$  antagonist felodipine. dihydropyridine binding prerequisites assessed from crystallographic data. *J. Med. Chem.*, 29:305–307, 1986.
- [145] J. Carson Meredith and Eric J. Amis. LCST phase separation in biodegradable polymer blends: poly(D,L-lactide) and poly( $\eta$ -caprolactone). *Macromol. Chem. Phys.*, 201:733–739, 2000.
- [146] Qiang Zheng, Mao Peng, Yihu Song, and Tiejun Zhao. Use of WLF-like function for describing the nonlinear phase separation behavior of binary polymer blends. *Macromol.*, 34:8483–8489, 2001.
- [147] Liang Cui and Yanchun Han. Honeycomb pattern formation via polystyrene/poly(2-vinylpyridine) phase separation. *Langmuir*, 21:11085–11091, 2005.
- [148] Khalil El-Mabrouk, Mohamed Belaiche, and Mosto Bousmina. Phase separation in PS/PVME thin and thick films. *J. Coll. & Interface Sci.*, 306:354–367, 2007.
- [149] Haijun Tao, Jun Zhang, and Jiali Gao. Phase separation and polymer crystallization in a poly(4-methyl-1-pentene)-dioctylsebacate-dimethylphthalate system via thermally induced phase separation. *J. Polym. Sci. B*, 45:153–161, 2007.

- [150] Yung-Hsu Wu, Da-Ming Wang, and Juin-Yi Lai. Effects of polymer chain length and stiffness on phase separation dynamics of semidilute polymer solution. *J. Phys. Chem. B*, 112:4604–4612, 2008.
- [151] Charles S. Johnson Jr. and Don A. Gabriel. *Laser Light Scattering*. Dover Publications, Inc., New York, 1994.
- [152] Benjamin Chu. *Laser Light Scattering: Basic Principles and Practice*. Academic Press, Ltd. London, 2nd edition, 1991.
- [153] Paul A. Webb. A primer on particle sizing by static laser light scattering. [http://www.particletesting.com/docs/primer\\_particle\\_sizing\\_laser.pdf](http://www.particletesting.com/docs/primer_particle_sizing_laser.pdf), January 2000. Accessed on 10/10/2010.
- [154] Takeji Hashimoto, Jiro Kumaki, and Hiromichi Kawai. Time-resolved light scattering studies on kinetics of phase separation and phase dissolution of polymer blends. 1. kinetics of phase separation of a binary mixture of polystyrene and poly(vinyl methyl ether). *Macromol.*, 16:641–648, 1983.
- [155] Takeji Hashimoto, Kouji Sasaki, and Hiromichi Kawai. Time-resolved light scattering studies on the kinetics of phase separation and phase dissolution of polymer blends. 2. phase separation of ternary mixtures of polymer A, polymer B and solvent. *Macromol.*, 17:2812–2818, 1984.
- [156] Takeshi Murashige, Hideo Fujikake, Hiroto Sato, Hiroshi Kikuchi, Taiichiro Kurita, and Fumio Sato. Light diffraction of aligned polymer fibers periodically dispersed by phase separation of liquid crystal and polymer. *Optical Rev.*, 11(11):349–352, 2004.
- [157] T. Matsumoto and G. Zografi. Physical properties of solid molecular dispersions of indomethacin with poly(vinylpyrrolidone) and poly(vinylpyrrolidone-co-vinylacetate) in relation to indomethacin crystallization. *Pharm. Res.*, 16:1722–1728, 1999.

- [158] Karine Khougaz and Sophie-Dorothée Clas. Crystallization inhibition in solid dispersions of MK-0591 and poly(vinylpyrrolidone) polymers. *J. Pharm. Sci.*, 89: 1325–1334, 2000.
- [159] George Zografi. States of water associated with solids. *Drug Dev. Ind. Pharm.*, 14:1905–1926, 1988.
- [160] Claes Ahlneck and George Zografi. The molecular basis of moisture effects on the physical and chemical stability of drugs in the solid state. *Int. J. Pharm.*, 62: 87–95, 1990.
- [161] Cynthia A. Oksanen and George Zografi. The relationship between the glass transition temperature and water vapor absorption by poly(vinylpyrrolidone). *Pharm. Res.*, 7(6):654–657, 1990.
- [162] Sheri L. Shamblin and George Zografi. The effect of absorbed moisture on the properties of amorphous mixtures containing sucrose. *Pharm. Res.*, 16(7):1119–1124, 1999.
- [163] Xiaolin Charlie Tang, Michael J. Pikal, and Lynne S. Taylor. A spectroscopic investigation of hydrogen bond patterns in crystalline and amorphous phases in dihydropyridine calcium channel blockers. *Pharm. Res.*, 19:477–483, 2002.
- [164] Christopher A. Lipinski. Drug-like properties and the causes of poor solubility and poor permeability. *J. Pharm. Tox. Meth*, 44:235–249, 2000.
- [165] Jan Westergren, Lennart Lindfors, Tobias Höglund, Kai Lüder, Sture Nordholm, and Roland Kjellander. *In Silico* prediction of drug solubility: 1. free energy of hydration. *J. Phys. Chem. B.*, 111(7):1872–1882, 2007.
- [166] Kai Lüder, Lennart Lindfors, Jan Westergren, Sture Nordholm, and Roland Kjellander. *In Silico* prediction of drug solubility: 2. free energy of solvation in pure melts. *J. Phys. Chem. B.*, 111(7):1883–1892, 2007.

- [167] Kai Lüder, Lennart Lindfors, Jan Westergren, Sture Nordholm, and Roland Kjellander. *In Silico* prediction of drug solubility. 3. free energy of solvation in pure amorphous matter. *J. Phys. Chem. B*, 111(25):7303–7311, 2007.
- [168] Kai Lüder, Lennart Lindfors, Jan Westergren, Sture Nordholm, Rasmus Persson, and Mikaela Pedersen. *In Silico* prediction of drug solubility: 4. will simple potentials suffice? *J. Comput. Chem.*, 30:1859–1871, 2009.
- [169] pION Inc. API-sparing small volume dissolution and solubility profiling of phenazopyridine.HCl. Technical Report D051001-2, pION Inc, Woburn, MA, USA, 5 Constitution Way, Woburn, MA 01801-1024, USA, November 2005.
- [170] Saša Baumgartner, Gojmir Lahajner, Ana Sepe, and Julijana Kristl. Quantitative evaluation of polymer concentration profile during swelling of hydrophilic matrix tablets using  $^1\text{H}$  NMR and MRI methods. *Eur. J. Pharm. Biopharm.*, 59:299–306, 2005.
- [171] C.A. Fyfe and A.I. Blazek. Complications in investigations of the swelling of hydrogel matrices due to the presence of trapped gas. *J. Control. Rel.*, 52:221–225, 1998.
- [172] Piotr Kulinowski, Przemysław Dorożyński, Renata Jachowicz, and Władysław P. Węglarz. An integrated system for dissolution studies and magnetic resonance imaging of controlled release, polymer-based dosage forms - a tool for quantitative assessment of hydrogel formation processes. *J. Pharm. Biomed. Anal.*, 48:685–693, 2008.
- [173] Ya Ying Chen, L.P. Hughes, L.F. Gladden, and M.D. Mantle. Quantitative ultra-fast MRI of HPMC swelling and dissolution. *J. Pharm. Sci.*, 99(8):3462–3472, 2010.
- [174] Ring Liu. *Water-Insoluble Drug Formulation*. CRC Press, 2007. 118 pp.

- [175] Zoe Langham, Jonathan Booth, Stephen Wren, Les Hughes, and Gavin Reynolds. An investigation into the impact of drug loading on the dissolution performance of amorphous felodipine/copovidone solid dispersions. In Preparation.
- [176] Wikipedia. Pearson product-moment correlation coefficient. [http://en.wikipedia.org/wiki/Pearson\\_product-moment\\_correlation\\_coefficient](http://en.wikipedia.org/wiki/Pearson_product-moment_correlation_coefficient). Accessed on 19/10/2010.
- [177] Han van de Waterbeemd. Physicochemical approaches to drug absorption. In Han van de Waterbeemd and Bernard Testa, editors, *Drug Bioavailability: Estimation of Solubility, Permeability, Absorption and Bioavailability*, volume 40 of *Methods and Principles in Medicinal Chemistry*, chapter 5, pages 71–99. Wiley-VCH, 2nd edition, 2009.
- [178] Alexander T Florence and David Attwood. *Physicochemical Principles of Pharmacy*, chapter 5: The solubility of drugs, pages 139–176. Pharmaceutical Press, London, 4th edition, 2006.